New transition metal carbene complexes for application in homogeneous catalysis

by

Gerrit R. Julius

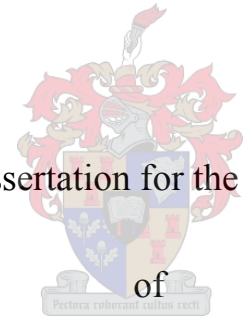

Dissertation for the degree

of

DOCTOR in PHILOSOPHY

at the

UNIVERSITY of STELLENBOSCH

Promoter: Prof H.G. Raubenheimer
Co-promoter: Dr S. Cronje

December 2005

Declaration

I, the undersigned, hereby declare that the work contained in this dissertation is my own original work and that I have not previously in its entirety or in part submitted it at any university for a degree.

Signature:……..

Date:……..

Abstract

This study comprises the preparation and full characterisation of new carbene complexes of group 10 metals (Ni, Pd or Pt), the group 9 metal, rhodium, as well as group 6 metals (Cr and/or W).

N-heterocyclic carbene (NHC) complexes of nickel and palladium were prepared *via* oxidative addition of the corresponding carbene precursors imidazolium-, imidazolinium-, pyridinium- and quinolinium chloride salts, to $M(PPh_3)_4$ (M = Ni or Pd). Three types of carbene complexes, namely the standard five-membered two-N carbene complexes, new six-membered NHC complexes and novel six-membered *r*NHC complexes received attention. In the *r*NHC complexes the heteroatom (N) is removed from the carbene carbon. These new square planar carbene complexes of the general formula *trans*-$[(PPh_3)_2MCl(L)]X$ (M = Ni or Pd; X = BF_4 or PF_6) L = 1,3-dimethyl-2,3-dihydro-1*H*-imidazol-2-ylidene, 1,3-dimethyl-2,3,4,5-tetrahydro-1*H*-imidazol-2-ylidene, 1-methyl-1,2-dihydro-pyridin-2-ylidene, 1-methyl-1,2-dihydro-quinolin-2-ylidene, 1,4-dimethyl-1,2-dihydro-quinolin-2-ylidene, 2-methoxy-1-methyl-1,4-dihydro-quinolin-4-ylidene, 1-methyl-1,4-dihydro-pyridin-4-ylidene) have been isolated and characterised. The preparation of the corresponding carbene complexes of platinum was complicated by the formation of $[PtCl(PPh_3)_3]BF_4$ and the desired carbene complexes could not be isolated in pure form. The investigation of *r*NHC complexes was extended to include the synthesis of $(CO)_5M\{CSC(CNCMe_2CH_2O)CHCH\}$ (M = Cr and W).

The molecular and crystal structures of thirteen of the new carbene complexes including the structures of both *cis*- (only formed below –20°C) and *trans*-chloro(1-methyl-1,2-dihydro-quinolin-2-ylidene)bis(triphenylphosphine)palladium(II) tetrafluoroborate were determined. The metal-carbene bond distances in both the palladium and nickel carbene families do not differ significantly. The carbene ligands can be arranged in a series of increasing *trans*-influence, using the metal-chloride bond distance as a guideline, as follows: 1,3-dimethyl-2,3-dihydro-1*H*-imidazol-2-ylidene and 1,3-dimethyl-2,3,4,5-tetrahydro-1*H*-imidazol-2-ylidene < 1-methyl-1,2-dihydro-pyridin-2-ylidene < 2-methoxy-1-methyl-1,4-dihydro-quinolin-4-ylidene, 1-methyl-1,4-dihydro-pyridin-4-ylidene. The crystal and molecular structures of two platinum compounds, *cis*-chloro(2-methoxy-1-methyl-1,4-dihydro-quinolin-4-ylidene)bis(triphenylphosphine)platinum(II) tetrafluoroborate and the byproduct $[PtCl(PPh_3)_3]BF_4$ were also determined.

Trans-chloro(2-methoxy-1-methyl-1,4-dihydro-quinolin-4-ylidene)bis(triphenylphosphine) palladium(II) tetrafluoroborate was found to be a very active catalyst, compared to simpler palladium carbene and phosphine complexes, in the Mizoroki-Heck and Suzuki-Miyaura coupling reactions. Quantum mechanical calculations indicated that the *r*NHC ligand in this complex is bound stronger to the palladium than a standard imidazole-derived NHC ligand. Further calculations suggested that the remote heteroatom carbene (*r*NHC) complexes of nickel(II) are significantly more stable when compared to the normal carbene (NHC) complexes. Energy decomposition analysis suggested that the *r*NHC ligands are strong σ-donors and weak π-acceptors.

Unsymmetrical imidazolium-derived bis(carbene) complexes, $[Rh(NHC)_2COD]Br$, bromo-mono(carbene) complexes, Rh(Br)COD(NHC), and chloro-mono(carbene) complexes, Rh(Cl)COD(NHC) where NHC = 1-R-3-methyl-2,3-dihydro-1*H*-imidazol-2-ylidene (R = ethyl, propyl or butyl), were formed in each reaction of the corresponding free carbene ligand with $[Rh(Cl)COD]_2$. [Rh(Br)COD(NHC)] formed as a result of substitution of a chloride ligand by a Br^--anion. The carbonyl complexes, *cis*-$[Rh(CO)_2X(NHC)]$ (X = Br or Cl; NHC = 1-ethyl-3-methyl-2,3-dihydro-1*H*-imidazol-2-ylidene) were isolated after the substitution of the COD ligand in Rh(X)COD(NHC) (X = Br or Cl) with CO. Isomerisation of these *cis*-carbonyl complexes to the *trans* isomers was observed.

Cis-[(η^4-1,5-cyclooctadiene)bis(1-butyl-3-methyl-2,3-dihydro-1*H*-imidazol-2-ylidene)rhodium(I)] bromide, bromo(η^4-1,5-cyclooctadiene)(1-methyl-3-propyl-2,3-dihydro-1*H*-imidazol-2-ylidene) rhodium(I) and *cis*-[(η^4-1,5-cyclooctadiene)bis(1-butyl-3-methyl-2,3-dihydro-1*H*-imidazol-2-ylidene)rhodium(I)]bromide were also characterised by single crystal X-ray diffraction.

The synthesis and structural characterisation of a series of acyclic and heterometallacyclic Fischer-type carbene complexes in which a soft donor atom (P) attached to the carbene side chain is either uncoordinated, $(CO)_5M{=}C(NMe_2)CH_2PPh_2$ (M = Cr or W), bonded to the original central metals (Cr or W) in four-membered chelates, $(CO)_4\overline{M{=}C(NMe_2)CH_2PPh_2}$, or coordinated to a second $M(CO)_5$ unit (only isolated for chromium) $(CO)_5Cr{=}C(NMe_2)CH_2P(Ph_2)Cr(CO)_5$, were carried out. These compounds were produced by the reaction of the anionic Fischer-type aminocarbene complexes, $[(CO)_5Cr{=}C(NMe_2)CH_2]Li$ (M = Cr or W), with $ClPPh_2$. The formation of the four-membered chelates, *via* cyclisation, occurs much faster for Cr than for W. The aminocarbene-phosphine

chelates represent the first examples of structurally characterised, four-membered C,P-chelate carbene complexes.

Opsomming

Hierdie studie behels die bereiding en volle karakterisering van nuwe karbeenkomplekse van groep 10 metale (Ni, Pd of Pt), die groep 9 metaal, rodium, asook groep 6 metale (Cr, en/of W).

N-heterosikliese karbeenkomplekse (NHC-komplekse) van nikkel en palladium is berei deur oksidatiewe addisie van die ooreenstemmende karbeenvoorlopers, imidasolium-, imidasolinium-, piridinium-, en kinoliniumchloriedsoute, aan $M(PPh_3)_4$ (M = Ni of Pd). Drie tipe karbeenkomplekse naamlik die standaard vyflid NHC-komplekse, seslid NHC-komplekse en seslid *r*NHC-komplekse word beskryf. In die *r*NHC-komplekse is die heteroatoom (N) verwyderd van die karbeenkoolstof. Die nuwe vierkantigvlak karbeenkomplekse met die algemene formule *trans*-$[(PPh_3)_2MCl(L)]X$ (M = Ni of Pd; X = BF_4 of PF_6) L = 1,3-dimetiel-2,3-dihidro-1*H*-imidasol-2-ilideen, 1,3-dimetiel-2,3,4,5-tetrahidro-1*H*-imidasol-2-ilideen, 1-metiel-1,2-dihidro-piridien-2-ilideen, 1-metiel-1,2-dihidro-kinolien-2-ilideen, 1,4-dimetiel-1,2-dihidro-kinolien-2-ilideen, 2-metoksie-1-metiel-1,4-dihidro-kinolien-4-ilideen, 1-metiel-1,4-dihidro-piridien-4-ilideen) is geisoleer. Die bereiding van die ooreenstemmende karbeenkomplekse van platinum is gekompliseer deur die vorming van $[PtCl(PPh_3)_3]BF_4$ en die verwagte karbeenkomplekse kon nie geïsoleer word nie. Die ondersoek van *r*NHC-komplekse is uitgebrei om die sintese van $(CO)_5M\{\underline{CSC(\overline{CNCMe_2CH_2O})CHCH}\}$ (M = Cr en W) in te sluit.

Die molekulêre en kristalstrukture van dertien van die karbeenkomplekse is bepaal. Interessant genoeg kon die strukture van beide *cis*- (vorm slegs benede –20°C) en *trans*-chloro(1-metiel-1,2-dihidro-kinolien-2-ilideen)bis(trifenielfosfien)palladium(II) tetrafluoroboraat eenduidig vasgelê word. Die metal-karbeen bindingslengtes in die palladium- en nikkelkarbeenkompleksfamilies verskil nie beduidend van mekaar nie. Die karbeenligande kan gerankskik word in ‘n reeks van toenemende *trans*-invloed, met die gebruik van die metaal-chloried bindingslengte as riglyn: 1,3-dimetiel-2,3-dihidro-1*H*-imidasol-2-ilideen en 1,3-dimetiel-2,3,4,5-tetrahidro-1*H*-imidasol-2-ilideen < 1-metiel-1,2-dihidro-piridien-2-ilideen < 2-metoksie-1-metiel-1,4-dihidro-kinolien-4-ilideen, 1-metiel-1,4-dihidro-piridien-4-ilideen. Die kristal- en molekulêre strukture van twee platinumkomplekse, *cis*-chloro(2-metoksie-1-metiel-1,4-dihidro-kinolien-4-ilideen) bis(trifenielfosfien)platinum(II) tetrafluoroboraat en $[PtCl(PPh_3)_3]BF_4$ is ook bepaal.

Trans-chloro(2-metoksie-1-metiel-1,4-dihidro-kinolien-4-ilideen)bis(trifenielfosfien)palladium(II) tetrafluoroboraat is ‘n baie aktiewe katalisator, in vergelyking met eenvoudiger palladiumkarbeen- en fosfienkomplekse vir die Mizoroki-Heck en Suzuki-Miyaura koppelingsreaksies. Kwantummeganiese berekeninge het getoon dat die *r*NHC-ligand in hierdie kompleks sterker aan die palladium gebind is as die standaard imodasool-afgeleide NHC-ligand. Verdere berekeninge wys daarop dat die verwyderde heteroatoomkarbeen (*r*NHC) komplekse van nikkel betekenisvol stabieler is as die normale NHC-komplekse. Energie ontbindingsanalises dui aan dat die karbeen ligande sterk σ-donors en swak π-akseptore is.

Die onsimmetriese, imidasool-afgeleide bis(karbeen)komplekse, $[Rh(NHC)_2COD]Br$, bromo-mono(karbeen)komplekse, Rh(Br)COD(NHC), en chloro-mono(karbeen)komplekse, Rh(Cl)COD(NHC), met NHC = 1-R-3-metiel-2,3-dihidro-1*H*-imidasol-2-ilideen (R = etiel, propiel of butiel), het gevorm in elke reaksie van die ooreenstemmende karbeenligand met $[Rh(Cl)COD]_2$. [Rh(Br)COD(NHC)] het ontstaan as gevolg van die substitusie van ‘n chloriedligand deur ‘n Br^--anioon. Die karbonielkomplekse, *cis*-$[Rh(CO)_2X(NHC)]$ (X = Br of Cl; NHC = 1-etiel-3-metiel-2,3-dihidro-1*H*-imidasol-2-ilideen) is berei deur die substitusie van die COD-ligand in Rh(X)COD(NHC) (X = Br of Cl) met CO. Isomerisasie van die *cis*-karbonielkomplekse na die *trans*-isomere is waargeneem.

Cis-[(η^4-1,5-siklo-oktadieen)bis(1-butiel-3-metiel-2,3-dihidro-1*H*-imidasol-2-ilideen)rodium(I)] bromied, bromo(η^4-1,5-siklo-oktadieen)(1-metiel-3-propiel-2,3-dihidro-1*H*-imidasol-2-ilideen) rodium(I) en *cis*-[(η^4-1,5-siklo-oktadieen)bis(1-butiel-3-metiel-2,3-dihidro-1*H*-imidasol-2-ilideen) rodium(I)]bromied is ook met behulp van enkelkristal X-straal diffraksie gekarakteriseer.

Die sintese en struktuurkarakterisering van ‘n reeks asikliese en heterometallasikliese Fischer-tipe karbeenkomplekse waarin ‘n sagte donoratoom (P) gebind is aan die karbeensyketting, $(CO)_5M{=}C(NMe_2)CH_2PPh_2$ (M = Cr or W), en met P verder gekoördineer aan die oorspronklike sentrale metale, Cr en W om vierlid-chelate, $(CO)_4\overline{M{=}C(NMe_2)CH_2PPh_2}$, te vorm of gekoördineer aan ‘n tweede $M(CO)_5$ eenheid (alleen geïsoleer vir chroom), $(CO)_5Cr{=}C(NMe_2)CH_2P(Ph_2)Cr(CO)_5$, is uitgevoer. Die verbindings is berei deur die reaksie van die anioniese Fischer-tipe aminokarbeenkomplekse, $[(CO)_5Cr{=}C(NMe_2)CH_2]Li$ (M = Cr of W) met $ClPPh_2$. Die vorming van die vierlid-chelate, *via* siklisering, vind vinniger plaas vir Cr as vir W.

Die aminokarbeen-fosfien-chelate verteenwoordig die eerste voorbeelde van struktureel-gekarakteriseerde vierlid C,P-chelaat-karbeenkomplekse.

To my mother

Acknowledgements

I would like to acknowledge and thank the following people for their contributions to my studies.

My Lord and heavenly Father for the ability, opportunity, love and grace to complete my studies.

Prof Raubenheimer for the support, guidance, inspiration, encouragement, challenging me and believing in me. It was great that we could reason together about chemistry and other aspects in life.

Dr Stephanie Cronje for the miles and miles that you walked with me, through the tough as well as the good periods of my studies. Your care, assistance, motivation and creativity were indispensable during this time.

My family for all your sacrifices and your unshakable support, especially during the tough times. Without you it would have been an uphill battle. Elize for your love and care. Also to my friends thank you for your support.

All the people with whom I worked in the lab, for the camaraderie and respect that we shared. It was special. Bertie Barnard, Jacorien en Karolien Coetzee for all your assistance in the lab. Your help was crucial and you saved me a lot of time. Elzet for the printing and binding of this thesis.

Prof Len Barbour, Drs Stefan Nogai and Catharine Esterhuysen for patience and help in the crystal structure determinations. Jean McKenzie and Elsa Malherbe in the NMR laboratory, for all the work you did for me and the many times that you went out of your way to help me. My gratitude also to Mr Ward, the glass blower (and a great friend). Thank you also to the other technical staff in the department.

Sabine Schneider from the group of Prof Dr Wolfgang Herrmann (Technical University of Munich, Germany), Christoph Loschen from the group of Prof Gernot Frenking (Phillips University Marburg, Germany) and Dr Patric Roembke for the fruitful collaboration.

Prof Wim Dehean for the four months that I spent with him at the Katholieke Universiteit Leuven, Belgium.

Sasol for the student sponsorship and more specifically, Dr Mike Green who financially supported the research project.

Dr Anton Vosloo, my mentor at Sasol, for your interest in my progress and assistance particularly in the last period of my studies.

Publications

Parts of this work have already been published or submitted for publication:

S. Cronje, G.R Julius, E. Stander, C. Esterhuysen, H.G. Raubenheimer – New reactions and new products derived from α-deprotonated Fischer-type carbene complexes, *Inorg. Chim. Acta*, 2005, **358**, 1581. (Special edition dedicated to F.G.A. Stone)

S.K. Schneider, P. Roembke, G.R. Julius, C. Loschen, H.G. Raubenheimer, G. Frenking, W.A. Herrmann - An Extension of the NHC Concept: C-C Coupling Catalysis by a Pd(II) Carbene (*r*NHC) Complex with Remote Heteroatoms, *Eur. J. Inorg. Chem*, 2005, 2973.

S.K. Schneider, G.R. Julius, C. Loschen, H.G. Raubenheimer, G. Frenking, W.A. Herrmann – A first structural and theoretical comparison of *r*NHC (*remote* N-Heterocyclic carbene) and HNC complexes of Ni(II) obtained by oxidative substitution, *Dalton Trans.*, 2005, in press.

S.K. Schneider, P. Roembke, G.R. Julius, H.G. Raubenheimer, W.A. Herrmann, Pyridin-, quinolin- and acridinylidene palladium carbene complexes as highly efficient C-C coupling catalysts, *Adv. Synth. Catal.*, 2005, submitted for publication.

Oral presentations

Cape Organometallic Symposium, Morgenhof, October 2003, Oral presentation by Gerrit Julius: "New unexpected and unusual carbene complexes of chromium, manganese, palladium and platinum".

37th National SACI Convention, Pretoria, July 2004, Oral Presentation by Gerrit Julius: "Variations on the theme by Öfele-Wanzlick, Fischer and Stone".

Parts of this work have also been presented by Prof Raubenheimer at various universities in Europe and conferences in South Africa.

Poster presentation

Cape Organometallic Symposium, Breakwater Lodge, Waterfront, Cape Town, October 2004; "New reactions and new products derived from α-deprotonated Fischer-type carbene complexes" G.R. Julius, E. Stander, S. Cronje, C. Esterhuysen, H.G. Raubenheimer.

Abbreviations

Å		Angström (10^{-10} m)
Δ		difference between two values
COD		η^4-1,5-cyclooctadiene
COE		cyclooctene
Cp		η-cyclopentadienyl
ghsqc		gradient heteronuclear single quantum coherence
ghmqc		gradient heteronuclear multiple quantum coherence
HUMO		highest occupied molecular orbital
LUMO		lowest unoccupied molecular orbital
MS		Mass Spectrometry
m/z		mass/charge
NMR		Nuclear Magnetic Resonance
NHC		*N*-heterocyclic carbene
*r*NHC		remote *N*-heterocyclic carbene
M-H		Mizoroki-Heck reaction
Ph		phenyl
PPh_3		triphenylphosphine
ppm		parts per million
S-M		Suzuki-Miyaura reaction
THF		tetrahydrofuran

IR	m	medium
	s	strong
	sh	shoulder
	w	weak

NMR	δ	chemical shift
	d	doublet
	dd	doublet of doublets
	dq	doublet of quartets

J	coupling constant
m	multiplet
q	quartet
s	singlet
t	triplet

Table of contents

Declaration

I, the undersigned, hereby declare that the work contained in this dissertation is my own original work and that I have not previously in its entirety or in part submitted it at any university for a degree.

Signature: C R Julius

Date: 28 · 11 · 05

Chapter 1

Introduction and Aims

1.1 Introduction

General

Carbenes are neutral compounds with a divalent carbon atom, which has two non-bonding electrons. These electrons can have the same spin (triplet state) or opposite spins (singlet state).[1,2] Carbenes and carbene complexes have played an important role as reactive intermediates in organic synthesis.[3,4] Doering introduced the term carbene into organic chemistry when dihalocarbenes were reacted with olefins to produce cyclopropanes (Scheme 1.1).[5] Fischer later developed this concept in organometallic chemistry by introducing carbenes as extremely useful ligands.[6] Free heterocyclic carbenes (usually derived from imidazolium salts) are examples of carbenes in the singlet state. Fischer carbene complexes contain the carbene ligand in the singlet state (compare the following section)

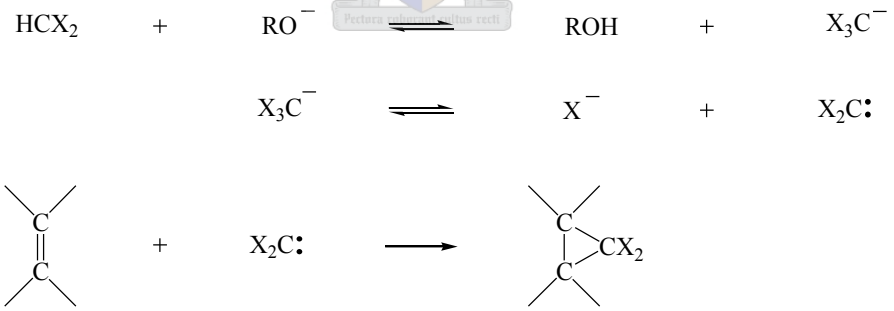

Scheme 1.1 (X = Cl, Br, I; R = *tert*-butyl)

---

[1] W.A. Herrmann, M. Elison, J. Fischer, C. Köcher, G.R.J. Artus, *Chem. Eur. J.*, 1996, **2**, 772.

[2] D. Bourissou, O. Guerret, F.P. Gabbai, G. Bertrand, *Chem. Rev.*, 2000, **100**, 39.

[3] N. Kuhn, T. Kratz, *Synthesis*, 1993, 561.

[4] M. Regitz, *Angew. Chem., Int. Ed., Engl.*, 1991, **30**, 674.

[5] W.von E. Doering, A.K. Hoffmann, *J. Am. Chem. Soc.*, 1954, **76**, 6162.

[6] E.O. Fischer, A. Maasböl, *Angew. Chem., Int. Ed., Engl.*, 1964, **3**, 580.

N-*Heterocyclic carbenes (NHC's) and their complexes*

The independent discovery of carbene complexes by Öfele[7] and Wanzlick[8] in 1968 [(**i**) and (**ii**) respectively, Scheme 1.2] and the isolation of the first stable free carbene by Arduengo[9] in 1991 [(**iii**), Scheme 1.3] were the landmarks that sparked the research of these interesting ligands, their metal complexes and their application in catalysis.

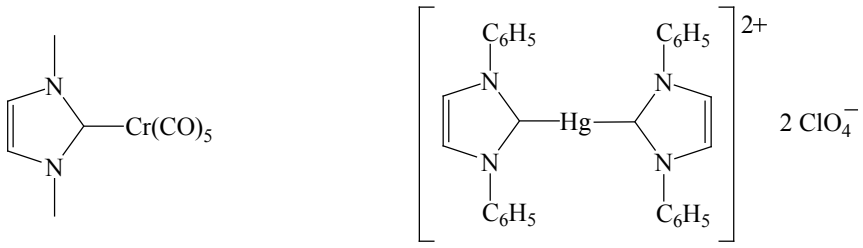

(**i**) (**ii**)

Scheme 1.2

These landmarks were followed by the isolation of more stable free carbenes [(**iii**) – (**vi**), Scheme 1.3][10,11,12] as well as the preparation of carbene complexes of almost all the transition metals, main group elements and rare earth metals.[2,13] Recently Kuhn and Al-Sheik[14] reviewed 2,3-dihydro-1*H*-imidazol-2-ylidenes and their main group element chemistry. Schumann and co-workers[15] described the first rare earth metal carbene complex, $Yb(C_5Me_4Et)_2(NHC)$ (NHC = 1,3,4,5-tetramethyl-2,3-dihydro-1*H*-imidazol-2-ylidene). A bis(carbene)proton compound has also been isolated.[16] Imidazolium-derived NHC's are σ-donating ligands with little π-acceptor ability and are

[7] K. Öfele, *J. Organomet. Chem.*, 1968, **12**, P42.

[8] H.W. Wanzlick, H.J. Schönder, *Angew. Chem., Int. Ed., Engl.*, 1968, **7**, 141.

[9] A.J. Arduengo, III, J.R. Goerlich, W.J. Marshall, *J. Am. Chem. Soc.*, 1991, **113**, 361.

[10] A.J. Arduengo,III, H.V.R. Dias, R.L. Harlow, M. Kline, *J. Am. Chem. Soc.*, 1992, **114**, 5530.

[11] A.J. Arduengo,III, J.R. Goerlich, W.J. Marshall, *J. Am. Chem. Soc.*, 1995, **117**, 11027.

[12] R.W. Alder, P.R. Allen, M. Murray, G. Orpen, *Angew. Chem., Int. Ed., Engl.*, 1996, **35**, 1121.

[13] W.A. Hermann, C. Köcher, *Angew. Chem., Int. Ed., Engl.*, 1997, **36**, 2162.

[14] N. Kuhn, A. Al-Sheikh, *Coord. Chem. Rev.*, 2005, **249**, 829.

[15] H. Schumann, M. Glanz, J. Winterfeld, H. Hemling, N. Kuhn, T. Kratz, *Angew. Chem., Int. Ed., Engl.*, 1994, **33**, 1733.

[16] A.J. Arduengo, III, S.F. Gamper, M. Tamm, J.C. Calabrese, F. Davidson, H.A. Craig, *J. Am. Chem. Soc.*, 1995, **117**, 572.

comparable to P, N and O-donating ligands rather than to Fischer and Schrock carbenes.[13,17] Imidazole-derived carbene ligands are however more basic than electron-rich phosphines like PMe_3 and $P(cyclohexyl)_3$ and increase the electron density at the metal center compared to these phosphines.[18] The successful application of carbene complexes (including NHC complexes) as active catalyst pre-cursors in olefin-metathesis reactions was honoured by the Nobel Prize for Chemistry in October 2005.[19] Y. Chauvin, for his proposed mechanism for metathesis, R.H. Grubbs, for developing the first generation of the Grubbs catalyst (carbene complexes as metathesis pre-catalysts), and R.R. Schrock, for the utilisation of specific carbene and carbyne complexes as metathesis pre-catalysts, shared the Nobel Prize.

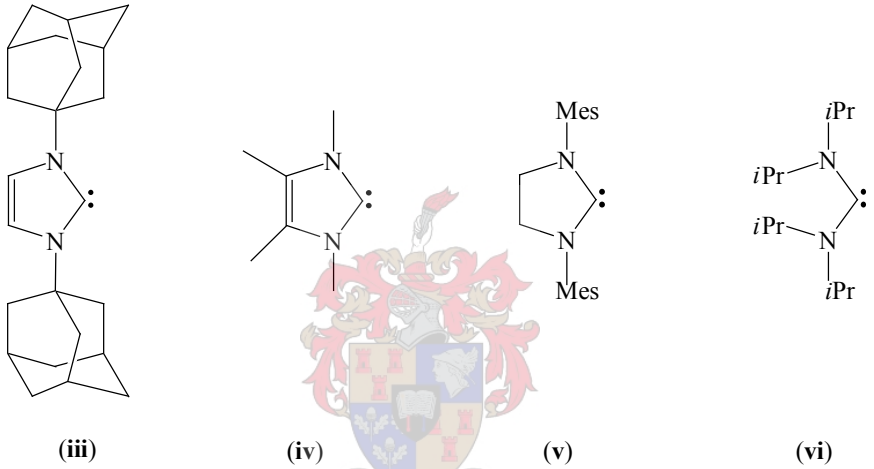

(iii) **(iv)** **(v)** **(vi)**

Scheme 1.3

Carbene complexes of nickel, palladium and platinum

In general the four-coordinated heterocyclic carbene complexes of nickel, palladium and platinum have a square planar geometry that is slightly distorted. In 1973 the group of Lappert described the carbene complexes of palladium and platinum of the type $MX_2(NHC)PR_3$ (M = Pd or Pt; X = Br or Cl, PR_3 = PEt_3, $P(n\text{-}Bu)_3$ or PMe_2Ph).[20] These complexes are produced from the reaction of the halogen-bridged dimers, $[M(\mu\text{-}X)(X)PR_3]_2$ with electron-rich olefins. The electron-rich olefins are

[17] T. Weskamp, V.P.W. Böhm, W.A. Herrmann, *J. Organomet. Chem.*, 2000, **600**, 12.

[18] W.A. Herrmann, G. Gerstberger, M. Spiegler, *Organometallics*, 1997, **16**, 2209.

[19] http://nobelprize.org/chemistry/laureates/2005/index.html (with links to the Curriculum Vitae of the prize winners as well as their publications lists).

[20] D.J. Cardin, B. Centinkaya, E. Centinkaya. M.F. Lappert, *J. Chem. Soc., Dalton Trans.*, 1973 514.

cleaved at elevated temperatures and the formed carbene ligands react with the metal dimers by cleaving their halogen bridges. A year later they reported more electron-rich olefin-derived carbene complexes of Pd(II) and Pt(II) as well as of Ni(II).[21] The precursor olefins react with the metal phosphine precursors and the resultant carbene ligands substitute a phosphine ligand on the metal complex. The ease of the phosphine displacement decreases as follows: Ni > Pd ≈ Pt. Ni(0) carbene complexes of the type $Ni(CO)_3(NHC)$, synthesized by the reaction of electron-rich olefins with $Ni(CO)_4$, were reported later by Lappert and Pye.[22] These zerovalent complexes were further reacted with another mole equivalent of carbene ligand or PPh_3 followed by the reaction with I_2 to form the Ni(II) carbene complexes $NiI_2(NHC)_2$ and $NiI_2(NHC)(PPh_3)$ respectively.

Synthetic routes to prepare carbene complexes have since been expanded to include the coordination of free carbenes to transition metal precursors as well as oxidative addition pathways. The free carbenes can be prepared separately or *in situ* before they react with the metal precursor. Palladium carbene complexes are prepared by the typical reaction shown in equation 1. The acetate acts as deprotonating agent during this reaction. It is noteworthy that the *cis* isomer has been isolated as the more stable isomer.[1,23] Lui *et al.* have observed the isomerisation of *trans*-dichlorobis(1,3-di(2-propene)-2,3,4,5-tetrahydro-1*H*-imidazol-2-ylidene)palladium(II), prepared by the transfer of the carbene from tungsten to the palladium, to yield the *cis* isomer.[24] The reaction of two mole equivalents of 1,3,4-trimethyl-4,5-dihydro-1*H*-1,2,4-triazol-5-ylidene with $Pd(OAc)_2$ in the presence of NaI yields the *trans*-bis(carbene) complex of palladium. The sterically demanding nature of the permethylated ligand has been proposed as reason for the isolation of the *trans*-isomer,[25] but a factor, like a difference in electronic properties of the two carbene ligands, may determine the formation of these isomers, as the steric demand of the 1,3,4-trimethyl-4,5-dihydro-1*H*-1,2,4-triazol-5-ylidene and the 1,3-dimethyl-2,3-dihydro-1*H*-imidazol-2-ylidene (equation 1) on the metal center is expected to be the same. Herrmann and co-workers[26] reported the preparation of the *cis*-diiodobis(1,4-dimethyl-4,5-dihydro-1*H*-1,2,4-triazol-5-ylidene)palladium(II) complex, *via* the same reaction shown in equation 1. This compound isomerises to the more stable *trans* isomer in the

[21] B. Centinkaya, P. Dixneuf, M.F. Lappert, *J. Chem. Soc., Dalton Trans.*, 1974, 1827.

[22] M.F. Lappert, P.L. Pye, *J. Chem. Soc., Dalton Trans.*, 1977, 2172.

[23] W.A. Herrmann, M. Elison, J. Fischer, C. Köcher, G.R.J. Artus, *Angew. Chem., Int. Ed., Engl.*, 1995, **34**, 2371.

[24] S-T. Liu, T-Y. Hsieh, G-H. Lee, S-M. Peng, *Organometallics*, 1998, **17**, 993.

[25] C. Buron, L. Stelzig, O. Guerret, H. Gornitzka, V. Romaneko, G. Bertrand, *J. Organomet. Chem.*, 2002, **664**, 70.

[26] W.A. Herrmann, J. Fischer, K. Öfele, G.R.J. Artus, *J. Organomet. Chem.*, 1997, **530**, 259.

presence of water. This is the opposite to what is observed when 1,3-di(2-propene)-2,3,4,5-tetrahydro-1*H*-imidazol-2-ylidene is the ligand, as indicated above.

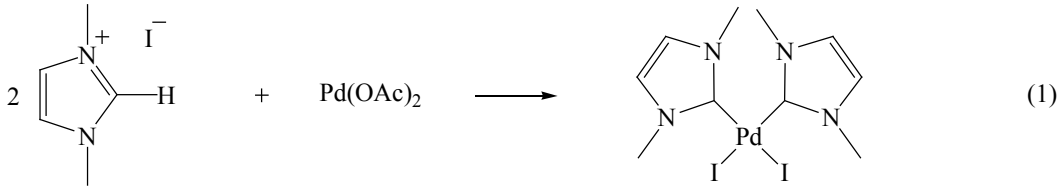

(1)

Steric effects become important when the *N*-substituents of imidazolium carbene ligands are cyclohexanol[27] or pyridyl and mesityl[28] or 1-phenylethyl,[29] as only the *trans*-bis(carbene) complexes of palladium(II) are formed. Reaction of imidazolium salts (with *N*-substituents such as cyclohexyl[18] or methyl and butyl[30]) with $Ni(OAc)_2$ also give the *trans*-bis(carbene) complexes of nickel(II).

Transfer of the carbene ligands [3-methyl-1-(methylacetyl)-2,3-dihydro-1*H*-imidazol-2-ylidene or 3-methyl-1-picolyl-2,3-dihydro-1*H*-imidazol-2-ylidene] from a Ag(I) carbene precursor to $PdCl_2(MeCN)_2$ yields the *cis*-bis(carbene) complexes of palladium, while the transfer of the carbenes to PdMeCl(COD) results in the formation of the *trans*-bis(carbene) complex of palladium with the Me and Cl *trans* towards each other.[31] The formation of the chloride-bridged dimer complexes $[(NHC)_2PdX]_2$ (X = Cl and I) are also observed during some of these reactions.[24,29,32] Bis(carbene) complexes of the type $[M\{bis(carbene)\}X_2]$ (M = Ni or Pd; X = Cl, Br, I, Me, or PMe_3) with the two carbene ligands connected by a $(CH_2)_n$ linker (n = 1, 2), also have seen the light.[33,34,35] In one instance where n = 1, the dinuclear, monodentately-coordinated carbene complex

[27] H. Glas, E. Herdweck, M. Spiegler, A-K. Pleier, W.R. Thiel, *J. Organomet. Chem.*, 2001, **626**, 100.

[28] S. Gründemann, M. Albrecht, A. Kovacevic, J.W. Faller, R.H. Crabtree, *J. Chem. Soc., Dalton Trans.*, 2002, 2163.

[29] W.A. Herrmann, V.P.W. Böhm, C.W.K. Gstöttmayr, M. Grosche, C-P. Reisinger, T. Weskamp, *J. Organomet. Chem.*, 2001, **617 - 618**, 616.

[30] D.S. McGuinness, W. Mueller, P. Wasserscheid, K.J. Cavell, B.W. Skelton, A.H. White, U. Englert, *Organometallics*, 2002, **21**, 175.

[31] D.S. McGuiness, K.J. Cavell, *Organometallics*, 2000, **19**, 741.

[32] W.A. Herrmann, L.J. Gooβen, M. Spiegler, *J. Organomet. Chem.*, 1997, **547**, 357.

[33] R.E. Douthwaite, D. Haüssinger, M.L.H. Green, P.J. Silcock, P.T. Gomes, A.M. Martins, A.A. Danopoulos, *Organometallics*, 1999, **18**, 4584.

[34] R.E. Douthwaite, M.L.H. Green, P.J. Silcock, P.T. Gomes, *Organometallics*, 2001, **20**, 2611.

of nickel has been isolated.[34] Bis(carbenes) with other linkers (like aromatic bridges) have been coordinated to palladium and nickel [36,37,38] and a tris(carbene) complex of nickel is also known.[39]

Stone and co-workers were first to exploit the ability of a metal to undergo oxidative addition to prepare carbene complexes. They describe the oxidative addition of *N*-methyl-2-chloro-5-methylthiazole tetrafluoroborate to the zerovalent $M(PR_3)_4$ (M = Ni, Pd or Pt; PR_3 = PEt_3, $PMePh_2$ or PPh_3) to generate the corresponding M(II) carbene complexes.[40] Several carbene complexes of palladium and platinum have since been synthesized using this method.[28,41,42,43,44] These include a hydrido-Pt carbene complex, *cis*-$[Pt(H)(NHC)(PPh_3)_2]BF_4$ (NHC = 1,3-dimethyl-2,3-dihydro-1*H*-imidazol-2-ylidene), isolated from the oxidative addition of the 1,3-dimethylidazolium cation to $Pt(PPh_3)_4$.[41,44] This reaction yields only 15% of the oxidative product relative to the unreacted starting materials.[44] The low yield of the oxidative product is not a result of a high barrier to oxidative addition but, rather, a representation of the equilibrium concentration of the reactants and the product. The yield of the hydrido-Pt carbene complex is improved to 63% when $Pt(PPh_3)_2$ serves as the metal precursor.[41] The oxidative substitution pathway will be employed as part of this research to prepare new NHC and rNHC carbene complexes of nickel, palladium and platinum.

Heterocyclic carbene complexes of palladium and platinum have also been prepared by the cyclization reaction of electrophilic metal-coordinated isocyanide ligands.[45,46,47] Equations 2 and 3 illustrates two such examples. The reaction of palladium or platinum isocyanide complexes with aziridine, thiirine or oxirane produces imidazolium, thiazolium or oxazolium carbene complexes of

---

[35] W.A. Herrmann, J. Schwarz, M.G. Gardiner, M. Spiegler, *J. Organomet. Chem.*, 1999, **575**, 80.

[36] W.A. Herrmann, *Angew. Chem., Int. Ed., Engl.*, 2002, **41**, 1290.

[37] M.V. Barker, B.W. Skelton, A.H. White, C.C. Williams, *J. Chem. Soc., Dalton Trans.*, 2001, 111.

[38] D.S. Clyne, J. Jin, E. Genest, J.C. Gallucci, T.V. RajanBabu, *Org. Lett.*, 2000, **2**, 1125.

[39] X. Hu, I. Castro-Rodrigues, K. Meyer, *Chem. Commun.*, 2004, 2164.

[40] P.J. Fraser, W.R. Roper, F.G.A. Stone, *J. Chem. Soc., Dalton Trans.*, 1974, 103.

[41] D.S. McGuinness, K.J. Cavell, B.F. Yates, B.W. Skelton, A.H. White, *J. Am. Chem. Soc.*, 2001, **123**, 8317.

[42] A. Fürstner, G. Seidel, D. Kremzow, C.W. Lehmann, *Organometallics*, 2003, **22**, 907.

[43] J. Schütz, E. Herdweck, W.A. Herrmann, *Organometallics*, 2004, **23**, 6084.

[44] D.S. McGuinness, K.J. Cavell, B.F. Yates, *Chem. Commun.*, 2001, 355.

[45] R. Bertini, M. Mozzon, R.A. Michelin, *Inorg. Chem.*, 1988, **27**, 2809.

[46] R.A. Michelin, L. Zanotto, D. Braga, P. Sabatino, R.J. Angelici, *Inorg. Chem.*, 1988, **27**, 85.

[47] R.A. Michelin, L. Zanotto, D. Braga, P. Sabatino, R.J. Angelici, *Inorg. Chem.*, 1988, **27**, 93.

palladium or platinum (equation 2).[45] The reaction of similar isocyanide complexes with 2-bromo-ethyl-ammonium bromide or 2-bromomethanol in the presence of a base also affords imidazolium or oxazolium carbene complexes of platinum or palladium.[46,47] Functionalised isocyanide ligands on a metal center can be intramolecularly cyclisised to furnish heterocyclic carbene complexes of platinum.[48,49]

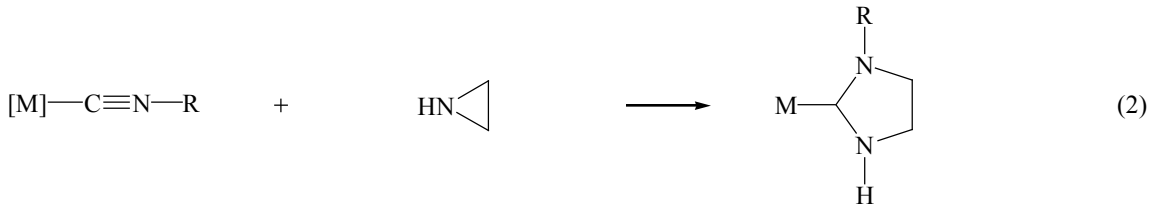

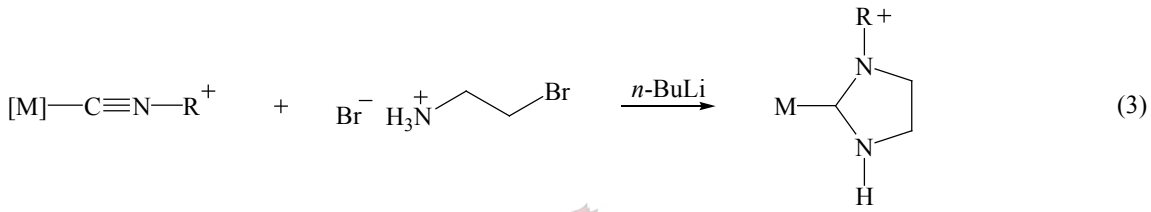

Equation 2: [M] = *cis*-$Cl_2(PPh_3)M$ (M = Pd or Pt); R = *tert*-Bu or *p*-$MeOC_6H_4$

Equation 3: [M] = *trans*-$[(PPh_3)_2MBr]BF_4$ (M = Pd or Pt); R = *tert*-Bu or *p*-$MeOC_6H_4$

Several heterocyclic carbene complexes of nickel(0), palladium(0) and platinum(0) are known. The reaction of $M(COD)_2$ (M = Ni or Pt) with two mole equivalents of 1,3-dimesityl-2,3-dihydro-1*H*-imidazol-2-ylidene yields the corresponding zerovalent bis(carbene) complex of nickel or platinum.[50] Co-condensation of nickel, palladium, or platinum vapor with an excess of 1,3-di-*tert*-butyl-2,3-dihydro-1*H*-imidazol-2-ylidene results in the formation of M(1,3-di-*tert*-butyl-2,3-dihydro-1*H*-imidazol-2-ylidene)$_2$ [M = Ni(0), Pd(0) or Pt(0)] in low yields (10 – 32%).[51,52] In addition to the nickel(0) carbene complexes $[Ni(CO)_3(NHC)]$ mentioned above, two carbene complexes $[Ni(CO)_2(NHC)]$ (NHC = 1,3-di-*tert*-butyl-2,3-dihydro-1*H*-imidazol-2-ylidene or 1,3-

[48] R.A. Michelin, G. Facchin, D. Braga, P. Sabatino, *Organometallics*, 1986, **5**, 2265.

[49] M. Basato, F. Benetollo, G. Facchin, R.A. Mechelin, M. Mozzon, S. Pugliese, P. Sgarbossa, S.M. Sbovata, A. Tassan, *J. Organomet. Chem.*, 2004, **689**, 454.

[50] A.J. Arduengo, III, S.F. Gamper, J.C. Calabrese, F. Davidson, *J. Am. Chem. Soc.*, 1994, **116**, 4391.

[51] P.L. Arnold, G.N. Cloke, T. Geldbach, P.B. Hitchcock, *Organometallics*, 1999, **18**, 3228.

[52] S. Caddick, F.G.N. Cloke, P.B. Hitchcock, A.K.de K. Lewis, *Angew. Chem., Int. Ed., Engl.*, 2004, **43**, 5824.

diadamantyl-2,3-dihydro-1*H*-imidazol-2-ylidene) have been described in literature as rare three-coordinate nickel carbonyl systems.[53]

Catalysis: C-C coupling reactions

Van Leeuwen called palladium catalysed C-C coupling reactions the new workhorse of organic synthesis.[54] These reactions include allylic alkylation, the Heck reaction, the cross coupling reaction, heteroatom-carbon bond formation and the Suzuki reaction. Allylic alkylation is, as the name states, the coupling of an allyl halide with a nucleophillic alkyl (reaction 1, Scheme 1.4). The Heck reaction involves the coupling of aryl halides with alkenes in the presence of a base (reaction 2, Scheme 1.4). During a cross-coupling reaction an aryl halide is coupled to a Grignard or lithium alkyl reagent (reaction 3, Scheme 1.4). Heteroatom-carbon bond formation includes the formation of carbon-to-nitrogen, carbon-to-oxygen and carbon-to-sulfur bonds as a result of the coupling of the corresponding organic substrates. The carbon-to-nitrogen bond formation is illustrated by reaction 4 (Scheme 1.4). The coupling of aryl halides with organometallic derivatives of boron or tin is called Suzuki (reaction 5, Scheme 1.4) and Stille[55] coupling reactions respectively. One equivalent of salt is formed with the organic products during the allylic alkylation, Heck and heteroatom-carbon bond formation reactions. The Suzuki-Miyaura (SM) and Mizoroki-Heck reaction (MH) will be described in this dissertation.

Pectora roborant cultus recti

Books[54,56] and reviews[57,58,59] as well as a vast amount of publications[60,61] are available today, covering various aspects of palladium catalyzed C-C coupling reactions including catalyst pre-cursors and their properties, mechanistic considerations, theoretical studies and applications of these

[53] R. Dorta, E.D. Stevens, C.D. Hoff, S.P. Nolan, *J. Am. Chem. Soc.*, 2003, **125**, 10490.

[54] P.W.N.M. van Leeuwen, *Homogeneous Catalysis, Understanding the Art*, Kluwer Academic Publishers, Dordrecht, 2004, p.271.

[55] J. Stille, *Angew. Chem., Int. Ed., Engl.*, 1998, **25**, 508.

[56] A. Yamamoto in: H. Kurosawa, A. Yamamoto (Eds), *Fundamentals of Molecular Catalysis*, Vol. 3, Elsevier, Amsterdam, 2003, p 1.

[57] U. Christmann, R. Vilar, *Angew. Chem., Int. Ed., Engl.*, 2005, **44**, 366.

[58] A.F. Littke, G.C. Fu, *Angew. Chem., Int. Ed., Engl.*, 2002, **41**, 4176.

[59] N.J. Whitcombe, K.K. Hii, S.E. Gibson, *Tetrahedron*, 2001, **57**, 7449.

[60] B-L. Lin, L. Liu, Y. Fu, S-W. Luo, Q. Chen, Q-X, Guo, *Organometallics*, 2004, **23**, 2114.

[61] K. Albert, P. Gisdakis, N. Rösch, *Organometallics*, 1998, **17**, 1608.

coupling reactions. Nickel complexes, as cheaper alternatives to palladium catalysts, have also been investigated as catalyst precursors despite the dominance of the palladium catalyst precursors.[59,60,62] The yields of the organic coupling products, however, are generally poor when nickel complexes are used as pre-catalysts. Nickel and palladium have been used in combination as a bimetallic catalyst system in the coupling of chloroarenes and olefins.[63] Platinum pre-catalysts have been used in the Heck reaction but are very ineffective and these expensive catalyst studies are not worth continuing.[64]

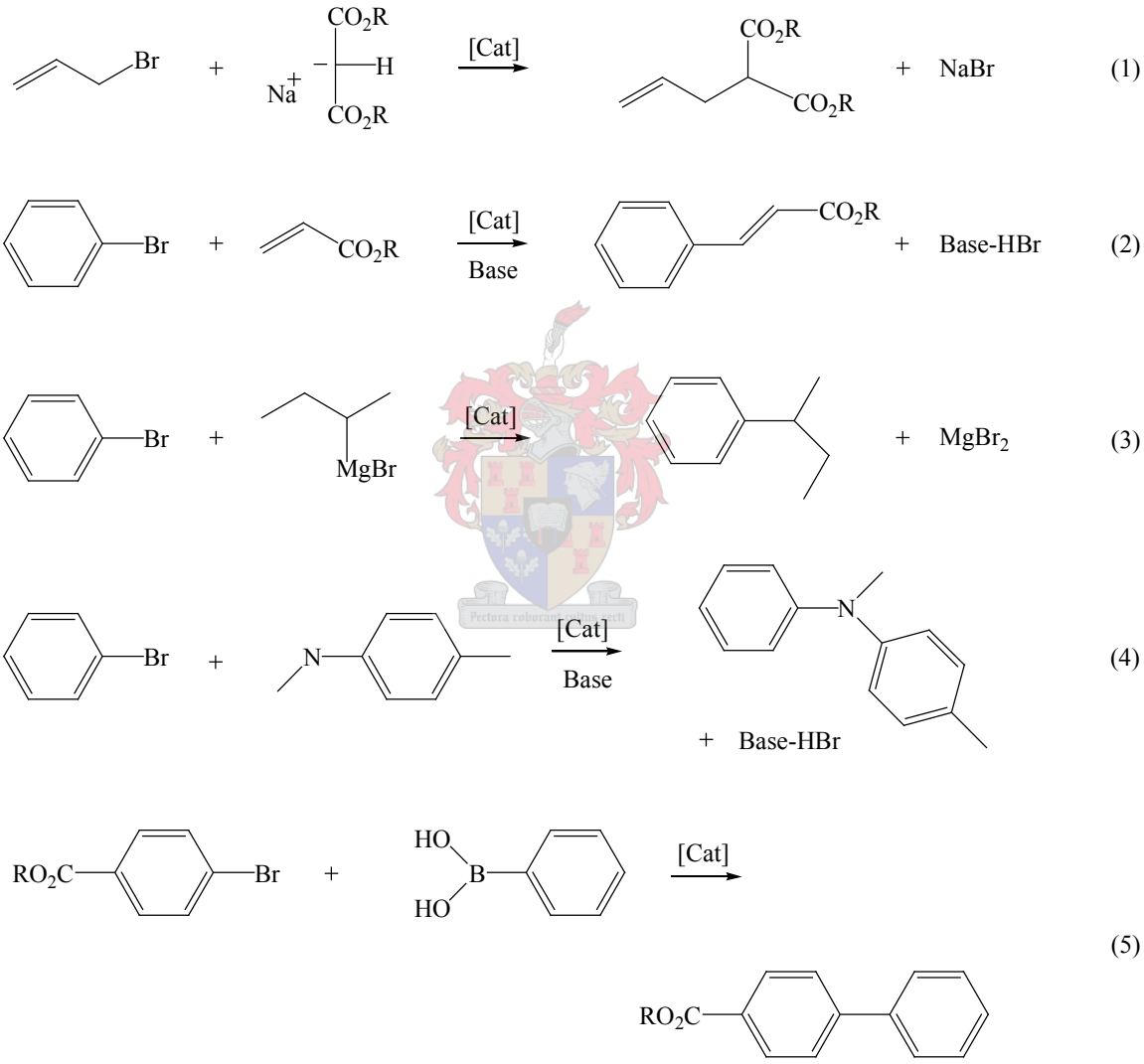

Scheme 1.4 {[Cat] = Pd(II) or Pd(0) pre-catalyst; R = organic moiety}

[62] K-C. Kong, C-H. Cheng, *Organometallics*, 1992, **11**, 1972 and references therein.

[63] J.J. Bozell, C.E. Vogt, *J. Am. Chem. Soc.*, 1988, **110**, 2655.

[64] I.P. Beletskaya, A.V. Cheprakov, *Chem. Rev.*, 2000, **100**, 3009.

Until recently cross-coupling reactions have been limited to aryl bromides and aryl iodides as substrates.[57,58] Despite their lower costs and the wider variety of available compounds when compared to the aryl bromides and aryl iodides, aryl chlorides are inactive under the conditions for the coupling of bromides and iodides.[58] This low reactivity of aryl chlorides can be attributed to the strength of the C-Cl bond (Ph-X: Cl = 96 kcal/mol ; Br: 81 kcal/mol ; I: 65 kcal/mol) that would make these substrates resistant to oxidative addition to Pd(0) catalysts. The development of palladium complexes, with electron-rich and bulky ligands (phosphines and carbenes), as catalyst precursors has been important as it may facilitate the oxidative addition of aryl chlorides to the active Pd(0) center. Phosphines like $P(^tBu)_3$,[65,66] and biphenyl-2-yl-di-*tert*-butyl-phosphine,[67] as well as imidazolium-derived carbenes (typical NHC's)[29,36,68,69] have been used as ligands to prepare palladium pre-catalysts. The ability of these ligands to stabilise monoligated palladium species results in enhanced reactivity and the steric bulk of the ligands are very important in the stabilisation of the unsaturated [PdL] species, needed to start the catalytic cycle.

Industrial applications

Some of the coupling reactions above are being applied very successfully in industry today.[54] The synthesis of the drug Merck L-699,392, used in the treatment of asthma and related diseases, requires the application of the Heck reaction twice. The cross-coupling reaction is implemented in the preparation of the non-steroidal anti-inflammatory drug, Diflunisal. Interestingly, it took Zambon 10 years to optimize this cross-coupling reaction, while today a few hundred tons of this drug are produced worldwide per year.[54] The Suzuki reaction is an important step in the synthesis of the anti-hypertensive drug, Losartan. These three drugs are shown in Scheme 1.5.

[65] A.F. Littke, C. Dai, G.C. Fu, *J. Am. Chem. Soc.*, 2000, **122**, 4020.

[66] I.D. Hills, G.C. Fu, *J. Am. Chem. Soc.*, 2004, **126**, 13178.

[67] J.P. Wolfe, R.A. Singer, B.H. Yang, S.L. Buchwald, *J. Am. Chem. Soc.*, 1999, **121**, 9550.

[68] J. Huang, S.P. Nolan, *J. Am. Chem. Soc.*, 1999, **121**, 9889.

[69] A.C. Frisch, A. Zapf, O. Briel, B. Kayser, N. Shaikh, M. Beller, *J. Mol. Cat. A: Chem.*, 2004, **214**, 231.

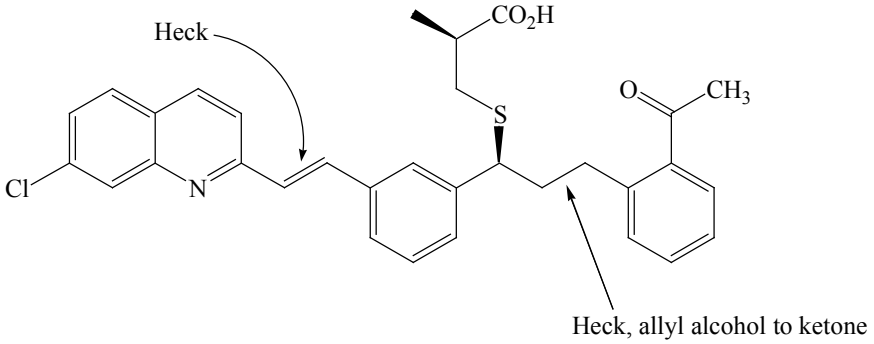

Merk L-699,392

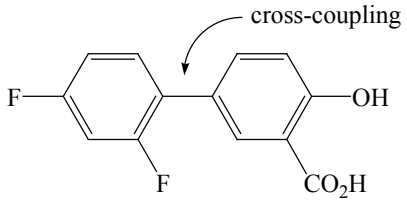

Diflunisal

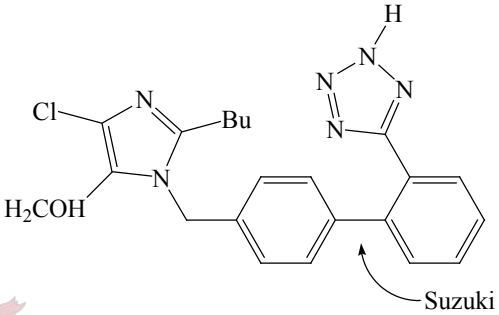

Losartan

Scheme 1.5

Carbene complexes of rhodium

Lappert and co-workers[70] have described synthetic routes to electron-rich olefin-derived square planar mono(carbene) complexes of rhodium(I). These complexes are prepared by ligand (PPh_3) displacement from $Rh(CO)Cl(PPh_3)$ or the splitting of the $(\mu\text{-}Cl)_2$-bridge of $[Rh(Cl)COD]_2$ by the carbene ligand. Other carbene complexes can be prepared by the substitution of one more ligand from the metal. The COD ligand in *cis*-[Rh(Cl)COD(NHC)] (NHC = 1,3-dimethyl-2,3,4,5-tetrahydro-1*H*-imidazol-2-ylidene), for example was substituted by two CO ligands to form *cis*-$[Rh(Cl)(CO)_2(NHC)]$. A dinuclear, monodentately-coordinated carbene complex of rhodium is prepared by the reaction of a $(CH_2)_2$-bridged electron-rich olefin with $[Rh(Cl)COD]_2$.[71] This type of complex can also be prepared by the reaction of free carbenes, prepared separately or *in situ*, with the starting materials like $[Rh(Cl)COD]_2$ or $[Rh(Cl)(CO)_2]_2$.[1,13,17] Potassium *tert*-butoxide or sodium hydride can be used as external bases in the deprotonation of the imidazolium salts.

[70] M.J. Doyle, M.F. Lappert, P.L. Pye, P. Terreros, *J. Chem. Soc., Dalton Trans.*, 1984, 2355.

[71] B. Cetinkaya, P.B. Hitchcock, M.F. Lappert, D.B. Shaw, K. Spyropoulos, N.J.W. Warhurst, *J. Organomet. Chem.*, 1993, **459**, 311.

$[Rh(OAc)COD]_2$ is conveniently reacted with imidazolium salts to prepare mono(carbene) complexes [Rh(Cl)COD(NHC)]. The acetate acts as the base for the deprotonation of the imidazolium salt.[1] Chelation of bis(carbene) ligands and the preparation of dinuclear, monodentately-coordinated carbene complexes of rhodium have been described by Matta *et al.*[72] and Herrmann *et al.*[1] A wide variety of carbene ligands including carbenes with chiral substituents,[73,74,75] functionalised carbenes,[32,76,77] acyclic carbenes like (aryl)(phosphino)carbene,[78] (aryl)(amino)carbene[79] and other acyclic carbenes[80,81] have been coordinated to rhodium. Mixed carbene-thione complexes of rhodium are also known.[82]

During the catalytic C-H activation and functionalisation, d^6 and d^8 14-electron metal complexes are of particular importance.[83] In the case of rhodium, the rhodium(III) complexes that are considered to be intermediates in the rhodium-catalyzed funtionalization of C-H bonds, are not easily isolated and characterised. Rhodium(III) complexes that form as a result of C-H activation have been isolated and characterised by NMR spectroscopy and single crystal structure dermination.[83,84] The rhodium(III) complex (**vii**) (Scheme 1.6) is produced from the reaction of $[Rh(Cl)(COE)_2]_2$ (COE = cyclooctene) and four mole equivalents of 1,3-bis(2,4,6-trimethylphenyl)-2,3-dihydro-1*H*-imidazol-2-ylidene (IMes).[84] The C-H bond of an aryl methyl group has been activated. As mentioned above the reaction of $[Rh(Cl)COD]_2$ with the carbene ligand affords the mono(carbene) complex. COE is a weaker coordinating ligand than COD and the relative ease of COE dissociation may be crucial in

Pectora roborant cultus recti

[72] J.A. Mata, A.R. Chianese, J.R. Miecznikowski, M. Poyatos, E. Peris, J.W. Faller, R.H. Crabtree, *Organometallics*, 2004, **23**, 1253.

[73] W.A. Herrmann, L.J. Gooβen, C. Köcher, G.R.J. Artus, *Angew. Chem., Int. Ed., Engl.*, 1996, **35**, 2805.

[74] M. Alcarazo, S.J. Roseblade, E. Alonso, R. Fernández, E. Alvarez, F.J. Lahoz, J.M. Lassaletta, *J. Am. Chem. Soc.*, 2004, **126**, 13242.

[75] H. Seo, B.Y. Kim, J.H. Lee, H-J. Park, S.U. Son, Y.K. Chung, *Organometallics*, 2003, **22**, 4783.

[76] W.A. Herrmann, C. Köcher, L.J. Gooβen, G.R.J. Artus, *Chem. Eur. J.*, 1996, **2**, 1627.

[77] W.A. Herrmann, L.J. Gooβen, M. Spiegler, *Organometallics*, 1998, **17**, 2162.

[78] E. Despagnet, K. Miqueu, H. Gornitzka, P.W. Dyer, D. Bourissou, G. Bertrand, *J. Am. Chem. Soc.*, 2002, **124**, 11834.

[79] X. Cattoën, H. Gornitzka, D. Bourissou, G. Bertrand, *J. Am. Chem. Soc.*, 2004, **126**, 1342.

[80] K. Denk, P. Sirsch, W.A. Herrmann, *J. Organomet. Chem.*, 2002, **649**, 219.

[81] V. Lavallo, J. Mafhouz, Y. Canac, B. Donnadieu, W.A. Schoeller, G. Bertrand, *J. Am. Chem. Soc.*, 2004, **126**, 8670.

[82] A. Neveling, G.R. Julius, S. Cronje, C. Esterhuysen, H.G. Raubenheimer, *Dalton Trans.*, 2005, 181.

[83] R. Dorta, E.D. Stevens, S.P. Nolan, *J. Am. Chem. Soc.*, 2004, **126**, 5054.

[84] J. Huang, E.D. Stevens, S.P. Nolan, *Organometallics*, 2000, **19**, 1194.

the formation of the bis(carbene) complex (**vii**).[84] The reaction of complex (**vii**) with H_2 gives the dihydride complex (**viii**) (Scheme 1.6)

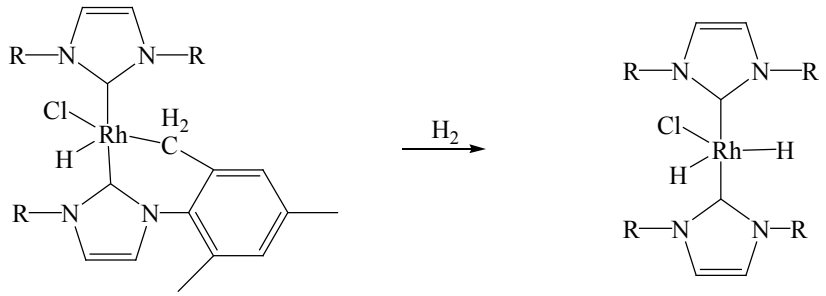

(vii) **(viii)**

Scheme 1.6 (R = 2,4,6-trimethylphenyl)

In a reaction of $[Rh(Cl)(COE)_2]_2$ with 1,3-di-*tert*-butyl-2,3-dihydro-1*H*-imidazol-2-ylidene (1 : 4.16) in hexane, the group of Nolan have also described the C-H activation in one methyl group of the *tert*-butyl substituent.[83] Complex (**ix**) in Scheme 1.7, shows the cyclometalated *tert*-butyl ligand with agostic interaction of a methyl proton of a *tert*-butyl group attached the other carbene ligand. The loss of H_2 produces a doubly cyclometalated complex (**x**) (Scheme 1.7). Complex (**x**) can also be obtained directly when the reaction is carried out in benzene instead of hexane.

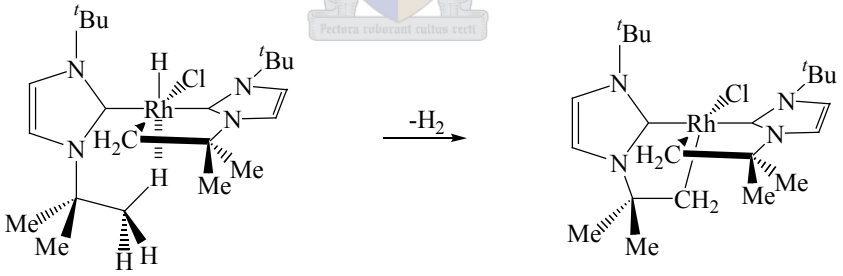

(ix) **(x)**

Scheme 1.7

The reaction of $[Rh(Cl)(COE)_2]_2$ with 1,3-di-*tert*-butyl-2,3-dihydro-1*H*-imidazol-2-ylidene (1 : 4.16) carried out in pentane yields the mixed dimer $[Rh(Cl)(COE)(NHC)]_2$. Addition of benzene to the reaction mixture produces complex (**x**) (Scheme 1.7), while the isolated $[Rh(Cl)(COE)(NHC)]_2$ is stable in benzene solution without additional free carbene. These experiments show that the complex formation is solvent dependent and that the dimer $[Rh(Cl)(COE)(NHC)]_2$ is a precursor for complexes (**ix**) and (**x**) with (**ix**) as the intermediate (Scheme 1.7). Furthermore, it demonstrates that

a single electron-donating carbene ligand is not sufficient to effect the intermolecular C-H activation. The ability of the rhodium complexes to invoke C-H activation could play an important role when they are used as pre-catalysts. The preparation of new carbene complexes of rhodium should allow the exploration of the catalytic properties of these compounds in reactions, such as hydroformylation.

Fischer-type carbene complexes

Fischer carbene complexes of group 6 transition metals are generally prepared by the reaction of $M(CO)_6$ (M = Cr, Mo or W) with RLi (R = Me, Ph, other organic group) to produce the carbene lithium salts such as (**xi**) (Scheme 1.8), which are usually alkylated with $[Me_3O][BF_4]$ or CF_3SO_3Me to yield neutral methoxy carbene complexes (**xii**).[6,85] Aminolysis with amines such as dimethyl amine leads to the conversion of the methoxy carbene complexes to the amino carbene complexes (**xiii**) (Scheme 1.8).[86,87]

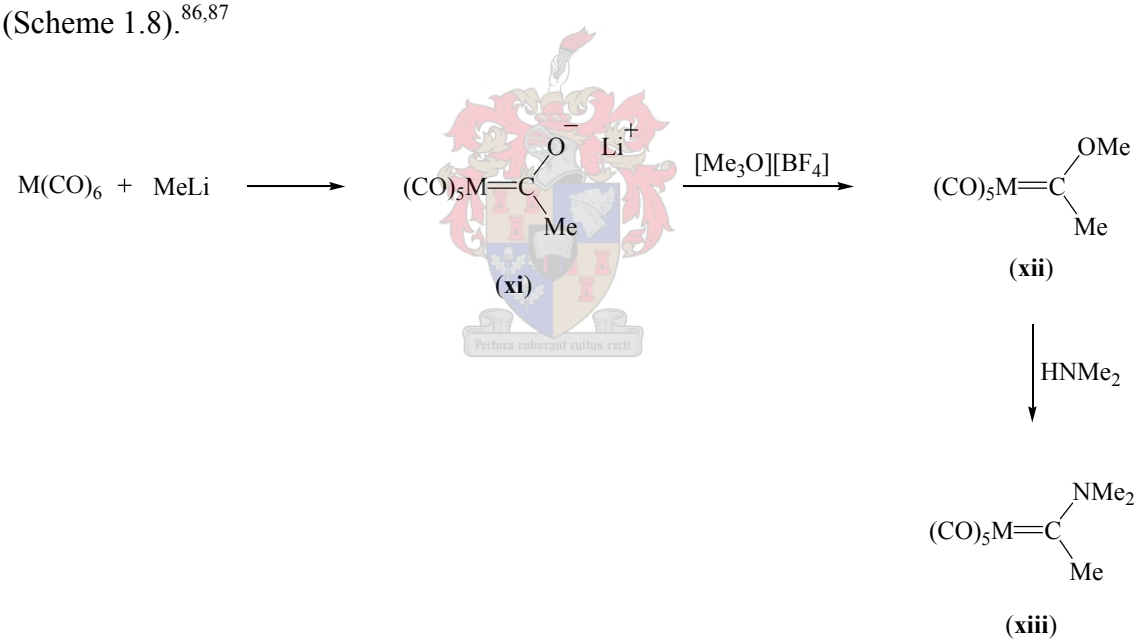

Scheme 1.8 (M = Cr, Mo or W)

Casey and co-workers have extensively investigated the acidity of the protons attached to the carbon α to the carbene carbon and the reactions of the carbene anions, $[(CO)_5M{=}C(OMe)CH_2]^-$ (M = Cr,

[85] F. Kreissl, in: W. A. Herrmann (Ed.), *Synthetic methods of Organometallic and Inorganic Chemistry, Volume 7, Transition Metals Part 1*, Georg Thieme Verlag, Stuttgart, 1997, p. 127.

[86] E.O. Fischer, M. Leupold, *Chem. Ber.*, 1972, **105**, 599.

[87] F.J. Brown, *Prog. Inorg. Chem.*, 1980, **27**, 1.

Mo or W), with carbon nucleophiles. These anions are produced by the deprotonation of the Fischer carbene $(CO)_5Cr{=}C(OMe)CH_3$ with a base such as *n*-BuLi. $(CO)_5Cr{=}C(OMe)CH_3$ has a p*K*a of ca. 8 in water.[88] The $[(CO)_5Cr{=}C(OMe)CH_2]M'$ [M' = Li^+ or $(PPh_3)_2N^+$] salts have been described.[89] The $[(CO)_5Cr{=}C(OMe)CH_2]^-$ anion reacts with epoxides (reaction 1, Scheme 1.8),[90,91,92] α-bromo esters[90] and aldehydes[88] to produce new Fischer carbene complexes. Bimetallic complexes are produced when the Fischer carbene anion is reacted with metal coordinated olefins (reaction 2, Scheme 1.9).[93] Reaction of the $[(CO)_5M{=}C(OEt)CH_2]^-$ anion (M = Cr or W) with $ClPPh_2$[94] and 2-chloro-1,3-dithiane[95] to produce $(CO)_5M{=}C(OEt)CH_2PPh_2$ and $(CO)_5M{=}C(OEt)CH_2\overline{CHS(CH_2)_3S}$ respectively, has also been carried out successfully.

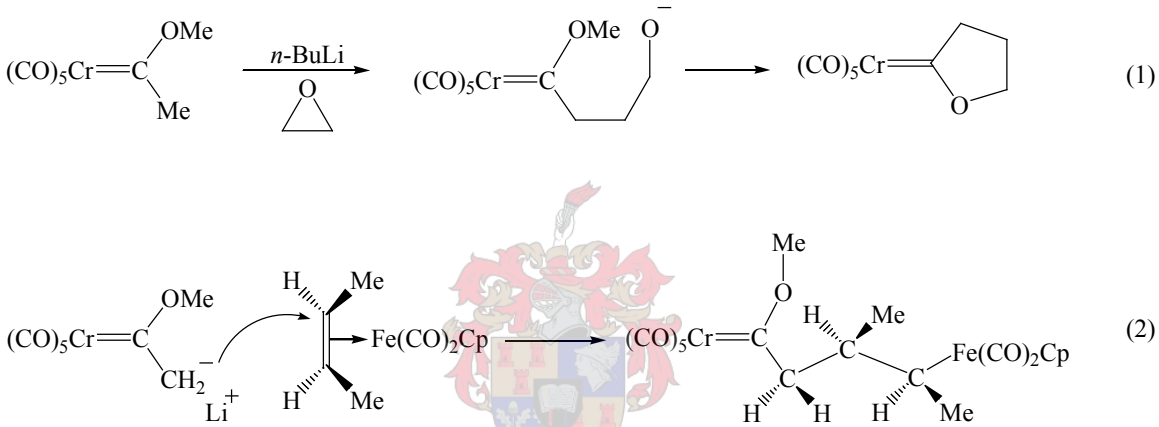

Scheme 1.9

Recently members of our group described the utilization of these *β*-deprotonated carbene complex anions as anionic vinyl synthons producing bimetallic gold(I) vinyl ether-group 6 metal complexes upon reaction with the electrophile Ph_3PAu^+ (Scheme 1.10).[96] These reactions show that the

[88] C.P. Casey, W.R. Burnsvold, *Inorg. Chem.*, 1977, **16**, 391.

[89] C.P. Casey, R.L. Anderson, *J. Am. Chem. Soc.*, 1974, **94**, 1230.

[90] C.P. Casey, R.L. Anderson, *J. Organomet. Chem.*, 1974, **73**, C28.

[91] C.P. Casey, W.R. Burnsvold, *J. Organomet. Chem.*, 1975, **102**, 175.

[92] C.P. Casey, W.R. Burnsvold, *J. Organomet. Chem.*, 1976, **118**, 309.

[93] C. Kelly, M.R. Terry, A.W. Kaplan, G.L. Geoffroy, N. Lugan, R. Mathieu, B.S. Haggerty, A.L. Rheingold, *Inorg. Chim. Acta*, 1992, **198 - 200**, 601.

[94] H.G. Raubenheimer, G.J. Kruger, H.W. Viljoen, S. Lotz, *J. Organomet. Chem.*, 1986, **314**, 281.

[95] H.G. Raubenheimer, G.J. Kruger, H.W. Viljoen, *J. Organomet. Chem.*, 1987, **319**, 361.

[96] H.G. Raubenheimer, M.W. Esterhuysen, A. Timoshkin, Y. Chen, G. Frenking, *Organometallics*, 2002, **21**, 3173.

reaction does not necessarily take place at the deprotonated carbon atom. A Fischer-type anionic carbene complex of a different kind, $[(CO)_5M{=}C(L)O]^-$ (M = Cr or W; L = 4-methylthiazolyl), that contains the two hard donor atoms (N and O) coordinates as an anionic bidentate ligand to other metals such as Cr(III), Fe(III), Co(III) to form polynuclear complexes that could be called 'complexes of complexes'.[97] As part of this current research, the reactivity of the $[(CO)_5Cr{=}C(OMe)CH_2]^-$ anion will be exploited to introduce another donor atom (phosphorus) to the carbene complex and this should allow the new carbene complexes (after aminolysis and N-deprotonation) to be used as a bidentate ligand towards other softer metals.

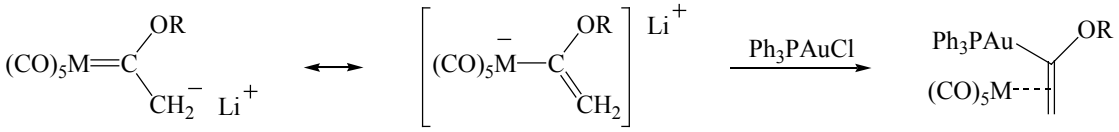

Scheme 1.10 (M = Cr or W, R = Me or Et; M = Mo, R = Me)

Lee and Hu[98] have performed a density functional study of *N*-heterocyclic (saturated and unsaturated imidazolium) and diamino carbene complexes of the type $(CO)_5Cr(L)$ (L = carbene ligand) also comparing carbene ligands with phosphines. The NHC ligand binding energies range from 44 – 54 kcal/mol. The binding energy for the carbene ligand $:C(Me)(NMe_2)$ is 49 kcal/mol and compares well with the values obtained for the NHC ligands while the energy for :C(Me)(OMe) (58 kcal/mol) is higher. The binding energy for the phosphines range from 25 to 37 kcal/mol and is lower than those for the NHC's as well as the Fischer-types carbenes. This study also indicates that the π-back-donation in the NHC-metal bonding is negligible, as was mentioned above (paragraph 2, page 2) It is shown that the $:C(Me)(NMe_2)$ unit is more basic than :C(Me)(OMe) based on lower νCO frequency and smaller force constant for the *trans* C-O bond observed for $:C(Me)(NMe_2)$ compared to :C(Me)(OMe). The nucleophilicity of ligands (the ability of the ligand to induce electron density charge at the metal center) decreases in the order: $:C(N^iPr_2)_2 > :C(NMe_2)_2 >$ $P(cyclohexyl)_3 > C(Me)(NMe_2) > PPh_3 >$ saturated imidazolium-derived carbenes > unsaturated imidazolium-derived carbenes > :C(Me)(OMe) > $P(alkyl)_3 > PH_3 > :C(OH)_2 > PF_3 > :CF_2$. In this thesis (chapter 2) quantum mechanical calculations were used to better our understanding of the

[97] A. Du Toit, M. Du Toit, S. Cronje, H.G. Raubenheimer, C. Esterhuysen, A.M. Crouch, J. An, L. van Niekerk, *Dalton Trans.*, 2004, 1173.

[98] M-T. Lee, C-H. Hu, *Organometallics*, 2004, **23**, 976.

metal carbene bonding of certain carbene complexes. Further, a simple way to evaluate the nucleophilicity (basicity) of carbene ligands is to compare the infrared data of complexes containing carbonyl ligands and this can be used to compare the basicity of carbene ligands in carbonyl-containing compounds.

1.2 Research goals and outline of thesis

The main aim of the research described in this dissertation is the preparation and characterisation of new carbene complexes of various transition metals, some of which could be useful as pre-catalysts in homogeneous catalysis involving unsaturated organic compounds.

A first target was the preparation and comparison of a series of related carbene complexes derived from heterocyclic ring systems: one group of ligands to be used would have a neighboring nitrogen atom such as in well-known NHC ligands but in the second family, called *r*NHC ligands, the heteroatom should be uniquely remote (or removed) from the carbene carbon. It was foreseen that both classes of compounds could be prepared by oxidative substitution of group 10 metal complexes (new for Ni) and then compared on the basis of structural characteristics (studies in solution as well as in the solid state) and by extracting chemical information from advanced theoretical calculations. Standard, well-studied, five-membered dinitrogen heterocyclic carbene complexes would serve as reference compounds. Finally, an experimental catalytic study carried out, by using them as pre-catalysts in coupling reactions, in collaboration with another laboratory (Inorganic Chemistry Institute, TU Munich), could indicate the usefulness of our new compounds in practice.

Second, although rhodium(I) compounds are well established as effective catalysts in the hydroformylation of alkenes, certain structural uncertainties still exist for their NHC complexes, especially when longer side chains are involved. Thus, it was envisaged to prepare and isolate such complexes and then embark on unequivocal structure-elucidation by means of single-crystal X-ray diffraction. Decomposition studies and the determination of isomerism in solution were identified as particularly important facets of the investigation.

Third, following the recent utilisation of anionic Fischer-type carbene complexes that contain two hard donor atoms (N and O) as ligands in 'complexes of complexes', the introduction of soft donor atoms - more specifically phosphorus - in the carbene ligand side chain was set as goal for this

section of the investigation. A deprotonation – C,P coupling pathway was chosen as possible pathway to place the phosphorus β to the carbene carbon.

Although continuously critically focusing on all three synthetic proposals, we decided, in addition, to keep the eyes wide open for previously unseen associations and potential serendipitous discoveries.

Chapter 2 describes the utilisation of oxidative substitution to prepare carbene complexes of nickel and palladium. Three types of carbene complexes namely, the standard two-N, five-membered NHC complexes, pyridine-derived one-N, six-membered NHC complexes and one-N, six-membered *r*NHC complexes are included. The catalytic properties and metal carbene bonding of selected compounds are compared by means of quantum mechanical calculations.

The synthesis and characterisation of mono(carbene) and bis(carbene) complexes of rhodium(I) with 1-R-3-methylimidazolium bromide salts (R = ethyl or propyl or butyl) as carbene precursors are presented in **Chapter 3**. The results, especially the crystal structure determination, allows the clarification of any uncertainty concerning the structure of chloro(η^4-1,5-cyclooctadiene)(1-butyl-3-methyl-2,3-dihydro-1*H*-imidazol-2-ylidene)rhodium(I), reported previously.[99] The carbonyl complexes $[Rh(CO)_2X(NHC)]$ (X = Br or Cl; NHC = 1-ethyl-3-methyl-2,3-dihydro-1*H*-imidazol-2-ylidene) are also described.

Chapter 4 illustrates the modification of the anionic Fischer-type carbene complex, $[(CO)_5M{=}C(OMe)CH_2]Li$ (M = Cr or W), by reaction diphenylphophinechloride. The isolated compounds include the desired acyclic animo-alkylphosphine Fischer-type carbene complexes as well as the novel four-membered carbene-phosphine chelate, formed as a result of CO substitution and coordination by the phosphorus atom to the present central metal. The bridged compound of chromium, $(CO)_5Cr{=}C(NMe_2)CH_2P(Ph_2)Cr(CO)_5$, is also described.

[99] A. Neveling, *Ph.D. Dissertation*, University of Stellenbosch, 2003.

Chapter 2

Unusual carbene complexes with the carbene carbon adjacent and removed from the heteroatom (N)

Abstract

New square planar *N*-heterocyclic carbene complexes of the type *trans*-[$(PPh_3)_2MCl(L)$]X (M = Ni or Pd; X = BF_4; L = 1,3-dimethyl-2,3-dihydro-1*H*-imidazol-2-ylidene, 1,3-dimethyl-2,3,4,5-tetrahydro-1*H*-imidazol-2-ylidene (for M = Ni; X = PF_6), 1-methyl-1,2-dihydro-pyridin-2-ylidene, 1-methyl-1,2-dihydro-quinolin-2-ylidene, 1,4-dimethyl-1,2-dihydro-quinolin-2-ylidene, 2-methoxy-1-methyl-1,4-dihydro-quinolin-4-ylidene, 1-methyl-1,4-dihydro-pyridin-4-ylidene) have been prepared *via* the oxidative addition of the corresponding imidazolium-, imidazolinium-, pyridinium- and quinolinium chloride salts to $M(PPh_3)_4$ (M = Ni or Pd). The molecular and crystal structures of 12 of these carbene complexes were determined and include structures of both unique *cis* (only at low temperature) and *trans*-chloro(1-methyl-1,2-dihydro-quinolin-2-ylidene)bis(triphenylphosphine)palladium(II) tetrafluoroborate. The crystal structure of *cis*-chloro(2-methoxy-1-methyl-1,4-dihydro-quinolin-4-ylidene)bis(triphenylphosphine)platinum(II) tetrafluoroborate is also reported here. The *r*NHC (*remote* N-Heterocyclic carbene) complexes, $(CO)_5M\{\underline{C}SC(\overline{CNCMe_2CH_2O})CH\underline{C}H\}$ (M = Cr or W) are also described in this chapter.

The one-*N*, six-membered heterocyclic carbene (*r*NHC) complex, *trans*-chloro(2-methoxy-1-methyl-1,4-dihydro-quinolin-4-ylidene)bis(triphenylphosphine)palladium(II) tetrafluoroborate is an active catalyst in the Mizoroki-Heck and Suzuki-Miyaura coupling reactions. Quantum mechanical calculations indicated that the palladium-carbene bond of this complex, where the N is removed from the carbene atom, is 20 kcal/mol stronger than that in the two-N, five-membered NHC complex, in which the N atoms are attached to the carbene carbon. Further calculations suggest that the one-*N*, six-membered *r*NHC complexes of nickel(II) are more stable when compared to the one-*N*, six-membered NHC complexes and the normal two-*N*, five-membered NHC complexes of nickel.

2.1 Introduction and aims

2.1.1 General

The synthesis of nickel, palladium, and platinum complexes by oxidative addition have been studied extensively and includes synthetic methodology, kinetic investigation, and other properties (such as bonding) of these complexes as well as theoretical and spectroscopic studies.[1,2,3,4,5] The synthesis generally proceeds *via* the oxidative addition of an aryl halide to $M(PR_3)_4$ (M = Ni, Pd or Pt; R = organic moiety).[6] Carbene complexes of these metals were only obtained at a later stage when the aryl group contained a heteroatom, generally nitrogen, conjugatively incorporated into a heterocyclic ring. Alkylation or protonation of this nitrogen either before or after complexation produces cationic carbene complexes. Stone and co-workers were first to use this method for preparing cationic pyridine- and thiazole-derived carbene complexes of rhodium and iridium.[7] The group of Crociani have prepared the former type of carbene complexes of palladium and platinum *via* the oxidative addition of 2-chloropyridine to $M(PPh_3)_4$. The *N*-protonation (by HCl or $HClO_4$) or N-methylation (Me_2SO_4, $NaClO_4$) of the neutral aryl complexes (**i**) produces the cationic carbene complexes (**ii**) (Scheme 2.1).[8,9]

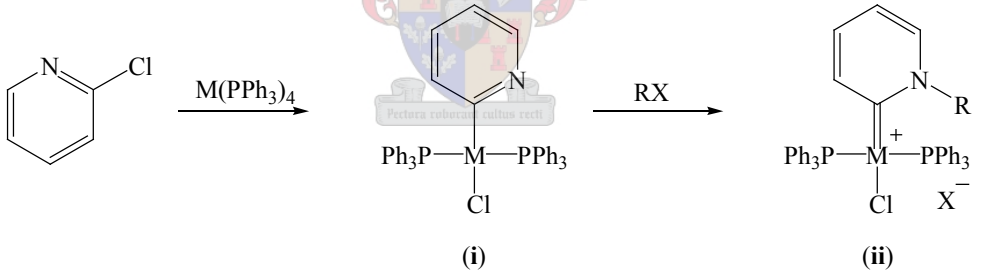

(i) **(ii)**

Scheme 2.1 M = Pd, Ni or Pt; R = H or Me; X = counter ion

---

[1] P. Fitton, E.A. Rick, *J. Organomet. Chem.*, 1971, **28**, 287.

[2] J-F. Fauvarque, F. Pflüger, M. Troupel, *J. Organomet. Chem.*, 1981, **208**, 419.

[3] G.W. Parshall, *J. Am. Chem. Soc.*, 1966, **88**, 704.

[4] G.W. Parshall, *J. Am. Chem. Soc.*, 1974, **96**, 2360.

[5] F.M. Bickelhaupt, T. Ziegler, P. von Ragué Schleyer, *Organometallics*, 1995, **14**, 2288.

[6] A. Yamamoto in: H. Kurosawa, A. Yamamoto (Eds), *Fundamentals of Molecular Catalysis*, Vol. 3, Elsevier, Amsterdam, 2003, p 1.

[7] P. J. Fraser, W. R. Roper and F. G. A. Stone, *J. Chem. Soc., Dalton Trans.,* 1974, 760.

[8] R. Bertani, A. Berton, F. Di Bianca, B. Crociani, *J. Organomet. Chem.*, 1986, **303**, 283.

[9] B. Crociani, F. Di Bianca, A. Giovenco, A. Berton, R. Bertani, *J. Organomet. Chem.*, 1989, **361**, 255.

Crociani and co-workers have also made the neutral complexes (**i**) in Scheme 2.1 from the reaction of [MX(μ-2-py)(PPh_3)] (M = Pd or Ni; X = Cl or Br; py = pyridyl) with two molar equivalents of phosphine (e.g. PPh_3 or PEt_3). The protonation or methylation of these neutral complexes yields the carbene complexes (**ii**) as shown in Scheme 2.1.[10,11] The potentially bifunctional 2,6-dichloropyridine only reacts with one mole equivalent of $M(PPh_3)_4$ (M = Pd or Pt) even if an excess of the metal(0) complex is used.[12] The higher electron density on the metallated aromatic ring probably inhibits the second oxidative addition. This study also reveals that the tendency to undergo oxidative addition of 2,6-dichloropyridine to $M(PPh_3)_4$ decreases in the order (reaction temperatures given in parenthesis): Ni (20°C) >> Pd (90°C) > Pt (110°).

N-heterocyclic carbene complexes have been prepared by the *in situ* oxidative addition of the imidazolium unit C-H[13,14] and imidazolium unit C-Cl bonds[15] to Pd(0). Cavell and co-workers have also studied the oxidative addition of the imidazolium cation to zerovalent Ni, Pd and Pt experimentally and theoretically.[16] This theoretical study suggests that these three zerovalent metals should readily undergo oxidative addition and that oxidative addition to Pt(0) and Ni(0) is more exothermic than to Pd(0). A *cis*-chelating ligand as well as a compact, strongly basic phosphine on the metal center lowers the activation barriers relative to modentate ligands. Finally, the study reveals that the oxidative addition of a halo-imidazolium to group 10 zerovalent metals is exothermically favoured over 2-H imidazolium ions followed by 2-alkylimidazolium ions. It is also important to note that the metal hydrides formed by the oxidative addition of an imidazolium ion could initiate many catalytical cycles involving unsaturated substrates. C-H and N-H activation by Pt(0) in N and O-heteroaromatic compounds are also known from the work of Chantson and Lotz to produce the corresponding Pt-hydride complexes.[17]

---

[10] B. Cociani, F. Di Bianca, A. Giovenco, A. Scrivanti, *J. Organomet. Chem.*, 1983, **251**, 393.

[11] B. Cociani, F. Di Bianca, A. Giovenco, A. Berton, *J. Organomet. Chem.*, 1987, **323**, 123.

[12] A. Mantovani, *J. Organomet. Chem.*, 1983, **255**, 385.

[13] S. Gründemann, M. Albrecht, A. Kovacevic, J.W. Faller, R.H. Crabtree, *J. Chem. Soc., Dalton Trans.*, 2002, 2163.

[14] C.J. Mathews, P.J. Smith, T. Welton, A.J.P. White, D.J. Williams, *Organometallics*, 2001, **20**, 3848.

[15] A. Fürstner, G. Seidel, D. Kremzow, C.W. Lehmann, *Organometallics*, 2003, **22**, 907.

[16] D.S. McGuinness, K.J. Cavell, B.F. Yates, B.W. Skelton, A.H. White, *J. Am. Chem. Soc.*, 2001, **123**, 8317.

[17] J.T. Chantson, S. Lotz, *J. Orgnanomet. Chem.*, 2004, **689**, 1315.

Recently, new diorgano carbene complexes with remote (or removed) heteroatoms (N and O) were prepared by oxidative addition in our Stellenbosch group. In these complexes the carbene carbon is bonded to two carbon atoms and not to one of the normally used heteroatoms (N, S or O). Although the heteroatoms are distant, they are still conjugated to the carbene carbon.[18] In this work the first structurally characterised remote carbene complex of palladium namely, chloro(2-methoxy-1-methyl-1,4-dihydro-quinolin-4-ylidene)bis(triphenyl-phosphine)palladium(II) tetrafluoroborate, is discussed. Alkylation may occur before or after oxidative substitution. Another example of a diorgano carbene complex, (**iii**) in Scheme 2.2, has been reported previously.[19,20] Heterocyclic carbene complexes with remote heteroatoms, *r*NHC complexes, of iron and gold have also been described previously by members of our group and are also shown in Scheme 2.2, (**iv**) and (**v**), (**vi**) respectively.[21,22] In this thesis carbene complexes of group 6 metals, containing this ligand, will be explored.

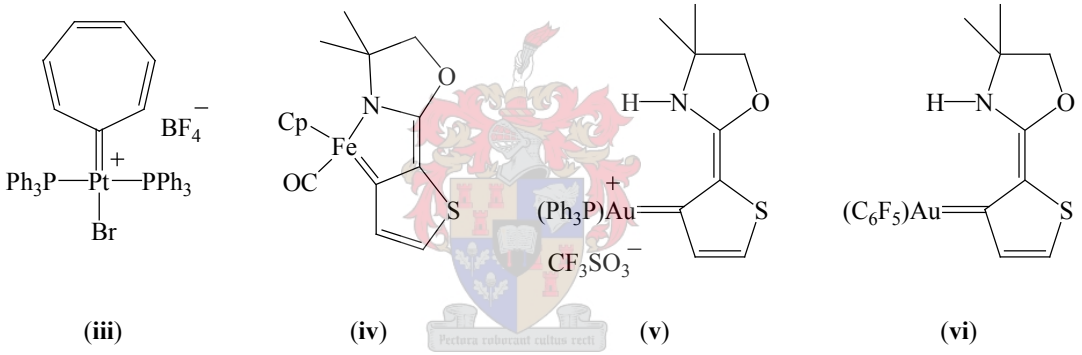

(**iii**) (**iv**) (**v**) (**vi**)

Scheme 2.2 (Cp = η-cyclopentadienyl)

More than 80% of all current pharmaceuticals and agrochemicals contain aromatic or heteroaromatic units as an essential component of their structure.[23] As a result of this, the modification of aryl halides is a critical part of the preparation of organic building blocks for new

---

[18] W.H. Meyer, M. Deetlefs, M. Pohlmann, R. Scholz, M.W. Esterhuysen, G.R. Julius, H. G. Raubenheimer, *J. Chem Soc., Dalton Trans*, 2004, 413.

[19] Z. Lu, K.A. Abboud, W.M. Jones, *J. Am. Chem. Soc.*, 1992, **114**, 10991.

[20] J. Klosin, W.M. Jones, K.A. Abboud, *Acta Cryst.*, 1996, **C52**, 1101.

[21] H.G. Raubenheimer, M. Desmet, P. Oliver, G.J. Kruger, *J. Chem. Soc., Dalton Trans*, 1996, 4431.

[22] M. Desmet, H.G. Raubenheimer, G.J. Kruger, *Organometallics*, 1997, **16**, 3324.

[23] A.C. Frisch, A. Zapf, O. Briel, B. Kayser, N. Shaikh, M. Beller, *J. Mol. Cat. A: Chem.*, 2004, **214**, 231.

active reagents. Catalysed reactions such as the Suzuki[24] and Heck [6,25,26] reactions provide ways to prepare such components and reduce the number of synthetic steps that the total synthesis of organic pharmaceuticals and agrochemicals would normally require. Despite this advantage these reactions have been applied in only a few instances on industrial scale.[6,27] Catalyst costs and leaching (> 1 ppm) of the catalysts are major drawbacks of these reactions. Lin and co-workers have compared the nickel and palladium catalysed Heck reaction theoretically. This comparison of the proposed steps of the reaction mechanism reveals that these two catalysed reactions are similar overall and that both metals have their advantages and disadvantages. The nickel-catalysed Heck reaction allows for the use of aliphatic halides (e.g. cyclohexyl bromide), which is a distinct advantage over the classical palladium-catalysed reaction.[28]

The use of phosphines as ligands in these reactions has been the norm and have led to high turnover numbers.[27] In a comparison of palladium carbene and palladium phosphine pre-catalysts in the coupling reactions of aryl halides, the phosphine pre-catalysts give better yields than the carbene pre-catalysts.[23] *N*-heterocyclic carbene (NHC) ligands have been implemented as alternatives to phosphines to overcome their shortcomings such as their sensitivity to air and water, which leads to their oxidation. *N*-heterocyclic carbenes are known to increase the electron density on the metal center and this could lead to an increase in the activity for the oxidative addition step in the catalytical cycle.[23]

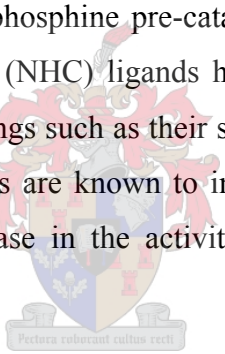

Recent successes include the use of imidazolium-derived NHC's as ligands in catalyst precursor complexes. Various groups, in particular the group of Herrmann, implement palladium(II) carbene complexes as pre-catalysts for C-C coupling reactions.[15,26,29,30,31,32] *N*-acyl-*N*-heterocyclic carbene

---

[24] A. Suzuki, *J. Organomet. Chem.*, 1999, **576**, 147.

[25] R.F. Heck, *Acc. Chem. Res.*, 1979, **12**, 146.

[26] N.J. Whitecombe, K.K. Hii, S.E. Gibson, *Tetrahedron*, 2001, **57**, 7449.

[27] P.W.N.M. van Leeuwen, *Homogeneous Catalysis, Understanding the Art*, Kluwer Academic Publishers, Dordrecht, 2004, p.271.

[28] B-L. Lin, L. Liu, Y. Fu, S-W. Luo, Q. Chen, Q-X, Guo, *Organometallics*, 2004, **23**, 2114.

[29] W.A. Herrmann, *Angew. Chem. Int. Ed. Engl.*, 2002, **41**, 1290.

[30] W.A. Hermann, M. Elison, J. Fischer, C. Köcher, G.R.J. Artus, *Angew. Chem. Int. Ed. Engl.*, 1995, **34**, 2371.

[31] W.A. Herrmann, V.P.W. Böhm, C.W.K. Gstöttmayr, M. Grosche, C-P. Reisinger, T. Weskamp, *J. Organomet. Chem.*, 2001, **617 - 618**, 616.

palladacycle and palladium(II) benzothiazole carbene complexes have also been used as catalyst precursors in the Suzuki-Miyaura and Heck reactions respectively.[33,34] The palladium imidazolylidene carbene complexes form during C-C coupling reactions in ionic liquids with the palladium sources $PdPh(PPh_3)_2Br$, $PdCl_2(PPh_3)_2$, $Pd(PPh_3)_4$[35] and $Pd(OAc)_2$.[36]

The mechanism for the (Pd-catalysed) Heck reaction when using Pd(0) as catalyst or when Pd(0) is formed in the reaction, is generally believed to consist of the following steps; 1) the oxidative addition of the aryl halide, 2) the coordination of the olefin and insertion of the olefin into the Pd-aryl bond, 3) β-hydrogen elimination which produces the coupling product and $PdH(X)L_2$, 4) regeneration of PdL_2 after the removal of HX from $PdH(X)L_2$ mediated by a base.[27,28,37] Both palladium(0) or palladium(II) catalyst precursors can be employed in C-C coupling reactions although greater uncertainty surrounds the latter situation.[27] Uncertainty also exists around the real active catalyst species in the process. The quest is to identify this species and the debate still continues.

2.1.2 Aims of the present study

After the already mentioned preparation of palladium and platinum carbene complexes with remote heteroatoms, for example chloro(2-methoxy-1-methyl-1,4-dihydro-quinolin-4-ylidene)bis(triphenylphosphine)palladium(II) tetrafluoroborate,[18] it became clear that the properties and reactivity of such complexes required further investigation. Especially the catalytic properties of *r*NHC complexes as well as their metal-carbene bond needed further clarification and should be compared to that of other known catalyst precursor complexes. The synthesis of new types of carbene complexes *via* oxidative addition reactions also needed to be extended to other metals like nickel.

---

[32] W.A. Herrmann, K. Öfele, D. v. Preysing, S.K. Sneider, *J. Organomet. Chem.*, 2003, **687**, 229.

[33] H. Palencia, F. Garcia-Jimenez, J.M. Takacs, *Tett. Lett.*, 2004, **44**, 3849.

[34] V. Calò, A. Nacci, L. Lopez, A. Napola, *Tett. Lett.*, 2001, **42**, 4701.

[35] F. McLachlan, C.J. Mathews, P.J. Smith, T. Welton, *Organometallics*, 2003, **22**, 5350.

[36] L. Xu, W. Chen, J. Xiao, *Organometallics*, 2000, **19**, 1123.

[37] C. Atmore. A. Jutand, *Acc. Chem. Res.*, 2000, **33**, 214.

The main aim of this study was to prepare, characterise and describe new carbene complexes of palladium, platinum and nickel, particularly carbene ligands with N atoms adjacent to the carbene carbon (NHC's) as well as carbene ligands with remote N atoms (*r*NHC) based on pyridine (a six-membered heterocycle). Imidazolium-derived complexes (typical NHC ligands) would be prepared to serve as reference complexes because the properties of this type of carbene compounds had already been studied extensively.

In an extension of the synthetic study, the use of 4,4-dimethyl-2-thiophen-2-yl-4,5-dihydro-oxazole as a ligand precursor and the consequent preparation of chromium and tungsten carbene complexes with the active N atom far removed from the carbene carbon (*r*NHC), were also targeted.

It was decided to include *trans*-chloro(2-methoxy-1-methyl-1,4-dihydro-quinolin-4-ylidene)bis(triphenylphosphine)palladium(II) tetrafluoroborate as a pre-catalyst in a comparative study of the homogeneous catalysis of C-C coupling (Mizoroki-Heck and Suzuki-Miyaura) reactions involving simple palladium carbene and phosphine complexes. In collaboration with the laboratory of Frenking at the Philips University, Marburg, quantum mechanical calculations were planned in order to better explain differences in the metal carbene bonding of NHC and *r*NHC ligands. A similar route (but without catalysis) was foreseen for NHC and *r*NHC complexes of nickel derived from readily available imidazole, pyridine and quinoline derivatives: 2-chloro-1,3-dimethylimidazolium tetrafluoroborate, 2-chloro-1-methylpyridinium tetrafluoroborate, 2-chloro-1-methylquinolinium tetrafluoroborate, 2-chloro-1,4-dimethylquinolinium tetrafluoroborate, 4-chloro-2-methoxy-1-methylquinolinium tetrafluoroborate, and 4-chloro-1-methylpyridinium tetrafluoroborate, compounds had to be prepared and fully characterised (again strengthened by quantum mechanical calculations) to find out if and how one-N, six-membered *r*NHC is different form their NHC analogues and from the better known two-N, five-membered heterocyclic carbene complexes. It was clear that crystal structure determinations of key complexes (by the author) would form an indispensable part of the investigation and would also underpin the quantum mechanical calculations.

2.2 Results and discussion

A. The preparation and characterisation of three reference complexes (two-N, five-membered heterocyclic carbene complexes)

2.2.1 Synthesis of 2-chloro-1,3-dimethylimidazolium tetrafluoroborate, 1

2-Chloro-1-methylimidazole (Scheme 2.3) was prepared by the chlorination of methylimidazolium, with CCl_4, after deprotonation at C^2 with *n*-BuLi at –78°C.[38] The *N*-methylation of 2-chloro-1-methylimidazole with trimethyloxonium tetrafluoroborate, $[Me_3O][BF_4]$, at room temperature yielded an off-white precipitate.[7] Repeated washing of this precipitate with THF and diethyl ether gave **1**, as a white microcrystalline material, in an overall yield of 28 %. Ligand precursor **1** is soluble in dichloromethane, but insoluble in diethyl ether, THF and other non-polar solvents like pentane.

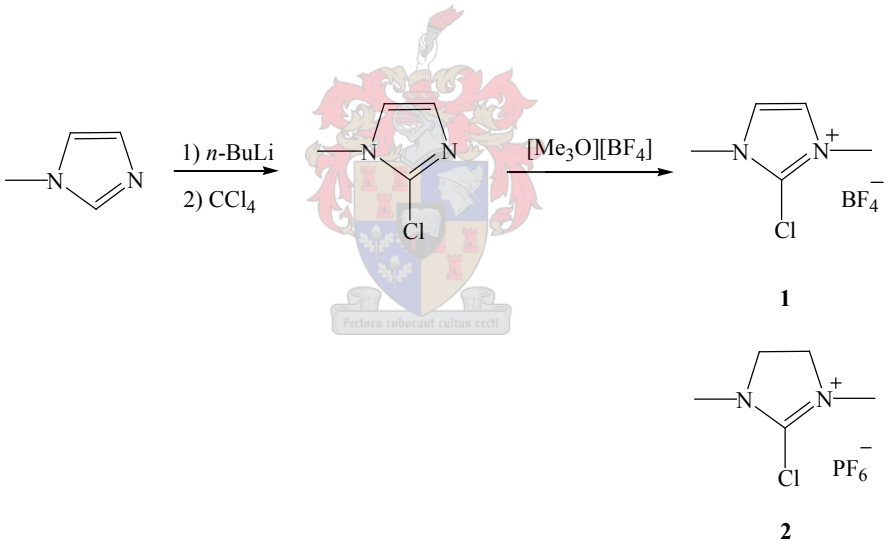

1

2

Scheme 2.3

[38] C. Boga, E. Del Vecchio, L. Forlani, P.E. Todesco, *J. Organomet. Chem.*, 2000, **601**, 233.

2.2.2 Spectroscopic characterisation of ligands 1 and 2

NMR spectroscopy.

2.2.2.1 2-Chloro-1,3-dimethylimidazolium tetrafluoroborate, 1

The NMR data for compound **1** are listed in Table 2.1 and compare well with those of 1,3-dimethylimidazolium iodide.[39,40] H^5 and H^4 appear as a singlet in the ^{1}H NMR spectrum of **1**. The NMe protons are also observed as a singlet at δ 3.88. In the ^{13}C NMR spectrum C^2 resonates at the lowest field of all the carbons because of the deshielding effect of the two adjacent N-atoms and the electron withdrawing Cl atom. C^4 and C^5 have a typical chemical shift of δ 124.6. NMe has the expected chemical shift in the ^{13}C NMR spectrum of **1**.

Table 2.1 ^{1}H and ^{13}C NMR data of compound **1** in CD_2Cl_2

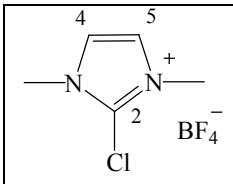

Assignment	δ / ppm	Assignment	δ / ppm
^{1}H NMR		**^{13}C NMR**	
H^4, H^5	7.54 (2H, s)	C^2	132.6 (s)
NMe	3.88 (6H, s)	C^4, C^5	124.5 (s)
		NMe	36.5 (s)

2.2.2.2 2-Chloro-1,3-dimethylimidazolinium hexafluorophosphate, 2

The NMR data of the saturated heterocycle, **2** (Table 2.2), are in agreement with the data for 2-chloro-1,3-dimethylimidazolinium hexachloroantimonate.[41] The aliphatic protons (H^4 and H^5) resonate at δ 4.06 as a singlet. These protons appear upfield (Δδ 3.48) compared to the more

[39] B.L. Benac, E.M. Burgess, A.J. Arduengo III, *Org. Synt.*, 1986, **64**, 92.

[40] W.A. Herrmann, C. Köcher, L.J. Gooβen, G.R.J. Artus, *Chem. Eur. J.*, 1996, **2**, 1627.

[41] A. Hamed, E. Müller, J.C. Jochims, *Tetrahedron*, 1986, **42**, 6645.

aromatic protons in **1**. The absence of aromaticity in compound **2** has the opposite effect on the NMe protons and they are deshielded by 0.68 ppm when compared to the NMe in **1**. C^2 appears at δ 156.8 in the ^{13}C NMR spectrum of **2**, downfield (Δδ 24.2) from the C^2 signal for **1**. This can be ascribed to the positive charge that cannot be delocalised through the imidazolinium ring and thus has a greater deshielding effect on C^2. C^4 and C^5 appear at much lower field (Δδ 74.4) than the signals of C^4 and C^5 in **1**.

Table 2.2 ^1H and ^{13}C NMR data of compound **2** in CD_2Cl_2

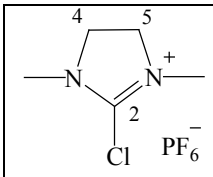

Assignment	δ / ppm	Assignment	δ / ppm
^{1}H NMR		**^{13}C NMR**	
H^4, H^5	4.06 (4H, s)	C^2	156.8 (s)
NMe	3.20 (6H, s)	C^4, C^5	50.2 (s)
^{31}P NMR		NMe	34.9 (s)
PF_6^-	-143.8 (hept, J_{P-F} = 710 Hz)		

Mass spectrometry

The structure of ligand **1** was confirmed by FAB MS, showing the fragment $[M - BF_4]^+$ (80%) as the base peak in the mass spectrum.

2.2.3 Synthesis of complexes 3a, 3b and 4b

Complex **3a** (Scheme 2.4) was synthesized *via* the oxidative substitution of $Pd(PPh_3)_4$ by compound **1**, in toluene at 60°C over a period of 16 hours. Recrystallisation yielded complex **3a** as colourless crystals. Complexes **3b** and **4b** were prepared in similar fashion but with $Ni(PPh_3)_4$ as metal-containing reactant and ligand precursors **1** and **2** respectively. The reactions proceeded incompletely and recrystallisation of the reaction mixtures yielded crystals of the complexes but still contained unreacted imidazolium and imidazolinium salts, all which were separated mechanically.

The new complexes are soluble in polar solvents like dichloromethane and acetone but insoluble in diethyl ether and non-polar solvents like pentane and hexane.

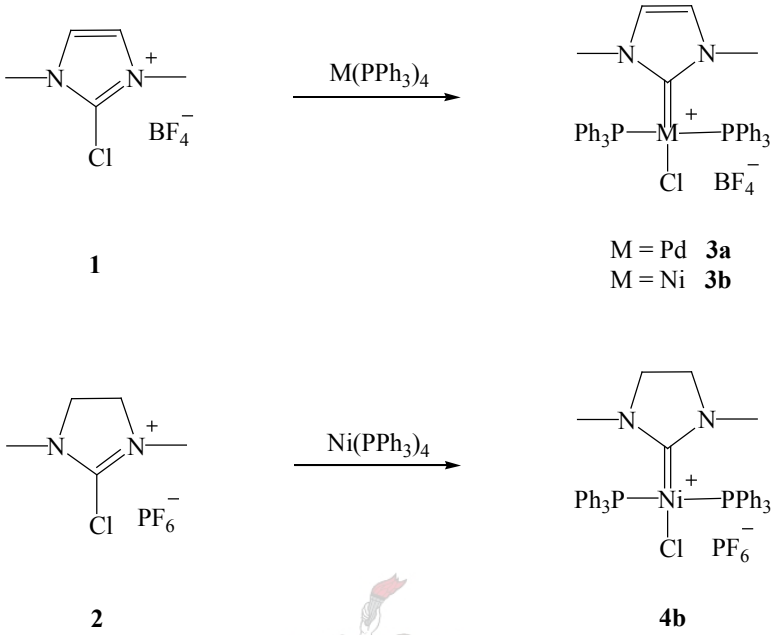

Scheme 2.4

2.2.4 Spectroscopic characterisation of complexes 3a, 3b and 4b

NMR spectroscopy.

2.2.4.1 Trans-*chloro(1,3-dimethyl-2,3-dihydro-1*H-*imidazol-2-ylidene)bis(triphenylphosphine) palladium(II) tetrafluoroborate, 3a, and* trans-*chloro(1,3-dimethyl-2,3-dihydro-1*H-*imidazol-2-ylidene)bis(triphenylphosphine)nickel(II) tetrafluoroborate, 3b*

The NMR data for complexes **3a** and **3b** are summarised in Table 2.3. H^4 and H^5 appear as a singlet in the ^{1}H NMR spectra of **3a** and **3b**, upfield ($\Delta\delta$ 1.0) compared to the signal of H^4 and H^5 in the spectrum of compound **1**. The singlet for NMe in both **3a** and **3b** also resonates upfield from the singlet resonance for NMe in **1**. The signals observed for the 1,3-dimethyl-2,3-dihydro-1*H*-

imidazol-2-ylidene ligand are similar to those observed for other palladium(II),[30,31] nickel(II),[42] rhodium(I) and iridium(I)[43,44] complexes with this carbene ligand.

Table 2.3 ^{1}H, ^{13}C and ^{31}P NMR data of complexes **3a** and **3b** in CD_2Cl_2

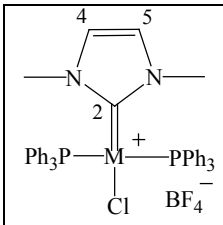

M = Pd **3a**
M = Ni **3b**

Assignment	δ / ppm **3a**	δ / ppm **3b**
^{1}H NMR		
Ph	7.52 (30H, m)	7.50 (30H, m)
H^4, H^5	6.56 (2H, s)	6.48 (2H, s)
NMe	3.16 (6H, s)	3.44 (6H, s)
^{13}C NMR		
C^2	161.2 (t, $^{2}J_{PC}$ = 11 Hz)	158.6 (t, $^{2}J_{P\text{-}C}$ = 36.7 Hz)
C_{ortho}, C_{para}	134.5 (m), 132.3 (s)	134.5 (m), 132.1 (s)
C_{meta}, C_{ipso}	129.7 (m), 129.1 (m)	129.6 (m), 129.0 (m)
C^4, C^5	125.4 (s)	126.7 (s)
NMe	37.3 (s)	37.3 (s)
^{31}P NMR		
PPh_3	22.8 (s)	20.3 (s)

Pectora roborant cultus recti

The triplet at the lowest field (δ 161.2) was assigned to C^2, the carbene carbon, in the ^{13}C NMR spectrum of **3a**. This chemical shift falls in the previously observed 157 - 169 ppm range for several palladium(II) imidazolium carbene complexes.[14,30,36,45,46] The carbon-phosphorus coupling constant is 11 Hz. The resonance for C^2 appears downfield (Δδ 28.6) when compared to the chemical shift of C^2 in **1**. C^2 in complex **3b** also appeared as a triplet at δ 158.6, 26.04 ppm downfield from the signal

[42] W.A. Herrmann, G. Gerstberger, M. Spiegler, *Organometallics*, 1997, **16**, 2209.

[43] W.A. Herrmann, M. Elison, J. Fischer, C. Köcher, G.R.J. Artus, *Chem. Eur. J.*, 1996, **2**, 772.

[44] M.V. Barker, S.K. Brayshaw, B.W. Skelton, A.H. White, *Inorg. Chim. Acta*, 2004, **357**, 2841.

[45] T. Strassner, M. Meuhlhofer, A. Zeller, E. Herdtweck, W.A. Herrmann, *J. Organomet. Chem.*, 2004, **689**, 1418

[46] D.S. McGuiness, N. Saendig, B.F. Yates, K.J. Cavell, *J. Am. Chem. Soc.*, 2001, **123**, 4029.

for C^2 in ligand **1**. The chemical shift of the carbene signals are similar to those (159 – 162 ppm) reported for several nickel(II) *N*-heterocyclic carbene complexes.[47,48] The phosphorus-carbon coupling experienced by the carbene carbon is 36.7 Hz. This coupling is comparable to the reported value of 30 Hz for the corresponding coupling in $[Ni\{=C(NH^tBu)Me\}Cl(PMe_3)_2]Cl$.[49] The signals for the phenyl carbons (*ortho*, *meta* and *ipso*) are observed as triplet-like multiplets for both complexes **3a** and **3b** due to carbons in the phenyl rings that are not magnetically equivalent.[50] Coupling between the P-atom and these phenyl carbons resulted in an AXX' spin system with $J_{xx'}$ = 0 (as the least complicated spin system). The signals show extra lines (second order spectrum) and coupling constants could not be determined as is usually done for first order spectra (when all the atoms are magnetically equivalent). These spectra can be analyzed by calculations performed by simulation and iteration methods[51] or direct methods[52] as can be done for an AA'XX' spin system. The *para* phenyl carbon appeared as a singlet. There are no significant differences between the chemical shifts for C^4, C^5 and NMe in complexes **3a** and **3b** and those signals in ligand precursor **1** and they compare well with those reported for palladium(II)[30,31] and nickel (II)[42] carbene complexes with 1,3-dimethyl-2,3-dihydro-1*H*-imidazol-2-ylidene as ligand.

The P-atoms resonate at similar chemical shifts (δ 22.8 and δ 20.3) in the ^{31}P NMR spectra of complexes **3a** and **3b** respectively. These chemical shifts do not differ from those reported (δ 22.9 and 21.8) for palladium(II) carbene complexes[14,15].

Pectora roborant cultus recti

2.2.4.2 Trans-*chloro(1,3-dimethyl-2,3,4,5-tetrahydro-1*H*-imidazol-2-ylidene)bis (triphenylphosphine)nickel(II) tetrafluoroborate, 4b*

The NMR data for complex **4b** are summarized in Table 2.4. The protons of the two chemically equivalent NMe groups resonated as a singlet at δ 3.14. This is in agreement with the chemical shift of compound **2** (δ 3.20). Fürstner and co-workers have reported the synthesis and characterisation

---

[47] X. Wang, S. Liu, G-X. Jin, *Organometallics*, 2004, **23**, 6002.

[48] C. Abernethy, J.A.C. Clyburne, A.H. Cowley, R.A. Jones, *J. Am. Chem. Soc.*, 1999, **121**, 2329.

[49] E. Carmona, P. Palma, M. Paneque, M.L. Poveda, *Organometallics*, 1990, **9**, 583.

[50] D.L. Pavia, G.M. Lampman, G.S. Kriz, *Introduction to Spectroscopy*, 3rd Edition, Harcourt College Publishers, Fort Worth, 2001, p. 228 - 231.

[51] H. Freibolin, *Basic One- and Two-Dimensional NMR Spectroscopy*, 3rd Edition, Wiley, Weinheim, 1998, p 124 - 125.

[52] H. Günther, *Angew. Chem. Int. Ed. Engl.*, 1972, **11**, 861.

of *trans*-chloro(1,3-dimethyl-2,3,4,5-tetrahydro-1H-imidazol-2-ylidene)bis(triphenylphosphine) palladium(II) tetrafluoroborate.[15] The NMe protons for this Pd-analogue appeared at δ 2.84, 0.4 ppm upfield compared to the chemical shift of the NMe protons in **2** and **4b**. H^4 and H^5 appear together, as a singlet, at δ 2.48. Small upfield shifts are obvious for the Pd-analogue but it is slightly less (Δδ 1.38) than that observed for complex **4b**. The signals for the carbene ligand compare well with those reported for a nickel(II) carbene complex prepared a long time ago.[53]

Table 2.4 ^1H, ^{13}C and ^{31}P NMR data of complex **4b** in CD_2Cl_2

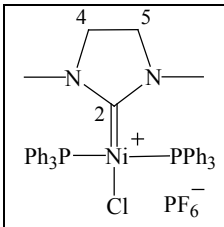

Assignment	δ / ppm
^{1}H NMR	
Ph	7.75 (12H, m), 7.60 (18H, m)
NMe	3.14 (6H, s)
H^4, H^5	2.48 (4H, s)
^{13}C NMR	
C^2	197.7 (t, $^2J_{P\text{-}C}$ = 32.8 Hz)
C_{ortho}, C_{para}	134.6 (m), 132.3 (s)
C_{meta}, C_{ipso}	129.4 (m)
C^4, C^5	51.2 (s)
NMe	36.9 (s)
^{31}P NMR	
PPh_3	21.5 (s)
PF_6^-	-143.9 (hept, $J_{P\text{-}F}$ = 711 Hz)

The carbene carbon, C^2, appears as a triplet at δ 197.7, with a coupling constant of 32.8 Hz for the carbon-phosphorus coupling. The resonance of the carbene carbon is equivalent to the carbene carbon resonance (δ 194) reported for another nickel(II) carbene complex with this carbene ligand.[53]

[53] M.F. Lappert, P.L. Pye, *J. Chem. Soc., Dalton Trans.*, 1977, 2172.

The coupling constant is similar to that ($^2J_{P-C}$ = 36.7 Hz) observed for **3b**. C^2 resonates downfield (Δδ 40.9) compared to the resonance of C^2 in ligand precursor **2**. The signals observed for the phenyl carbons, C^4, C^5 and NMe are as expected.[53]

The singlet observed for the two equivalent PPh_3 ligands appears at δ 21.5 in the ^{31}P NMR spectrum of **4b**. This chemical shift is similar to that reported (δ 22.8) for the Pd-analogue of **4b**.[15] The chemical shift for PF_6^- in the ^{31}P NMR spectrum was not affected during the formation of complex **4b**.

Mass spectrometry

The FAB mass spectrometry data for complexes **3a** – **4b** are given in Table 2.5. All the complexes show a similar fragmentation pattern with the cation observed as the highest peak. The loss of one PPh_3 ligand is followed by the loss of Cl. PPh_3 is only observed in the mass spectrum of complex **4b**.

Table 2.5 Mass spectrometry data for complexes **3a** - **4b**

Complex	m/z	Relative intensity (%)	Fragment ion
3a	761	18	$[M - BF_4]^+$
	499	5	$[M - BF_4 - PPh_3]^+$
	464	6	$[M - BF_4 - PPh_3 - Cl]^+$
3b	713	7	$[M - BF_4]^+$
	451	22	$[M - BF_4 - PPh_3]^+$
	416	10	$[M - BF_4 - PPh_3 - Cl]^+$
4b	715	30	$[M – PF_6]^+$
	453	100	$[M - PF_6 - PPh_3]^+$
	418	39	$[M - PF_6 - PPh_3 - Cl]^+$
	262	42	$[PPh_3]^+$

B. Heterocyclic carbene complexes with the N atom adjacent to the carbene carbon (one-N, six-membered NHC complexes)

2.2.5 Synthesis of compounds 2-chloro-1-methylpyridinium tetrafluoroborate, 5, 2-chloro-1-methylquinolinium tetrafluoroborate, 6, and 2-chloro-1,4-dimethylquinolinium tetrafluoroborate, 7

Ligand precursors **5**, **6** and **7** were prepared according to the method of Stone and co-workers[7] by *N*-methylation of the corresponding starting compounds with $[Me_3O][BF_4]$ in CH_2Cl_2:CH_3CN (3:1) as solvent system (Scheme 2.5) in very good yields (85 – 90%). Compounds **5** - **7** are soluble in dichloromethane, but not in THF, diethyl ether and pentane. The CH_2Cl_2 solution of compound **7** has a light pink colour.

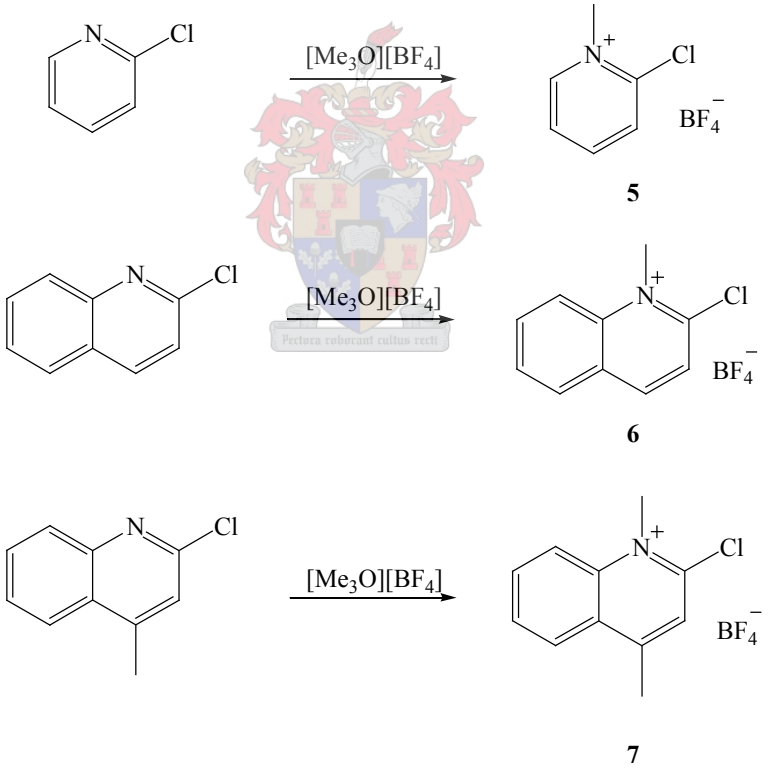

Scheme 2.5

2.2.6 Spectroscopic characterisation of 2-chloro-1-methylpyridinium tetrafluoroborate, 5, 2-chloro-1-methylquinolinium tetrafluoroborate, 6, and 2-chloro-1,4-dimethylquinolinium tetrafluoroborate, 7

NMR spectroscopy

The assignments of the peaks for **5** – **7** (Tables 2.6 – 2.8) were confirmed by two-dimensional NMR techniques, namely ghsqc (gradient heteronuclear single quantum coherence) and ghmqc (gradient heteronuclear multiple quantum coherence) NMR spectra.

2.2.6.1 2-Chloro-1-methylpyridinium tetrafluoroborate, 5

The group of Stone[7] has reported the NMR data for **5** (measured in CD_2Cl_2) but the exact assignment of the signals was not done because of the low resolution of the NMR spectra. The aromatic protons were reported as a multiplet at τ1.70 (δ 8.30, δ = 10 – τ).[54] It was, therefore, important to reassign the signals unambiguously.

H^6 (Table 2.6) appears at the lowest field (δ 9.02) as a multiplet in the ^1H NMR spectrum of **5** due to its location closest to the positively charged N-atom, which has a deshielding effect on H^6. Considering the possible resonance structures of **5** (Scheme 2.6), the positive charge on the N-atom can be localised at C^2, C^4 and C^6 and has a deshielding effect on the protons attached to the corresponding carbon atoms.[55] Deshielding, due to the adjacent N-atom combined with the further deshielding as a result of the resonance effect, substantiate the chemical shift of H^6 even more. The coupling constant for the coupling of H^6 with H^5 and H^4 could not be determined. The doublet of doublets at δ 8.46 is assigned to H^4, showing the coupling of H^4 with H^5 and H^3 and the longer range coupling of H^4 with H^6. H^4 appears upfield from H^6 because it is located further away from the N-atom than H^6 while both experience deshielding due to the resonance effect. H^4 resonates at lower field than H^3 and H^5 as a result of the resonance effect.

---

[54] D.L. Pavia, G.M. Lampman, G.S. Kriz, *Introduction to Spectroscopy*, 3rd Edition, Harcourt College Publishers, Fort Worth, 2001, p. 111

[55] D.L. Pavia, G.M. Lampman, G.S. Kriz, *Introduction to Spectroscopy*, 3rd Edition, Harcourt College Publishers, Fort Worth, 2001, p. 257.

Table 2.6 ^{1}H and ^{13}C NMR data of compound **5** in CD_2Cl_2

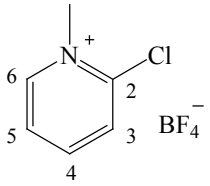

Assignment	δ / ppm
^{1}H NMR	
H^6	9.02 (1H, m)
H^4	8.46 (1H, td, $^{3}J_{H\text{-}H}$ = 8.0 Hz, $^{4}J_{H\text{-}H}$ = 1.3 Hz)
H^3	8.06 (1H, dd, $^{3}J_{H\text{-}H}$ = 8.7 Hz, $^{4}J_{H\text{-}H}$ = 1.9 Hz)
H^5	8.01 (1H, m)
NMe	4.46 (3H, s)
^{13}C NMR	
C^6	149.0 (s)
C^2	147.9 (s)
C^4	147.4 (s)
C^3	130.1 (s)
C^5	127.1 (s)
NMe	48.5 (s)

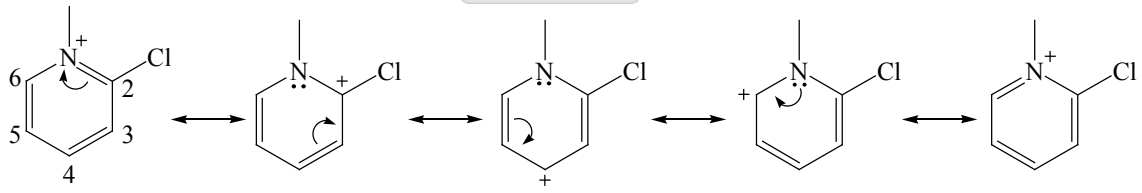

Scheme 2.6

The doublet of doublets at δ 8.06 is assigned to H^3 showing coupling with H^4 and H^5. The multiplet at δ 8.01 was assigned to H^5. The NMe protons appear (δ 4.46) at the expected chemical shift. All the coupling constants determined are normal for aromatic protons.[56]

[56] D.L. Pavia, G.M. Lampman, G.S. Kriz, *Introduction to Spectroscopy*, 3rd Edition, Harcourt College Publishers, Fort Worth, 2001, p. 261, 265 - 266.

C^6 resonates as a singlet (δ 149.1) at a slightly lower field than C^2 (δ 147.9). The negative inductive effect (-I) of the Cl-atom[57] did not result in significant deshielding that would have allowed C^2 to resonate at a lower field than C^6. The signals for C^4 and C^2 are similar in chemical shift (Δδ 0.5). C^3 and C^5 appear at a somewhat higher field strength than C^4 because they are not deshielded in the same manner as C^4 because of the resonance effect (Scheme 2.6).

2.2.6.2 2-Chloro-1-methylquinolinium tetrafluoroborate, 6

In the ^{1}H NMR spectrum of compound **6** (Table 2.7) the doublet at the lowest field (δ 8.98) is assigned to H^4. This low field resonance of H^4 results from the deshielding due to the resonance effect in ligand **6** as was observed for H^4 in ligand **5**. The resonance structures of ligand **6** are shown in Scheme 2.7. H^4 couples with H^3 with a coupling constant of 8.8 Hz. H^8 appears as a doublet at δ 8.42 in the ^{1}H NMR spectrum of **6**. The coupling between H^8 and H^7 is 9 Hz. According to the resonance structures (Scheme 2.7) H^8 is expected to resonate at a higher field than H^7 and H^5 as these two protons would be deshielded because of the delocalised positive charge on C^7 and C^5. However, H^8 appears downfield from H^5 and H^7, probably because it is located closer to the deshielding N-atom than H^7 and H^5. The σ-effect (inductive) is apparent. The mulitplet at δ 8.30 is due to the presence of H^7 and H^5.

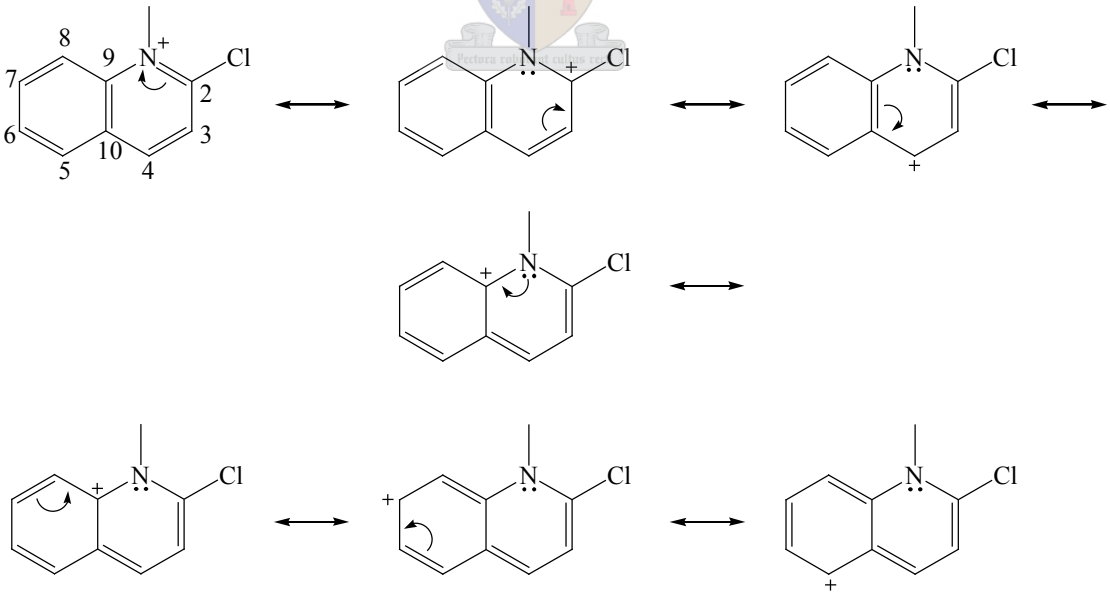

Scheme 2.7

[57] J. McMurray, *Organic Chemistry*, 4th Edition, Brooks/Cole Publishing Company, Pacific Grove, 1996, p. 548 – 595.

The doublet at δ 8.07 with the same coupling constant ($^3J_{H-H}$ = 8.8 Hz) as the doublet for H^4 is assigned to H^3. H^6 resonates as a triplet at δ 8.02. H^6 does not show coupling to H^8. H^3 and H^6 do resonate at higher fields because these protons do not experience deshielding as a result of the resonance effect. The NMe protons have the same chemical shift (δ 4.46) as the NMe resonance in the spectrum of **5**.

Table 2.7 ^{1}H and ^{13}C NMR data of compound **6** in CD_2Cl_2

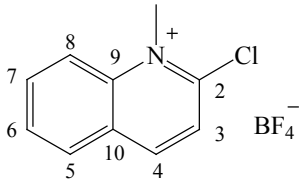

Assignment	δ / ppm
^{1}H NMR	
H^4	8.98 (1H, d, $^3J_{H-H}$ = 8.8 Hz)
H^8	8.42 (1H, d, $^3J_{H-H}$ = 9.0 Hz)
H^7, H^5	8.30 (2H, m)
H^3	8.07 (1H, d, $^3J_{H-H}$ = 8.8 Hz)
H^6	8.02 (1H, t, $^3J_{H-H}$ = 7.7 Hz)
NMe	4.46 (3H, s)
^{13}C NMR	
C^2	152.4 (s)
C^4	148.4 (s)
C^9	141.2 (s)
C^7	137.7 (s)
C^5	131.4 (s)
C^6	131.0 (s)
C^{10}	128.6 (s)
C^3	124.8 (s)
C^8	119.3 (s)
NMe	42.2 (s)

In the ^{13}C NMR spectrum of **6**, C^2 resonates at the lowest field (δ 152.4) as a singlet followed by the triplet for C^4 at δ 148.4. C^2 is expected to appear at a lower field than C^4 because of the extra contribution of the -I effect of the Cl-atom to the deshielding of C^2. The quaternary carbon, C^9,

appears at δ 141.2 and resonates at a lower field than C^{10} (δ 128.6) because of the electronegative N adjacent thereto as well as the deshielding contributed by the resonance effect (Scheme 2.7). C^7 and C^5 appear at lower field than C^6, C^3 and C^8 as expected and are in accordance with the resonance effect. The chemical shift of the signal for NMe (δ 42.2) is normal.

2.2.6.3 2-Chloro-1,4-dimethylquinolinium tetrafluoroborate, 7

The NMR data of compound **7** are summarized in Table 2.8. The assignment of the signals in the ^{1}H NMR spectrum of **7** was done in a similar fashion as for the signals in the spectrum of compound **6**. H^8 appears at the lowest field of the protons as it does in the spectrum of **6** where it appears lower than all the protons apart from H^4.

H^5 and H^7 are well resolved as a doublet and multiplet respectively compared to **6** where these two protons are observed together as a multiplet. The singlet at δ 7.93 is assigned to H^3 and it appears at a higher field than H^3 in **6**. The protons of CMe resonate as a singlet at δ 3.01.

The chemical shifts of the signals for the C-atoms in the ^{13}C NMR spectrum of ligand precursors **7** and **6** do not differ much except for C^4 and C^5. C^4 appears at δ 160.2, 11.8 ppm downfield compared to C^4 in **6** as a result of the Me-substitution of H^4. C^5 appears upfield (Δδ 4.1) from C^5 in **6**. CMe resonates at δ 20.4 as a singlet

Pectora roborant cultus recti

Table 2.8 ^{1}H and ^{13}C NMR data of compound **7** in CD_2Cl_2

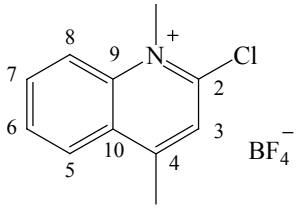

Assignment	δ / ppm
^{1}H NMR	
H^8	8.98 (1H, d, $^{3}J_{H-H}$ = 8.7 Hz)
H^5	8.42 (1H, dd, $^{3}J_{H-H}$ = 8.3 Hz, $^{4}J_{H-H}$ = 1.5 Hz)
H^7	8.27 (1H, m)
H^6	8.03 (1H, m)
H^3	7.93(1H, s)
NMe	4.68 (3H, s)
CMe	3.01 (3H, s)
^{13}C NMR	
C^4	160.2 (s)
C^2	151.1 (s)
C^9	140.4 (s)
C^7	137.0 (s)
C^6	130.6 (s)
C^{10}	128.2 (s)
C^5	127.3 (s)
C^3	125.2 (s)
C^8	119.8 (s)
NMe	41.8 (s)
CMe	20.4 (s)

Mass spectrometry

The cations are observed as the only fragments in the FAB MS spectra of compounds **5** – **7** (Table 2.9).

Table 2.9 Mass spectrometry data for compounds **5 – 7**

Complex	m/z	Relative intensity (%)	Fragment ion
5	128	100	$[M - BF_4]^+$
6	178	100	$[M - BF_4]^+$
7	192	100	$[M - BF_4]^+$

2.2.7 Synthesis of complexes 8a, 8b, 9a, 9b, 10a and 10b.

Complexes **8a**, **8b**, **9a**, **9b**, **10a** and **10b** were again prepared by the oxidative substitution reaction of compounds **5 – 8** to $M(PPh_3)_4$ (M = Pd or Ni) in toluene at 60°C over a period 16 hours (Scheme 2.8). Complexes **8a** and **9a** formed as white precipitates while **10a** was obtained as a pink precipitate. These precipitates were collected by filtration, washed with toluene and dried under vacuum as white microcrystalline materials. The precipitate obtained from the reactions of the ligand precursors with $Ni(PPh_3)_4$ which always contained impurities, was filtered over dried celite and washed well with toluene. Subsequently the product was washed through celite with dichloromethane, leaving the impurities on the celite. These filtrates were concentrated, the products precipitated with pentane and collected by filtration. Complexes **8b**, **9b** and **10b** were dried as yellow, red-purple and dark purple microcrystalline materials respectively.

During the slow crystallisation of **9a** from a concentrated CH_2Cl_2 solution layered with pentane, decomposition of **9a** resulted in the formation of yellow crystals. X-ray crystal structure determination of these yellow crystals revealed $PdCl_2(PPh_3)_2$ as one of the decomposition products. The X-ray crystal structure of this product has been reported in literature previously.[58] Already in 1974 Parshall proposed the formation of $NiX_2(PEt_3)_2$ as a decomposition product of $NiX(aryl)(PEt_3)_2$ by successive ligand redistribution and reductive elimination.[4] Thus, a possible formation of $PdCl_2(PPh_3)_2$ from **9a** is illustrated in equation 1 (L = 1-methyl-1,2-dihydroquinolin-2-ylidene), a rearrangement affording more uniformly ligated products.

$$2\ PdCl(L)(PPh_3)_3 \rightleftharpoons Pd(L)_2(PPh_3)_2 + PdCl_2(PPh_3)_2 \qquad (1)$$

[58] R. Oilunkaniemi, R.S. Laitinen, M.S. Hannu-Kuure, M. Ahlgrén, *J. Organomet. Chem.*, 2003, **678**, 95.

Complexes **9b** and **10b** contained small amounts of impurities and they could not be purified by crystallisation because of complete decomposition during the crystallisation process. These complexes are soluble in dichloromethane and acetone, but less soluble in diethyl ether, hexane and pentane.

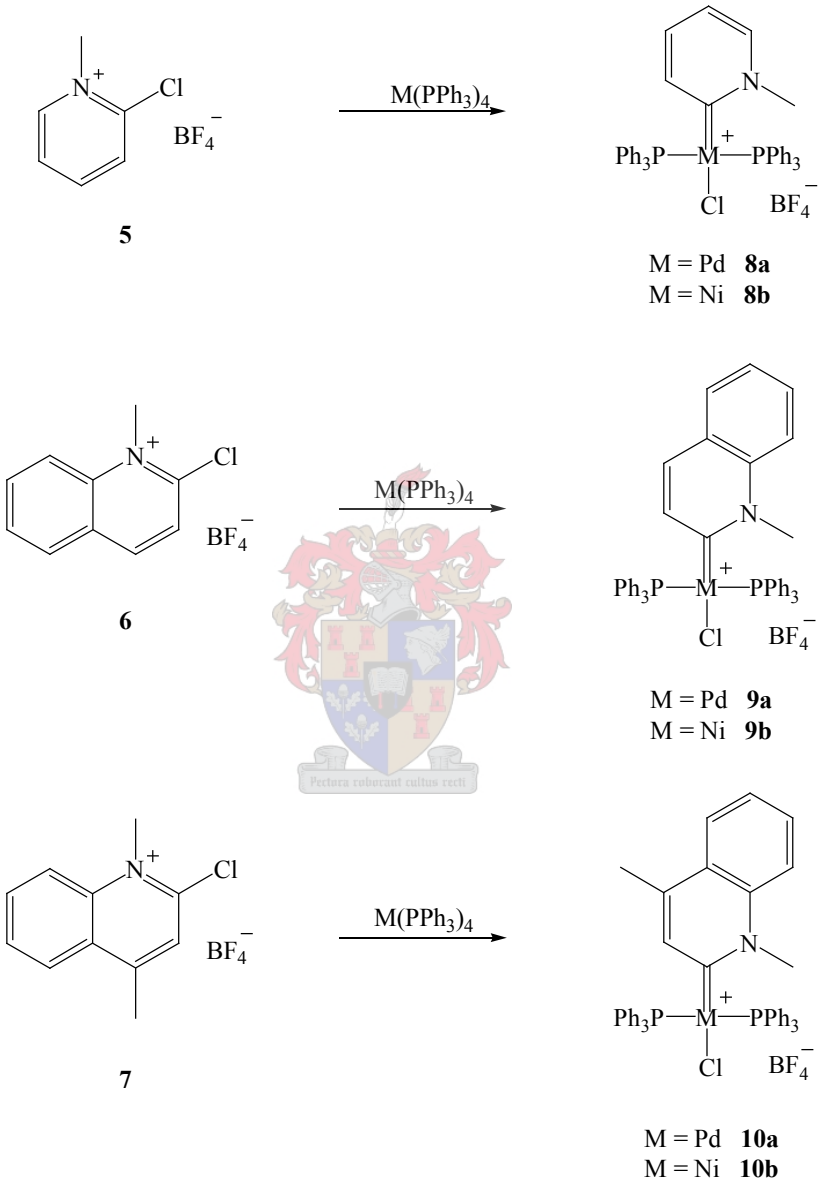

Scheme 2.8

2.2.8 Spectroscopic characterisation of complexes 8a, 8b, 9a, 9b, 10a and 10b

NMR spectroscopy

The assignments of the peaks in the NMR spectra were carried out with the aid of ghsqc (of **8b**, **9a**, **10b**) and ghmqc (of **10a**) two-dimensional NMR spectra.

2.2.8.1 **Trans-*chloro(1-methyl-1,2-dihydro-pyridin-2-ylidene)bis(triphenylphosphine) palladium(II) tetrafluoroborate, 8a, and* trans-*chloro(1-methyl-1,2-dihydro-pyridin-2-ylidene)bis(triphenylphosphine)nickel(II) tetrafluoroborate, 8b***

The ^{1}H NMR data of complexes **8a** and **8b** are summarized in Table 2.10. All the protons of the carbene ligand in complexes **8a** and **8b**, due to coordination, appear at a higher field compared to the signals for compound **5**. Stone and co-workers also observed this upfield shift when they prepared the Ir and Rh complexes of compound **5** *via* oxidative addition.[7] The ^{1}H NMR data of **8a** and **8b** are similar to those reported for *trans*-chloro(1-methyl-1,2-dihydro-pyridin-2-ylidene)bis(triethylphosphine)palladium(II) perchlorate,[10] *trans*-chloro(1,2-dihydro-pyridin-2-ylidene)bis(triphenylphosphine)palladium(II) perchlorate and *trans*-chloro(1,2-dihydro-pyridin-2-ylidene)bis(triethylphosphine)palladium(II) perchlorate[11] with the difference that H^6 resonates downfield from H^3 in these reported complexes. The proton signals of the carbene ligands in the complexes with PEt_3 as ligand have lower chemical shifts than those in complexes with PPh_3 as ligand because PPh_3 has a greater shielding effect on these protons than PEt_3 (and PMe_2Ph).[10]

The doublet at the lowest field (δ 7.80) in the ^{1}H NMR spectrum of complex **8a**, is assigned to H^3. H^3 appeared Δδ 0.26 upfield from H^3 in ligand **5**. Coupling of H^3 with H^4 and H^5 is observed with the coupling constants of 6.0 Hz and 1.3 Hz respectively. The chemical shift of H^6 could not be observed as it appears in the same region as the phenyl protons. The positive charge is primarily located on the metal. H^4 and H^5 appear together as a multiplet, upfield (Δδ 1.47 and Δδ 1.07 respectively) compared to H^4 and H^5 in ligand **5**. The largest upfield shift is observed for H^4 as it is more shielded in complex **8a** compared to H^4 in **5**. The singlet for NMe appears also upfield (Δδ 0.52) from NMe in ligand **5**.

The signals in the ^{1}H NMR spectrum of complex **8b** are assigned in the same manner as for complex **8a**. In a similar fashion to complex **8a**, the signals ($\Delta\delta$ 0.21 – 1.55) in the spectrum of complex **8b** are observed upfield compared to the corresponding signals for ligand **5**. The signal of H^4 is shielded more than the other protons ($\Delta\delta$ 1.55). H^4 and H^5 are well resolved and H^4 appears as a triplet of doublets, while H^5 appeared as a multiplet at highest field. H^5 in complex **8b** is observed more upfield than H^5 in complex **8a** while NMe in complex **8a** resonates more upfield than NMe in complex **8b**.

Table 2.10 ^{1}H, ^{13}C and ^{31}P NMR data of complexes **8a** and **8b** in CD_2Cl_2

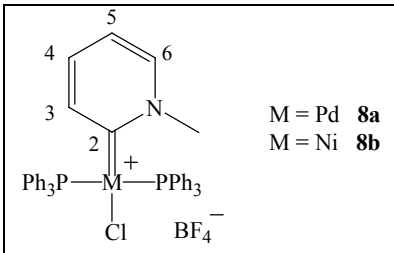

Assignment	δ / ppm **8a**	δ / ppm **8b**
^{1}H NMR		
H^3	7.80 (1H, dd, $^{3}J_{H-H}$ = 6.0 Hz, $^{4}J_{H-H}$ = 1.3 Hz)	7.85 (1H, m)
Ph, H^6	7.54, 7.42 (31H, 2 x m)	7.56, 7.42 (31H, 2 x m)
H^5, H^4	6.99 (1H, m)	
H^4		6.91 (1H, td, $^{3}J_{H-H}$ = 7.8 Hz, $^{4}J_{H-H}$ = 1.3 Hz)
H^5		6.80 (1H, m)
NMe	3.94 (3H, s)	4.21 (3H, s)
^{13}C NMR		
C^2	189.5 (t, $^{2}J_{P-C}$ = 6.5 Hz)	193.5 (t, $^{2}J_{P-C}$ = 33.6 Hz)
C^6	145.4 (s)	145.7 (s)
C^3	138.2 (t, $^{3}J_{P-C}$ = 3.8 Hz)	138.1 (m)
C^4	137.4 (s)	134.8 (s)
C_{ortho}, C_{para}	134.4 (m), 131.9 (s)	134.5 (m), 131.8 (s)
C_{meta}, C_{ipso}	129.4 (m), 129.00 (m)	129.4 (m), 129.2 (m)
C^5	122.4 (s)	121.5 (s)
NMe	52.8(s)	52.4 (s)
^{31}P NMR		
PPh_3	22.8 (s)	21.1 (s)

In the ^{13}C NMR spectrum of **8a** the carbene carbon, C^2, appears as a triplet at δ 189.5, 41.6 and 28.3 ppm downfield compared to C^2 in **5** and **3a** respectively. The phosphorus-carbon coupling for C^2 of 6.5 Hz, is smaller than the coupling in **3a** (11 Hz). The chemical shift and the coupling constant are similar to those (δ 185, $^2J_{P\text{-}C}$ = 7.5 Hz) reported for *trans*-chloro(1-methyl-1,2-dihydro-pyridin-2-ylidene)bis(triethylphosphine)palladium(II) perchlorate.[10] All signals for the protons in the ^1H NMR spectrum of complex **8a** have moved upfield compared to ligand **5**, but not all the carbon signals display this upfield shift in the ^{13}C NMR spectrum of **8a**. Similar to C^2, the signals for C^3 (Δδ 8.1) and NMe (Δδ 4.3) also resonate downfield compared to the same signals in ligand **5** while the signals for C^6 (Δδ 3.6), C^4 (Δδ 10.0) and C^5 (Δδ 4.7) appear upfield. This phenomenon can be explained in terms of the components that contribute to the total chemical shift (σ) namely a paramagnetic contribution (σ_p) and a diamagnetic contribution (σ_d) in the equation $\sigma = \sigma_p + \sigma_d$. The paramagnetic component (σ_p) can be ignored in ^1H NMR where the chemical shifts reflect shielding and deshielding.[59] The diamagnetic contribution (σ_d) plays a more significant role in ^{13}C NMR and cannot be ignored. The ^{13}C NMR chemical shifts of the signals for C^2, C^3 and NMe do not reflect shielding experienced by the protons. The triplet at δ 138.2 is assigned to C^3. The coupling between C^3 and the P-atoms of the PPh_3 ligands is 3.8 Hz. The phenyl carbon resonances in **8a**, **8b**, **3a** and **3b** are alike.

The carbene carbon atom, C^2, of complex **8b** also appears as a triplet at δ 193.5 with a coupling constant of 33.6 Hz due to carbon-phosphorus coupling. C^2 appears 45.6 ppm downfield from C^2 in ligand **5**. The chemical shift of the carbene signals in **8a** and **4b** (δ 197.7) are comparable, while this signal for **3b** (δ 158.6) appears at a higher field. The coupling constant for the phosphorus-carbon coupling of the carbene carbon in complex **8b** is similar to the same coupling constant in **3b** and **4b**. Similarly the signals for C^3 (Δδ 8.0) and NMe (Δδ 3.9) in **8a** appear downfield compared to corresponding signals in ligand **5** whereas C^6 (Δδ 3.3), C^4 (Δδ 12.6) and C^5 (Δδ 5. 6) have moved upfield. The signal for C^4 is more shielded (Δδ 2.6) in complex **8b** than in complex **8a** while the shifts of the other signals are comparable. A multiplet is observed for C^3 in the ^{13}C NMR spectrum of **8b** indicating carbon-phosphorus coupling does occur but the coupling constant could not be determined.

---

[59] R.F. Fenske in: B.L. Shapiro (Ed), *Organometallic Compounds, Synthesis, Structure and Theory*, Texas A & M University Press, Texas, 1983, p 305.

The signals for the two equivalent P-atoms in complex **8a** and **8b** appear as singlets at δ 22.8 and δ 21.1 respectively in the ^{31}P NMR spectra for these complexes. These resonances are the same as the corresponding resonances in **3a**, **3b**, **4b** and *trans*-chloro(1,2-dihydro-pyridin-2-ylidene)bis(triethylphosphine)nickel(II) perchlorate.[11] The *trans* positioning of the PPh_3-ligands, deduced from the ^{31}P NMR spectra has been confirmed by the single crystal structure determination of **8a** and **8b** (Section 2.2.17).

2.2.8.2 **Trans-***chloro(1-methyl-1,2-dihydro-quinolin-2-ylidene)bis(triphenylphosphine) palladium(II) tetrafluoroborate, 9a, and* **trans-***chloro(1-methyl-1,2-dihydro-quinolin-2-ylidene)bis(triphenylphosphine)nickel(II) tetrafluoroborate, 9b*

The NMR data of complexes **9a** and **9b** are summarized in Table 2.11. Similar to complexes **8a** and **8b**, all the signals in the ^{1}H NMR spectra of both **9a** and **9b** are found upfield when compared to the same signals in compound **6.** The greatest upfield change in chemical shift in the ^{1}H NMR spectrum of **9a** are observed for H^4 (Δδ 1.36) and H^8 (Δδ 0.99) because these two protons are more deshielded as a result of the resonance effect in compound **6** while in complex **9a** the deshielding is minimized with the positive charge now located primarily on the metal. The doublet of doublets at lowest field (δ 7.81) in the ^{1}H NMR spectrum of **9a** is assigned to H^5. This proton experiences coupling with H^6 and H^7. The multiplet at δ 7.78 is assigned to H^7 while H^3 and H^6 appear together as one multiplet (δ 7.68). H^4 (δ 7.61) and H^8 (δ 7.43) both are observed as a doublet each. The singlet assigned to NMe appears upfield (Δδ 0.24) when compared to the same signal for compound **6**. The signals for the phenyl protons are normal.

Despite several attempts, a well-resolved ^{1}H NMR spectrum of **9b** could not be obtained and the signals of H^7, H^6, H^4 and H^3 (δ 7.53) could not be assigned unambiguously. H^8 (δ 7.43) resonates 0.97 ppm upfield and H^5 (δ 7.81) 0.49 ppm upfield compared to the chemical shift of the corresponding protons in ligand precursor **6**. The chemical shift of the NMe signal in the spectrum of **9b** and **6** are the same (while the singlet assigned to NMe for **9a** is upfield).

Table 2.11 ^{1}H, ^{13}C and ^{31}P NMR data of complexes **9a** and **9b** in CD_2Cl_2

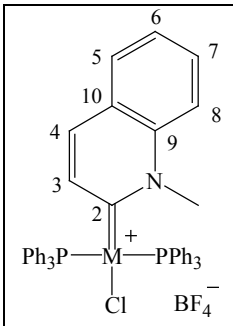

M = Pd **9a**
M = Ni **9b**

Assignment	δ / ppm **9a**	δ / ppm **9b**
^{1}H NMR		
H^5	7.81 (1H, dd, $^{3}J_{H-H}$ = 8.1 Hz, $^{4}J_{H-H}$ = 1.2Hz)	8.12 (1H, d, $^{3}J_{H-H}$ = 8.8 Hz)
H^7	7.78 (1H, m)	7.53 (1H, m)
H^3, H^6	7.68 (2H, m)	7.53 (2H, m)
H^4	7.62 (1H, d, $^{3}J_{H-H}$ = 8.3 Hz)	7.53 (1H, m)
Ph	7.56, 7.37, 7.28 (30H, 3 x m)	7.60, 7.40, 7.28 (30H, 3 x m)
H^8	7.43 (1H, d, $^{3}J_{H-H}$ = 8.7 Hz)	7.47 (1H, d, $^{3}J_{H-H}$ = 8.8 Hz)
NMe	4.22 (3H, s)	4.43 (3H, s)
^{13}C NMR		
C^2	199.9 (t, $^{2}J_{P-C}$ = 5.5 Hz)	207.0 (t $^{2}J_{P-C}$ = 31.6 Hz)
C^9	140.7 (s)	141.8 (s)
C^4	138.1 (s)	135.1 (s)
C_{ortho}, C_{para},	134.3 (m), 131.8 (s)	134.5 (m), 131.9 (s)
C_{meta}, C_{ipso}	129.1 (m), 128.6 (m)	129.3 (m), 128.7 (m)
C^7	133.4 (s)	133.1 (s)
C^3	132.0 (t, $^{3}J_{P-C}$ = 3.7 Hz)	131.5 (t, $^{3}J_{P-C}$ = 3.7 Hz)
C^5	130.0 (s)	130.3 (s)
C^6	128.9 (s)	128.9 (s)
C^{10}	126.6 (s)	126.4 (s)
C^8	116.8 (s)	115.8 (s)
NMe	49.5 (s)	49.5 (s)
^{31}P NMR		
PPh_3 *trans*	22.2 (s)	21.2
PPh_3 *cis* at -20°C	31.1 ($^{2}J_{P-P}$ = 26.6 Hz), 21.0 ($^{2}J_{P-P}$ = 26.6 Hz)	

Pectora roborant cultus recti

C^2 is observed as a triplet at δ 199.9 with a phosphorus-carbon coupling of 5.5 Hz, in the ^{13}C NMR spectrum of **9a**. The coupling constant compares well with that of complex **8a** ($^2J_{P-C}$ = 6.5 Hz). The signal appears 47.5 and 10.4 ppm downfield compared to the signal for C^2 of ligand precursor **6** and complex **8a** respectively. Similar to complexes **8a** and **8b**, the chemical shifts of all the signals in the ^{13}C NMR spectrum of **9a** do not reflect the deshielding (or shielding) displayed by the protons in the carbene ligand. C^4, C^7, C^6, C^{10} and C^8 appeared upfield (Δδ 2.0 –10.3) while C^3 (Δδ 7.2) and NMe (Δδ 7.3) like C^2 appears downfield compared to the corresponding signals in compound **6**. The chemical shifts of C^9 and C^5 in **9a** and **6** are the same. C^3 is observed as a triplet as a result of phosphorus-carbon coupling with a coupling constant of 3.7 Hz. The coupling constant is the same as determined for the same coupling in **8a**. The resonances for the phenyl carbons are similar to those observed for **8a** and **8b**.

The assignment of the signals in the ^{13}C NMR spectrum of **9b** has been done in similar fashion to **9a**. The carbene carbon, C^2 appears as a doublet at δ 207.0, 54.6 and 13.5 ppm downfield compared to C^2 in **6** and **8b**. The phosphorus-carbon coupling constant of 31.6 Hz compares well with that of **8b**. The same up and downfield shifts of signals in the ^{13}C NMR spectrum compared to that of **6** are observed for **9b** as were for **9a.** C^9 and C^5 in both **9a** and **6** have the same chemical shifts. C^3 in complex **9b** couples with the two equivalent P-atoms with a coupling constant of 3.7 Hz and appears as triplet in the ^{13}C NMR spectrum as is also observed for **9a**. The signals assigned to the phenyl carbons are similar to those of **8a**, **8b** and **9a**.

The signal for the two equivalent PPh_3 ligands in complexes **9a** and **9b** are observed as singlets at δ 22.2 and δ 21.2 respectively in the ^{13}P NMR spectra of the two complexes. The chemical shifts of these signals are the same as those in complexes **8a** and **8b**. The molecular structures of ***trans*-9a** (crystallysed at room temperature) and ***cis*-9a** (crystallysed at –20°C) were determined (Section 2.2.17). Therefore, the ^{31}P NMR of **9a** was also recorded at –20°C where the two doublets resulting from the presence of ***cis*-9a** in low a concentration are present. The two doublets (δ 31.1 and 21.0) show the coupling of the two P atoms at 26.6 Hz. These values are the same as those (δ 31.8 and 21.2, $^2J_{P-P}$ = 24 Hz) that are known for *cis*-chloro(1,3-dimethyl-2,3,4,5-tetrahydro-1*H*-imidazol-2-ylidene)bis(triphenylphosphine)palladium(II) hexafluorophosphate.[15]

2.2.8.3 **Trans-*chloro(1,4-dimethyl-1,2-dihydro-quinolin-2-ylidene)bis(triphenylphosphine) palladium(II) tetrafluoroborate, 10a, and* trans-*chloro(1,4-dimethyl-1,2-dihydro-quinolin-2-ylidene)bis(triphenylphosphine)nickel(II) tetrafluoroborate, 10b***

The signals in the NMR spectra of complexes **10a** and **10b** (Table 2.12) have been assigned using the same principles applied for **9a** and **9b**. A well-resolved ^{1}H NMR spectrum of complex **10b** could not be obtained, and the unambiguous assignment of the multiplets observed for the protons of the carbene ligand was not possible. The signals for all the protons in both **10a** and **10b** appear upfield compared to those of compound **7**. This trend is also observed for **8a**, **8b**, **9a** and **9b**. H^5 resonates at lower field in the ^{1}H NMR spectrum of **10a**, 0.58 ppm upfield compared to the signal of H^5 in **7**. H^5 also resonates at lower field in the ^{1}H NMR spectrum of **9a** and **9b**. The upfield shift ($\Delta\delta$ 1.5) of the singlet assigned to H^8 is the largest of all the protons. NMe appears at the same chemical shift in the ^{1}H NMR spectrum of both **10b** and ligand **7** and this phenomenon is similar to that of complex **9b** and ligand **6**. The chemical shift of the CMe protons is found at higher field ($\Delta\delta$ 0.79) compared to the CMe resonance for **7**.

C^2, C^3 and NMe in the ^{13}C NMR spectra of **10a** and **10b** appear downfield ($\delta\Delta$ 7.4 – 47.7), while the signals for the other carbon atoms appear upfield ($\delta\Delta$ 2 – 12.1) compared to the corresponding signals of **7**. The chemical shift of C^9 in **10a**, **10b** and **7** is virtually the same. The chemical shift of the triplet assigned to the carbene carbon, C^2, in the ^{13}C NMR spectrum of **10a** and **10b** and the coupling constant for the carbon-phosphorus coupling compares well with the other palladium (**8a** and **9a**) and nickel complexes (**8b** and **9b**) respectively. A multiplet is observed for C^3 in both **10a** and **10b**, indicating carbon-phosphorus coupling.

The signals in the ^{13}P NMR spectra of **10a** and **10b** are as expected and compare well with the other palladium and nickel complexes respectively, that have been discussed above.

Table 2.12 ^{1}H, ^{13}C and ^{31}P NMR data of complexes **10a** and **10b** in CD_2Cl_2

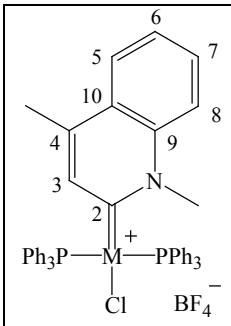

M = Pd **10a**
M = Ni **10b**

Assignment	δ / ppm **10a**	δ / ppm **10b**
^{1}H NMR		
H^5	7.84 (1H, dd, $^{3}J_{H-H}$ = 7.4 Hz, $^{4}J_{H-H}$ = 1.2Hz)	7.60 (1H, m)
H^7	7.78 (1H, m)	7.60 (1H, m)
H^6	7.68 (1H, m)	7.60 (1H, m)
Ph	7.57, 7.37, 7.28 (30H, 3 x m)	7.62, 7.38, 7.29 (30H, 3 x m)
H^8	7.48 (1H, d, $^{3}J_{H-H}$ = 8.8 Hz)	7.60 (1H, m)
H^3	7.34 (1H, s)	7.60 (1H, m)
NMe	4.31 (3H, s)	4.60 (3H, s)
CMe	2.26 (3H, s)	2.22 (3H, s)
^{13}C NMR		
C^2	198.8 (t, $^{2}J_{P-C}$ = 4.9 Hz)	205.2 (t, $^{2}J_{P-C}$ = 31.8 Hz)
C^4	148.1 (s)	144.8 (s)
C^9	139.8 (s)	140.7 (s)
C_{ortho}, C_{para}	134.3 (m), 131.7 (s)	134.4 (m), 131.8 (s)
C_{meta}, C_{ipso}	129.0 (m), 128.8 (m)	129.2 (m), 129.0 (m)
C^7	133.0 (s)	132.6 (s)
C^3	132.6 (m)	132.4 (m)
C^6	128.6 (s)	128.4 (s)
C^{10}	126.1 (s)	126.2 (s)
C^5	126.0 (s)	126.2 (s)
C^8	117.1 (s)	115.9 (s)
NMe	49.2 (s)	49.3 (s)
CMe	19.3 (s)	19.0 (s)
^{31}P NMR		
PPh_3	22.5 (s)	21.2 (s)

Mass spectrometry

The FAB mass spectrometry data for complexes **8a** – **10b** are summarized in Table 2.13. All the complexes show a similar fragmentation pattern and the cation is observed as the fragment with highest m/z value. The loss of one PPh_3 ligand is followed by the loss of Cl. A fragment indicating the loss of the carbene ligand (L) is only observed for complex **10a**.

Table 2.13 Mass spectrometry data for Pd complexes **8a** – **10b**

Complex	m/z	Relative intensity (%)	Fragment ion
8a	758	7	$[M - BF_4]^+$
	498	5	$[M - BF_4 - PPh_3]^+$
	461	5	$[M - BF_4 - PPh_3 - Cl]^+$
8b	710	25	$[M - BF_4]^+$
	448	76	$[M - BF_4]^+ - PPh_3$
	413	35	$[M - BF_4 - PPh_3 - Cl]^+$
9a	809	17	$[M - BF_4]^+$
	546	12	$[M - BF_4 - PPh_3]^+$
	510	7	$[M - BF_4 - PPh_3 - Cl]^+$
9b	761	14	$[M - BF_4]^+$
	499	36	$[M - BF_4 - PPh_3]^+$
	464	11	$[M - BF_4 - PPh_3 - Cl]^+$
10a	823	12	$[M - BF_4]^+$
	562	10	$[M - BF_4 - PPh_3]^+$
	524	6	$[M - BF_4 - PPh_3 - Cl]^+$
	368	5	$[M - BF_4 - PPh_3 - Cl - L]^+$
10b	775	12	$[M - BF_4]^+$
	512	24	$[M - BF_4 - PPh_3]^+$
	477	9	$[M - BF_4 - PPh_3 - Cl]^+$

C. Heterocyclic carbene complexes with their N atoms remote from the carbene carbons (one-N, six-membered rNHC complexes)

2.2.9 Synthesis of 4-chloro-2-methoxy-1-methylquinolinium tetrafluoroborate, 11, and 4-chloro-1-methylpyridinium tetrafluoroborate, 12

Compound **11** was prepared by *N*-methylation of 4-chloro-1-methyl-1*H*-quinolin-2-one with $[Me_3O][BF_4]$ in CH_2Cl_2:CH_3CN (3:1) as solvent system (Scheme 2.9) in a yield of 36%.[18] Compound **12** was prepared in the same manner, in a yield of 81%, but only after the 4-chloropyridine hydrochloride had been treated with aqueous NaOH. The 4-chloropyridine was extracted with diethyl ether. The ligand precursors **11** and **12** are soluble in polar solvents like CH_2Cl_2 but less soluble to insoluble in diethyl ether, THF and other non-polar solvents like pentane.

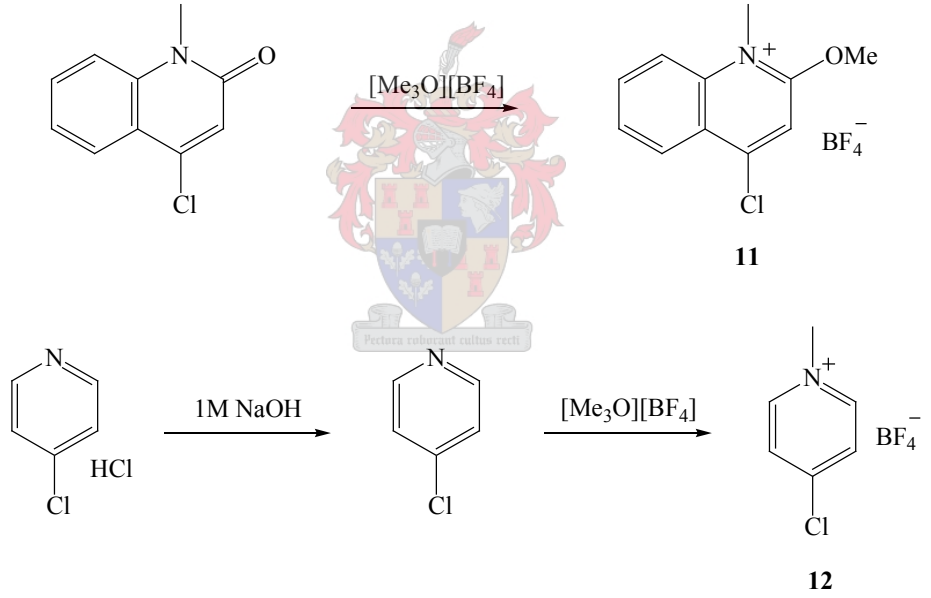

Scheme 2.9

2.2.10 Spectroscopic characterisation of 4-chloro-2-methoxy-1-methylquinoliniumtetrafluoroborate, 11, 4-chloro-1-methylpyridinium tetrafluoroborate, 12

NMR spectroscopy.

The NMR data of compound **11** agree with the data previously reported.[18]

2.2.10.1 Spectroscopic characterisation of 4-chloro-1-methylpyridinium tetrafluoroborate, 12

The assignments of the signals were confirmed with gshqc and gshqm two-dimensional NMR experiments. The NMR data of ligand **12** are summarized in Table 2.14. The two doublets (δ 8.69 and δ 7.99) in the ^{1}H NMR spectrum of **12** are assigned to H^2, H^6 and H^3, H^5 respectively. H^2 and H^6 resonate at a lower field than H^3 and H^5 because the neighbouring N atom deshields these protons more. H^2 and H^6 might be deshielded even more as a result of the resonance effect, illustrated by the resonance structures of ligand **12** (Scheme 2.10). The chemical shift of the NMe protons (δ 4.40) is comparable to the NMe resonance for ligands **5** – **7**.

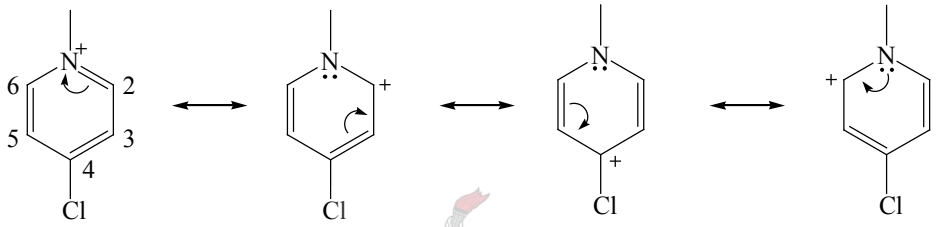

Scheme 2.10

Table 2.14 ^{1}H and ^{13}C NMR data of ligand **12** in CD_2Cl_2

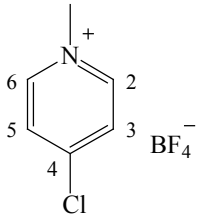

Assignment	δ / ppm
^{1}H NMR	
H^2, H^6	8.69 (2H, d, $^{3}J_{H\text{-}H}$ = 7.1 Hz)
H^3, H^5	7.99 (2H, d, $^{3}J_{H\text{-}H}$ = 6.6 Hz)
NMe	4.40 (3H, s)
^{13}C NMR	
C^4	154.6 (s)
C^2, C^6	146.5 (s)
C^3, C^5	129.0 (s)
NMe	48.9(s)

The singlet at lowest field is assigned to C^4. C^4 is well deshielded by the electronegative Cl-atom and as a result of the resonance effect in the ligand. C^2 and C^6 are less deshielded than C^4 despite their location next to the N-atom and resonate at higher field than C^4 ($\Delta\delta$ 8.1).

Mass spectrometry

The structure of compound **12** was confirmed by FAB MS. The cation is observed as the only peak in the mass spectrum of **16**.

2.2.11 Synthesis of complexes 13a, 13b, 13c, 14a and 14b.

Complex **13a**, **13c** and **14a** were prepared in the same manner as complexes **8a**, **9a** and **10a** in reasonable to good yields (78 – 95%), according to the reaction shown in Scheme 2.11. Complex **13c** is the exception, as ***cis*-13c** was isolated as the kinetic product, while the trans products for the other compounds were found. This *cis* product isomerises to the thermodynamic *trans* product in solution (CD_2Cl_2) and both isomers are present in solution at room temperature in a *cis* : *trans* ratio of 2.5 : 1.

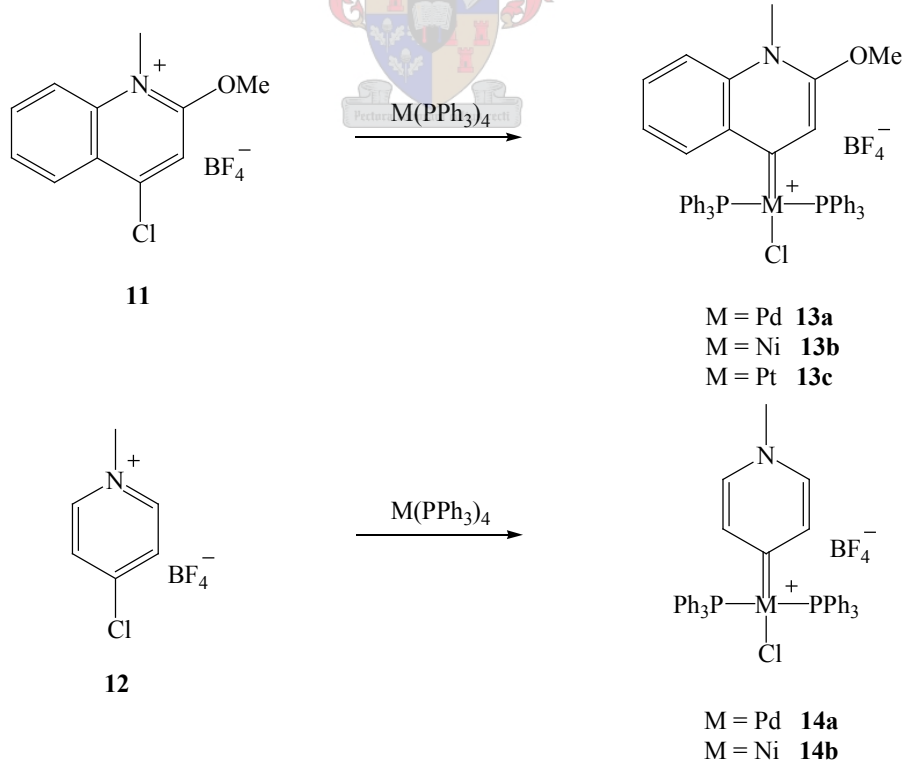

Scheme 2.11

Complexes **13b** and **14b** were prepared similarly to complexes **8b**, **9b** and **10b**. The yield of complex **13a** was 66% while complex **14b** could only be isolated in a very low yield of 6%. These microcrystalline materials are soluble in polar solvents like dichloromethane and acetone and insoluble in pentane and diethyl ether.

2.2.12 Spectroscopic characterisation of complexes 13b, 14a and 14b

NMR spectroscopy.

The assignments of the peaks in the NMR spectra were performed with the aid of ghsqc (of **13b** and **14a**) and ghmqc (of **13b**) two-dimensional NMR spectra. The NMR data of complexes **13a** and **13c** have been reported previously.[18]

2.2.12.1 Trans-*chloro(2-methoxy-1-methyl-1,4-dihydro-quinolin-4-ylidene)bis (triphenylphosphine)nickel(II) tetrafuoroborate, 13b*

The NMR data of complex **13b** are summarised in Table 2.15. All the signals for the protons move upfield (Δδ 0.24 - 0.89) compared to the same signals observed for compound **11** except for H^5, which moved downfield by 1.21 ppm. This downfield shift of H^5 is also observed for H^5 in **13a** (Δδ 0.40) and **13c** (Δδ 0.72) but the downfield shifts are smaller than those observed for **13b**. The signal for H^8 is not observed as it is masked by the signal for some the phenyl protons. As expected the singlet due to OMe resonates at lower field than that of the NMe.

Table 2.15 ^{1}H, ^{13}C and ^{31}P NMR data of complex **13b** in CD_2Cl_2

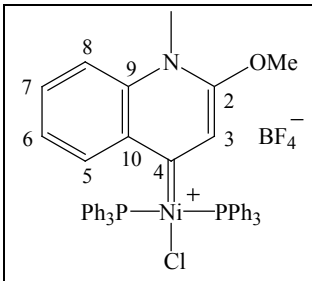

Assignment	δ / ppm
^{1}H NMR	
H^5	9.70 (1H, dd, $^{3}J_{H-H}$ = 8.1 Hz, $^{4}J_{H-H}$ = 1.3Hz)
H^7	7.94 (1H, m)
Ph	7.59, 7.41, 7.30 (30H, 3 x m)
H^6	7.51 (1H, t, $^{3}J_{H-H}$ = 7.6 Hz)
H^8	7.41 (1H, m) masked by Ph
H^3	6.88 (1H, s)
OMe	3.81 (3H, s)
NMe	3.55 (3H, s)
^{13}C NMR	
C^4	215.3 (t, $^{2}J_{P-C}$ = 30.9 Hz)
C^2	151.7 (t, $^{4}J_{P-C}$ = 2.0 Hz)
C^5	135.0 (s)
C_{ortho}, C^7	134.9 (m)
C_{para}, C_{ipso}, C_{meta}	131.4 (s), 129.9 (m), 128.8 (m)
C^9	132.8 (s)
C^{10}	132.4 (s)
C^6	126.4 (s)
C^8	116.8 (s)
C^3	115.0 (t, $^{3}J_{P-C}$ = 3.9 Hz)
OMe	59.1 (s)
NMe	32.0 (s)
^{31}P NMR	
PPh_3	21.8 (s)

The carbene carbon, C^4, resonates as a triplet at δ 215.3 in the ^{13}C NMR spectrum of **13b**, 59.5 ppm downfield compared to C^4 in ligand **11**. It is of interest to note that this carbene carbon appears at

the lowest field of all the complexes prepared and characterised in this study including complex **13a** (C^4 at δ 208.1) and complex **13c** (C^4 at δ 201.8).[18] The coupling of C^4 with the two P-atoms is 30.9 Hz and compares well with the corresponding coupling constant for the other Ni-complexes (**4b**, **8b**, **9b**, **10b**). A downfield appearance (Δδ 7.3 – 9.1) compared to the signals in **11** is observed for C^5, C^{10} and C^3 and is similar to the signals downfield observed for **13a** and **13c** although the downfield resonance changes of C^4, C^{10} and C^5 are significantly larger for **13b**. The downfield movement of the signal for C^5 reflects the deshielding of H^5, while the chemical shift of C^3 does not reflect the shielding of H^3. All the signals for the other carbon atoms appear upfield when compared to the signals observed for ligand **11** and reflects the shielding of the protons in the ^{1}H NMR spectrum of **13b**. The upfield movement of the signal for C^6 is contrary to the downfield appearance of the signal of C^6 in **13a** and **13c** when compared to ligand **11**. The upfield move of the resonance of C^9 (Δδ 5.9) compared to ligand **11** is larger than that observed for **13a** (Δδ 2.1) and **13c** (Δδ 3.0).

The singlet at δ 21.8 for the two P-atoms in the ^{31}P NMR spectrum of **13b**, compares well with all the nickel (and palladium) complexes described in this chapter, but appears upfield by 6 ppm compared to the signal observed for **13a**.

Pectora roborant cultus recti

2.2.12.2 Trans-chloro(1-methyl-1,4-dihydro-pyridin-4-ylidene)bis(triphenylphosphine) palladium(II) tetrafluoroborate, 14a, and trans-chloro(1-methyl-1,4-dihydro-pyridin-4-ylidene)bis(triphenylphosphine)nickel(II) tetrafluoroborate, 14b

The NMR data for complexes **14a** and **14b** are summarized in Table 2.16. The signals for the phenyl protons appear where they are expected. H^3 and H^5 appear as a doublet at δ 7.33, due to coupling of 6.3 Hz with H^2 and H^6 respectively. H^2 and H^6 are also observed as a doublet at δ 7.08. H^3 and H^5 appear at a lower field than H^2 and H^6, the opposite from ligand **12**, and this change of positions can be attributed to the positive charge which is now located more on the metal and thus decreases the deshielding effect of the aromatic ring current on the protons of the carbene ligand. Similarly to complex **8a** and **9a**, the signals for the protons in the carbene ligand appear at a higher field (Δδ 0.63 – 1.61) when they are compared to the shifts of these protons in ligand **12**.

The ^{1}H NMR spectrum of **14b** is very similar to that of **14a**. However, H^3 and H^5 are not observed as their signals are obscured by the signals for the phenyl protons. H^2 and H^6 resonate at δ 6.84 as a doublet with coupling constant of 6.3 Hz. H^2 and H^6 (Δδ 1.85) and NMe (as a singlet, Δδ 0.73) appear upfield when compared to the signals in ligand **12**. This upfield movement of the signals is slightly larger for complex **14b** than for complex **14a**.

Table 2.16 ^{1}H, ^{13}C and ^{31}P NMR data of complexes **14a** and **14b** in CD_2Cl_2

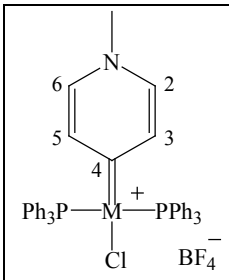

M = Pd **14a**
M = Ni **14b**

Assignment	δ / ppm **14a**	δ / ppm **14b**
^{1}H NMR		
Ph, H^3, H^5		7.67, 7.49, 7.40 (32H, 3 x m)
Ph	7.61, 7.48, 7.38 (30H, 3 x m)	
H^3, H^5	7.33 (2H, d, $^{3}J_{H-H}$ = 6.3 Hz)	
H^2, H^6	7.08 (2H, d, $^{3}J_{H-H}$ = 6.3 Hz)	6.84 (2H, d, $^{3}J_{H-H}$ = 6.3 Hz)
NMe	3.77 (3H, s)	3.67 (3H, s)
^{13}C NMR		
C^4	196.9 (t, $^{2}J_{P-C}$ = 5.5 Hz)	205.3 (t, $^{2}J_{P-C}$ = 31.6 Hz)
C^2, C^6	136.9 (s)	136.4 (s)
C^3, C^5	136.4 (t, $^{3}J_{P-C}$ = 3.7 Hz)	137.5 (m)
C_{ortho}, C_{para}	134.8 (m), 131.4 (s)	135.1 (m), 131.5 (s)
C_{ipso}, C_{meta}	129.6 (m), 128.9 (m)	130.0 (m), 129.1 (m)
NMe	46.4 (s)	46.1 (s)
^{31}P NMR		
PPh_3	23.2 (s)	22.8 (s)

In the ^{13}C NMR spectrum of **14a**, the carbene carbon, C^4, appears as a triplet at δ 196.9 downfield by 42.3 ppm when compared with C^4 in ligand precursor **12**. The coupling constant for the carbon-phosphorus coupling is 5.5 Hz. The chemical shift and phosphorus-carbon coupling are in the same order as those observed for **9a** and **10a**. The singlet at δ 136.9 is assigned to C^2 and C^6 and this

singlet appears upfield compared to the signal for C^2 and C^6 in **12**. This upfield change is due to less deshielding that C^2 and C^6 are experiencing in complex **14a**, where the positive charge is located more on the metal than on the N-atom, when compared to **12**. C^3 and C^5 appeared together as a triplet (7.4 ppm downfield from C^3 and C^5 in **12**) as a result of carbon-phosphorus coupling of 3.7 Hz. This coupling constant compares well with the coupling constant determined for C^3 in complex **8a** ($^3J_{PC}$ = 3.8 Hz). The singlet at δ 46.4 is assigned to NMe and is observed upfield (Δδ 2.5) from the singlet for NMe in ligand precursor **12**.

The signals in the ^{13}C NMR spectrum of **14b** are assigned in the same manner as for **14a**. The carbene signal is a triplet at δ 205.3 with a carbon-phosphorus coupling of 31.6 Hz. These values compare well with those listed for **9b** and **10b**. The carbene carbon appears 50.7 ppm downfield from the signal for C^4 in **12**. Similarly to **14a**, the signals for C^2, C^6 and NMe in **14b** resonate upfield while the C^3 and C^5 signals appear downfield compared to the corresponding signals in **12**. The coupling constant for the coupling of C^3 and C^5 and the two P-atoms of the two PPh_3 ligands could not be determined because C^3 and C^5 are observed together as a multiplet in the ^{13}C NMR spectrum of **14b**.

The chemical shifts for the P-atoms in the ^{31}P NMR spectra for **14a** (δ 23.2) and **14b** (δ 22.8) are of the same magnitude. Single crystal structure determinations of both complexes **14a** and **14b** confirm the *trans* disposition of the two PPh_3 ligands (Section 2.2.17).

Mass spectrometry

The FAB mass spectrometry data for complexes **13b, 14a** and **14b** are given in Table 2.17. The complexes exhibit a fragmentation pattern in which the cation is observed as the fragment with the highest molecular mass. The loss of one PPh_3 ligand is followed by the loss of Cl. The fragment, after the loss of the second PPh_3 ligand is only observed for complex **13b**.

Table 2.17 Mass spectrometry data for complexes **13b** – **14a**

Complex	m/z	Relative intensity (%)	Fragment ion
13b	791	6	$[M - BF_4]^+$
	528	26	$[M - BF_4 - PPh_3]^+$
	493	5	$[M - BF_4 - PPh_3 - Cl]^+$
	266	9	$[M - BF_4 - 2\ PPh_3]^+$
14a	760	4	$[M - BF_4]^+$
	498	12	$[M - BF_4 - PPh_3]^+$
	463	4	$[M - BF_4 - PPh_3 - Cl]^+$
14b	710	7	$[M - BF_4]^+$
	448	6	$[M - BF_4 - PPh_3]^+$
	413	5	$[M - BF_4 - PPh_3 - Cl]^+$

D. Heterocyclic carbene complexes with their active N atoms remote from the carbene carbons (based on 4,4-dimethyl-2-thiophen-2-yl-4,5-dihydro-oxazole)

The current investigation to prepare *r*NHC carbene complexes was extended to the synthesis of carbene complexes of chromium(0) and tungsten(0) with 4,4-dimethyl-2-thiophen-2-yl-4,5-dihydro-oxazole, **15**, as carbene ligand precursor (Scheme 2.13), as was mentioned in the introduction. Compound **16**, 4,4-dimethyl-2-(5-methyl-thiophen-2-yl)-4,5-dihydro-oxazole, produced by the selective methylation of **15** in the 5-position (Scheme 2.12), was also used as a carbene precursor. This position was blocked in an attempt to prepare diorgano carbene complexes chromium(0) and tungsten(0) with the $M(CO)_5$ group in the 3-position (Scheme 2.14). As mentioned before, in a diorgano carbene complex, the carbene carbon is not connected to a heteroatom but to two other carbon atoms.

2.2.13 Synthesis of CHSC(COCH$_2$CMe$_2$N)CHCH, 15, and CMeSC(COCH$_2$CMe$_2$N)CHCH], 16

Compounds **15** and **16** were prepared following literature procedures (Scheme 2.12).[60] Compound **15** resulted from the reaction of thiophene-2-carboxylic acid with thionyl chloride followed by the reaction of the resultant thiophene-2-carbonyl chloride with 2-amino-2-methylpropan-1-ol to produce *N*-(2-hydroxyl-1,1-dimethylethyl)thiophene-2-carboxamide. This amide was reacted with thionyl chloride in toluene to yield 4,4-dimethyl-2-thiophen-2-yl-4,5-dihydro-oxazole, **15**, after purification. Compound **15** was deprotonated selectively[60] at the 5-position with LDA (lithium diisoproplylamide) and alkylated with $CF_3SO_3CH_3$ to produce 4,4-dimethyl-2-(5-methyl-thiophen-2-yl)-4,5-dihydro-oxazole, **16**, in a yield of 80%. Compounds **16** and the unreacted **15** could not be separated chromatographically and this mixture was used without further purification.

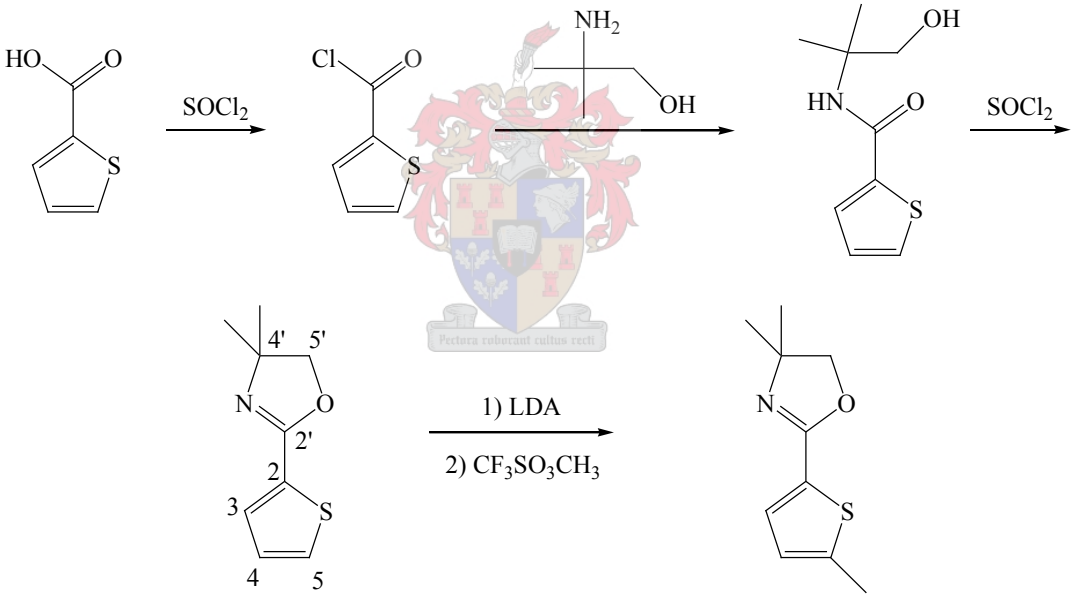

15 **16**

Scheme 2.12

[60] A.J. Carpenter, D.J. Chadwick, *J. Chem. Soc., Perkin Trans. I*, 1985, 173.

2.2.14 Synthesis of $(CO)_5Cr\{CSC(CNMeCMe_2CH_2O)CHCH\}$, 17a, and $(CO)_5W\{CSC(CNMeCMe_2CH_2O)CHCH\}$, 17b

Complexes **17a** and **17b** (Scheme 2.13) were prepared employing the same procedure as described by Stander[61] with the modification that THF was used as solvent rather than diethyl ether. THF facilitates homogeneous reaction conditions at –78°C. The best selectivity for deprotonation (ß-lithiation) at the 3-position is found when hexane (-78°C) is used as solvent and *n*-BuLi as base during this heterogeneous reaction.[60] Compound **15**, dissolved in THF, was treated with *n*-BuLi at -78°C. After 15 minutes the temperature was raised to –30°C before $[(CO)_5MX][NEt_4]$ (M = Cr or W, X = Cl or Br) was added to the reaction mixture. Methylation with $CF_3SO_3CH_3$ was carried out in CH_2Cl_2 (complex **17a**) or THF (complex **17b**) at an initial temperature of –50°C. The resultant residues were chromatographed and complexes **17a** and **17b** were isolated as the last fractions from the column.

The methylation with $CF_3CO_3CH_3$ in the preparation of complex **17b** should rather be carried out in CH_2Cl_2, as described for complex **17a**, as the work-up is easier and methylation with $CF_3CO_3CH_3$ in THF carries the risk of THF ring opening and polymerization. Complexes **17a** and **17b** are soluble in polar solvents (CH_2Cl_2 and THF) as well as in non-polar solvents like pentane.

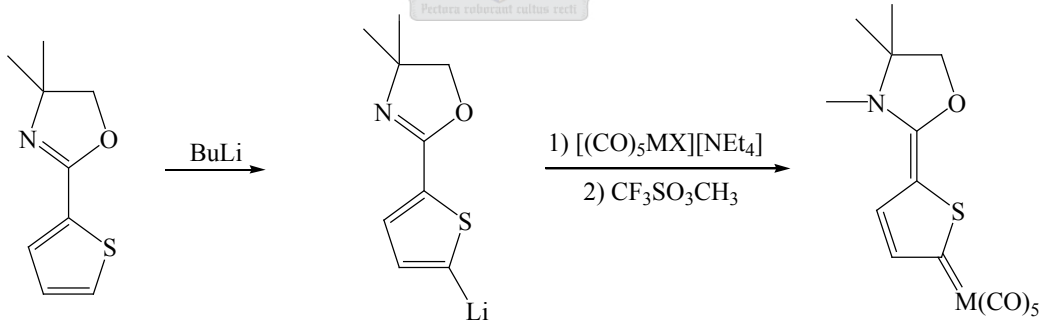

15

M = Cr **17a**
M = W **17b**

Scheme 2.13 X = Cl or Br

The attempt to prepare the diorgano carbene complexes **I** an **II** with C^3 as the carbene carbon (Scheme 2.14) were not successful. Complexes **17a** and **17b** were isolated and identified products

[61] Y. Stander, *M.Sc. Thesis*, Rand Afrikaans University, 1996, p. 110.

of these reactions, respectively. The formation of **17a** and **17b** is a result of the presence of compound **15**, that could not be separated form compound **16** that was metallated only, as shown in Scheme 2.13. The other compounds in the reaction mixtures were separated by column chromatography, but none could be identified as **I** or **II**.

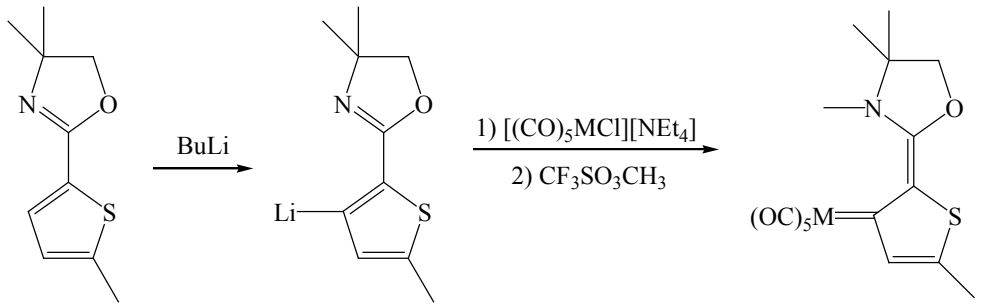

16

Scheme 2.14

2.2.15 Spectroscopic characterisation of $(CO)_5Cr\{\underline{CSC(\overline{CNMeCMe_2CH_2O})CHCH}\}$, 17a, and $(CO)_5W\{\underline{CSC(\overline{CNMeCMe_2CH_2O})CHCH}\}$, 17b

NMR spectroscopy

Preliminary NMR data of complexes **17a** and **17b** had been reported previously and were assigned on the premise that the matallation and trans metallation occurred in the 3-position of the oxazoline-containing carbene ligand.[61] The crystal structure determination of **17a** and **17b** now revealed that the $M(CO)_5$ group was in reality bonded in the 5-position and not in the 3-position (Section 2.2.17). The NMR data of these two complexes **17a** and **17b** (Table 2.18) are rather similar to those reported for these complexes previously, however, with some new observations that have to be taken into account. All the protons in **17a** and **17b** are deshielded ($\Delta\delta$ 0.15 – 0.54) compared to the corresponding signals in the spectrum of **15**. No resonance for H^5 was observed in the NMR spectrum of **17a** and **17b**. H^3 resonates at lowest field. H^3 and H^4 appeared as doublets as a result of their coupling to each other.

Table 2.18 ^{1}H and ^{13}C NMR data of complexes **17a** and **17b** in CD_2Cl_2

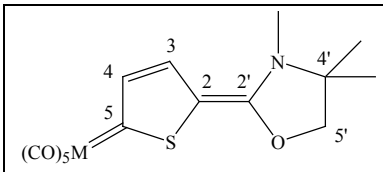

M = Cr **17a**
M = W **17b**

Assignment	δ / ppm **17a**	δ / ppm **17b**
^{1}H NMR		
H^3	7.93 (1H, d, $^{3}J_{H-H}$ = 3.7 Hz)	7.86 (1H, d, $^{3}J_{H-H}$ = 3.7 Hz)
H^4	7.54 (1H, d, $^{3}J_{H-H}$ = 3.7 Hz)	7.60 (1H, d, $^{3}J_{H-H}$ = 3.7 Hz)
$H^{5'}$	4.52 (2H, s)	4.53 (2H, s)
NMe	3.41 (3H, s)	3.41 (3H, s)
C(*Me*$_2$)	1.48 (6H, s)	1.49 (6H, s)
^{13}C NMR		
CO_{trans}	226.2 (s)	205.8 (s, J_{W-C} = 136.2 Hz)
CO_{cis}	220.6 (s)	200.5 (s, J_{W-C} = 125.9 Hz)
C^5	-	200.3 (s)
$C^{2'}$	-	161.0 (s)
C^2	143.2 (s)	143.9 (s)
C^3	138.5 (s)	139.4 (s)
C^4	132.9 (s)	122.1 (s)
$C^{5'}$	80.1 (s)	80.2 (s)
$C^{4'}$	66.5 (s)	66.6 (s)
NMe	29.6 (s)	29.7 (s)
C(*Me*)$_2$	24.1 (s)	24.1 (s)

Pectora roborant cultus recti

The signal for the carbene carbon and $C^{2'}$ is not observed in the ^{13}C NMR spectrum of **17a** but, nevertheless, the structure was confirmed by the single crystal structure determination (Section 2.2.17). The atoms, C^2, C^3 and C^4 resonate at lower field and C(*Me*)$_2$ at higher field compared to the same resonances in **15**, while $C^{5'}$, $C^{4'}$ have similar chemical shifts compared to those in **15**. The carbene signal (C^5) of **17b** is observed δ 200.3 as a singlet and not at δ 191.3 [$W(CO)_6$!] as reported previously.[61] This signal appears downfield by 70.6 ppm in comparison with the C^5 signal (δ 129.7) in compound **15**. The carbons in **17b** are deshielded compared to the carbons in **15**, while the $C^{5'}$, $C^{4'}$ resonances do not change after complex formation. In contrast to **17a**, C^4 in **17b** is shielded by 5.7 ppm. The tungsten-carbon couplings are only observed for the carbonyl signals. These

couplings are similar to those observed for the tungsten complexes reported in literature (and in Chapter 4).[62]

Mass spectrometry

The fragmentation patterns for complexes **17a** and **17b** are shown in Table 2.19. The molecular ion peaks for both complexes are observed. The sequential loss of the CO ligands in complexes **17a** (5 CO ligands) and **17b** (3 CO ligands) is followed by the dissociation of the carbene ligand from the metal. The fragments representing the carbene ligands have the largest intensities.

Table 2.19 Mass spectrometry data for complexes **17a** and **17b**

Complex	m/z	Relative intensity (%)	Fragment ion
17a	387	9	M^+
	359	3	$[M - CO]^+$
	331	5	$[M - 2CO]^+$
	303	4	$[M - 3CO]^+$
	275	9	$[M - 4CO]^+$
	247	6	$[M - 5CO]^+$
	196	36	$[CSC(COCH_2CMe_2NMe)CHCH]^+$
17b	519	9	M^+
	491	4	$[M - CO]^+$
	463	5	$[M - 2CO]^+$
	435	7	$[M - 3CO]^+$
	196	41	$[CSC(COCH_2CMe_2NMe)CHCH]^+$

Infrared spectroscopy

The IR spectra of compounds **17a** and **17b** (Table 2.20) are typical for octahedral transition metal pentacarbonyl complexes. The local symmetry of the $M(CO)_5$ unit is C_{4v} and the expected four

[62] K. Issberner, E. Niecke, E. Wittchow, K.H. Dötz, M. Nieger, *Organometallics*, 1997, **16**, 2370.

infrared active bands are observed for **17b**.[63,64,65] The normally weak B_1 band is not present in the spectrum of **17a**.

Table 2.20 The infrared data of complexes **17a** and **17b** in CH_2Cl_2

Complex	ν(CO) / cm^{-1} (Intensity)	Assignment
17a	2045 (m)	$A_1^{(1)}$
	1918 (s)	E
	1881 (sh)	$A_1^{(2)}$
17b	2054 (m)	$A_1^{(1)}$
	1958 (w)	B_1
	1914 (s)	E
	1881 (sh)	$A_1^{(2)}$

2.2.16 Platinum analogues: Complications and side reactions.

During the attempted preparation of the platinum(II) carbene complexes using the ligands shown in Scheme 2.15 by oxidative substitution of the ligand precursors to $Pt(PPh_3)_4$ in toluene, the unexpected formation of $[PtCl(PPh_3)_3]BF_4$ and in some reactions, an unknown platinum phosphine complex, were observed. Subsequently, the reactions were carried out in toluene at 60°C and then at room temperature to establish the role of temperature in these complicating reactions. Precipitates formed during these procedures were collected by filtration, washed with toluene and stripped of solvent in vacuum. The ^1H and ^{31}P NMR and FAB-MS data of the residues were obtained.

Pectora roborant cultus recti

[63] S. Lotz, *Ph.D. Dissertation*, Rand Afrikaans University, 1978.

[64] J.A. Connor, E.O. Fischer, *J. Chem. Soc. (A)*, 1969, 578.

[65] E.O. Fischer, H-J. Kollmeier, *Chem. Ber.*, 1971, **104**, 1339.

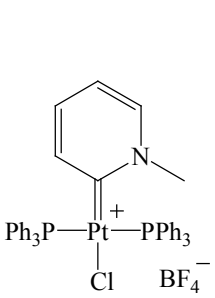

***trans*-8c**

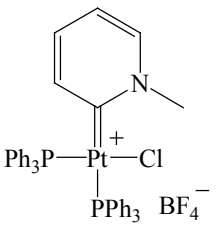

***cis*-8c**

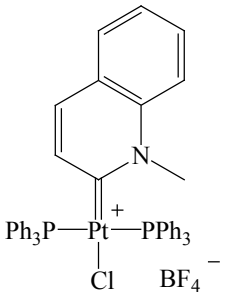

***trans*-9c**

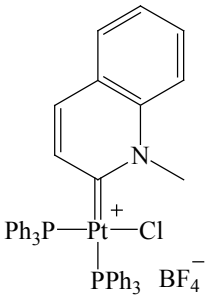

***cis*-9c**

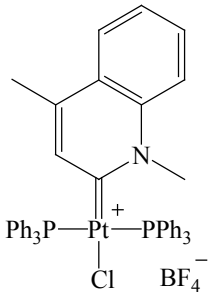

***trans*-10c**

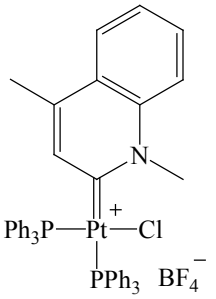

***cis*-10c**

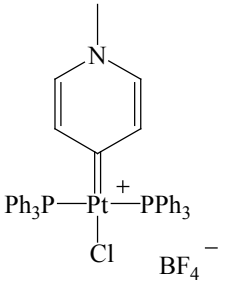

***trans*-14c**

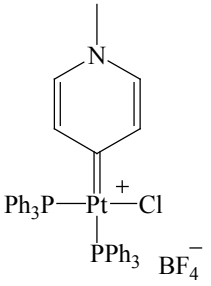

***cis*-14c**

Scheme 2.15

NMR spectroscopy

The ^{31}P NMR data of the reaction residues dissolved in CD_2Cl_2 are summarized in Table 2.21. $[PtCl(PPh_3)_3]BF_4$ together with an unknown species (singlet at δ 7.5) were the two products of the attempted preparation of **8c** at 60° for 32 hours. No signals indicated the formation of **8c**. The ^{31}P NMR data for $[PtCl(PPh_3)_3]BF_4$ are exactly the same as the data reported for this complex previously.[66] De Jung and co-workers reported the synthesis of complexes of the type $[PtX(PPh_3)_3]X$ (where X = Cl and or NO_3).[67] The doublet at δ 23.2 indicated the two PPh_3 ligands in the *trans* arrangement. These equivalent phosphines experienced phosphorus-phosphorus coupling of 18.5 Hz with the other PPh_3 (*trans* to Cl). The PPh_3 *trans* to the Cl in turn couples with the two equivalent PPh_3 ligands and appears as a triplet at δ 13.0. This triplet has half the intensity of the doublet observed for the two *trans* PPh_3 ligands. The ^{31}P - ^{31}P and ^{195}Pt - ^{31}P coupling

[66] P.S. Pregosin, R. Favez, R. Roulet, T. Boschi, R.A. Michelin, R. Ros, *Inorg. Chim. Acta*, 1980, **45**, L7.

[67] F. De Jong, J.J. Bour, P.P.J. Schelbos, *Inorg. Chim. Acta*, 1988, **154**, 89.

constants (the latter determined from the platinum satellites) are as expected. If the signals for the phosphines are of too low intensity, no platinum satellites are observed and, therefore, the ^{195}Pt - ^{31}P coupling constants could not be determined in those instances. An unknown *trans* platinum phosphine complex is observed as having a singlet at δ 7.5. $[PtCl(PPh_3)_3]BF_4$ and the lower unknown species were also products in the preparation of **13c**, but then in lower yields.

In the attempted preparation of **8c** stirring was reduced to 16 hours (at 60°C) and then two doublets (δ 16 and 13.9) are observed for two non-equivalent PPh_3 ligands in ***cis*-8c**. The PPh_3 *trans* to the carbene ligand appeared at δ 16.0 and the PPh_3 *trans* to Cl resonated at δ 13.9. The ^{195}Pt - ^{31}P coupling for the PPh_3 *trans* to the carbene is smaller than the coupling for the other PPh_3 ligand, due to the larger *trans*-influence of the carbene ligand compared to the Cl. $[PtCl(PPh_3)_3]BF_4$ as well as the unknown *trans* platinum phosphine complex (δ 8.03) formed during the reaction but as minor products. Similar reactions at room temperature and 35°C produced, for the first time, ***trans*-8c**, with the equivalent phosphines observed as a singlet in the ^{31}P NMR spectrum. The ^{195}Pt - ^{31}P coupling of 3685 Hz is similar to the coupling observed for the PPh_3 ligand *trans* to the carbene ligand in ***cis*-8c** indicating similar *trans*-influences of the carbene ligand. $[PtCl(PPh_3)_3]BF_4$ formed in a greater yield than ***trans*-8c** during the reaction at room temperature.

The attempted synthesis of **9c** at 60° yielded ***cis*-9c** (two doublets observed), $[PtCl(PPh_3)_3]BF_4$ (as major product) and two unknown *trans* platinum phosphine complexes with signals at δ 18.8 and 7.6. The reaction at room temperature resulted in the formation of ***cis*-9c** as major product (doublets at δ 15.5 and 12.8), ***trans*-9c** (singlet at δ 14.4) and $[PtCl(PPh_3)_3]BF_4$ as the other products. The ^{195}Pt - ^{31}P coupling for ***trans*-9c** (3678 Hz) is similar to that observed for ***trans*-8c** (3685 Hz).

***Cis*-10c** (resonates at δ 15.4 in the ^{31}P NMR spectrum) was produced in low concentrations during the synthesis at 60°C (16 hours), with $[PtCl(PPh_3)_3]BF_4$ as the major product of the reaction. Similar to **9c**, the process carried out at 60°C also produced two unknown *trans* platinum phosphine complexes with signals at δ 19.2 and 7.6 in the ^{31}P NMR spectrum. The room temperature synthesis yielded ***trans*-10c** (singlet at δ 14.4) with a ^{195}Pt - ^{31}P coupling of 3680 Hz, similar to that observed for ***trans*-8c** and ***trans*-9c**. $[PtCl(PPh_3)_3]BF_4$ and an unknown complex (δ 7.2) were minor products of this conversion.

Table 2.21 ^{31}P NMR data of the reaction mixtures of **8c** - **10c** and **14c** in CD_2Cl_2

Reaction mixtures	Pt carbene complex	$[PtCl(PPh_3)_3]BF_4$ and other side products
	δ / ppm	
8c (60°C, 32 hours)		23.2 (d, J_{Pt-P} = 2482 Hz, $^2J_{P-P}$ = 18.5 Hz), 12.5 (t, J_{Pt-P} = 3641 Hz, $^2J_{P-P}$ = 18.5 Hz), 7.5 (s)
8c (60°C, 16 hours)	16.0 (d, J_{Pt-P} = 2020 Hz, $^2J_{P-P}$ = 18.6 Hz), 13.9 (d, J_{Pt-P} = 3874 Hz, $^2J_{P-P}$ = 18.6 Hz)	23.7 (d, $^2J_{P-P}$ = 18.6 Hz), 13.0 (t, $^2J_{P-P}$ = 18.6 Hz), 8.0 (s)
8c (r.t., 20 hours; 35°C, 21 hours)	14.4 (s, J_{Pt-P} = 3685 Hz)	23.5 (d, J_{Pt-P} = 2483 Hz, $^2J_{P-P}$ = 18.5 Hz), 12.7 (t, J_{Pt-P} = 3644 Hz, $^2J_{P-P}$ = 18.6 Hz)
9c (60°C, 16 hours)	15.4 (d, J_{Pt-P} = 2017 Hz, $^2J_{P-P}$ = 18.6 Hz), 12.7 (m, J_{Pt-P} = 3881 Hz, $^2J_{P-P}$ = 16.0 Hz)	23.3 (d, J_{Pt-P} = 2485 Hz, $^2J_{P-P}$ = 18.5 Hz), 12.7 (m, J_{Pt-P} = 3643 Hz, $^2J_{P-P}$ = 18.6 Hz), 18.8 (s, J_{Pt-P} = 2672 Hz), 7.6 (s)
9c (r.t., 41 hours)	15.5 (d, J_{Pt-P} = 2015 Hz, $^2J_{P-P}$ = 18.5 Hz), 12.8 (d, J_{Pt-P} = 3875 Hz, $^2J_{P-P}$ = 18.6 Hz), 14.4 (s, J_{Pt-P} = 3678 Hz)	23.4 (d, J_{Pt-P} = 2479 Hz, $^2J_{P-P}$ = 16.9 Hz)
10c (60°C, 16 hours)	15.4 (d, $^2J_{P-P}$ = 18.5 Hz)	23.3 (d, J_{Pt-P} = 2482 Hz, $^2J_{P-P}$ = 18.5 Hz), 12.5 (t, J_{Pt-P} = 3641 Hz, $^2J_{P-P}$ = 18.6 Hz), 19.2 (s, J_{Pt-P} = 2682 Hz), 7.6 (s)
10c (r.t., 41 hours)	14.4 (s, J_{Pt-P} = 3680 Hz)	23.4 (d, J_{P-P} = 18.5 Hz)
14c (60°C, 16 hours)	14.3 (s, J_{Pt-P} = 3683 Hz), 17.6 (d, $^2J_{P-P}$ = 15.1 Hz), 15.1 (d, $^2J_{P-P}$ = 16.9 Hz)	21.8 (s, J_{Pt-P} = 2820 Hz)
14c (r.t., 20 hours; 35°C, 21 hours)	14.5 (s, J_{Pt-P} = 3690 Hz)	23.6 (d, J_{Pt-P} = 2483 Hz, $^2J_{P-P}$ = 18.6 Hz), 12.8 (t, $^2J_{P-P}$ = 18.5 Hz)

***Cis*-14c** (doublets at δ 17.6, 15.1) and ***trans*-14c** (^{31}P NMR singlet at δ 14.3) in a lower concentration, formed both during the preparation at 60°C. No signals for $[PtCl(PPh_3)_3]BF_4$ are observed in the spectrum, while another unknown *trans* platinum complex (singlet at δ 21.8) is present. This unknown complex is different to the one observed in the preparations of **9c** and **10c** at 60°C because the ^{195}Pt - ^{31}P coupling between the former and the latter differ. ***Trans*-14c** (δ 14.5)

was the major product of the synthesis carried out at room temperature and 35°C, while $[PtCl(PPh_3)_3]BF_4$ was a minor product.

Despite the observation of the expected *trans*-platinum carbene complexes in the ^{31}P NMR spectra, signals of the carbene complex are only clearly identifiable in the ^{1}H NMR spectrum of **9c** (collected of the reaction mixture at room temperature). The most notable signal is the singlet for NMe (δ 4.83) of **9c** in the ^{1}H NMR spectrum. The low concentration signals for the carbene complexes in the ^{1}H NMR spectra are overshadowed by the presence of $[PtCl(PPh_3)_3]BF_4$.

It is clear from the NMR data that the *cis*-phosphine-platinum complexes are formed at 60°C, while the *trans*-phosphine complexes are produced at room temperature. The formation of the *cis*-complex at 60°C was also observed for **13c** in the first preliminary work.[18] Complex ***cis*-9c** is an exception, and is the major isomer at room temperature. $[PtCl(PPh_3)_3]BF_4$ is a side product of all the reactions except in the synthesis of **14c** at 60°C. This complex is the major product of the reactions carried out at 60°C, with the exception of the synthesis of **9c** at 60° with 16 hours stirring. $[PtCl(PPh_3)_3]BF_4$ is a minor product of the reactions at room temperature, except in the synthesis of **14c**, where it was the major species. The two unknown *trans* platinum phosphine complexes that resonate at δ 7.6 and 19.0 were only produced at higher temperatures. It is also clear from the coupling constants that 1-methyl-1,2-dihydropyridin-2-ylidene in **8c** and 1-methyl-1,2-dihydroquinolin-2-ylidene in **9c**, exhibit similar *trans*-influences since the PPh_3 *trans* to both these carbene ligands experience a ^{195}Pt - ^{31}P coupling of 2017 Hz. Reaction time, temperature and perhaps the carbene ligand itself are contributing factors to the product distribution obtained from the reactions.

Mass spectrometry

The FAB MS data of the residues obtained from the attempted room temperature synthesis of complexes **8c** - **10c** and **14c** are summarized in Table 2.22. The cationic complex is observed for **8c**, **10c** and **14c** while a second fragment, after the loss of a PPh_3 ligand and a Cl, is observed for **10c**. The fragmentation pattern for complex **9c** is similar to that of the palladium and nickel complexes prepared as part of this study. The expulsion of PPh_3 is followed by the loss of Cl and then the

second PPh_3. The $[PtCl(PPh_3)_3]^+$ cation is also observed in all the MS spectra. The fragmentation pattern for $[PtCl(PPh_3)_3]^+$ is the same as the pattern for **9c**.

Table 2.22 Mass spectrometry data for (room temperature) reaction mixtures for complexes **8c**- **10c** and **14c**

Complex	m/z	Relative intensity (%)	Fragment ion
8c	848	2	$[M - BF_4]^+$
	1017	11	$[PtCl(PPh_3)_3]^+$
	754	22	$[PtCl(PPh_3)_2]^+$
	718	25	$[Pt(PPh_3)_2]^+$
	454	9	$[Pt(PPh_3)]^+$
9c	898	42	$[M -BF_4]^+$
	636	9	$[M - BF_4 - PPh_3]^+$
	599	26	$[M - BF_4 - PPh_3 - Cl]^+$
	337	8	$[M - BF_4 - PPh_3 - Cl - PPh_3]^+$
	1017	3	$[PtCl(PPh_3)_3]^+$
	754	6	$[PtCl(PPh_3)_2]^+$
	718	8	$[Pt(PPh_3)_2]^+$
	454	7	$[Pt(PPh_3)]^+$
10c	912	3	$[M - BF_4]^+$
	613	2	$[M - BF_4 - PPh_3 - Cl]^+$
	1017	3	$[PtCl(PPh_3)_3]^+$
	754	5	$[PtCl(PPh_3)_2]^+$
	718	6	$[Pt(PPh_3)_2]^+$
14c	848	1	$[M - BF_4]^+$
	1017	4	$[PtCl(PPh_3)_3]^+$
	754	6	$[PtCl(PPh_3)_2]^+$
	718	6	$[Pt(PPh_3)_2]^+$
	454	3	$[Pt(PPh_3)]^+$

Pectora roborant cultus recti

2.2.17 Crystal and molecular structure determinations by means of X-ray diffraction

The molecular and crystal structures of 14 compounds, characterised above, were determined. Only the molecular structures of the cations of the complexes are shown in all the figures except in Figures 2.23 and 2.25 where the molecular structures of neutral carbene complexes of chromium and tungsten are shown. The hydrogen atoms, counter ions and the solvent molecules are omitted from these figures for clarity. Hydrogen atoms are also not shown in the packing diagrams of the complexes. The orientations of the carbene ligand with respect to the coordination plane is the angle between the least square plane through the atoms of the carbene ligand and the least square plane through the central metal and the four atoms coordinated to it, unless stated otherwise. No short intermolecular contacts occur in all the unit cells of the structures determined and the crystal lattices are organised by van der Waals interactions.

In the following section very standard two-N, five-membered NHC complexes of palladium and nickel are discussed.

2.2.17.1 The crystal and molecular structure of trans-*chloro(1,3-dimethyl-2,3-dihydro-1*H-*imidazol-2-ylidene)bis(triphenylphosphine)palladium(II) tetrafluoroborate,* ***3a***

The crystal and molecular structure of **3a** is shown in Figure 2.1. Apart from the expected square-planar coordination of the palladium atom, this study revealed that the two PPh_3 ligands occupy the *trans* positions. Selected bond lengths and angles are listed in Table 2.23. The carbene backbone is orientated at an angle of 85.6(1)° with respect to the coordination plane defined by C(1), Pd(1), P(1), P(2) and Cl(1). The deviation from this calculated least square plane of the five atoms in the coordination plane is small with the maximum deviation from the plane only 0.035(1)Å by Pd(1). The geometry at the palladium atom is only slightly distorted square planar with the two types of angles ranging from 88.4(1) to 91.6(2)° and 176.9(2) to 178.2(1)°.

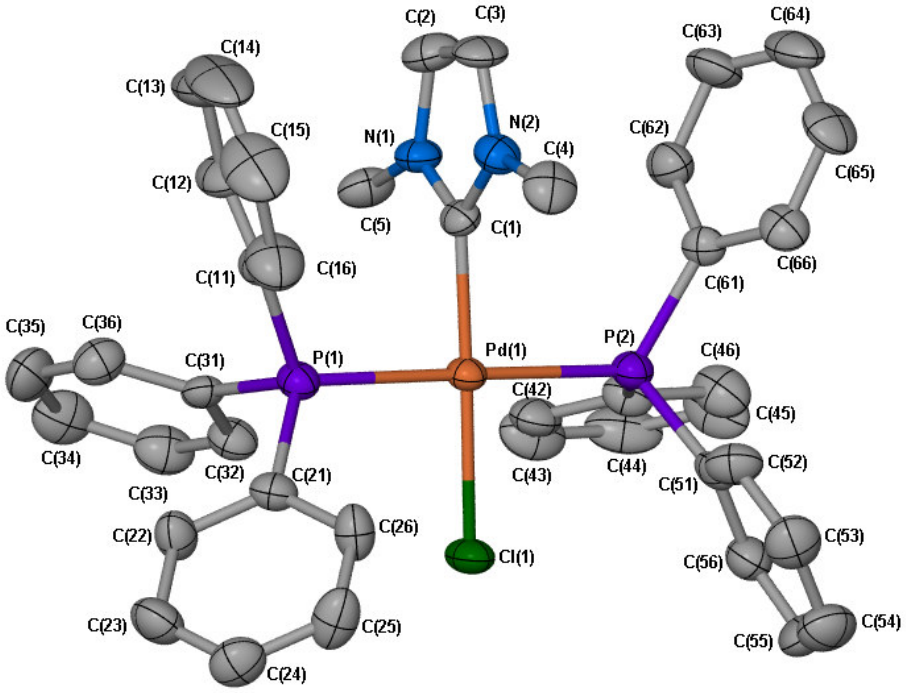

Figure 2.1 Molecular structure of **3a**, showing the numbering scheme, generated in POV-Ray

The bond lengths and angles of the carbene ligand compare well to the carbene ligands in similar complexes: chloro(1-butyl-3-methyl-2,3-dihydro-1*H*-imidazol-2-ylidene)bis(triphenylphosphine) palladium(II) tetrafluoroborate, (**A**),[14] bromo{1,3-bis(2-pyridyl)-2,3-dihydro-1*H*-imidazol-2-ylidene}bis(triphenylphosphine)palladium(II) bromide[68] (**B**) and in chloro(η^4-1,5-cyclooctadiene)(1,3-dimethyl-2,3-dihydro-1*H*-imidazol-2-ylidene)rhodium(I).[44] The Pd-$C_{carbene}$ bond length of 1.996(5) Å is the same as observed for **A** [1.999(13) Å], **B** [2.002(5) Å] and **13a** [1.986(3) Å][18]. These distances are well within the range [1.91 – 2.10 Å] reported for various palladium(II) carbene complexes.[18] The Pd-P bond lengths are normal. The Pd-Cl distance in **3a** [2.336(1) Å] and **A** [2.333(1) Å] are identical but significantly smaller than the same bond in **13a** [2.380(1) Å].[18] This difference indicates that the carbene ligands in 5-membered *N*-heterocyclic carbene complexes **3a** and **A** have a much smaller *trans*-influence than the one N, ligand in the 6-membered *r*NHC complex **13a.**

[68] J.C.C. Chen, I.J.B. Lin, *Organometallics*, 2000, **19**, 5113.

Table 2.23 Selected bond lengths (Å) and angles (°) for **3a**

Pd(1)-C(1)	1.996(5)	C(1)-N(1)	1.335(7)
Pd(1)-P(1)	2.335(1)	C(1)-N(2)	1.340(7)
Pd(1)-P(2)	2.337(1)	N(1)-C(2)	1.380(8)
Pd(1)-Cl(1)	2.336(1)	C(2)-C(3)	1.319(9)
N(1)-C(5)	1.461(8)	N(2)-C(3)	1.366(8)
N(2)-C(4)	1.458(8)		
C(1)-Pd(1)-Cl(1)	176.9(2)	N(1)-C(1)-N(2)	105.7(5)
P(1)-Pd(1)-P(2)	178.2(1)	C(1)-N(1)-C(2)	109.4(5)
C(1)-Pd(1)-P(1)	89.3(2)	C(1)-N(2)-C(3)	110.5(6)
C(1)-Pd(1)-P(2)	91.6(2)	N(1)-C(2)-C(3)	107.7(6)
Cl(1)-Pd(1)-P(1)	90.7(1)	C(2)-C(3)-N(2)	106.7(6)
Cl(1)-Pd(1)-P(2)	88.4(1)	C(1)-N(1)-C(5)	126.9(5)
Pd(1)-C(1)-N(1)	126.5(4)	C(1)-N(2)-C(4)	125.3(5)
		Pd(1)-C(1)-N(2)	127.9(4)

The cations in complex **3a** are stacked on top of each other forming layers parallel to the a-axis and c-axis (Figure 2.2). In one layer (along the c-axis) the carbene ligand is pointed forward and in the next layer (down along the b-axis) it is pointing backwards. The BF_4^- counter ions and CH_2Cl_2 solvent molecules are located in the spaces between the layers of cations.

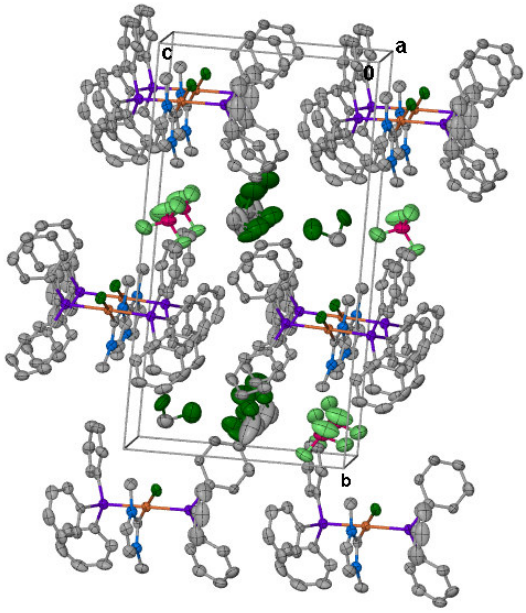

Figure 2.2 Packing diagram of the molecules of **3a** along the a-axis

2.2.17.2 The crystal and molecular structure of trans-*chloro(1,3-dimethyl-2,3-dihydro-1*H-*imidazol-2-ylidene)bis(triphenylphosphine)nickel(II) tetrafluoroborate,* ***3b***

Figure 2.3 shows the molecular structure of the square planar complex **3b**, with the PPh_3 ligands occupying the *trans* positions, similar to its palladium analogue, complex **3a**. Selected bond lengths and angles are summarized in Table 2.24. There is little deviation from this square planar geometry around the nickel atom. Deviations from the least square plane calculated through C(1), Ni(1), P(1), P(2) are very small [0.003(1) – 0.005(1) Å] and the angles around the central metal range from 88.4(1) to 91.2(2)°. The P(1)-Ni(1)-P(2) angle [179.2(1)°] is almost linear but the C(1)-Ni(1)-Cl(1) angle [172.8(2)°] is bent out of the plane. No apparent reason for this deviation could be deduced from the packing of **3b** in the unit cell. The angle between the least square planes through the atoms of the carbene ligand and the five atoms of the coordination plane of **3b** is 87.0(1)° and is similar to the same angle determined for **3a** [85.6(1)°].

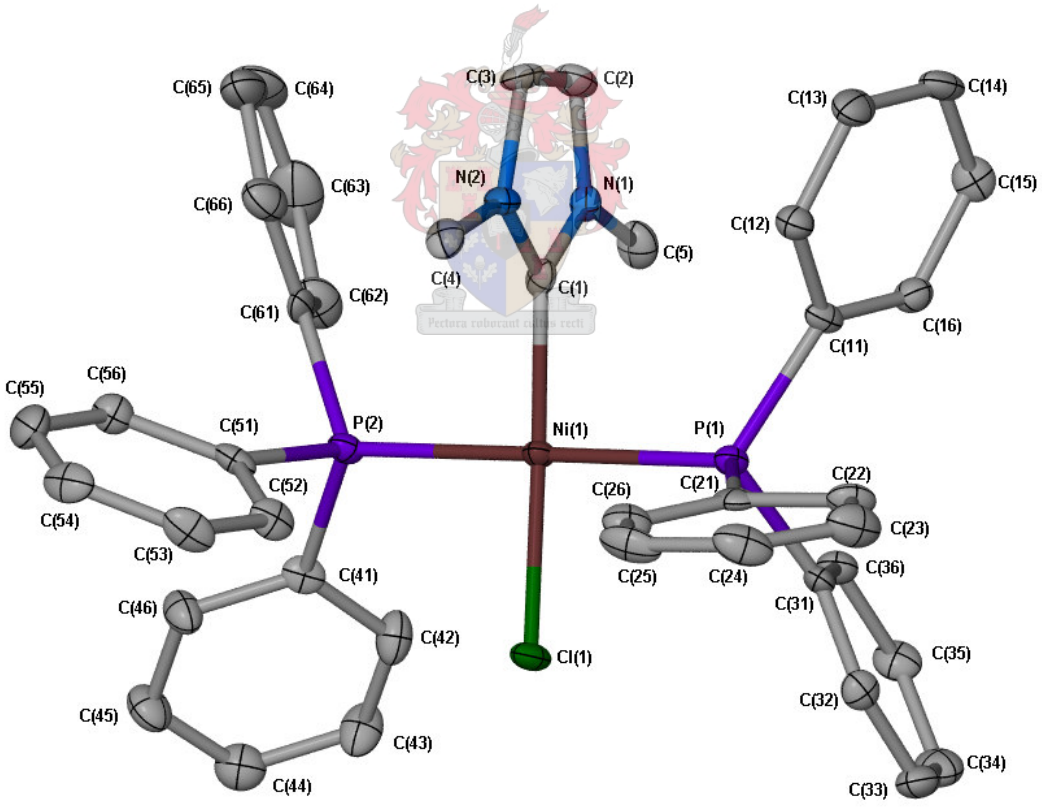

Figure 2.3 Molecular structure of **3b**, showing the numbering scheme, generated in POV-Ray

The Ni-$C_{carbene}$ bond length [1.881(5) Å] falls well in the range 1.83 – 1.95 Å reported for such nickel(II) complexes.[42,69,70,71,72] The Ni(1)-Cl(1) distance [2.187(1) Å] is similar to the same distances [2.195(1) and 2.200(1) Å] in nickel complexes with the Cl atom *trans* to an imidazolylidene carbene ligand.[70] The bond lengths and angles of the carbene ligand in **3b** are the same as those in **3a**, **A**,[14] **B**[68] and other complexes containing the same heterocyclic ring.[44,48]

Table 2.24 Selected bond lengths (Å) and angles (°) for **3b**

Ni(1)-C(1)	1.881(5)	C(1)-N(1)	1.355(6)
Ni(1)-P(1)	2.239(1)	C(1)-N(2)	1.333(7)
Ni(1)-P(2)	2.233(1)	N(1)-C(2)	1.368(7)
Ni(1)-Cl(1)	2.187(1)	C(2)-C(3)	1.339(9)
N(1)-C(5)	1.462(8)	N(2)-C(3)	1.385(7)
N(2)-C(4)	1.482(7)		
C(1)-Ni(1)-Cl(1)	175.8(2)	N(1)-C(1)-N(2)	105.0(4)
P(1)-Ni(1)-P(2)	179.2(1)	C(1)-N(1)-C(2)	110.6(5)
C(1)-Ni(1)-P(1)	91.2(2)	C(1)-N(2)-C(3)	111.0(5)
C(1)-Ni(1)-P(2)	89.6(2)	N(1)-C(2)-C(3)	107.2(5)
Cl(1)-Ni(1)-P(1)	88.4(1)	C(2)-C(3)-N(2)	106.3(5)
Cl(1)-Ni(1)-P(2)	90.9(1)	C(1)-N(1)-C(5)	125.6(5)
Ni(1)-C(1)-N(1)	127.3(4)	C(1)-N(2)-C(4)	125.3(4)
		Ni(1)-C(1)-N(2)	127.8(4)

The arrangement of the molecules of **3b** in the unit cell (Figure 2.4) is similar to that of complex **3a**. The cations are again packed on top of each other along the a-axis and the c-axis with the Cl-atoms pointing to the back and to the front alternatively in the layers along the c-axis as one moves down the b-axis.

[69] D.S. McGuiness, W.A. Mueller, P. Wasserscheid, K.J. Cavell, B.W. Skelton, A.H. White, U. Englert, *Organometallics*, 2002, **21**, 175.

[70] R.E. Douthwaite, D. Haüssinger, M.L.H. Green, P.J. Silcock, P.T. Gomes, A.M. Martins, A.A. Danopoulos, *Organometallics*, 1999, **18**, 4584.

[71] M.V. Baker, B.W. Skelton, A.H. White, C.C. Williams, *Organometallics*, 2002, **21**, 2674.

[72] E. Baba, T.R. Cundari, I. Firkin, *Inorg. Chim. Acta*, 2005, **358**, 2867.

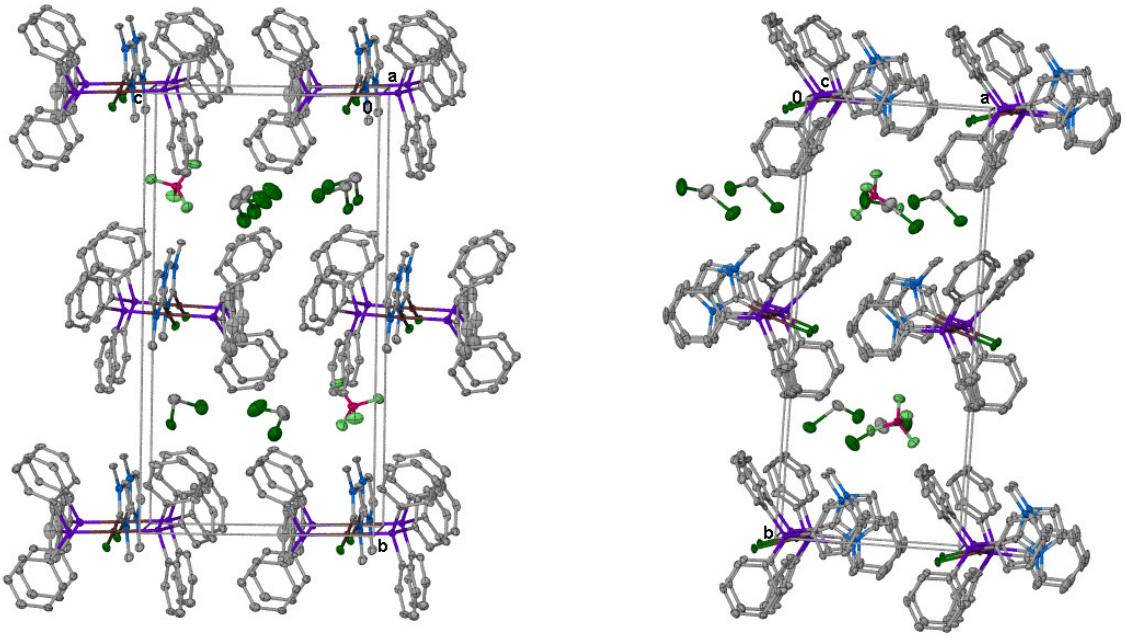

A B

Figure 2.4 Packing diagram of the molecules of **3b** viewed along the a-axis (A) and b-axis (B)

2.2.17.3 The crystal and molecular structure of trans-*chloro(1,3-dimethyl-2,3,4,5-tetrahydro-1*H-*imidazol-2-ylidene)bis(triphenylphosphine)nickel(II) tetrafluoroborate,* ***4b***

The asymmetric unit of the complex **4b** consists of two independent molecules of which one cation is shown in Figure 2.5 and selected bond lengths are combined in Table 2.25. The bond lengths and angles in these two independent molecules are the same. The deviations from the least square planes calculated through the atoms of the carbene ligand on the one hand and the five atoms of the coordination plane on the other, is smaller (0.001 - 0.010 and 0.038 - 0.069 Å respectively) in the independent molecule shown in Figure 2.5 when compared to the other independent molecule (0.004-0.022 and 0.018-0.132 Å respectively). The square planar geometry of the nickel is slightly distorted with the angles around the metal ranging from 87.4(1) – 91.9(1)° and with C(11)-N(11)-Cl(11) [174.2(1)°] and P(11)-N(11)-P(12) [176.7(1)°] slightly bent away from linearity. The carbene ligand is orientated at an angle of 88.5(1)° with respect to the coordination plane of the nickel, determined from the calculated least square planes through these two sets of atoms. This angle compares well with the angle in the imidazolylidene complex **3b** [87.0(1)°] but is closer to 90° than the same angle calculated for imidazolylidene complex, **3a** [85.6(1)°].

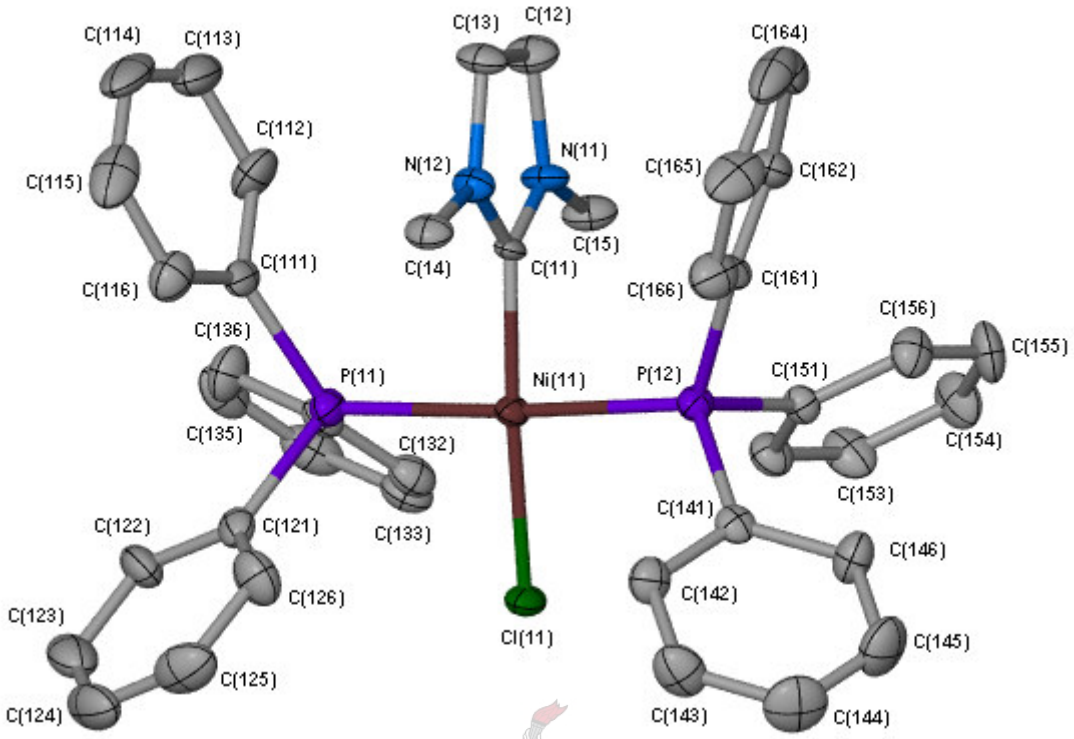

Figure 2.5 Molecular structure of **4b**, showing the numbering scheme, generated in POV-Ray

Despite the reported isolation of nickel(II) complexes with this standard carbene as a ligand, no crystal structures have been reported.[53] The Ni-$C_{carbene}$ distance [1.857(4) Å] and Ni-Cl [2.191(1) Å] separation in **4b** are similar to the corresponding bonds in **3b** [1.881(5) and 2.187(1) Å respectively] despite the saturation of the carbene ligand in **4b**. The similar Ni-Cl distances in these two complexes demonstrate the similar *trans*-influences of the two carbene ligands. The bond lengths and angles of the carbene ligand in **4b** are the same as those of the carbene ligand in the palladium analogue of complex of **4b**.[15]

Table 2.25 Selected bond lengths (Å) and angles (°) for **4b**

Ni(11)-C(11)	1.857(4)	C(11)-N(11)	1.332(6)
Ni(11)-P(11)	2.239(1)	C(11)-N(12)	1.335(5)
Ni(11)-P(12)	2.233(1)	N(11)-C(12)	1.458(6)
Ni(11)-Cl(11)	2.191(1)	C(12)-C(13)	1.549(6)
N(11)-C(15)	1.447(5)	N(12)-C(13)	1.466(6)
N(12)-C(14)	1.446(5)		
C(11)-Ni(11)-Cl(11)	174.2(1)	N(11)-C(11)-N(12)	109.2(4)
P(11)-Ni(11)-P(12)	176.7(1)	C(11)-N(11)-C(12)	113.3(3)
C(11)-Ni(11)-P(11)	89.3(1)	C(11)-N(12)-C(13)	112.8(4)
C(11)-Ni(11)-P(12)	87.4(1)	N(11)-C(12)-C(13)	102.3(4)
Cl(11)-Ni(11)-P(11)	91.9(1)	C(12)-C(13)-N(12)	102.4(3)
Cl(11)-Ni(11)-P(12)	91.4(1)	C(11)-N(11)-C(15)	126.3(4)
Ni(11)-C(11)-N(11)	124.6(3)	C(11)-N(12)-C(14)	125.2(4)
		Ni(11)-C(11)-N(12)	126.2(4)

The cations of complex **4b** are stacked on top of each other forming layers parallel to the a-axis (Figure 2.6). The carbene ligands are orientated in an alternating up and down fashion in the layer. The PF_6^- counter ion and CH_2Cl_2 solvent molecules occupy the spaces in the unit cell.

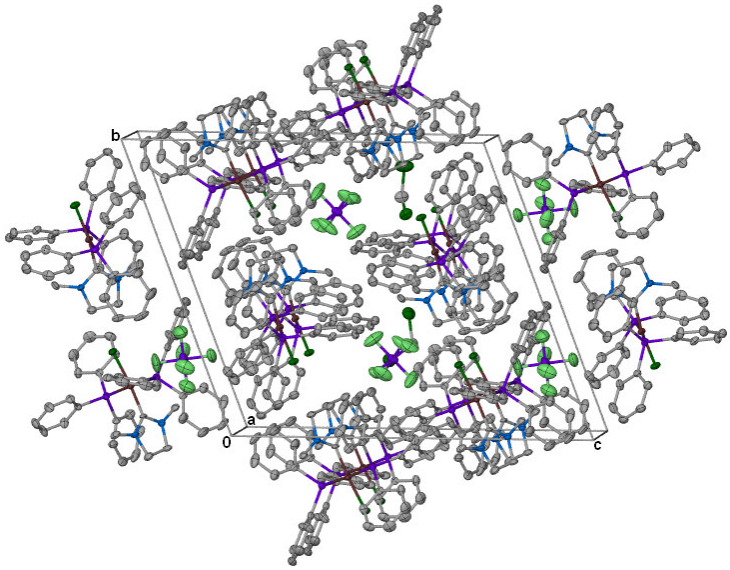

Figure 2.6 The packing diagram the of molecules of **4b** along the a-axis

In this second section structures of pyridinylidene-type and quinolinylidene-type, one-N, six-membered NHC complexes, are discussed.

2.2.17.4 The crystal and molecular structure of trans-*chloro(1-methyl-1,2-dihydro-pyridin-2-ylidene)bis(triphenylphosphine)palladium(II) tetrafluoroborate,* ***8a***

The molecular structure of the pyridine-derived 6-membered *N*-heterocyclic carbene complex **8a** is shown in Figure 2.7. Selected bond lengths and angles are summarized in Table 2.26. The palladium again resides in a square planar environment, defined by the carbene carbon, the Cl-atom and the two phosphine atoms occupying the *trans* positions on the metal center. The atoms C(1), Pd(1), P(1), P(2) and Cl(1) all deviate from the least square plane calculated through these five atoms by 0.137(2), -0.075(10, -0.088(1), -0.089(1) and 0.115(1) Å respectively thus showing the slight distortion of the square plane. The coordination plane around the central metal is rather regular with angular values in the range 88.8(1) – 91.5(1)° and the P(1)-Pd(1)-P(2) angle is almost linear [179.3(1)°]. The C(1)-Pd(1)-Cl(1) angle [169.1(1)°] is significantly smaller than 180° and this could result from the close proximity of the BF_4^- counter ion to the NMe group, causing the pyridine ring to bend away from the BF_4^- counter ion. The pyridine ring is very nearly perpendicular to the square plane with the torsion angle [P(2)-Pd(1)-C(1)-C(2) = 89.4(2)°] which is similar to the torsion angle [90.0(1)°] reported for *trans*-chloro(1,2-dihydro-pyridin-2-ylidene)bis(dimethylphenylphosphine)palladium(II) perchlorate (**C**), one of the few pyridine-derived carbene complexes known.[73] The angle between the least square planes calculated through the atoms of the carbene ligand and the atoms of the coordination plane is 88.8(1)°.

[73] F. Benetollo, G. Bombieri, F. DiBianca, B. Crociani, *Inorg. Chim. Acta*, 1991, **188**, 51.

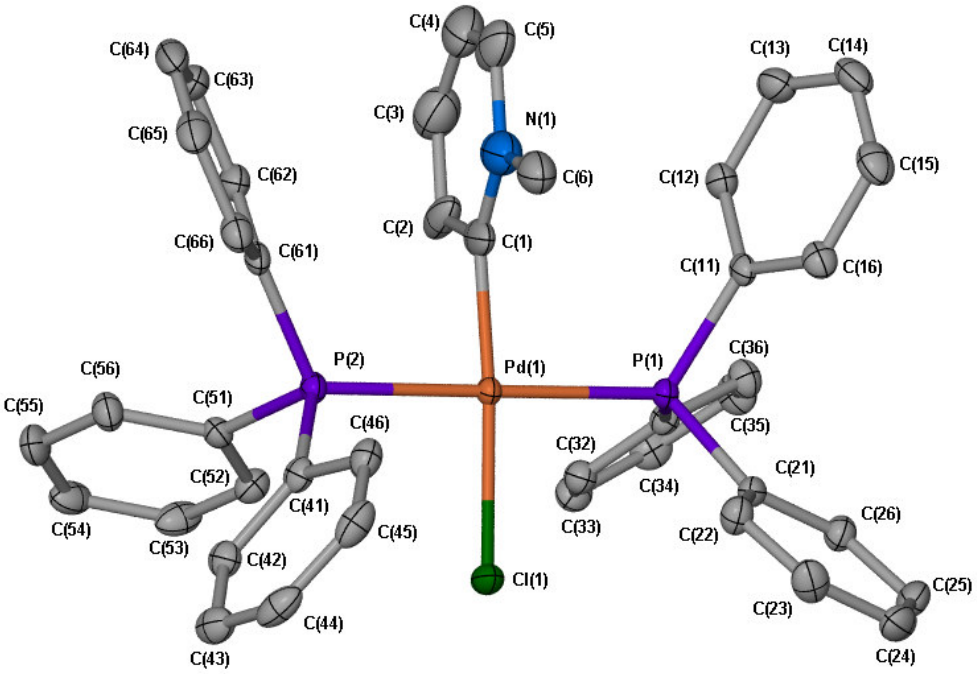

Figure 2.7 Molecular structure of **8a**, showing the numbering scheme, generated in POV-Ray

The Pd(1)-C(1) [1.995(3) Å] and Pd(1)-Cl(1) [2.363(1) Å] bond lengths in **8a** compare well with Pd(1)-C(1) [1.970(5) Å] and Pd(1)-Cl(1) [2.368(2) Å] in **C**. The Pd-$C_{carbene}$ bond length does not differ significantly from the Pd-$C_{carbene}$ bond length in the imidazolylidene complex **3a** [1.996(5) Å] and the quinolinylidene complex **13a** [1.986(3) Å]. The Pd-Cl bond length in **8a** however is longer than Pd-Cl in **3a** [2.336(1) Å] but shorter than Pd-Cl in **13a** [2.380(1) Å]. These distances are related to the difference in the *trans*-influence of the carbene ligands. The carbene ligand in **8a** has a greater *trans*-influence than the carbene ligand in **3a** and a slightly smaller *trans*-influence than the carbene ligand in **13a**. The *r*NHC ligand, in **13a**, has a greater *trans*-influence than the NHC ligands with one or two N atoms attached to the carbene carbon. The C(1)-N(1) bond distance [1.314(5) Å] in **8a** is significantly shorter than C(1)-N(1) [1.362(7) Å] in **C** but longer than the C(sp^2)=N(sp^2) double bond (1.27 Å)[74]. This indicates that the C(1)-N(1) bond does have partial double bond character and that the most important contributing structures of **8a** in the solid state is (**vii**) and (**ix**) (Scheme 2.16). The other bond lengths of the carbene ligand are the same as that reported for **C** except C(1)-C(2) [1.503(6) Å] and N(1)-C(5) [1.416(5) Å] which are significantly longer than the same bonds [1.366(7) Å] and [1.344(8) Å] in **C** respectively.

[74] B. Crociani, M. Sala, A. Polo, G. Bombieri, *Organometallics*, 1986, **5**, 1369.

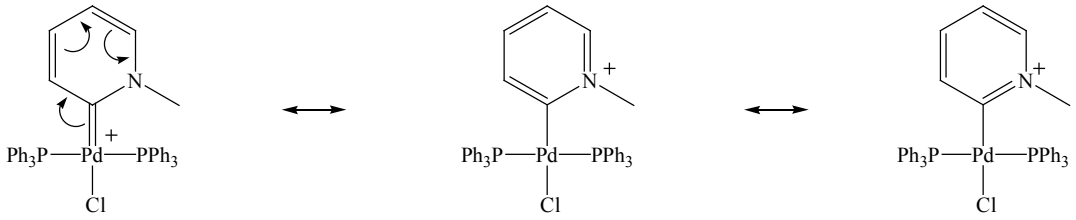

(**vii**) (**viii**) (**ix**)

Scheme 2.16

Table 2.26 Selected bond lengths (Å) and angles (°) for **8a**

Pd(1)-C(1)	1.995(3)	C(1)-C(2)	1.503(6)
Pd(1)-P(1)	2.341(1)	C(2)-C(3)	1.378(5)
Pd(1)-P(2)	2.334(1)	C(3)-C(4)	1.379(6)
Pd(1)-Cl(1)	2.363(1)	C(4)-C(5)	1.336(6)
N(1)-C(6)	1.410(5)	C(5)-N(1)	1.416(5)
		C(1)-N(1)	1.314(5)
C(1)-Pd(1)-Cl(1)	169.1(1)	N(1)-C(1)-C(2)	116.8(3)
P(1)-Pd(1)-P(2)	179.3(1)	C(1)-C(2)-C(3)	117.8(4)
C(1)-Pd(1)-P(1)	88.9(1)	C(2)-C(3)-C(4)	119.6(4)
C(1)-Pd(1)-P(2)	91.0(1)	C(3)-C(4)-C(5)	124.5(4)
Cl(1)-Pd(1)-P(1)	91.5(1)	C(4)-C(5)-N(1)	115.8(4)
Cl(1)-Pd(1)-P(2)	88.8(1)	C(1)-N(1)-C(5)	125.4(4)
C(1)-N(1)-C(6)	116.6(3)	C(5)-N(1)-C(6)	117.9(3)
Pd(1)-C(1)-N(1)	127.7(3)	Pd(1)-C(1)-C(2)	115.6(2)

Figure 2.8 illustrates the packing of the molecules of **8a** and the CH_2Cl_2 solvent molecules in the unit cell. The cations are stacked on top of each other along the a-axis and the b-axis with the BF_4^- anions and CH_2Cl_2 molecules filling the spaces in the unit cell. The cations are stacked on top of each other in such a way that the carbene ligands point down in one layer and then up in the next layer parallel to the a-axis and b-axis (A and B).

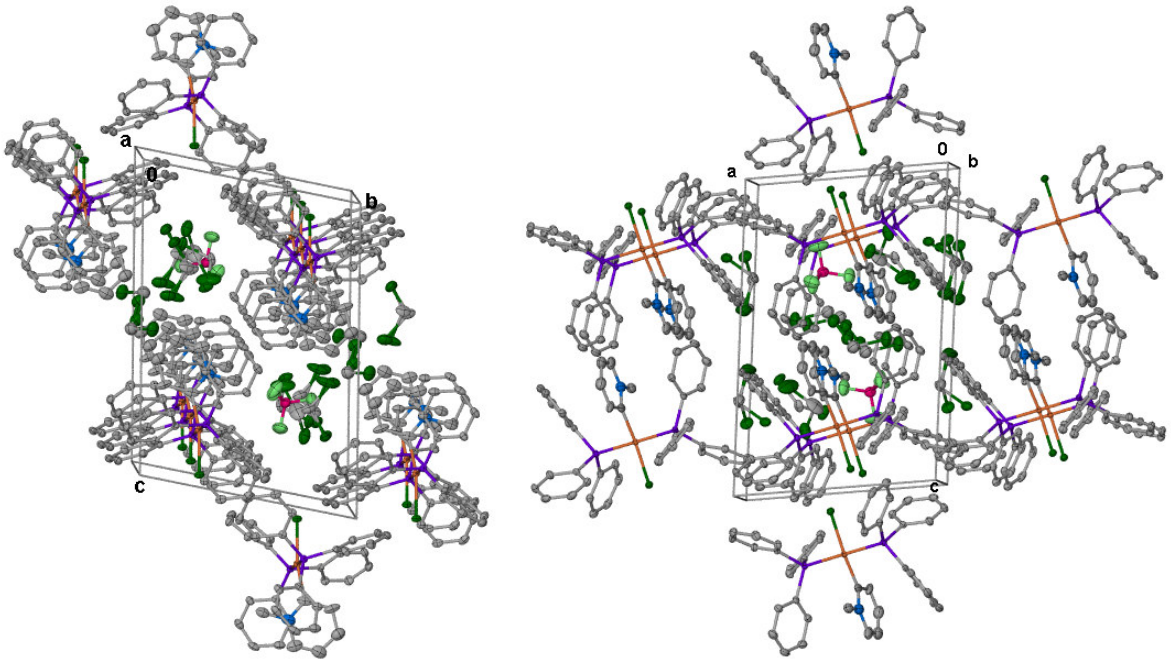

Figure 2.8 Packing diagram of the molecules of **8a** along the a-axis (A) and the b-axis (B)

2.2.17.5 The crystal and molecular structure of trans-*chloro(1-methyl-1,2-dihydro-pyridin-2-ylidene)bis(triphenylphosphine)nickel(II) tetrafluoroborate,* ***8b***

The molecular structure of the cation of the nickel complex **8b** (Figure 2.9) shows the square planar geometry of the nickel(II) atom with the PPh_3 in the *trans* positions. Selected bond lengths and angles are listed in Table 2.27. Similar to the crystal structure of complex **13a**, there is a mirror plane through the atoms of the carbene ligand, N(1), Cl(1), B(1), F(2) and F(3).[18] The one PPh_3 and F(4) are related by symmetry to the rest of the molecule. The angles around the Ni center are close to 90° but the C(1)-Ni(1)-Cl(1) [161.9(2)°] and the P(1)-Ni(1)-P(1)' angle [164.5(1)°] are well bent away from linearity. This may be the result of the presence of the BF_4^- counter ion close (3.17 Å) to the NMe group of the carbene ligand. This deviation from linearity is accompanied by Ni(1) that shows maximum deviation [0.208(2) Å] from the least square plane calculated through C(1), Ni(1), P(1), P(1)' and Cl(1). The least square plane through the atoms of the carbene ligand is orientated at an angle of 76.8(1)° with respect to the least square plane through the five atoms of the coordination plane in **8b**. This angle is much smaller than the corresponding angle in **8a** [88.8(1)°].

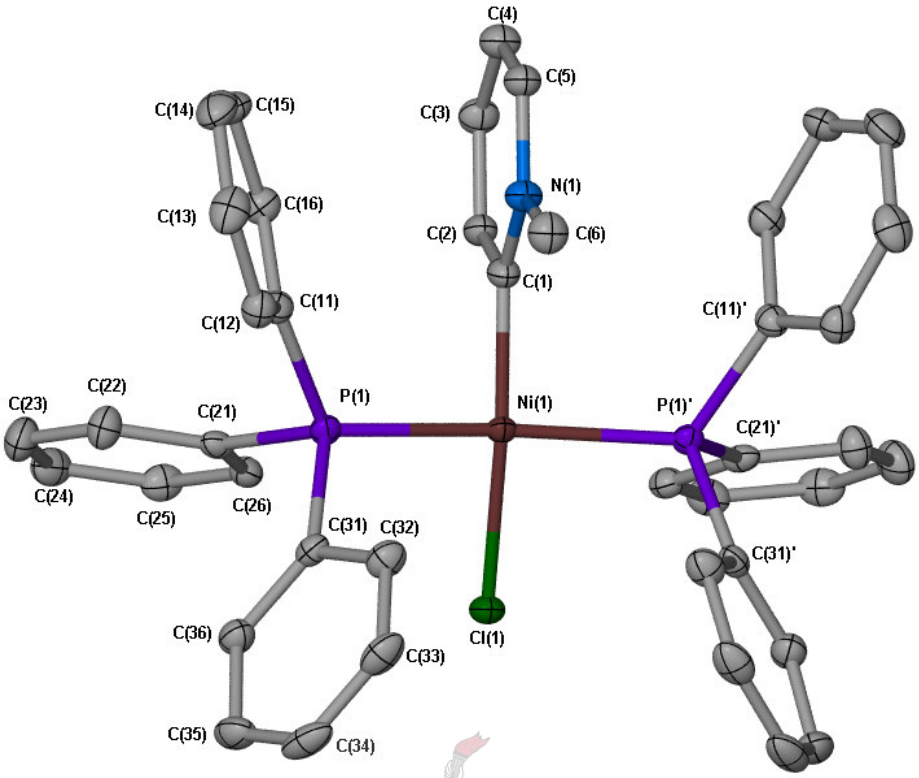

Figure 2.9 Molecular structure of **8b**, showing the numbering scheme, generated in POV-Ray

Ni-$C_{carbene}$ bond distance [1.863(3) Å] does not differ significantly from the same distance in **3b** [1.881(5) Å] and **4b** [1.857(4) Å]. The Ni(1)-Cl(1) length in **8b** [2.203(1) Å] is just significantly longer than the same bond in the five-membered carbene complexes **3b** [2.187(1) Å] and **4b** [2.191(1) Å] and is an indication of the slightly larger *trans*-influence of the carbene ligand compared to the carbene ligands in complexes **3b** and **4b**. The bond lengths of the carbene ligand in **8b** compare well with that of **8a** with the exception that C(1)-C(2) in **8b** [1.431(7) Å] is significantly shorter than the same bond in **8a** [1.503(6) Å] while N(1)-C(5) and C(1)-N(1) in the two complexes differ just slightly. Bond distances and angles in the carbene ligand in **8b** are the same as the carbene ligand in *trans*-chloro(1,2-dihydro-pyridin-2-ylidene)bis(dimethylphenylphosphine) palladium(II) perchlorate (**C**),[73] with the exception that C(1)-C(2) in **8b** is longer than the same bond in **C** [1.366(7) Å]. The C(1)-N(1) bond lengths in **8b** [1.349(6) Å] and **C** [1.362(7) Å] are just longer than C(1)-N(1) in **8a** [1.314(5) Å] and much longer than the shorter $C(sp^2)=N(sp^2)$ double bond (1.27 Å)[74] but shorter than N(1)-C(6) [1.460(6) Å] indicating the double bond character of C(1)-N(1) in the three complexes. The most important resonance structures for **8b** are the same as those proposed for **8a** [(**vii**) and (**ix**) in Scheme 2.16]. The difference in these bond lengths suggest that the C(1)-N(1) bond in **8b** has slightly less double bond character than the same bond in **8a**.

Table 2.27 Selected bond lengths (Å) and angles (°) for **8b**.

Ni(1)-C(1)	1.863(5)	C(1)-C(2)	1.431(7)
Ni(1)-P(1)	2.228(1)	C(2)-C(3)	1.374(7)
Ni(1)-Cl(1)	2.203(1)	C(3)-C(4)	1.385(7)
N(1)-C(6)	1.460(6)	C(4)-C(5)	1.361(7)
C(1)-N(1)	1.349(6)	C(5)-N(1)	1.381(6)
C(1)-Ni(1)-Cl(1)	161.9(2)	C(1)-C(2)-C(3)	120.8(5)
P(1)-Ni(1)-P(1)'	164.5(1)	C(2)-C(3)-C(4)	119.5(5)
C(1)-N(1)-P(1)	92.0(1)	C(3)-C(4)-C(5)	120.2(5)
Cl(1)-Ni(1)-P(1)	90.4(1)	C(4)-C(5)-N(1)	119.8(4)
N(1)-C(1)-C(2)	116.9(4)	C(1)-N(1)-C(5)	122.8(4)
Ni(1)-C(1)-C(2)	114.4(3)	C(5)-N(1)-C(6)	117.1(4)
Ni(1)-C(1)-N(1)	128.7(4)	C(1)-N(1)-C(6)	120.1(4)

The packing diagram (Figure 2.10) of **8b** shows the cations stacked on top of each other along the c-axis and along the a-axis. The carbene ligands of the cations are directed in one direction in one layer parallel to the a-axis and in the opposite direction in the next layer below or above. The BF_4 anions are packed between the carbene ligands of two cations in each layer (along the c-axis). Two CH_2Cl_2 molecules between two phenyl rings each are also packed between two cations in each layer down the c-axis.

Pectora roborant cultus recti

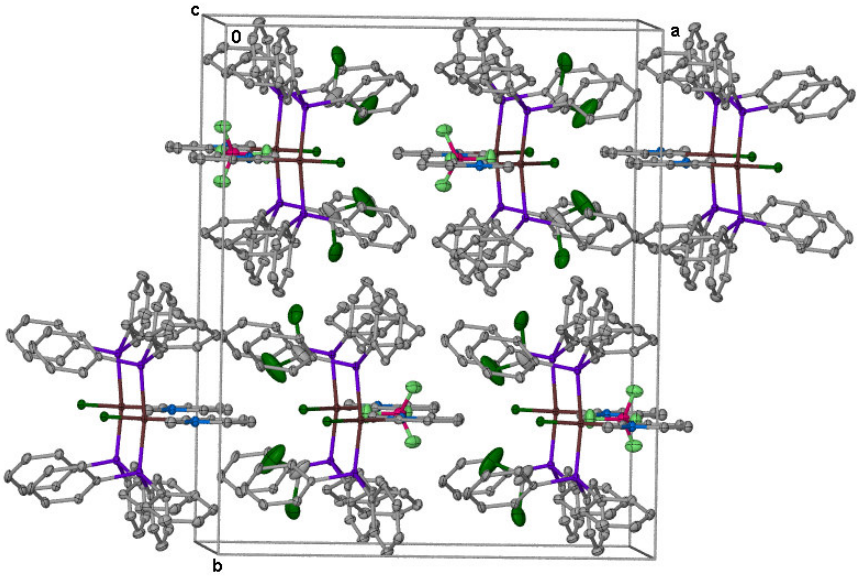

Figure 2.10 Packing diagram of the molecules of **8b** along the c-axis

2.2.17.6 The crystal and molecular structure of trans*-chloro(1-methyl-1,2-dihydro-quinolin-2-ylidene)bis(triphenylphosphine)palladium(II) tetrafluoroborate,* **trans-*9a***

The molecular structure of ***trans*-9a**, with one of the two disordered carbene ligands, is shown in Figure 2.11 and selected bond lengths are summarized in Table 2.28. The carbene ligand is disorded over two sites (A and B) with site occupation factors of 0.57 and 0.43 respectively and with a C(1A)-Pd(1)-C(1B) angle of 19.2(3)°. The palladium atom is located in a distorted square planar environment and the maximum deviation from the square plane calculated through C(1A), C(1B), Pd(1), P(1), P(2) is 0.311(6) and -0.339(7) Å by C1A and C1B respectively. The angles around the metal center range from 86.5(1) - 94.3(4)° and the angles C(1A)-Pd(1)-Cl(1) [170.6(3)°] and P(1)-Pd(1)-P(2) [176.2(1)°] underline the distortion of the square planar environment of the palladium atom. The least square plane calculated through the atoms of the two disordered carbene ligands, A and B, are orientated at an angle of 86.4(3)° and 83.0(4)° respectively with respect to the plane calculated through C(1A), C(1B), Pd(1), P(1), P(2). The bond lengths and angles of the carbene ligand are the same as restraints were applied in the refinement to deal with the disorder.

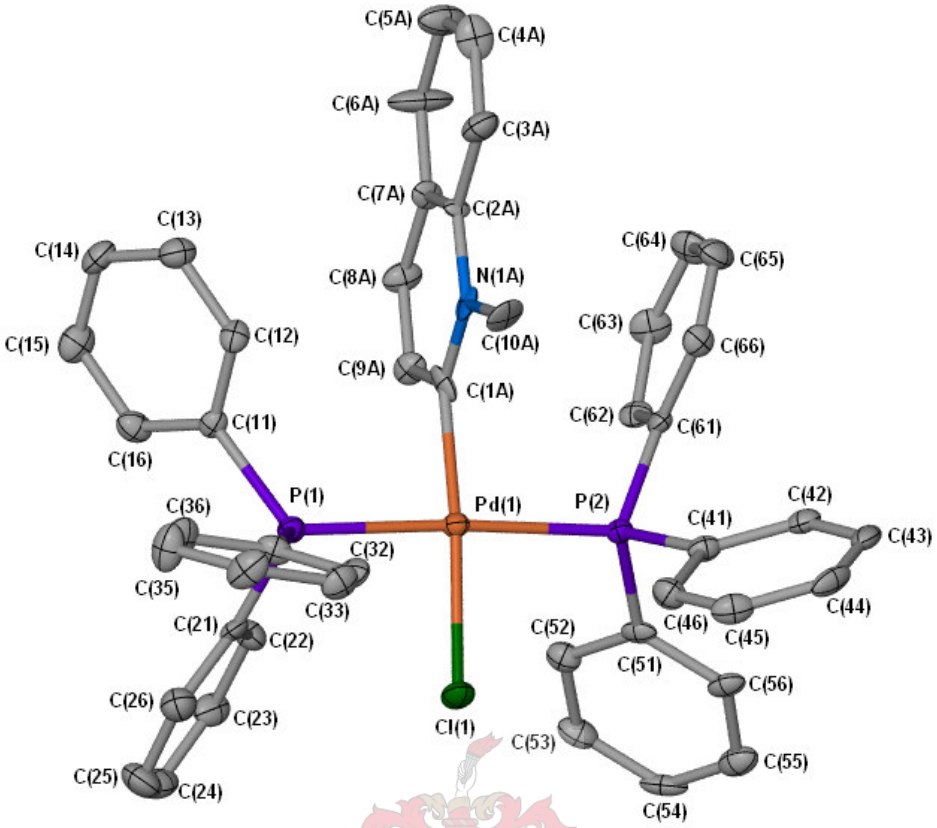

Figure 2.11 Molecular structure of ***trans*-9a**, showing the numbering scheme, generated in POV-Ray

The Pd(1)-C(1A) bond length [2.031(10) Å] does not differ significantly from the Pd-$C_{carbene}$ bond lengths in **3a** [1.996(5) Å], **8a** [1.995(3) Å], *trans*-chloro(2-tert-butyl-1,2,3,4-tetrahydro-isoquinolin-3-ylidene)bis(trimethylphosphine)palladium(II) tetraphenylborate (**D**) [2.011(14) Å],[75] and other Pd(II) carbene complexes with the Cl atom located *trans* to the carbene ligand.[14,15,68] The Pd(1)-C(1B) bond length [1.939(12) Å] is however, significantly shorter than Pd(1)-C(1A) and this could be the result of the disorder in the carbene ligand. The distances Pd(1)-P(1) [2.320(1) Å] and Pd(1)-P(1) [2.329(1) Å] are similar as expected for two PPh_3 ligands orientated *trans* to each other. Pd(1)-Cl(1) [2.347(1) Å] is significantly longer than the same bond in **3a** [2.336(1) Å] but shorter than the same bond in **8a** [2.363(1) Å]. From these differences it can be concluded that the *trans*-influence of the carbene ligand in ***trans*-9a** is greater than that of the carbene in **3a** but smaller than the *trans*-influence of the carbene ligand in **8a**. The C(1A)-N (1A) distance [1.340(10) Å] does not differ significantly from the same distances in **8a** [1.314(5) Å], **8b** [1.349(6) Å], and (**D**) [1.31(3) Å][75] but

[75] J. Cámpora, C. Graiff, P. Palma, E. Carmona, A. Tiripicchio, *Inorg. Chim. Acta*, 1998, **269**, 191.

this bond is shorter than N(1A)-C(10A) [1.461(19) Å] and longer than the $C(sp^2)=N(sp^2)$ double bond (1.27 Å).[74] This analysis confirms the partial double bond character of C(1A)-N(1A) and that the main contributing structures for ***trans*-9a** in the solid phase are similar to those proposed for **8a** [(**vii**) and (**ix**), Scheme 2.16]. All the C-C bond lengths fall into the range for typical conjugated aromatic rings (1.36 – 1.43 Å).[18]

Table 2.28 Selected bond lengths (Å) and angles (°) for ***trans*-9a**

Pd(1)-C(1A)	2.031(10)	C(3A)-C(4A)	1.343(19)
Pd(1)-C(1B)	1.939(12)	C(4A)-C(5A)	1.415(19)
Pd(1)-P(1)	2.320(1)	C(5A)-C(6A)	1.403(18)
Pd(1)-P(2)	2.329(1)	C(6A)-C(7A)	1.420(20)
Pd(1)-Cl(1)	2.347(1)	C(7A)-C(8A)	1.399(12)
C(1A)-N(1A)	1.340(10)	C(8A)-C(9A)	1.370(20)
N(1A)-C(10A)	1.461(19)	C(9A)-C(1A)	1.420(20)
N(1A)-C(2A)	1.397(10)	C(7A)-C(2A)	1.402(14)
C(2A)-C(3A)	1.397(13)		
C(1A)-Pd(1)-Cl(1)	170.6(3)	N(1A)-C(1A)-C(9A)	117.3(13)
C(1B)-Pd(1)-Cl(1)	170.2(3)	C(1A)-N(1A)-C(2A)	122.6(8)
P(1)-Pd(1)-P(2)	176.2(1)	N(1A)-C(2A)-C(7A)	119.4(9)
C(1A)-Pd(1)-P(1)	91.8(3)	C(2A)-C(7A)-C(8A)	119.2(9)
C(1A)-Pd(1)-P(2)	91.3(3)	C(7A)-C(8A)-C(9A)	119.0(12)
Cl(1)-Pd(1)-P(1)	86.5(1)	C(1A)-C(9A)-C(8A)	122.5(17)
Cl(1)-Pd(1)-P(2)	90.1(1)	Pd(1)-C(1A)-N(1A)	125.5(7)
C(1A)-Pd(C(1B)	19.2(3)	Pd(1)-C(1A)-C(9A)	117.3(11)

The packing of ***trans*-9a** in the unit cell along the b-axis (A) and the c-axis (B) is shown in Figure 2.12. The cations are stacked on top of each other along the b-axis and c-axis forming layers along the b-axis and c-axis. The BF_4^- counter ions and CH_2Cl_2 molecules are located in the spaces amongst the cations. The carbene ligands point to the left in two layers and then to the right in the next two layers parallel to the b-axis (B). In the two layers where the carbene ligands are pointing in the same direction, the carbene ligands are pointing slightly down in the one layer and slightly up in the other layer.

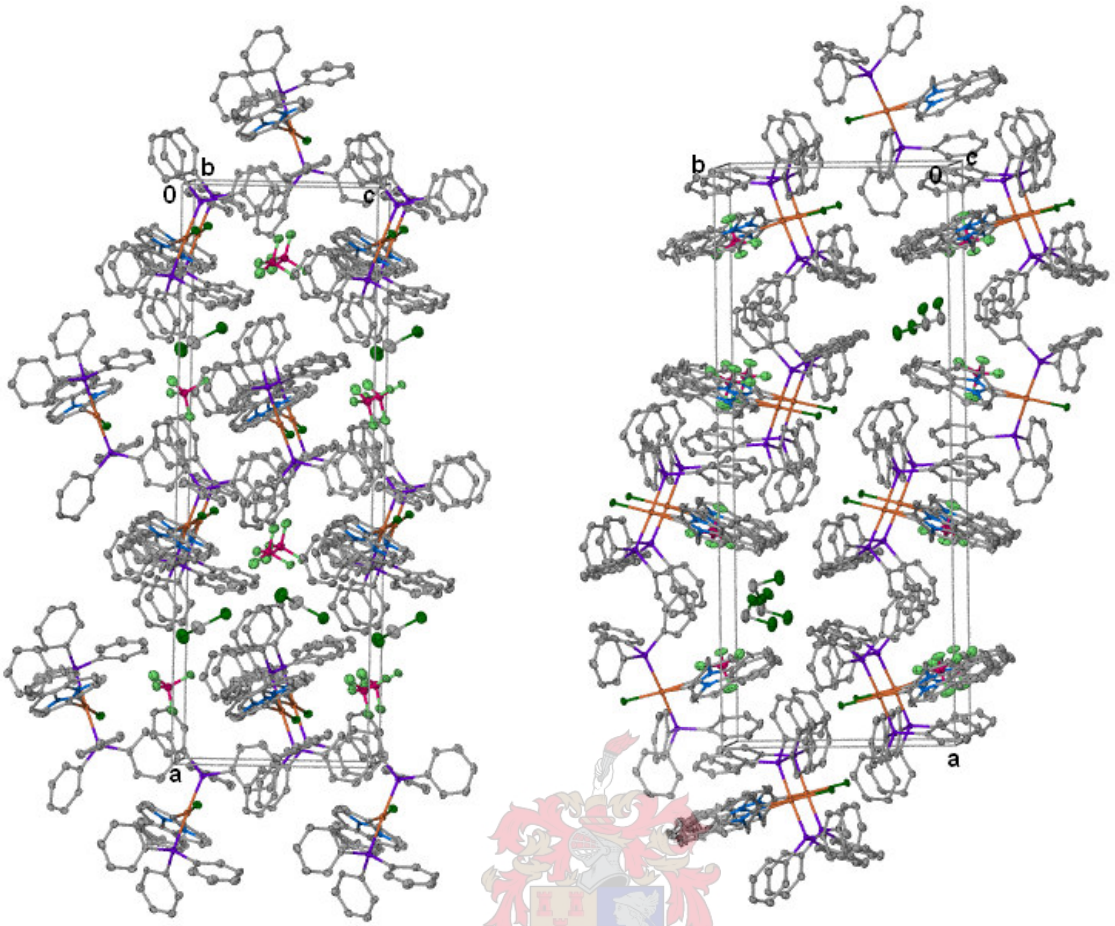

A B

Figure 2.12 Packing diagram of the molecules of ***trans*-9a** along the b-axis (A) and c-axis (B)

2.2.17.7 The crystal and molecular structure of cis-*chloro(1-methyl-1,2-dihydro-quinolin-2-ylidene)bis(triphenylphosphine)palladium(II) tetrafluoroborate,* ***cis*-9a**

This is the first *cis* structure in this study that is reported here. The structure is also unique as the structures of both the *cis* and *trans* isomers of **9a** were determined. Figure 2.13 shows one of the two independent molecules in the unit cell of the square planar complex ***cis*-9a** crystallised at –20°C. The molecular structure of ***cis*-9a** shows the two PPh_3 ligands in the *cis* positions while the NMR data at room temperature indicate two equivalent phosphines. The two doublets expected for ***cis*-9a** were observed only at –20°C in the ^{31}P NMR spectrum of complex **9a** (Section 2.2.8.2). This indicates that the *cis*-*trans* isomerisation is temperature-dependent with the *cis* isomer more stable at lower temperatures. Both *cis* and *trans* isomers for the platinum quinolinylidene, **13c**, were observed also by ^{31}P NMR spectroscopy, in solution at room temperature, but only the crystal

structure of this ***cis*-13c** could be determined. Selected bond lengths and angles are summarized in Table 2.29.

Deviations from the least square plane calculated through the five atoms C(10), Pd(11), P(11), P(12) and Cl(11) range from -0.050(2) to 0.208(3) Å and the angles around the Pd center deviate significantly from 90° due to the rather bulky PPh_3 ligands in the *cis* positions. The angle (P11)-P(11)-P(12) [100.64(7)] is expanded to accommodate the two PPh_3 ligands next to each other. The C(10)-Pd(11)-Cl(11) angle of 85.7(2)° on the other hand is the smallest of the four angles and the carbene and the Cl ligands are forced closer together. The two angles C(10)-Pd(11)-P(11) [165.8(2)°] and Cl(11)-Pd(11)-P(12) [170.39(70°] are also much smaller than 180°. All the atoms of the carbene ligand are practically in one plane [maximum deviation 0.012(7) Å by C(18) and C(19)] and the carbene ligand is orientated at an angle of 82.5(1)° with respect to the coordination plane of the Pd center.

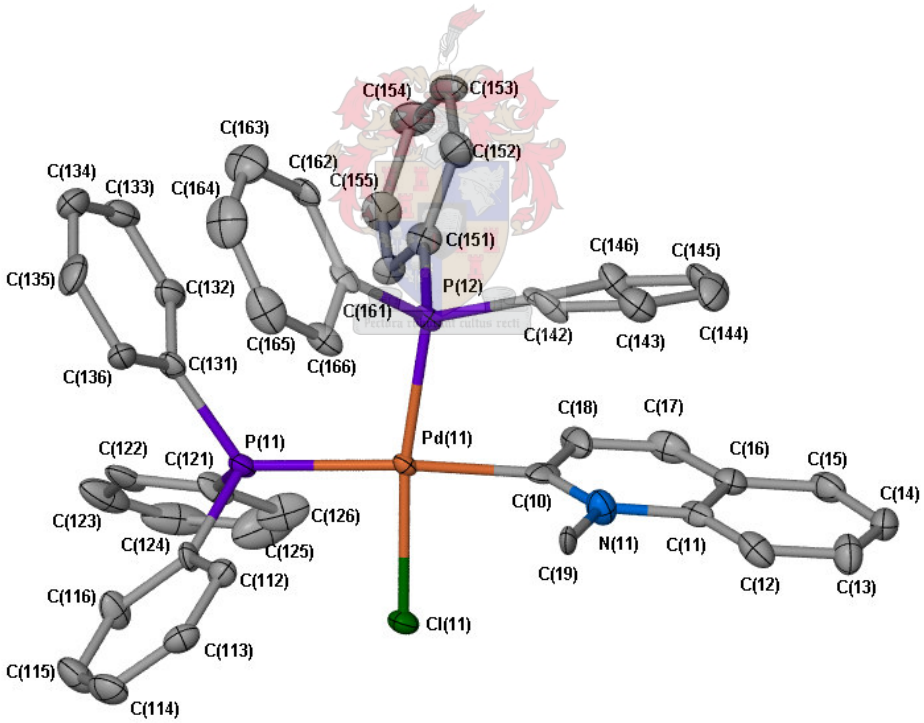

Figure 2.13 Molecular structure of ***cis*-9a**, showing the numbering scheme, generated in POV-Ray

The Pd-carbene bond [2.033(8)Å] is only slightly longer than the Pd-$C_{carbene}$ bond in **8a** [1.995(3) Å] and **13a** [1.986(3) Å] as a result of the greater *trans*-influence of PPh_3 (in ***cis*-9a**) compared to chloride (in **13a** and **9**). The Pd(11)-P(11) distance [2.386(2) Å] is also larger than the Pd(11)-P(12)

bond length [2.268(2) Å] due to the greater *trans*-influence of the carbene ligand in comparison to chloride. The C(10)-N(11) bond length [1.319(10) Å] in ***cis*-9a** does not differ significantly from the corresponding C(1)-N(1) distance in **8a** [1.314(5) Å] , ***trans*-9a** [1.340(10) Å] as well in *trans*-chloro(2-tert-butyl-1,2,3,4-tetrahydro-isoquinolin-3-ylidene)bis(trimethylphosphine)palladium(II) tetraphenylborate (**D**) [1.31(3) Å].[75] The most important contributing structure of ***cis*-9a** in the solid state is similar to that of **8a**, **8b** and ***cis*-9a** (except that the two PPh_3 ligands are now in the *cis* positions) with the Pd(11)-C(10) and C(10)-N(11) bonds both having partial double bond character. The bond lengths and angles of the carbene ligand in ***trans*-9a** and ***cis*-9a** are similar.

Table 2.29 Selected bond lengths (Å) and angles (°) for ***cis-9a***

Pd(11)-C(10)	2.033(8)	C(12)-C(13)	1.363(12)
Pd(11)-P(11)	2.386(2)	C(13)-C(14)	1.400(12)
Pd(11)-P(12)	2.268(2)	C(14)-C(15)	1.368(12)
Pd(11)-Cl(11)	2.347(2)	C(15)-C(16)	1.446(12)
C(10)-N(11)	1.319(10)	C(16)-C(17)	1.402(12)
N(11)-C(11)	1.421(10)	C(17)-C(18)	1.375(12)
N(11)-C(19)	1.423(10)	C(18)-C(10)	1.449(12)
C(11)-C(12)	1.379(12)	C(11)-C(16)	1.427(11)
C(10)-Pd(11)-Cl(11)	85.7(2)	N(11)-C(10)-C(18)	119.2(8)
P(11)-Pd(11)-P(12)	100.6(1)	C(10)-N(11)-C(11)	122.9(7)
C(10)-Pd(11)-P(11)	165.8(2)	N(11)-C(11)-C(16)	118.0(7)
C(10)-Pd(11)-P(12)	87.1(2)	C(11)-C(16)-C(17)	119.3(8)
Cl(11)-Pd(11)-P(11)	87.8(1)	C(16)-C(17)-C(18)	120.4(8)
Cl(11)-Pd(11)-P(12)	170.4(1)	C(10)-C(18)-C(17)	120.1(9)
Pd(11)-C(10)-N(11)	125.5(6)	Pd(11)-C(10)-C(18)	115.2(6)

The cations of ***cis-9a*** are stacked on each other along the a-axis (A) and b-axis (B) forming layers on top of each other (Figure 2.14). The cations are arranged in such a way that the carbene ligands of the cations are pointing towards each other with the benzene ring of two cations overlapping each other, forming a cavity that hosts the BF_4^- counter ions (A). The Cl atoms are pointing up in one layer parallel to the a-axis and down in the next layer (B).

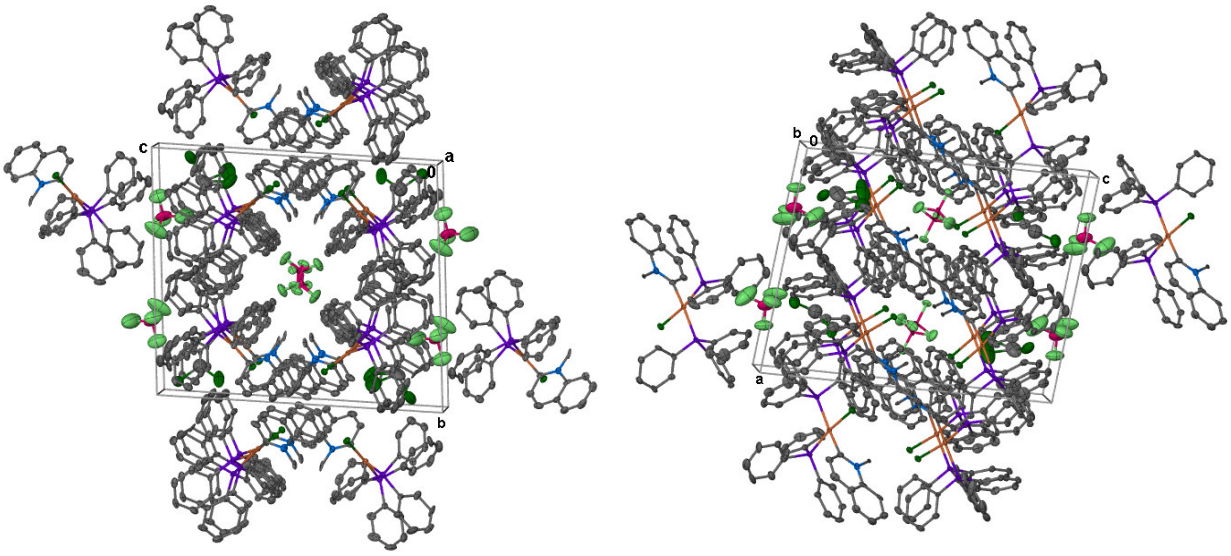

A B

Figure 2.14 Packing diagram of the molecules of ***cis-9a*** along the a-axis (A) and b-axis (B)

The one-N, six-membered *r*NHC complexes of nickel, palladium and platinum are described next.

2.2.17.8 The crystal and molecular structure of trans-*chloro(2-methoxy-1-methyl-1,4-dihydro-quinolin-4-ylidene)bis(triphenylphosphine)nickel(II) tetrafuoroborate,* ***13b***

The crystal structure of **13b** is shown in Figure 2.15 and is very similar to the crystal structure of **13a**.[18] Selected bond lengths and angles are summarized in Table 2.30. The carbene ligand backbone, Ni(1), Cl(1), B(1), F(1) and F(2) are situated in a mirror plane that relates one half of the molecule to the other. The two PPh_3 ligands occupy mutually *trans* positions. The Ni metal center is square planar and the maximum deviation from the least square plane through C(1), Ni(1), P(1), P(2) and Cl(1) is 0.003(3)Å. The mirror plane intersects the Ni square plane at an angle of 89.9(1)° and it is the same as in **13a** [90.0(1) °]. The angles around the Ni center do not deviate much from 90° or from 180°as a result of the mirror plane present in **13b**.

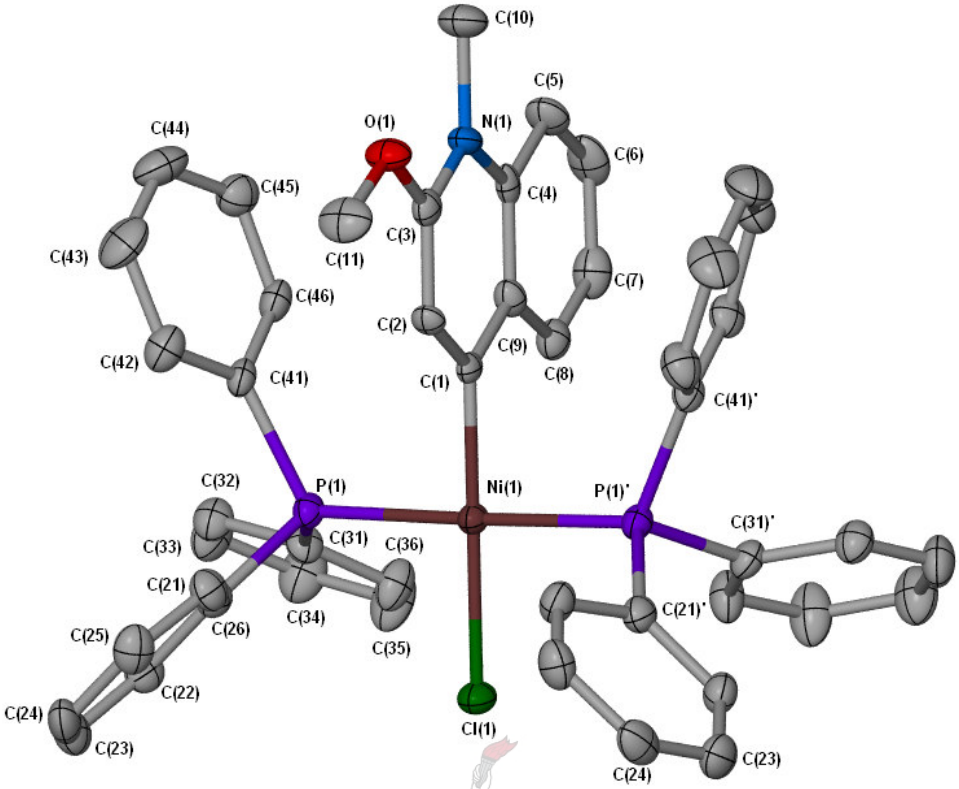

Figure 2.15 Molecular structure of **13b**, showing the numbering scheme, generated in POV-Ray

The Ni-$C_{carbene}$ bond is not different from the others in the complexes described in this chapter but the Ni-Cl distance could be a way of discriminating between *r*NHC and NHC complexes. The Ni(1)-Cl(1) distances in **13b** [2.216(2) Å] and **8b** [2.203(1) Å] do not just differ significantly but the Ni(1)-Cl(1) distance is longer than the same bond in **3b** [2.187(1) Å] and **4b** [2.191(1) Å], illustrating the smaller *trans*-influence of the two NHC carbene ligands compared to the *r*NHC ligand. The bond lengths and angles in the carbene ligand do not differ significantly from the corresponding bonds and angles of the carbene ligand in **13a**.[18] All the other bonds are normal. The resonance structures in Scheme 2.17 indicate that some positive charge is located on N(1) (**xi**) and O(1) (**xii**) and this electron distribution contributes to the overall structure of **13b** [**xiii**].

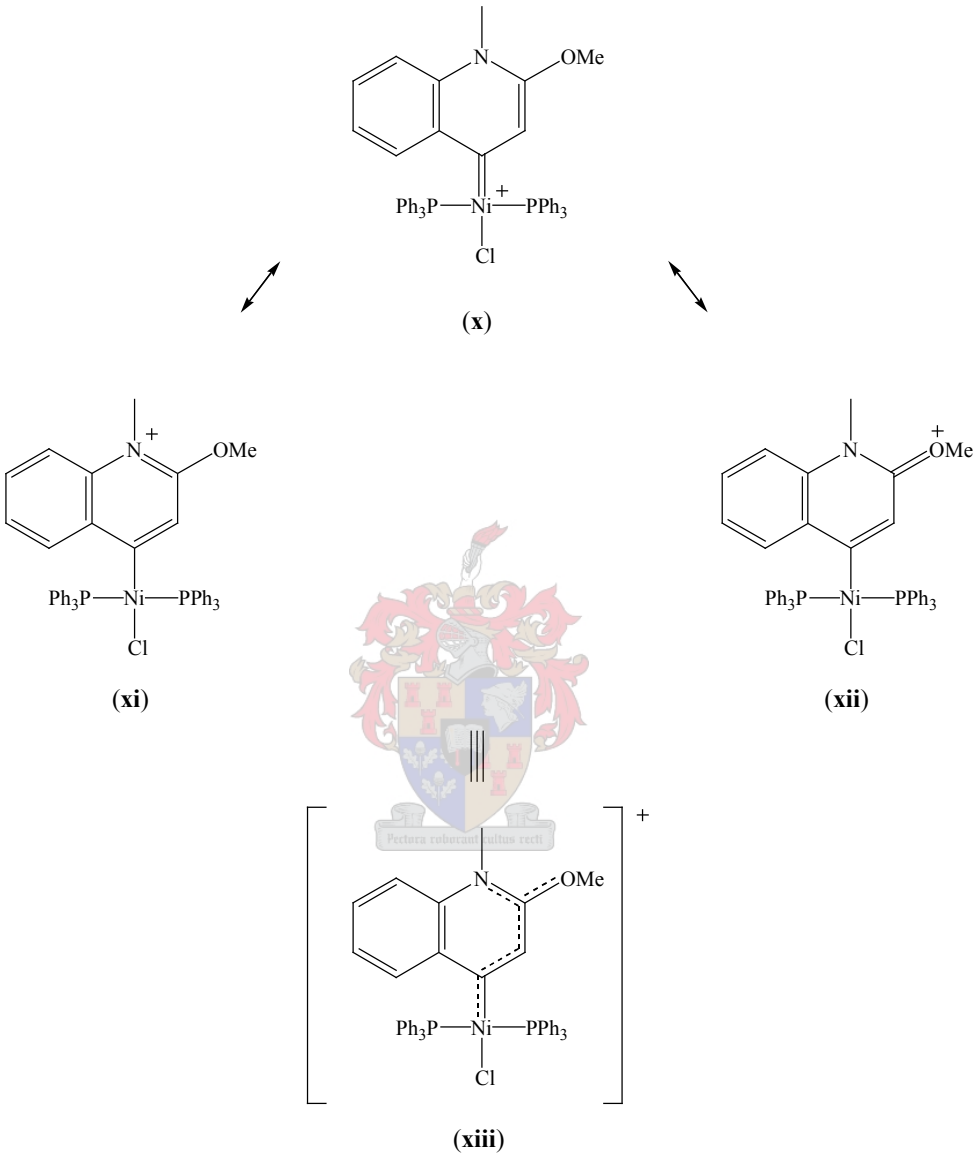

Scheme 2.17

Table 2.30 Selected bond lengths (Å) and angles (°) for **13b**

Ni(1)-C(1)	1.871(5)	N(1)-C(10)	1.476(7)
Ni(1)-P(1)	2.235(1)	N(1)-C(4)	1.401(7)
Ni(1)-Cl(1)	2.216(2)	C(4)-C(5)	1.395(8)
C(1)-C(2)	1.376(7)	C(5)-C(6)	1.365(9)
C(1)-C(9)	1.432(7)	C(6)-C(7)	1.392(9)
C(2)-C(3)	1.385(7)	C(7)-C(8)	1.381(8)
C(3)-N(1)	1.352(7)	C(8)-C(9)	1.405(8)
C(3)-O(1)	1.335(6)	C(4)-C(9)	1.405(8)
O(1)-C(11)	1.447(7)		
C(1)-Ni(1)-Cl(1)	179.8(2)	C(2)-C(1)-C(9)	117.9(5)
P(1)-Ni(1)-P(1)'	178.4(1)	C(1)-C(2)-C(3)	120.8(5)
C(1)-Ni(1)-P(1)	89.2(1)	C(2)-C(3)-N(1)	122.0(5)
Cl(1)-Ni(1)-P(1)	90.8(1)	C(3)-N(1)-C(4)	119.9(5)
Ni(1)-C(1)-C(2)	122.2(4)	N(1)-C(4)-C(9)	119.0(5)
Ni(1)-C(1)-C(9)	119.9(4)	C(1)-C(9)-C(4)	120.3(5)
C(3)-N(1)-C(10)	121.4(5)	C(3)-O(1)-C(11)	117.6(4)
C(4)-N(1)-C(10)	118.7(5)	O(1)-C(3)-N(1)	113.6(5)

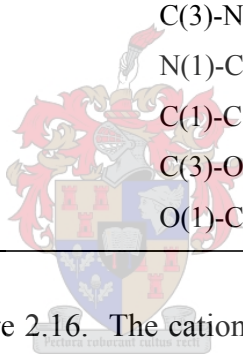

The unit cell of **13b** is shown in Figure 2.16. The cations form layers parallel to the a-axis, b-axis and c-axis in the unit cell of complex **13b**. The cations are packed along the b-axis in such a manner that the carbene ligands are almost in a straight line pointing in one direction in one layer and in the opposite direction in the next layer of cations. The PPh_3 ligands are thus also stacked on top of each other. Each BF_4^- anion is packed in the space between the carbene ligand of one cation and the Cl-ligand of a following one.

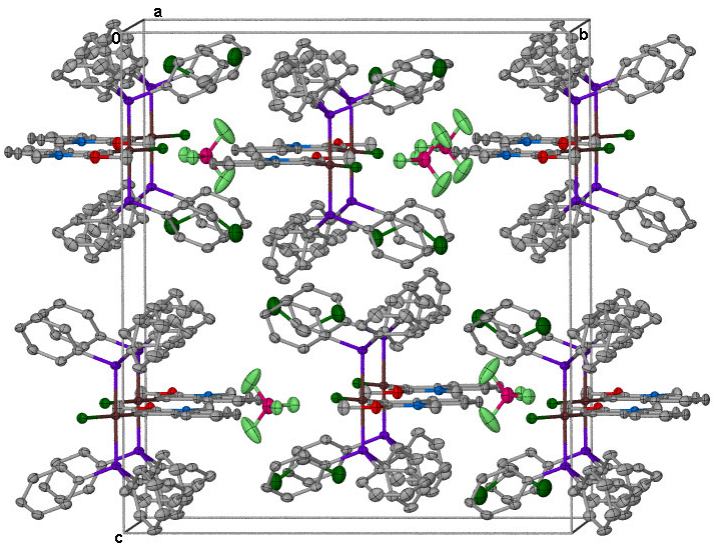

Figure 2.16 Packing diagram of the molecules of **13b** along the a-axis

The *r*NHC complex, with the heaviest element in group 10, Pt, follows. This time, however, the *cis* complex was isolated.

2.2.17.9 The crystal and molecular structure of cis*-chloro(2-methoxy-1-methyl-1,4-dihydro-quinolin-4-ylidene)bis(triphenylphosphine)platinum(II) tetrafuoroborate,* ***13c***

Despite the presence of both *cis* and *trans* isomers in solution as found by ^{31}P NMR study of the product mixture in the attempted preparation of **13c** at room temperature, only the molecular structure of the *cis* isomer could be determined after crystallisation (–20°C). The structure on **13c** (Figure 2.17) shows an approximate square planar coordination. Selected bond lengths and angles are summarized in Table 2.31. It is clear, however, that the coordination sphere is distorted and the plane of the heterocyclic carbene is rotated with respect to the main coordination plane resulting in a dihedral angle of 87.6(1)°. This value is still within the range 77 - 90° already reported for square planar platinum carbene complexes.[76] The maximum deviation from the coordination plane is 0.026(3) Å by the C(1). The atoms of the carbene ligand deviate only slightly from the least square plane calculated through the atoms of the ligand. The four angles around Pt(1) are well bent away from the ideal 90° due to the close proximity of the two bulky PPh_3 groups. The angles range from

[76] L. Garlaschelli, M.C. Malatesta, S. Panzeri, A. Albinati, F. Ganazzoli, *Organometallics*, 1987, **6**, 63.

85.6(2)° to 98.2(1)°. The accommodation of the steric requirements of the two *cis* PPh_3 ligands is also reflected by the two angles C(1)-Pt(1)-P(1) [172.7(2) Å] and Cl(1)-Pt(1)-P(2) [174.5(1) Å].

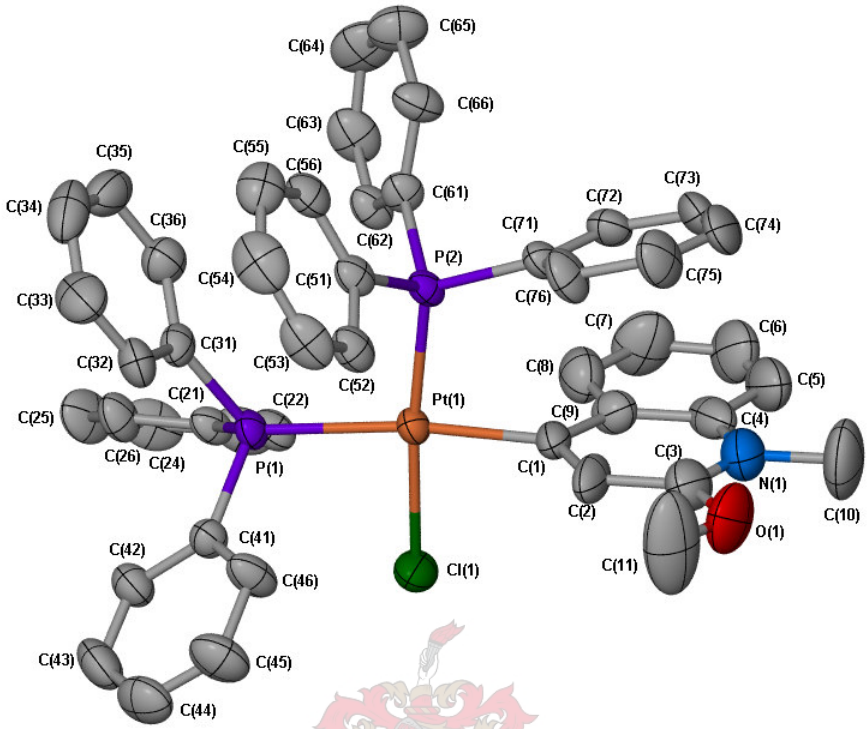

Figure 2.17 Molecular structure of **13c**, showing the numbering scheme, generated in POV-Ray

The Pt(1)-C(1) bond length of 2.054(6) Å in **13c** is significantly longer than other Pt-$C_{carbene}$ distances of square planar platinum(II) carbene complexes, which generally occur in the range 1.82 - 2.01 Å when a chloride occurs *trans* to the carbene ligand.[77] The longer Pt-$C_{carbene}$ bond length is due to the greater *trans*-influence of PPh_3 in comparison to chloride. The Pt-Cl bond length [2.361(2) Å] compares well with the Pt-Cl bond lengths [2.356(4) - 2.369(2) Å] of similar but *trans* complexes.[78] This similarity in the Pt-Cl distance indicates that the carbene ligand in **13c** and PPh_3 exhibit the same *trans*-influence. The Pt(1)-P(1) bond [2.365(1) Å] is significantly longer than the Pt(1)-P(2) bond [2.242(1) Å] as a result of the greater *trans*-influence of the carbene ligand over the chloride. This result now also confirms the assignments and coupling constants of the peaks and satellites in the ^{31}P NMR spectrum of **13c**.[18] The internal bond lengths of the carbene ligand does not differ significantly from those in **13a** and **13b** except for C(5)-C(6), C(8)-C(9) and C(3)-N(1) which are somewhat shorter than those in **13a** and **13b** and C(3)-O(1) that is longer than the same

[77] R.A. Michelin, L. Zanotto, D. Braga, P. Sabatino, R.J. Angelici, *Inorg. Chem.*, 1998, **27**, 85.

[78] R.A. Michelin, G. Facchin, D. Braga, P. Sabatino, *Organometallics*, 1986, **5**, 2265.

bond in **13a**. The C(3)-N(1) distance [1.278(10) Å] compares well with that of a $C(sp^2)=N(sp^2)$ double bond (1.27 Å),[74] indicating also that the C(3)-N(1) has much more double bond character than C(3)-N(1) in **13a** and **13b**. This phenomenon suggests that the positive charge is mostly located on N(1) and that resonance structure **(xiv)** in Scheme 2.18 might even be more important for **13c** in the solid state than for both **13a** and **13b**.

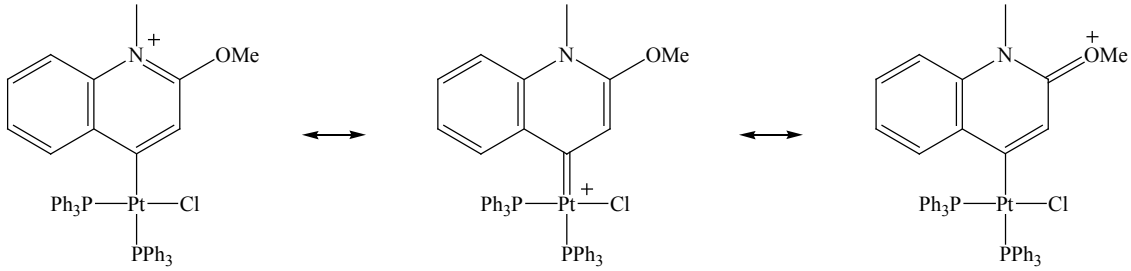

(xiv) **(xv)** **(xvi)**

Scheme 2.18

Table 2.31 Selected bond lengths (Å) and angles (°) for **13c**.

Pt(1)-C(1)	2.054(6)	O(1)-C(11)	1.446(12)
Pt(1)-P(1)	2.365(1)	N(1)-C(10)	1.474(10)
Pt(1)-P(2)	2.242(1)	N(1)-C(4)	1.424(10)
Pt(1)-Cl(1)	2.361(2)	C(4)-C(5)	1.374(11)
C(1)-C(2)	1.398(10)	C(5)-C(6)	1.277(13)
C(1)-C(9)	1.429(9)	C(6)-C(7)	1.389(13)
C(2)-C(3)	1.397(10)	C(7)-C(8)	1.378(11)
C(3)-N(1)	1.278(10)	C(8)-C(9)	1.356(10)
C(3)-O(1)	1.362(9)	C(4)-C(9)	1.434(10)
C(1)-Pt(1)-Cl(1)	85.6(2)	C(2)-C(1)-C(9)	118.4(6)
C(1)-Pt(1)-P(1)	172.7(2)	C(1)-C(2)-C(3)	120.2(8)
C(1)-Pt(1)-P(2)	88.9(2)	C(2)-C(3)-N(1)	122.0(8)
P(1)-Pt(1)-P(2)	98.2(1)	C(3)-N(1)-C(4)	122.8(7)
Cl(1)-Pt(1)-P(1)	87.3(1)	N(1)-C(4)-C(9)	117.3(6)
Cl(1)-Pt(1)-P(2)	174.5(1)	C(1)-C(9)-C(4)	119.0(4)
Pt(1)-C(1)-C(2)	118.9(5)	C(3)-O(1)-C(11)	117.1(7)
Pt(1)-C(1)-C(9)	122.7(5)	O(1)-C(3)-N(1)	114.6(7)
C(3)-N(1)-C(10)	120.7(7)	C(4)-N(1)-C(10)	116.5(7)

The packing diagram of **13c** shows the packing of the cations on top of each other along the a-axis (Figure 2.18). Along the b-axis the cations are packed in layers with the carbene ligand and Cl pointing down in one layer and up in the next layer and with the carbene ligands pointing to the left in both layers. The cations of the next layer (down the b-axis and c-axis) are packed in line with the space between the two cations of the layers above and below that particular layer along both the axes creating cavities that host CH_2Cl_2 molecules. The BF_4 counter ions are packed between two cations in line with the Pt-atoms down the a-axis.

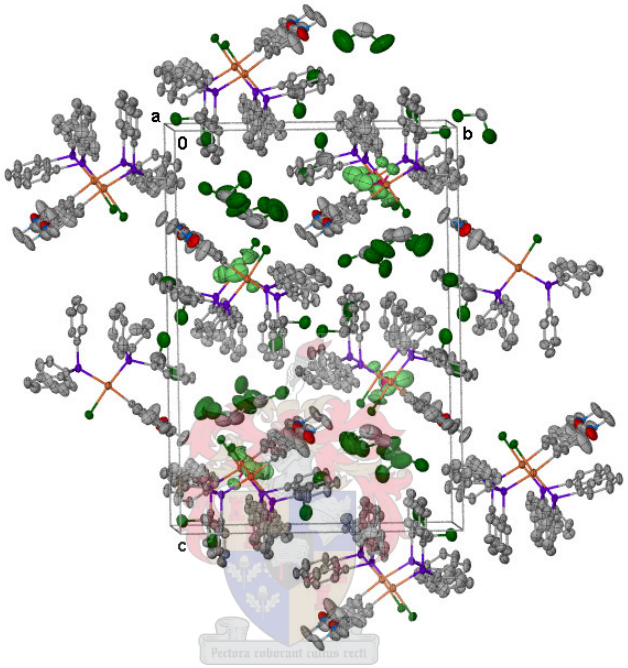

Figure 2.18 Packing diagram of the molecules of **13c** along the a-axis

The simplest *r*NHC complexes based on pyridine contain no substituents on the six-membered heterocycle. Two examples of unprecedented structures are reported here.

2.2.17.10 The crystal and molecular structure of trans-*chloro(1-methyl-1,4-dihydro-pyridin-4-ylidene)bis(triphenylphosphine)palladium(II) tetrafluoroborate,* ***14a***

Selected bond lengths and angles are listed in Table 2.32 and the molecular structure appears in Figure 2.19. The square plane is only slightly distorted with a maximum deviations of 0.018(3) Å from the least square plane calculated through C(1), Pd(1), P(1), P(2) and Cl(1). The carbene ligand is essentially flat, not perpendicular to the square plane formed by Pd and the four atoms coordinated to it but turned at an angle of 77.8(1)°. The C(1)-Pd(1)-P(2) angle is essentially 90°

while the three other angles around the Pd-center deviate slightly from this ideal angle but C(1)-Pd(1)-Cl(1) is really bent [175.3(2)°]. P(1)-Pd(1)-P(2) [177.4(1)°] is slightly smaller than 180°.

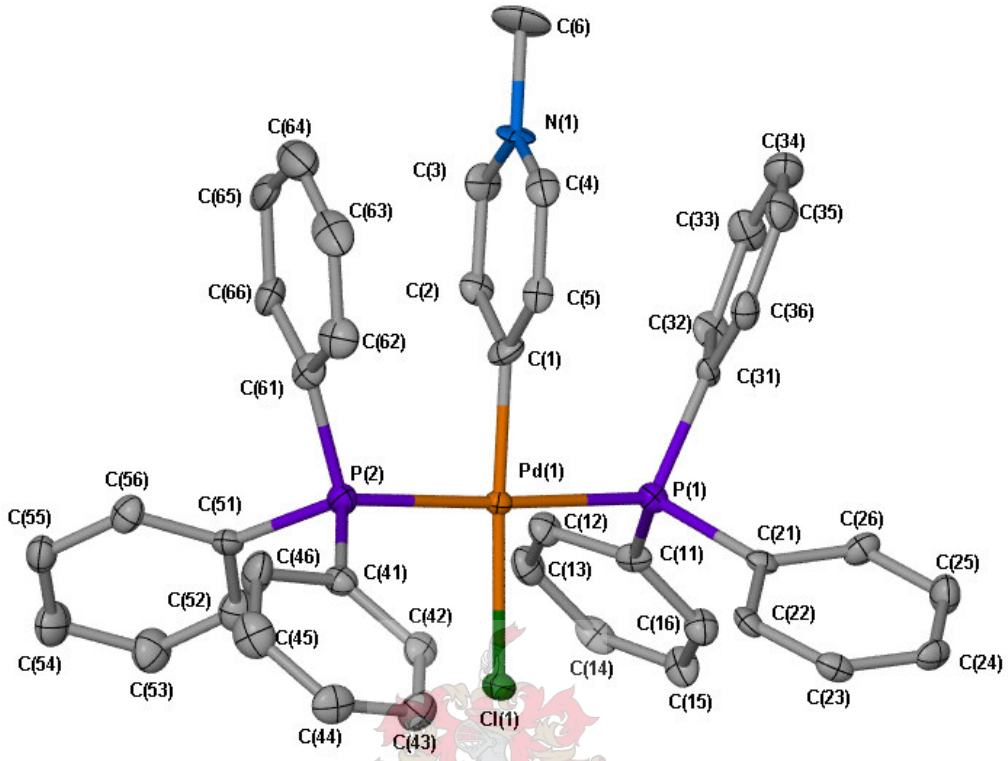

Figure 2.19 Molecular structure of **14a**, showing the numbering scheme, generated in POV-Ray

The Pd(1)-C(1) distance of 1.983(7) Å compares well with the same distance in other already-mentioned Pd carbene complexes. From the various bond lengths one could confidently say that delocalisation of electron density occurs between the metal and the heterocyclic ring (Scheme 2.19) The positive charge is thus partially located on the N atom [(**xvii**) and (**xix**)] and the structure (**xx**) represent the overall structure for **14a**.

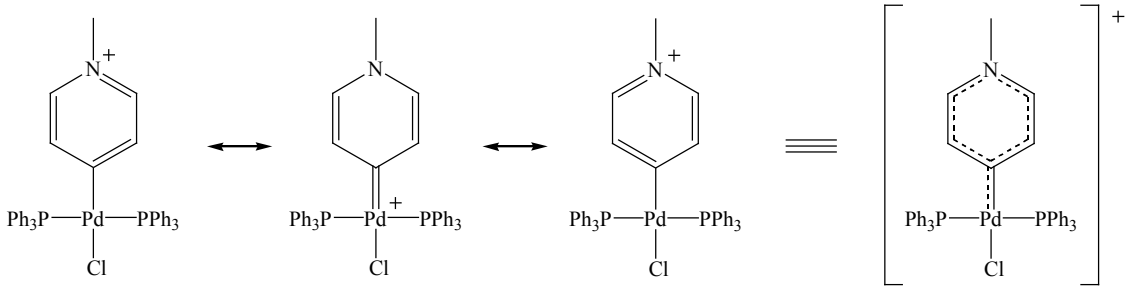

(**xvii**) (**xviii**) (**xix**) (**xx**)

Scheme 2.19

The Pd-Cl distance [2.394(2) Å] in **14a** is much longer than the same bond length in **3a** [2.336(1) Å], **8a** [2.363(1) Å] but close to Pd-Cl in **13a** [2.380(1) Å]. The carbene ligands can be arranged in order of increasing *trans*-influence: 1,3-dimethyl-2,3-dihydro-1*H*-imidazol-2-ylidene (in **3a**) < 1-methyl-1,2-dihydro-pyridin-2-ylidene (in **8a**) < 2-methoxy-1-methyl-1,4-dihydro-quinolin-4-ylidene (in **13a**), 1-methyl-1,4-dihydro-pyridin-4-ylidene (in **14a**).

Table 2.32 Selected bond lengths (Å) and angles (°) for **14a**

Pd(1)-C(1)	1.983(7)	C(3)-N(1)	1.351(8)
Pd(1)-P(1)	2.345(2)	N(1)-C(4)	1.342(9)
Pd(1)-P(2)	2.364(2)	C(4)-C(5)	1.376(9)
Pd(1)-Cl(1)	2.394(2)	C(1)-C(5)	1.406(9)
C(1)-C(2)	1.420(9)	N(1)-C(6)	1.477(9)
C(2)-C(3)	1.365(10)		
C(1)-Pd(1)-Cl(1)	175.3(2)	C(2)-C(3)-N(1)	119.2(6)
P(1)-Pd(1)-P(2)	177.4(1)	C(3)-N(1)-C(4)	122.1(6)
C(1)-Pd(1)-P(1)	87.7(2)	N(1)-C(4)-C(5)	119.8(6)
C(1)-Pd(1)-P(2)	89.7(2)	C(1)-C(5)-C(4)	121.8(6)
Cl(1)-Pd(1)-P(1)	87.9(1)	C(3)-N(1)-C(6)	119.3(6)
Cl(1)-Pd(1)-P(2)	94.6(1)	C(4)-N(1)-C(6)	118.6(6)
C(2)-C(1)-C(5)	114.8(6)	Pd(1)-C(1)-C(2)	120.7(5)
C(1)-C(2)-C(3)	122.3(6)	Pd(1)-C(1)-C(5)	124.5(5)

The packing of the molecules in the asymmetric unit of **14a** in the unit cell along the a-axis (A) and b-axis (B) is shown in Figure 2.20. The cations are packed on top of each other along the a-axis and form layers along the b-axis. The layers along the b-axis are packed in such a way that the cations in the next layer are positioned in line with the space between the two cations of the layers above and below that particular layer.

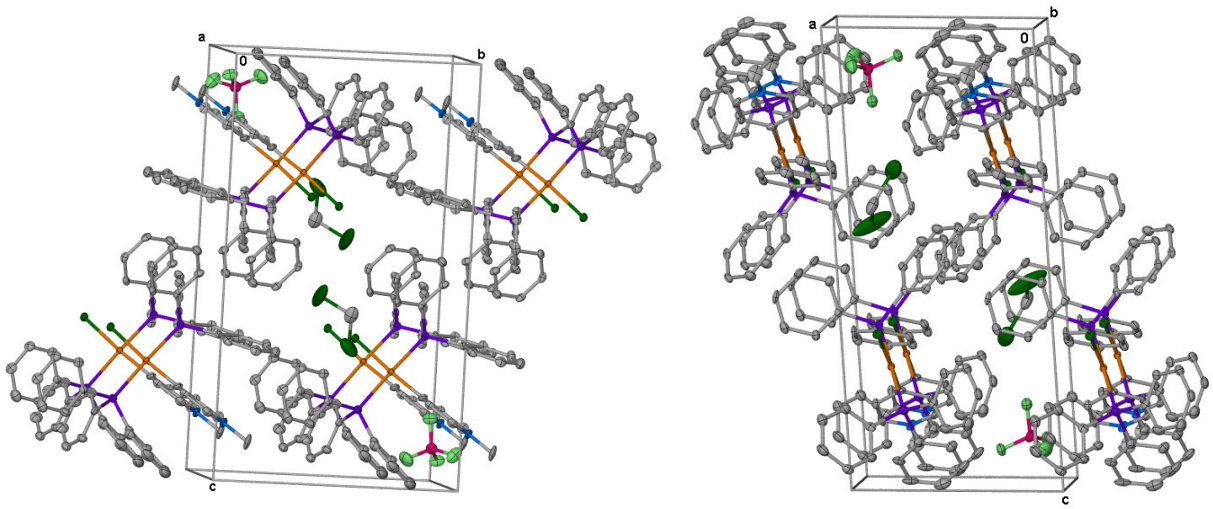

A B

Figure 2.20 Packing diagram of the molecules of **14a** along the a-axis

2.2.17.11 The crystal and molecular structure of trans-*chloro(1-methyl-1,4-dihydro-pyridin-4-ylidene)bis(triphenylphosphine)nickel(II) tetrafluoroborate,* ***14b***

The molecular structure of **14b** is shown is Figure 2.21 and selected bond lengths and angles in Table 2.33. The geometry around the nickel is distorted square planar with the maximum deviation [0.149(1) Å] from this plane by the two PPh_3 ligands in the *trans* positions and by Cl(1) [-0.133(2) Å]. This deformation is accompanied by the out of plane bending of the P(1)-Ni(1)-P(2) [169.5(1)°] and Cl(1)-C(1)-Ni(1)-Cl(1) [176.2(2)°] angles. The four angles around the nickel central metal are close to 90°. The carbene ligand is rotated with respect to the coordination plane, defined by C(1), Ni(1), P(1), P(2), at an angle of 83.5(1)°.

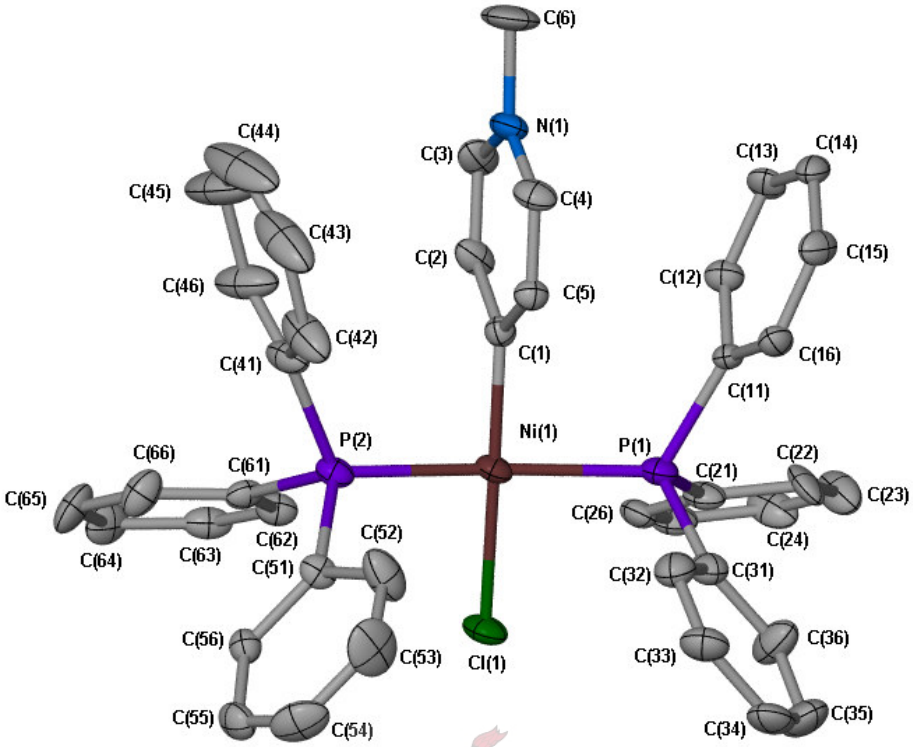

Figure 2.21 Molecular structure of **14b**, showing the numbering scheme, generated in POV-Ray

The Ni-$C_{carbene}$ bond length in **14b** [1.863(5) Å] is similar to Ni-$C_{carbene}$ in **3b** [1.881(5) Å], **4b** [1.857(4) Å], **8b** [1.863(3) Å] and **13b** [1.871(5) Å]. The bond lengths and angles of the carbene ligand in **14b** and **14a** do not differ significantly. Complex **14b** also has delocalised electron density that includes the metal and the carbene ligand, similar to **14a**. The Ni(1)-Cl(1) distance in **14b** [2.217(1) Å] and **13b** [2.216(2) Å] are equal but these bonds are longer than Ni-Cl in **3b** [2.187(1) Å], **4b** [2.191(1) Å] and **8b** [2.203(1) Å]. The carbene ligands in these nickel complexes can be arranged with increasing *trans*-influence as follows: 1,3-dimethyl-2,3-dihydro-1*H*-imidazol-2-ylidene (in **3b**), 1,3-dimethyl-2,3,4,5-tetrahydro-1*H*-imidazol-2-ylidene (in **4b**) < 1-methyl-1,2-dihydro-pyridin-2-ylidene (in **8b**) < 2-methoxy-1-methyl-1,4-dihydro-quinolin-4-ylidene (in **13b**), 1-methyl-1,4-dihydro-pyridin-4-ylidene (in **14b**).

Table 2.33 Selected bond lengths (Å) and angles (°) for **14b**

Ni(1)-C(1)	1.863(5)	C(3)-N(1)	1.342(7)
Ni(1)-P(1)	2.222(2)	N(1)-C(4)	1.348(6)
Ni(1)-P(2)	2.226(2)	C(4)-C(5)	1.350(7)
Ni(1)-Cl(1)	2.217(1)	C(1)-C(5)	1.399(7)
C(1)-C(2)	1.402(6)	N(1)-C(6)	1.484(6)
C(2)-C(3)	1.359(7)		
C(1)-Ni(1)-Cl(1)	176.2(2)	C(2)-C(3)-N(1)	120.9(5)
P(1)-Ni(1)-P(2)	169.5(1)	C(3)-N(1)-C(4)	119.8(4)
C(1)-Ni(1)-P(1)	89.8(2)	N(1)-C(4)-C(5)	120.7(5)
C(1)-Ni(1)-P(2)	89.9(2)	C(1)-C(5)-C(4)	122.1(5)
Cl(1)-Ni(1)-P(1)	90.3(1)	C(3)-N(1)-C(6)	121.7(5)
Cl(1)-Ni(1)-P(2)	90.7(1)	C(4)-N(1)-C(6)	118.4(5)
C(2)-C(1)-C(5)	114.9(4)	Ni(1)-C(1)-C(2)	122.8(4)
C(1)-C(2)-C(3)	121.5(5)	Ni(1)-C(1)-C(5)	122.2(4)

The packing diagram in the unit cell of **14b** is shown is Figure 2.22. The cations of complex **14b** are packed on top of each other along the a-axis and in a layer parallel to the c-axis. In the layers along the c-axis the cations are packed with the carbene ligand alternating up and down. The BF_4^- anions are situated between the carbene ligands of two cations packed on top of each other along the a-axis. CH_2Cl_2 molecules fill some of the spaces in the unit cell formed as a result of the packing of **14b**.

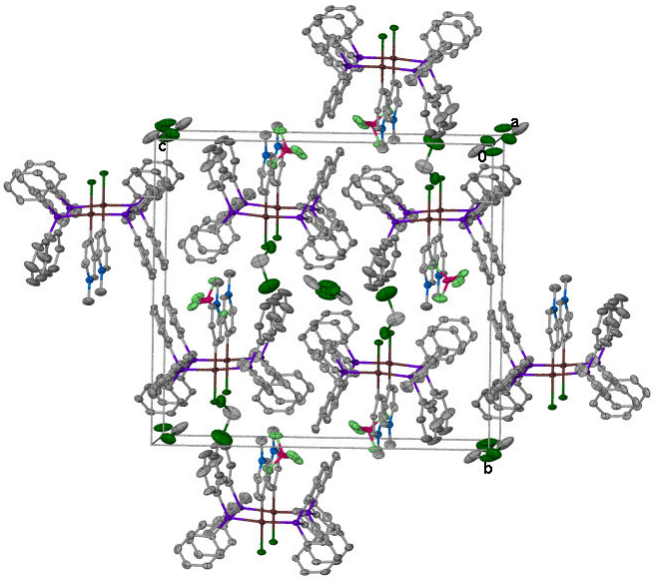

Figure 2.22 Packing diagram of the molecules of **14b** along the a-axis

Two *r*NHC complexes of chromium(0) and tungsten(0), derived form 4,4-dimethyl-2-thiophen-2-yl-4,5-dihydro-oxazole, with the active heteroatom, N, removed from the carbene carbon, are discussed in the following section.

2.2.17.12 The crystal and molecular structure of $(CO)_5Cr\{\underline{C}SC(\overline{CNMeCMe_2CH_2O})CH\underline{C}H\}$, ***17a***

Figure 2.23 shows the molecular structure of **17a**, with the $(CO)_5Cr$ group situated adjacent to the sulfur atom. Selected bond lengths and angles are listed in Table 2.34. The octahedral environment of the Cr atom is distorted and the angles around the Cr atom range from 86.8(2) – 92.0(2)° and 176.3(2) - 179.0(1)°. The plane through the thienyl ring [C(1), C(2), C(3), C(4) and S(1)] is rotated at an angle of 46.4(1)° with respect to the plane through Cr(1), C(1), C(13) and C(15). The least square plane through the thienyl ring is orientated at an angle of 9.7(1)° with respect to the bent plane calculated through the oxazole ring [C(5), C(6), C(7), O(1) and N(1)].

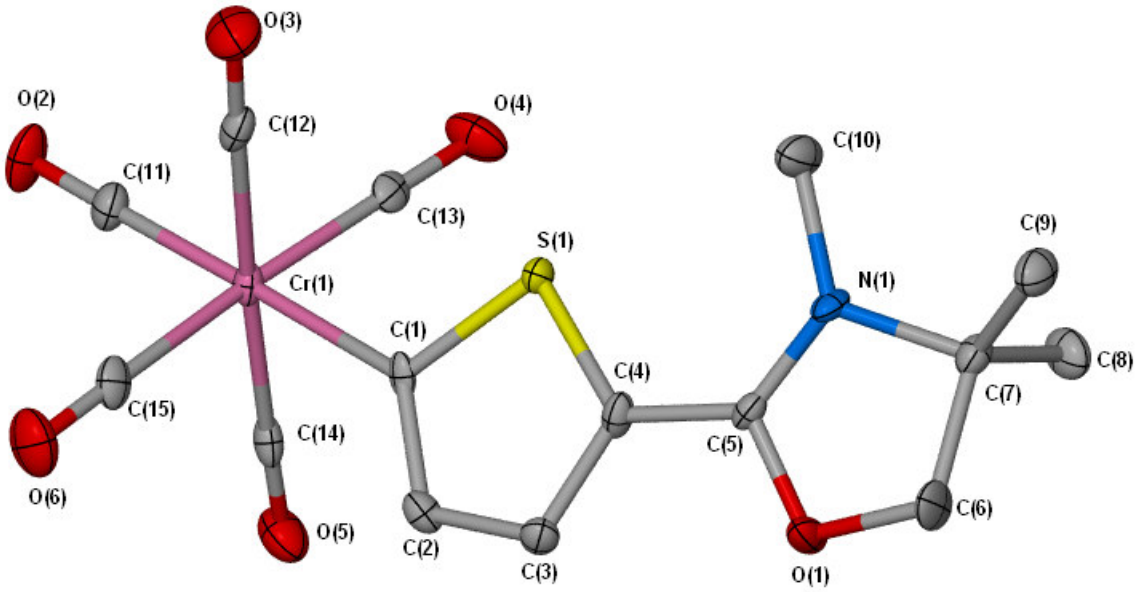

Figure 2.23 Molecular structure of **17a**, showing the numbering scheme, generated in POV-Ray

The Cr-$C_{carbene}$ [2.102(3) Å] and C(1)-S(1) distance [1.722(3) Å] in **17a** is longer than the 2.0 - 2.06 Å and 1.40 – 1.70 Å ranges reported for Cr-$C_{carbene}$ and $C_{carbene}$-S distances respectively in chromium thiocarbene complexes of the type $(CO)_5Cr=C(SR)R'$.[79] These two bond lengths are similar to the Cr-$C_{carbene}$ [2.09 Å] and $C_{carbene}$-S [1.73 Å] bond lengths in $(CO)_5Cr=\{\overline{CSC(SMe)C(COOEt)NH}\}$.[80] The bond lengths of the carbene ligand in **17a**, compare well with the oxazoline ligands in the dimeric complex $[Au\{\underline{C=C(\overline{C=NCMe_2CH_2O})SCH=CH}\}]_2$, **E**.[22] The following bond lengths, C(1)-C(2), and C(2)-C(3), in **17a** fall in the 1.36 – 1.43 Å range for aromatic conjugated systems.[18] C(5)-N(1) [1.311(4) Å] also has double bond character as it is shorter than N(1)-C(10) [1.466(4) Å]. The most important resonance structure for **17a** in the solid state is shown by (**xxi**) and (**xxii**) in Scheme 2.20 with (**xxiii**) as the overall structure. The Cr-$C_{carbonyl}$ distances in **17a** are surprisingly similar, indicating that the carbene ligand and CO show *trans*-influences of the same magnitude.

[79] U. Schubert, *Coord. Chem. Rev.*, 1984, **55**, 261.

[80] W.P. Fehlhammer, D. Achatz, U. Plaia, A. Volkl, *Z. Natuforsch., B: Chem. Sci.*, 1987, **42**, 720

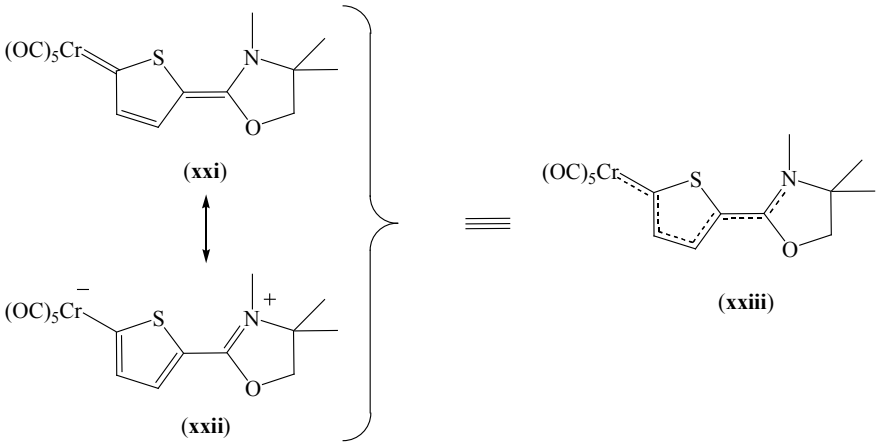

Scheme 2.20

Table 2.34 Selected bond lengths (Å) and angles (°) for **17a**

Cr(1)-C(1)	2.102(3)	N(1)-C(10)	1.466(4)
C(1)-C(2)	1.402(5)	C(7)-C(8)	1.531(5)
C(2)-C(3)	1.389(5)	C(7)-C(9)	1.502(5)
C(3)-C(4)	1.395(5)	Cr(1)-C(11)	1.870(4)
C(4)-S(1)	1.743(3)	Cr(1)-C(12)	1.895(5)
S(1)-(C1)	1.722(3)	Cr(1)-C(13)	1.891(4)
C(4)-C(5)	1.415(5)	Cr(1)-C(14)	1.888(5)
C(5)-O(1)	1.339(4)	Cr(1)-C(15)	1.903(5)
O(1)-C(6)	1.463(4)	C(11)-O(2)	1.147(4)
C(6)-C(7)	1.531(5)	C(12)-O(3)	1.149(5)
C(7)-N(1)	1.498(4)	C(13)-O(4)	1.142(5)
N(1)-C(5)	1.311(4)	C(14)-O(5)	1.156(5)
		C(15)-O(6)	1.141(5)
C(1)-Cr(1)-C(11)	179.0(1)	C(4)-S(1)-C(1)	95.0(2)
C(12)-Cr(1)-C(14)	176.9(2)	N(1)-C(5)-O(1)	112.0(3)
C(13)-Cr(1)-C(15)	176.3(2)	C(5)-O(1)-C(6)	107.5(3)
Cr(1)-C(1)-S(1)	121.2(2)	O(1)-C(6)-C(7)	104.4(3)
C(2)-C(1)-S(1)	107.0(2)	C(6)-C(7)-N(1)	97.8(3)
C(1)-C(2)-C(3)	116.6(3)	C(7)-N(1)-C(5)	111.0(3)
C(2)-C(3)-C(4)	112.7(3)	C(5)-N(1)-C(10)	126.1(3)
C(3)-C(4)-S(1)	108.7(2)	C(8)-C(7)-C(9)	112.6(3)

The molecules of complex **17a** are packed (viewed along the a-axis, Figure 2.24) with the oxazoline-containing carbene ligands of the different layers (parallel to the b-axis) aligned on top of each other and the $Cr(CO)_5$ groups of the different layers overlapping. The $Cr(CO)_5$ groups are pointing in one direction in one layer parallel to the b-axis and in the opposite direction in the next layer.

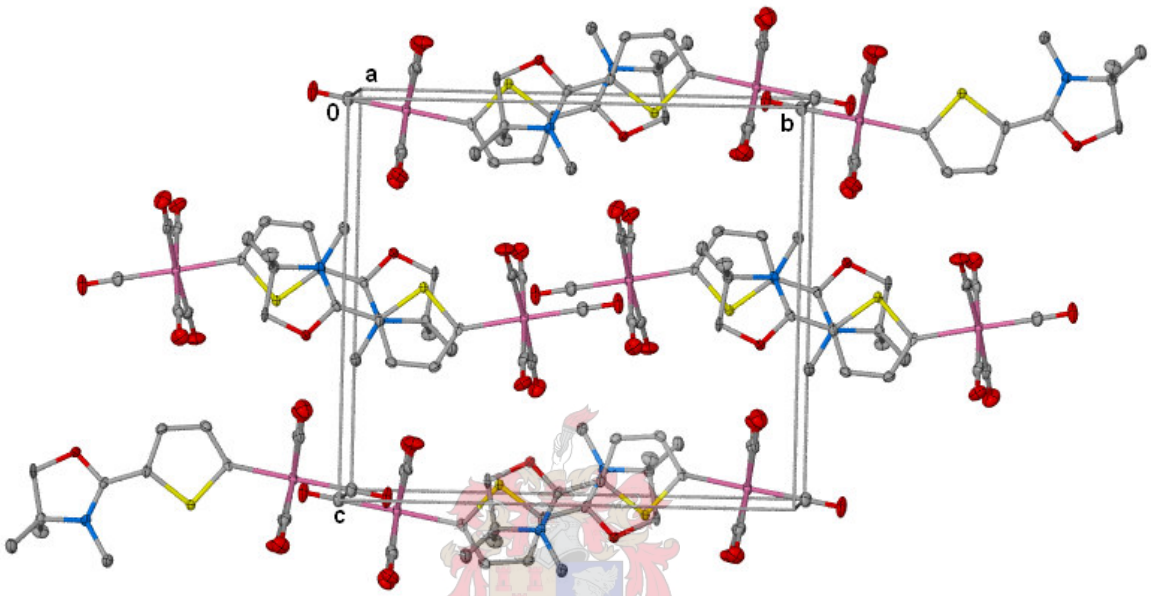

Figure 2.24 Packing diagram of the molecules of **17a** along the a-axis

2.2.17.13 The crystal and molecular structure of $(CO)_5W\{\underline{CSC(CNMeCMe_2CH_2O)CHCH}\}$, ***17b***

The molecular structure of complex **17b** shows that the metal fragment is again connected to the carbon atom adjacent to the sulfur atom (Figure 2.25). Selected bond lengths and angles are listed in Table 2.35. The atoms of the oxazole ring, except C(5), are disordered over two positions with site occupancy factors of 0.46 and 0.54 respectively, and with an angle of 25.8(4)° between the least square planes through these two disordered rings. The bond lengths and angles of the two disordered rings differ significantly. The angle between the least square plane through the thienyl ring and the disordered oxazoline rings is 15.8(5) and 15.9(2)° respectively. The thienyl ring is orientated at 47.2(5)° with respect to the least square plane through C(1), W(1), C(11), C(13) and C(15). The angles around W(1) deviate slightly [86.7(5) – 92.1(5) and 177.1(5) – 178.3(5)°] from the respective ideal 90° and 180° angles expected for the octahedral $W(CO)_5$ group.

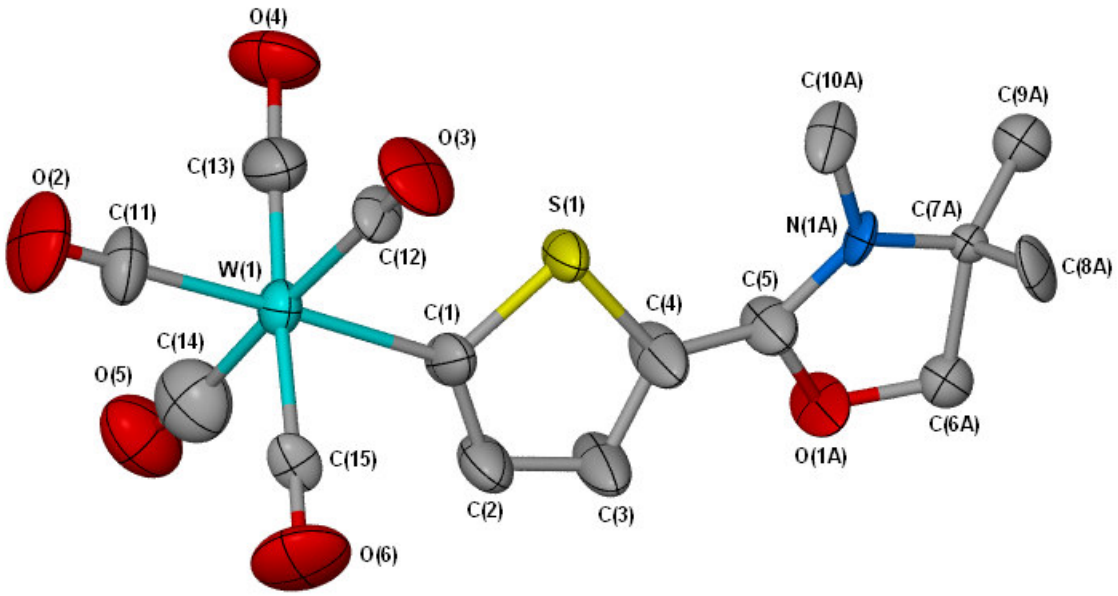

Figure 2.25 Molecular structure of **17b**, showing the numbering scheme, generated in POV-Ray

The W(1)-C(1) [2.231(3) Å] distance compares well with distances [2.23(2) Å[81] and 2.262(7) Å[82]] reported for tungsten carbene complexes with a sulfur connected to the carbene carbon. The C(1)-S(1) bond length [1.720(3) Å] is only slightly longer than literature values [1.63(2) – 1.690(3) Å][81,83] but is similar to $C_{carbene}$-S bonds [1.694(7)[82] and 1.740(6) Å[84]] in reported crystal structures of tungsten carbene complexes. The bond lengths of the carbene ligand in **17b**, compare well with the oxazoline ligands in the dimeric complex, **E**,[22] despite the disorder in the carbene ligand in **17a**. Similar to **17a**, the three distances, C(1)-C(2), C(2)-C(3), C(4)-C(5) are in the range for conjugated aromatic systems. Despite the long N(1A)-C(5) distance due to the disorder, the overall structure of **17a** in the solid state [(**xxiii**) in Scheme 2.20], can be expected for **17b** in the solid state. The W-$C_{carbonyl}$ distances in **17b** are similar with the exception of W(1)-C(12), which is somewhat longer than the rest. This again confirms the similar *trans*-influence of the carbene ligand and the CO ligand, as was observed for **17a**.

---

[81] H.G. Raubenheimer, G.J. Kruger, C.F. Marais, J.T.Z. Hattingh, L. Linford, *J. Organomet. Chem.*, 1998, **355**, 337.

[82] H.G. Raubenheimer, G.J. Kruger, C.F. Marais, R. Otte, J.T.Z. Hattingh, *Organometallics*, 1998, **7**, 1853.

[83] H.G. Raubenheimer, G.J. Kruger, L. Linford, C.F. Marais, R. Otte, J.T.Z. Hattingh. A. Lombard, *J. Chem. Soc., Dalton Trans.*, 1989, 1565.

[84] S. Anderson, D.J. Cook, A.F. Hill, J.M. Malget, A.J.P. White, D.J. Williams, *Organometallics*, 2004, **23**, 2552.

Table 2.35 Selected bond lengths (Å) and angles (°) for **17b**

W(1)-C(1)	2.231(3)	N(1A)-C(10A)	1.41(3)
C(1)-C(2)	1.382(5)	C(7A)-C(8A)	1.36(3)
C(2)-C(3)	1.396(4)	C(7A)-C(9A)	1.494(15)
C(3)-C(4)	1.372(5)	W(1)-C(11)	1.991(3)
C(4)-S(1)	1.752(3)	W(1)-C(12)	2.111(16)
S(1)-C(1)	1.720(3)	W(1)-C(13)	1.950(17)
C(4)-C(5)	1.412(6)	W(1)-C(14)	2.008(16)
C(5)-O(1A)	1.330(12)	W(1)-C(15)	2.040(12)
O(1A)-C(6A)	1.430(16)	C(11)-O(2)	1.159(5)
C(6A)-C(7A)	1.708(13)	C(12)-O(3)	0.993(15)
C(7A)-N(1A)	1.450(20)	C(13)-O(4)	1.326(18)
N(1A)-C(5)	1.430(30)	C(14)-O(5)	1.111(16)
		C(15)-O(6)	1.178(15)
C(1)-W(1)-C(11)	177.9(5)	C(4)-S(1)-C(1)	94.5(2)
C(12)-W(1)-C(14)	177.1(5)	N(1A)-C(5)-O(1A)	110.0(11)
C(13)-W(1)-C(15)	178.3(5)	C(5)-O(1A)-C(6A)	111.7(11)
W(1)-C(1)-S(1)	120.7(2)	O(1A)-C(6A)-C(7A)	104.1(7)
C(2)-C(1)-S(1)	107.6(2)	C(6A)-C(7A)-N(1A)	96.1(12)
C(1)-C(2)-C(3)	115.9(3)	C(7A)-N(1A)-C(5)	113.8(15)
C(2)-C(3)-C(4)	113.5(3)	C(5)-N(1A)-C(10A)	124.8(18)
C(3)-C(4)-S(1)	108.3(3)	C(8A)-C(7A)-C(9A)	112.9(11)

Pectora roborant cultus recti

The packing of complex **17b** (Figure 2.26) in the unit cell is similar to that of complex **17a**.

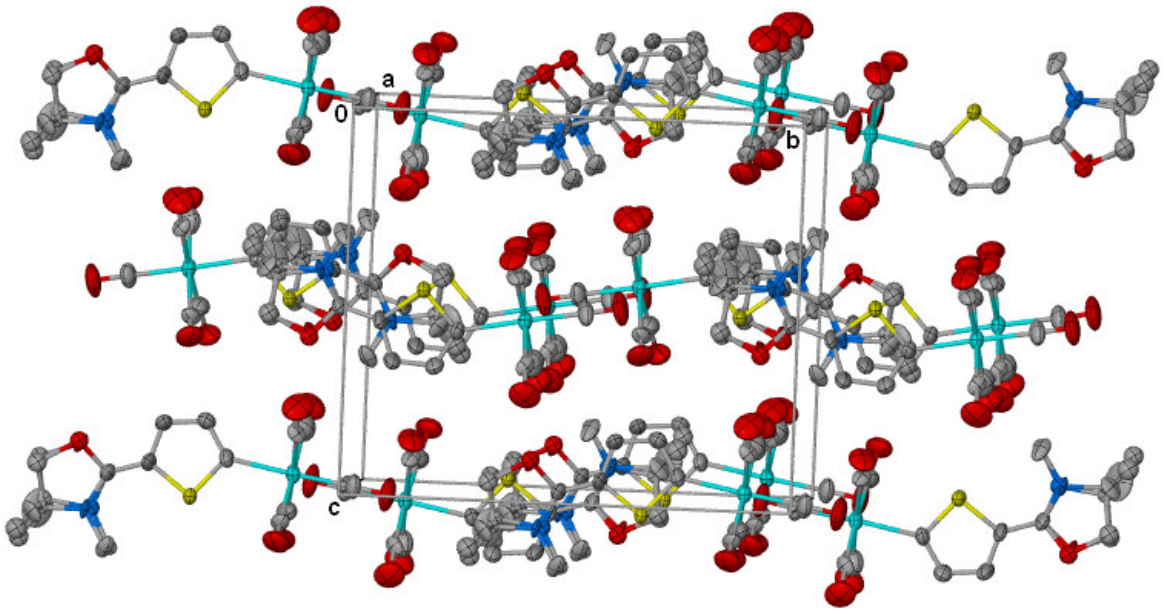

Figure 2.26 The packing diagram of the molecules of **17b** viewed along a-axis

As mentioned previously (section 2.27) crystals of the complex $[PtCl(PPh_3)_3]BF_4$ form during the crystallisation of the one-N, six-membered NHC complex of palladium, **9a**, at –20°C. The crystal structure and molecular structure of this phosphine complex was determined and will be discussed next.

2.2.17.14 The crystal and molecular structure of $[PtCl(PPh_3)_3]BF_4$

The molecular structure of $[PtCl(PPh_3)_3]BF_4$ (Figure 2.27) shows that the Pt atom resides in a distorted square-planar environment defined by three P atoms and Cl(1). Table 2.36 contains the selected bond lengths and angles. The distortion results from the close proximity of the sterically demanding PPh_3 ligands that must be accommodated around the platinum atom. Deviations from the least square plane through Pt(1), P(1), P(2), P(3) and Cl(1) range from 0.008(1) – 0.232(1) Å. This distortion is also evident in the magnitude of the four angles around Pt(1) that vary from 83.5(1) to 98.9(1)° and the two angles Cl(1)-Pt(1)-P(2) [169.8(1)°] and P(1)-Pt(1)-P(3) [162.5(1)°] that are both significantly smaller than 180°.

This is the most distorted square planar structure determined in this study. This complex can be compared to $[PtCl(PEt_3)_3]BF_4$, $[PtF(PEt_3)_3]BF_4$ and $[PtH(PEt_3)_3]PF_6$[85] that are also similarly distorted.

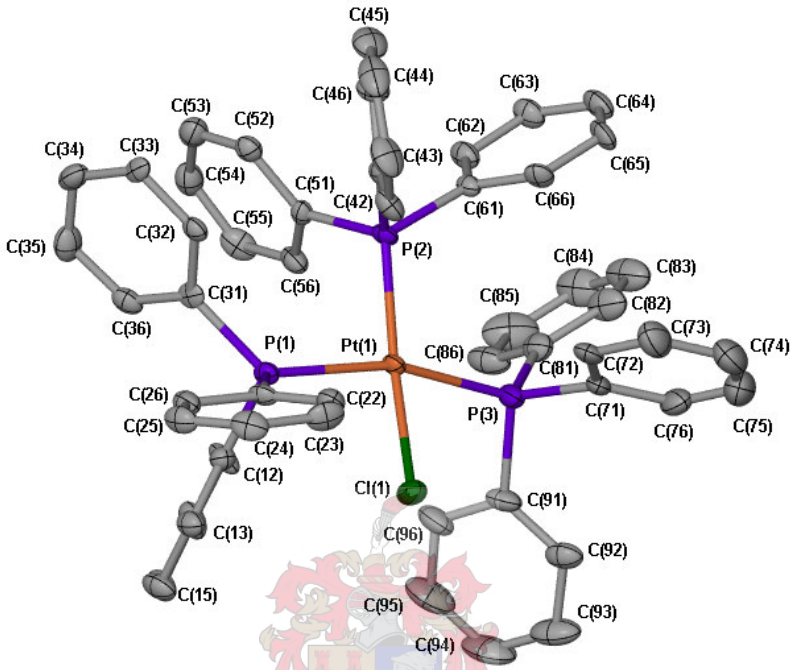

Figure 2.27 Molecular structure of $[PtCl(PPh_3)_3]BF_4$, showing the numbering scheme, generated in POV-Ray

Table 2.36 Selected bond lengths (Å) and angles (°) for $[PtCl(PPh_3)_3]BF_4$

Pt(1)-Cl(1)	2.358(2)	Pt(1)-P(2)	2.256(2)
Pt(1)-P(1)	2.357(2)	Pt(1)-P(3)	2.353(2)
Cl(1)-Pt(1)-P(1)	83.8(1)	P(1)-Pt(1)-P(2)	95.7(1)
Cl(1)-Pt(1)-P(2)	169.8(2)	P(1)-Pt(1)-P(3)	162.5(1)
Cl(1)-Pt(1)-P(3)	83.5(1)	P(2)-Pt(1)-P(3)	98.8(1)

The Pt(1)-P(1) [2.357(2) Å] and the Pt(1)-P(3) [2.353(2) Å] distances are identical but significantly longer than the Pt(1)-P(2) bond length of 2.256(2) Å which is a result of the greater *trans*-influence

[85] D.R. Russel, M.A. Mazid, P.A. Tucker, *J. Chem. Soc., Dalton Trans.*, 1980, 1737.

of PPh_3 compared to chloride. These three separations and the Pt(1)-Cl(1) bond length do not differ from corresponding bond lengths reported for $[PtCl(PEt_3)_3]BF_4$.[85]

The cations of $[PtCl(PPh_3)_3]BF_4$ are packed on top of each other along the b-axis as shown in Figure 2.28. The cations are also stacked on top of each other along the a-axis and the c-axis. The BF_4^- anions and CH_2Cl_2 solvent molecules are located in the spaces between the cations.

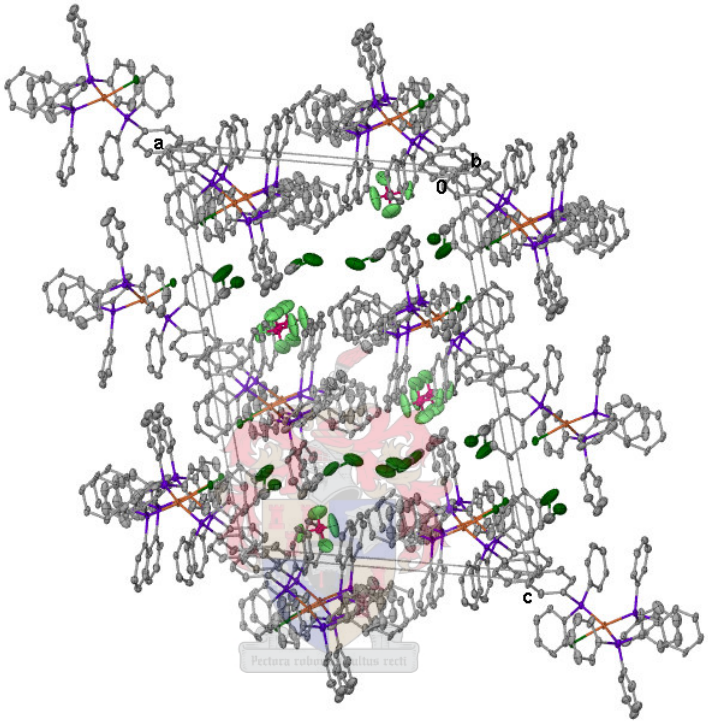

Figure 2.28 The packing diagram of the molecules of $[PtCl(PPh_3)_3]BF_4$ along b-axis

2.2.18 Catalysis (C-C coupling reactions) and quantum mechanical calculations

Palladium complexes

In order to compare the *r*NHC-type complexes as catalyst precursors for C-C coupling reactions, the compound **13a** was again prepared by the author and with **3a** submitted for testing in the laboratory of W. Herrmann in Munich. The results are, for completeness sake, briefly reported here. In addition, G. Frenking in Marburg was approached with the request to carry out comparative calculations involving the ligands in as well as the complexes **3a** and **13a**. The results are important

and differentiate clearly between the well-known and new class of carbenes and carbene complexes. Again, the results are summarised below.

The catalyst precursors, shown in Scheme 2.21, were tested for their activity and efficiency in well-known M-H (Mizoroki-Heck) and S-M (Suzuki-Miyaura) reactions and the results obtained are collected in Tables 2.37 and 2.38. The superiority of the stable *r*NHC complex, **13a**, which gives high conversions even at low concentration, can be clearly seen from the data. Under the chosen conditions TON's of 9.1 x 10^5 in the M-H and 3.2 x 10^6 in the S-M coupling were reached. Catalyst loading in the latter situation, however, is too low and affects the efficiency of the process as a yield of only 32% was obtained. Arylchlorides couple successfully at 0.5% loading level of the *r*NHC complex in the M-H reaction, and at 1.0% in the S-M reaction without any evidence of palladium black formation, even after stirring for 3 hours.

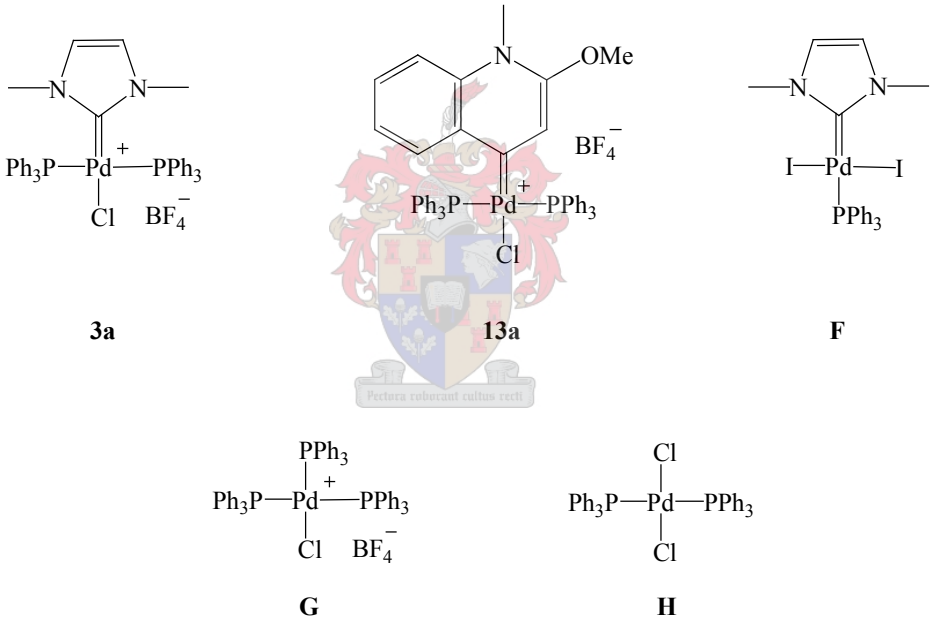

3a **13a** **F**

G **H**

Scheme 2.21

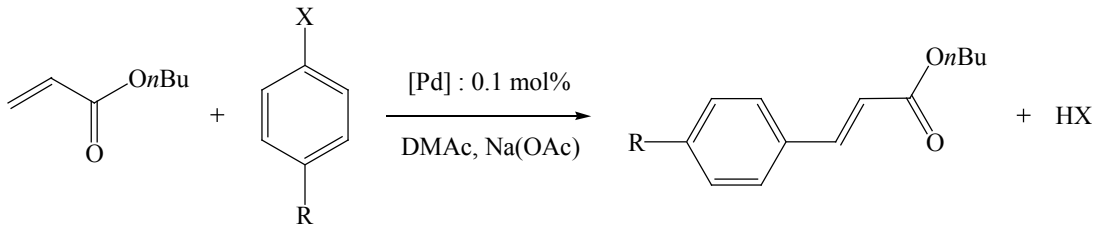

Table 2.37 Mizoroki-Heck reaction

Entry[i]	R	X	mol% Pd	Temperature [°C]	Catalyst	Conversion [%][ii]	Yield [%][ii]	TON [mol.product.mol. cat^{-1}]
1	$C(O)CH_3$	Br	0.01	130	**13a**	>99.99	94	9 400
2	$C(O)CH_3$	Br	0.01	130	**F**	45	41	4 100
3	$C(O)CH_3$	Br	0.001	145	**13a**	>99.99	94	94 000
4	OCH_3	Br	0.5	145	**13a**	84	80	160
5	$C(O)CH_3$	Br	0.0001	145	**13a**	92	91	910 000
6	$C(O)CH_3$	Br	0.0001	145	**F**	8	6	60 000
7	$C(O)CH_3$	Cl	0.5[iii]	150	**13a**	85	81	162
8	H	Cl	0.5[iii]	150	**13a**	64	55	110
9[iv]	H	Br	0.1	145	**13a**	>99.99	95	950
10	H	Br	0.1	145	**3a**	68	66	660
11	H	Br	0.1	145	**F**	20	17	170
12	H	Br	0.1	145	**G**	38	34	340
13	H	Br	0.1	145	**H**	39	37	370

[i] Ratio of aryl halide/olefin/NaOAc = 1:1.5:1.5; solvent: DMAc (dimethylacetamide); [ii] GC-yield and conversion using diethyleneglycol/di-*n*-butylether as internal standard; [iii] 0.2 mole equivalents of $[R_4N]Br$ added to the reaction mixture; [iv] For entries 9 – 13 also compare Figure 2.29.

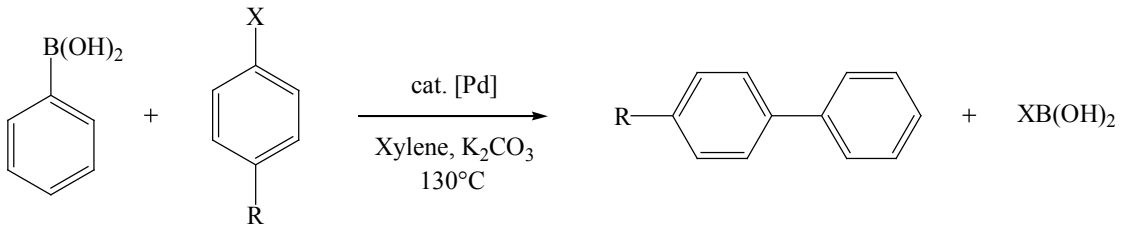

Table 2.38. Suzuki-Miyaura coupling

Entry[i]	R	X	mol% Pd	Catalyst	Time[ii]	Yield [%][ii]	TON [mol.product.mol. cat^{-1}]
1	$C(O)CH_3$	Br	0.0001	**13a**	13 h	>99.99	1 000 000
2	$C(O)CH_3$	Br	10-5	**13a**	13 h	32	3 200 000
3	H	Br	0.01	**13a**	13 h	>99.99	10 000
4	H	Br	0.001	**13a**	13 h	98	98 000
5	H	Br	0.1	**13a**	10 min	95	950
6	H	Br	0.1	**F**	10 min	16	160
7	$C(O)CH_3$	Cl	1.0[iii]	**13a**	14 h	46	460
8[iv]	OCH_3	Br	0.1	**13a**	13 h	>99.99	1 000
9	OCH_3	Br	0.1	**3a**	13 h	85	850
10	OCH_3	Br	0.1	**F**	13 h	32	320
11	OCH_3	Br	0.1	**G**	13 h	72	720
12	OCH_3	Br	0.1	**H**	13 h	77	770
13	OCH_3	Br	0.01	**13a**	13 h	54	5 400

[i] Ratio of aryl halide/phenylboronic acid/K_2CO_3 = 1:1.2:1.5; solvent: xylene; T = 130°C; [ii] GC-yield using diethyleneglycol/di-*n*-butylether as internal standard; [iii] Cs_2CO_3 used as base, [iv] For entries 8 – 12 also compare Figure 2.30.

The time conversion curves in Figure 2.29 and Figure 2.30, determined under similar conditions for the two types of C-C couplings respectively, provide a better picture of the catalyst activities.

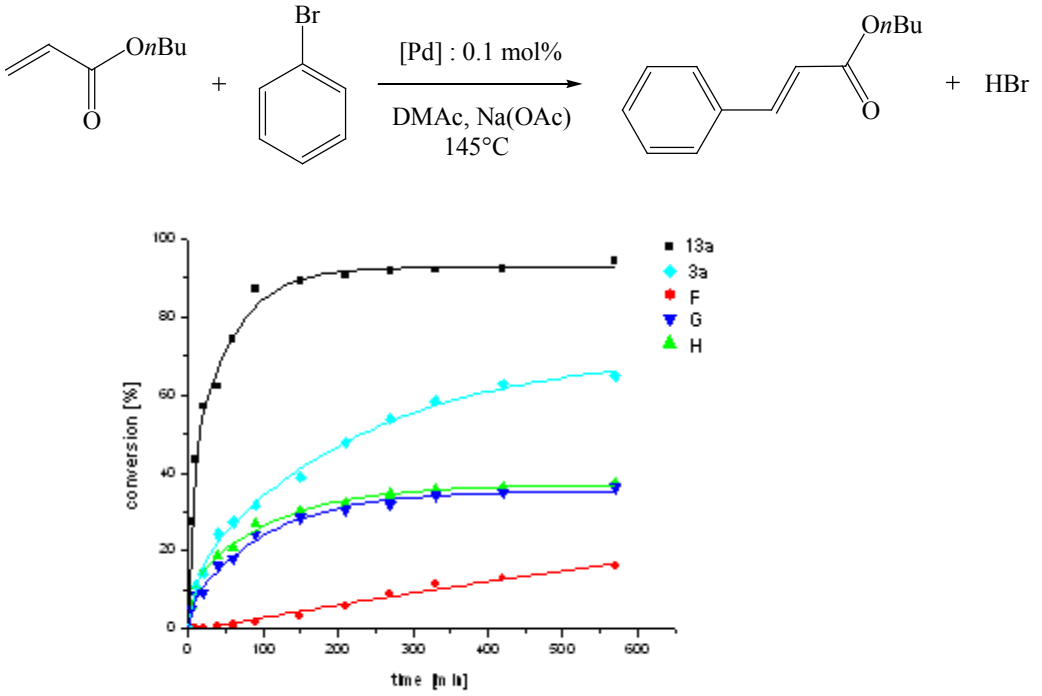

Figure 2.29 Time-conversion-curves: Mizoroki-Heck reaction.

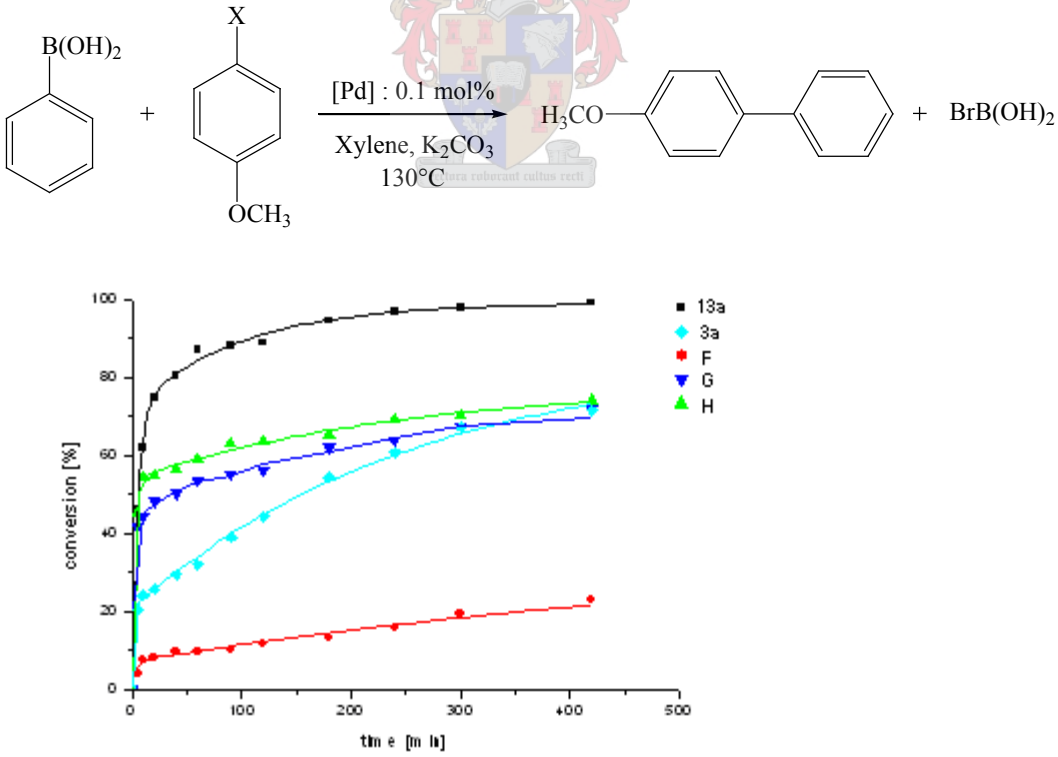

Figure 2.30 Time-conversion-curves: Suzuki-Miyaura reaction.

The two sets of curves are surprisingly similar, although this is not a necessary or expected condition[86] and the *r*NHC complex, which requires no induction period, is the most active catalyst under the catalytic conditions. The catalyst precursors were chosen to determine the influence of the cationic charge or the number of phosphine ligands present, on the catalytic reactions. The cationic charge in the complex is not an important parameter for the halo-phosphine complexes **G** and **H**, but differentiates dramatically between NHC complexes **3a** and **F**.

Quantum mechanical calculations

To understand from a chemical viewpoint the reasons behind the exceptional activity of the one-N, six-membered *r*NHC complex, **13a**, when compared with the standard two-N, five membered imidazolydine complex, **3a**, the metal-carbene bonds were analyzed theoretically. This implies calculation of bond lengths (ligands and complexes; Figure 2.31), NBOs (natural bond orbitals) charges (ligands and complexes; Figure 2.32) and frontier orbitals (ligands; Figure 2.33). To carry out the calculations within reasonable time limits, model compounds **3aM** and **13aM** with phenyl (on P) and methyl (on N and O) substituents replaced by hydrogen atoms, were chosen. Their geometries were optimized at the RI-BP86/SV level.[87]

The crystal and molecular structure of **3a** was determined in this study (Section 2.2.17) while that of **13a** was reported previously.[18] Figure 2.31 shows the most important bond lengths of the calculated molecules and the experimental data for **3a** and **13a**. The agreement between calculated and experimental bond lengths is quite good indicating that the models are satisfactory. The Pd-C(carbene) bond lengths of the two complexes with *r*NHC and NHC ligands are very similar but both the experimental (as discussed in Section 2.2.17) and theoretical values of the Pd-Cl distance in

---

[86] I.D. Hills, G.C. Fu, *J. Am. Chem. Soc.*, 2004, **126**, 13178.

[87] The calculations were carried out using the program package TURBOMOLE: (a) R. Ahlrichs, M. Bär, M. Häser, H. Horn, C. Kölmel, *Chem. Phys. Lett.* 1989, **162**, 165; (b) O. Treutler, R. Ahlrichs, *J. Chem. Phys.* 1995, **102**, 346. Becke-Perdew(BP86) exchange-correlation functional and Resolution-of-the-Identity- Approximation (RI): (c) S. H. Vosko, L. Wilk, M. Nusair, *Can. J. Phys.* 1980, **58**, 1200; (d) J. P. Perdew, *Phys. Rev. B*, 1986, **33**, 8822; (e) D. Becke, *Phys. Rev. A*, 1988, **38**, 3098. Erratum: J. P. Perdew, *Phys. Rev. B* **1986**, *34*, 7406; (f) K. Eichkorn, O. Treutler, H. Öhm, M. Häser, R. Ahlrichs, *Chem. Phys. Lett.* 1995, **242**, 652. For the calculations an SVP basis set was used: (g) A. Schäfer, H. Horn, R. Ahlrichs, *J. Chem. Phys.* 1992, **97**, 2571.

the *r*NHC complex are significantly larger than in complex **3a**. This difference (exp. 0.044 Å) in Pd-Cl bond length (calculated as well as experimentally determined) between the two complexes, illustrates and confirms the larger *trans*-influence exhibited by the *r*NHC ligand when compared to the NHC ligand.

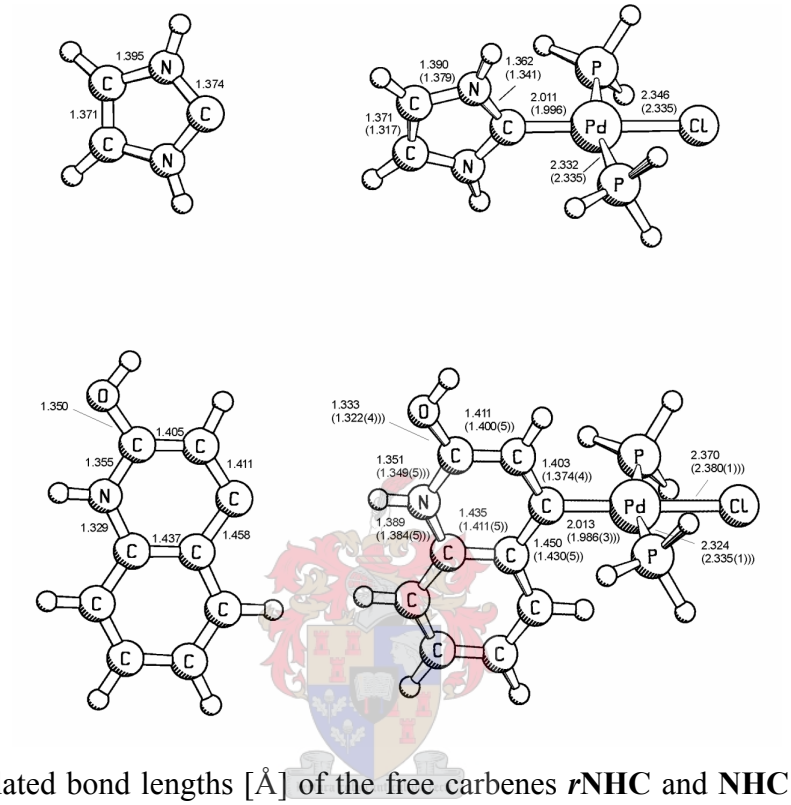

Figure 2.31 Calculated bond lengths [Å] of the free carbenes ***r*NHC** and **NHC** and the complexes **3aM** and **13aM**. Experimental values of **3a** and **13a** are given in parentheses.

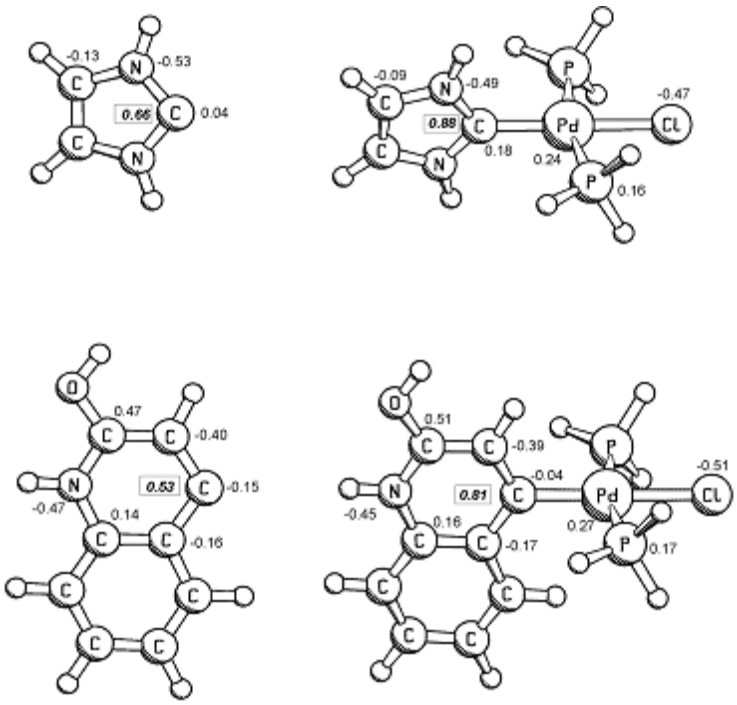

Figure 2.32 NBO charges of the atoms and Mullikan population at the carbene p(π) orbitals

Different methods were used to extract chemical bonding information in **13aM** and **3aM**. Figure 2.33 shows the most important frontier orbitals of the two free carbene ligands ***r*NHC** and **NHC**. The HOMO is an σ-donor orbital, which in ***r*NHC** is higher in energy (1.28 eV) than in **NHC**. The HOMO-1 is the highest lying occupied π-orbital and has a much larger coefficient at the carbene C-atom in **NHC** than in ***r*NHC**. This is the reason for the higher population of the C(carbene) p(π) AO (atomic orbital) in **NHC** (0.66) than in ***r*NHC** (0.53) (Figure 2.32 shows some partial charges.). This is disadvantageous for M-L π back donation in **NHC**. The lowest-lying π-acceptor orbital (LUMO) of **NHC** (not shown) is a π^* orbital of the C=C double bond which has a node at the C(carbene) atom. The next low-lying π-acceptor orbital is the LUMO+1 which has a large coefficient for the C(carbene) p(π) AO. The π-acceptor LUMO of ***r*NHC** is lower in energy than the LUMO+1 of **NHC** but it is much more delocalised. The increase in the p(π) AO population in the carbene carbon atom of ***r*NHC** after formation of the complex **13aM** (Δq_π = 0.28e) which is larger than in **NHC** (Δq_π = 0.20e) suggests that the former ligand may be a stronger π-acceptor than the latter species.

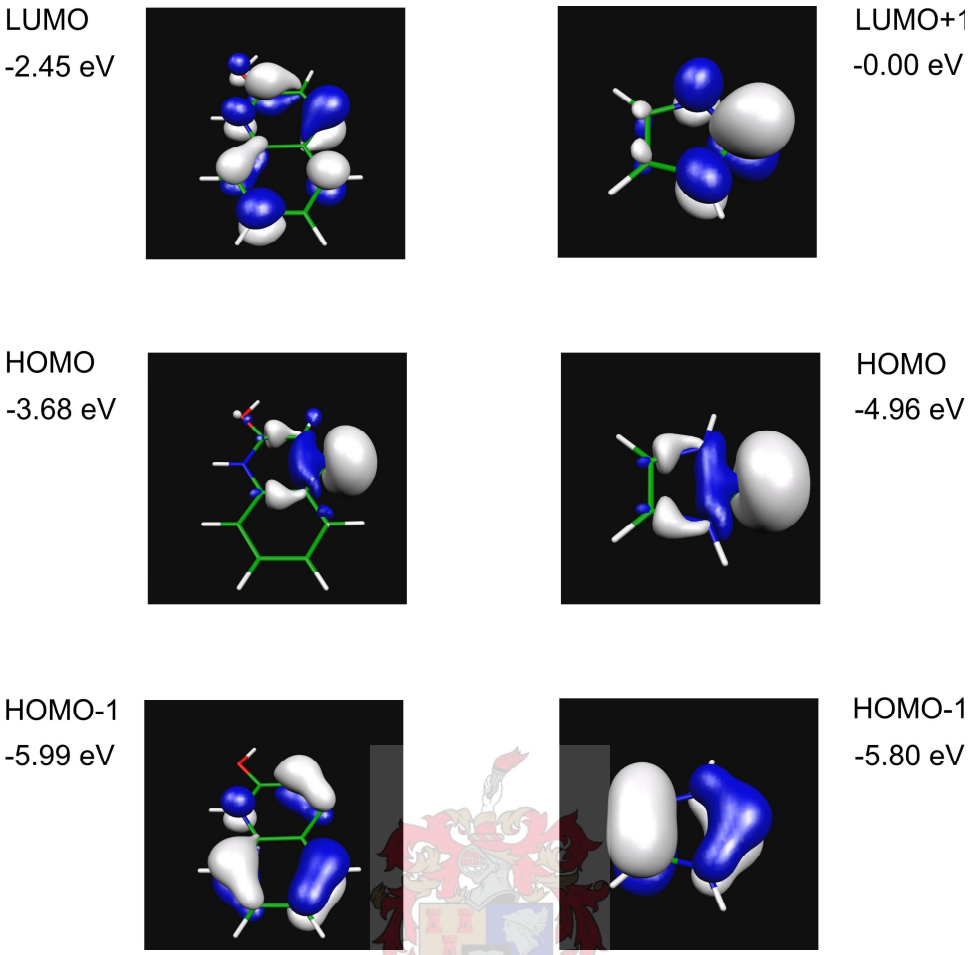

Figure 2.33 Frontier orbitals of the free carbenes ***r*NHC** (left) and **NHC** (right) carbenes.

The energy decomposition analysis (EDA) of **13aM** and **3aM** provided a deeper insight into the metal-carbene bonding situation (Table 2.39).[88,89] The metal-carbene interactions in the ***r*NHC** carbene complex, **13aM** (ΔE_{int} = -107.6 kcal/mol), are significantly stronger than in **3aM** (ΔE_{int} = -85.5 kcal/mol). The calculated geometry relaxation of the fragments, ΔE_{prep}, is rather small which

[88] The EDA calculations were performed using the program package ADF: (a) F.M. Bickelhaupt, E.J. Baerends, *Rev. Comput. Chem.*, Vol. 15, p. 1, K.B. Lipkowitz, D.B. Boyd (Eds), Wiley-VCH, New York, **2000**; (b) G. te Velde, F.M. Bickelhaupt, E.J. Baerends, S.J.A. van Gisbergen, C. Fonseca Guerra, J.G. Snijders, T. Ziegler, *J. Comput. Chem.* 2001, **22**, 931. The calculations have been carried out at the BP86 level [87c-e] using uncontracted Slater-type orbitals (STOs) as basis functions: (c) J.G. Snijders, E.J. Baerends, P. Vernooijs, *At. Nucl. Data Tables*, 1982, **26**, 483. The basis sets have TZP quality. An auxiliary set of s, p, d, f and g STOs was used to fit the molecular densities and to represent the Coulomb and exchange potentials accurately in each SCF cycle. (d) J. Krijn, E.J. Baerends, *Fit Functions in the HFS-Method*, Internal Report (in Dutch), Vrije Universiteit Amsterdam, The Netherlands, 1984.

[89] For a review of EDA results on bonding in transition metal complexes see: G. Frenking, K. Wichmann, N. Fröhlich, C. Loschen, M. Lein, J. Frunzke, V.M. Rayón, *Coord. Chem. Rev.*, 2003, **238**, 55.

indicates, extremely significantly, that the former complex also has a bond dissociation energy (ΔE) which is ~20 kcal/mol higher than the latter species. The metal-carbene bonding in both complexes comes mainly from classical electrostatic interactions, ΔE_{elstat}, which contribute ~70% to the attractive forces.

Table 2.39 Energy decomposition analyses of **13aM** and **3aM**.[i]

	13aM		**3aM**	
ΔE_{int}	-107.6		-85.5	
ΔE_{Pauli}	184.9		157.9	
ΔE_{elstat}	-204.6	(69.9%)	-171.8	(70.6%)
ΔE_{orb}	-87.9	(30.1%)	-71.5	(29.4%)
a'	-72.8	(82.8%)	-60.4	(84.5%)
a"	-15.1	(17.2%)	-11.1	(15.5%)
ΔE_{prep}	3.6		2.4	
$\Delta E=-D_e$	-104.0		-83.1	

[i] Energy given in kcal/mol

The most interesting part of the EDA was the breakdown of the total orbital interaction term ΔE_{orb} into orbital contributions of different symmetry. Both complexes **3aM** and **13aM** have C_s symmetry which means that the strength of the σ-bonding is given by the a' contribution and π-bonding by the a" contribution. Table 2.39 shows that 82.8% of ΔE_{orb} comes from the σ-orbitals while only 17.2% come from the π-orbitals in **13aM**. Similar to **13aM**, the greatest contribution to ΔE_{orb} comes from the σ-orbitals (84.5%) where the π-orbitals only contribute 15.5% in **3aM**. This clearly shows that the carbene ligand in both **13aM** and **3aM** is mainly a σ-donor.

Nickel complexes

Here, a different approach was taken since it became essential to compare **NHC** and ***r*NHC** complexes of the same (one-N, six-membered) family. Again the main aim was differentiation, if possible, and directed at the metal carbene bond.

The geometries of the ligand precursors **1**, **6 – 8, 11** and **12** and the model complexes **3bM**, **8bM – 10bM**, **13bM** and **14bM** wherein the bulky PPh_3 groups are replaced by PH_3 were firstly optimised at BP86/TZVP.[87,90] Figure 2.34 shows the most important bond lengths of the molecules. The theoretical bond lengths of **3bM**, **8bM**, **13bM and 14bM** are in good agreement with the experimental values determined for **3b**, **8b**, **13b** and **14b** (Section 2.2.17). The calculated geometries also indicate that the bond lengths of the ligand precursor molecules do not change significantly after complexation to the metal.

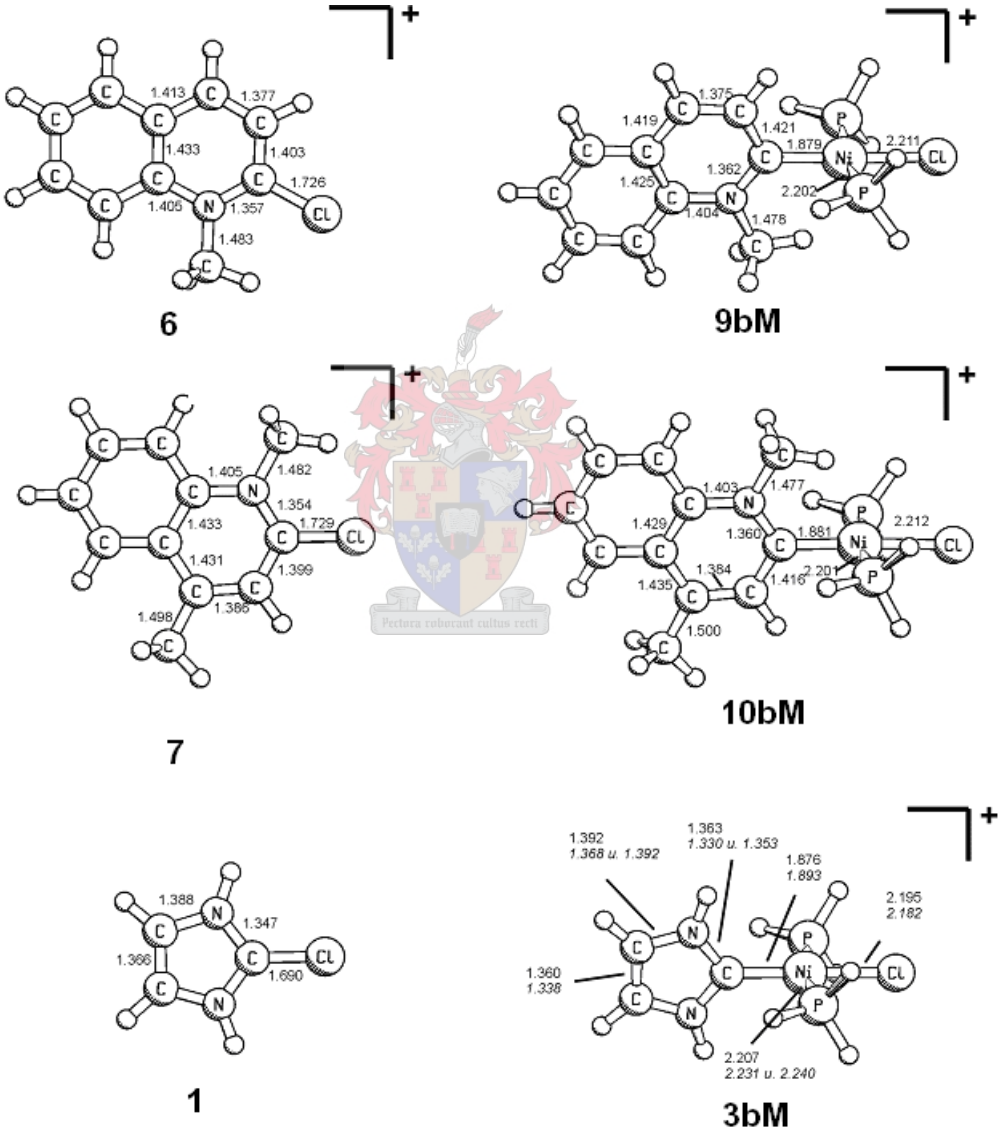

[90] (a) D. Nemcsok, K. Wichmann, G. Frenking, *Organometallics*, 2004, **23**, 3640; (b) G. Frenking, N. Froehlich, *Chem. Rev.*, 2000, **100**, 717.

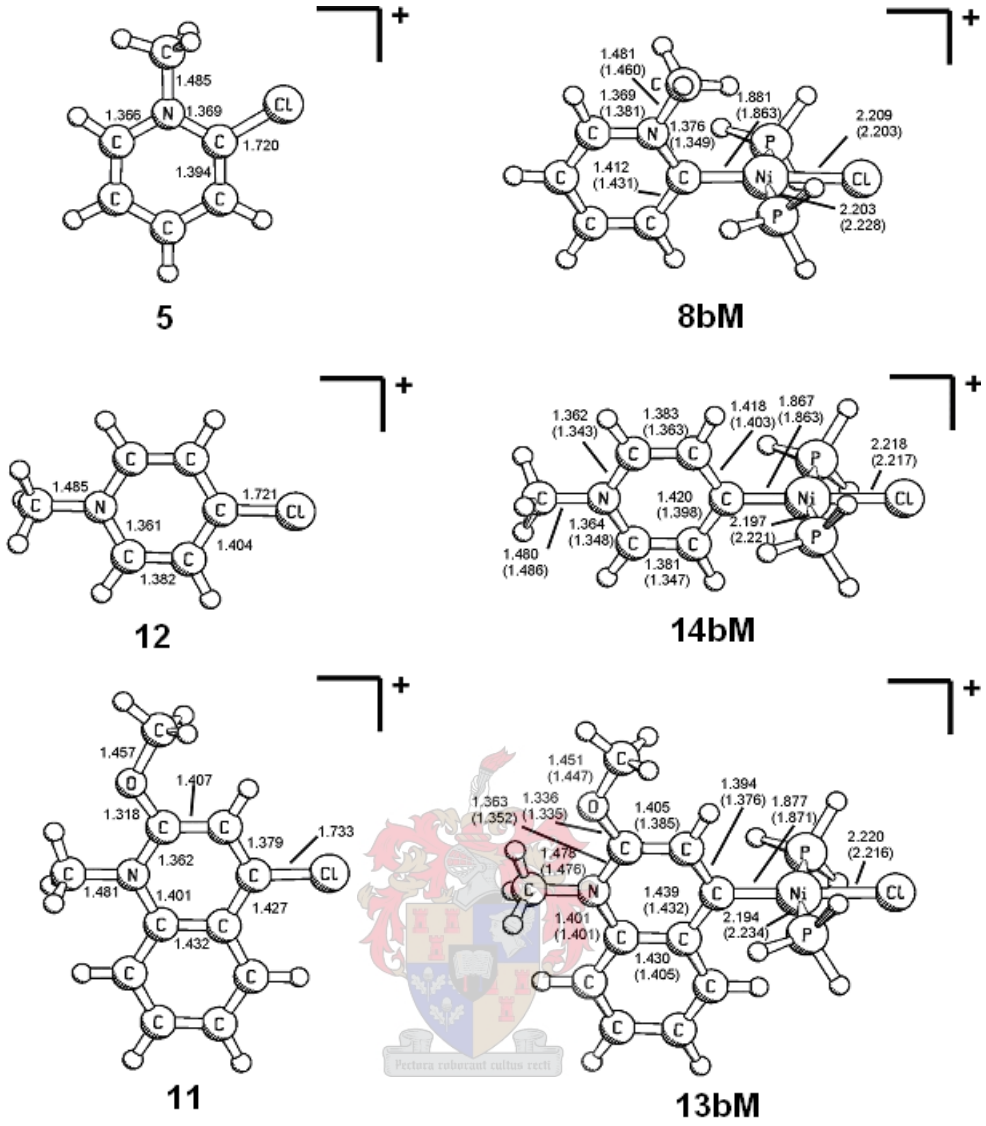

Figure 2.34 Calculated bond lengths at BP86/TZVP of the ligand precursor compounds **1, 6 – 8**, **11** and **12** and the model complexes **3bM**, **8bM** – **10bM**, **13bM** and **14bM**. Experimental values are given in parentheses

The theoretically predicted free reaction energies show that the reactions are all exergonic by 20.4 - 36.2 kcal/mol. Furthermore, the results indicate that the preference for substitutive oxidative addition to occur follows the order **3bM** > **8bM** > **9bM** > **10bM** > **14bM** > **13bM** (Table 2.40). Although the absolute values for the reaction energies of the true molecules **3b**, **8b** – **10b**, **13b** and **14b** will be different and probably also less exergonic than for the formation of the calculated nickel complexes (**3bM**, **8bM** – **10bM**, **13bM** and **14bM**) because PPh_3 binds stronger than PH_3, the trend should remain the same. The process should be facilitated by π-donation of neighboring or distant nitrogen atoms, which also stabilizes the formed free carbene.

Table 2.40 Calculated reactions energies ΔE, reaction enthalpies ΔH (0K) and Gibbs Free Energies ΔG (333.15K and 1bar) in kcal/mol at the RI-BP86/TZVP level

Reaction	ΔE	ΔH	ΔG
1 + $Ni(PH_3)_4$ → 2 PH_3 + **3bM**	-27.5	-27.0	-36.2
6 + $Ni(PH_3)_4$ → 2 PH_3 + **8bM**	-16.8	-19.3	-28.0
7 + $Ni(PH_3)_4$ → 2 PH_3 + **9bM**	-16.6	-18.9	-27.1
8 + $Ni(PH_3)_4$ → 2 PH_3 + **10bM**	-15.5	-17.7	-25.9
11 + $Ni(PH_3)_4$ → 2 PH_3 + **13bM**	-9.2	-11.7	-20.4
12+ $Ni(PH_3)_4$ → 2 PH_3 + **14bM**	-12.0	-14.3	-23.1

The nature of the nickel-carbene interactions was investigated with the help of energy decomposition analysis (EDA, Table 2.41).[88,89,91] The instantaneous interaction energies, ΔE_{int}, between the frozen fragment $Ni(PH_3)_2Cl^+$ and the neutral carbene ligands **1**, **6** – **8, 11** and **12** gives the important result that the **metal-*r*NHC** bonds in **13bM** and **14bM** are significantly stronger than those found between nickel and the carbons situated adjacent to N in **3bM**, **8bM - 10bM.** The calculations thus show that the Ni-carbene bonds in the six calculated nickel complexes become weaker when the carbene ligand has a π-donor group in the α position. The weakening effect of two π-donor groups in the α position of **3bM** is larger (D_e = 90.6 kcal/mol) than in **8bM** (D_e = 97.4 kcal/mol) and **9bM** (D_e = 99.8 kcal/mol) which have only one α nitrogen.

Finally, the EDA calculations[89] indicate (Table 2.41) that classical electrostatic interactions contribute ca. 2/3 of the total attractive interactions while approximately 1/3 results from orbital contributions. The largest part of the latter ΔE_{orb}-term comes from σ-overlap. The π-bonding contributes only between 17.2% - 20.5% of the total orbital interactions.

[91] THE EDA method has been suggested by (a) K. Morokuma, *J. Chem. Phys.*, 1971, **55**, 1236; (b) T. Ziegler, A. Rauk, *Theor. Chim. Acta*, 1977, **46**, 1.

Table 2.41 Energy decomposition analysis of the Ni-C bonds in compounds **3bM**, **8bM** – **10bM**, **13bM** and **14bM** at BP86/TZP

	3bM		**8bM**		**9bM**	
ΔE_{int}	-93.8		-100.9		-103.4	
ΔE_{pauli}	152.7		165.9		167.9	
ΔE_{elstat}[i]	-167.2	(67.8%)	-181.8	(68.1%)	-182.9	(67.4%)
ΔE_{orb}[i]	-79.3	(32.2%)	-85.1	(31.9%)	-88.4	(32.6%)
ΔE_{orb} (a')[ii]	-65.7	(82.8%)	-69.2	(81.3%)	-70.3	(79.5%)
ΔE_{orb} (a'')[ii]	-13.6	(17.2%)	-15.9	(18.7%)	-18.1	(20.5%)
ΔE_{prep}	3.2		3.6		3.6	
$\Delta E = -D_e$	-90.6		-97.4		-99.8	
q $[NiCl(PH_3)_2]^+$	0.627		0.633		0.626	
	10bM		**13bM**		**14bM**	
ΔE_{int}	-105.2		-118.1		-116.0	
ΔE_{Pauli}	168.3		177.3		172.4	
ΔE_{elstat}[i]	-184.5	(67.4%)	-201.6	(68.3%)	-197.9	(68.6%)
ΔE_{orb}[i]	-89.1	(32.6%)	-93.8	(31.7%)	-90.6	(31.4%)
ΔE_{orb} (a')[ii]	-71.0	(79.7%)	-75.6	(80.6%)	-73.1	(80.6%)
ΔE_{orb} (a'')[ii]	-18.1	(20.3%)	-18.2	(19.4%)	-17.5	(19.4%)
ΔE_{prep}	3.7		4.0		3.6	
$\Delta E = -D_e$	-101.6		-114.1		-112.4	
q $[NiCl(PH_3)_2]^+$	0.615		0.595		0.626	

[i] The value in parentheses gives the percentage contribution to the total attractive interactions $\Delta E_{elstat} + \Delta E_{orb}$.

[ii] The value in parentheses gives the percentage contribution to the total orbital interactions ΔE_{orb}.

2.3 Conclusions and future work

The preparation and characterisation of palladium and nickel carbene complexes with imidazole, pyridine and quinoline-derived carbene ligands were successful and 12 new complexes were fully characterized – 9 by crystal structure determinations (7 carried out by the author himself). All the metal centers in these complexes have a square planar geometry with the carbene ligand orientated almost perpendicular to the coordination plane of the metal. For the first time we report both the *cis* and *trans* isomers of a Pd carbene complex participating in *cis*-*trans* isomerisation on solution. The presence of the ***cis*-9a** isomer, however, was observed in solution only at –20°C by ^{31}P NMR spectroscopy. The carbene ligands in these nickel and palladium complexes, using the M-Cl bond distance as probe, can be arranged in a series of increasing *trans*-influence: 1,3-dimethyl-2,3-dihydro-1*H*-imidazol-2-ylidene, 1,3-dimethyl-2,3,4,5-tetrahydro-1*H*-imidazol-2-ylidene < 1-methyl-1,2-dihydro-pyridin-2-ylidene < 2-methoxy-1-methyl-1,4-dihydro-quinolin-4-ylidene, 1-methyl-1,4-dihydro-pyridin-4-ylidene. The crystal structure determinations also revealed that the positive charge of these complexes is not located only on the metal but also partially on the heteroatom (mainly N, but also O in **13b** and **13c**) in the solid state. The crystal structure of the platinum *r*NHC complex, **13c**, is also described here.

While mainly the *trans* isomers of the corresponding platinum carbene complexes were obtained during room temperature preparations, higher temperature (60°C) synthesis yielded the *cis* complexes. The preparation of the platinum carbene complexes was complicated by the formation of $[Pt(Cl(PPh_3)_3]BF_4$ and other unknown *trans* platinum phosphine complexes as products. The formation of these products is dependent on the reaction conditions (time and temperature) and probably on the carbene ligand itself. Room temperature preparations effected a decrease in the amount of $[Pt(Cl(PPh_3)_3]BF_4$ formed. The other unknown *trans* platinum complexes did not form during these reactions carried out at room temperature. $[Pt(Cl(PPh_3)_3]BF_4$ was characterised by crystal structure determination (carried out by the author himself). Further work is required to increase the selectivity towards platinum carbene complex formation.

Single crystal structure determination of chromium and tungsten *r*NHC complexes derived from 4,4-dimethyl-2-thiophen-2-yl-4,5-dihydro-oxazole (**17a** and **17b**) revealed that the $M(CO)_5$ units were bound at the 5-position, rather than the 3-position. The attempted preparation of the carbene complex with the $M(CO)_5$ fragment bonded in the 3-position with the ligand precursor that was

blocked in the 5-position using a methyl group (the reaction mixture contained 20% unblocked precursor) was unsuccessful. This experiment should be investigated further with a clean ligand precursor (blocked in the 5-position) to confirm whether the accommodation of the $M(CO)_5$ group in the 3-position is possible. The use of diethyl ether or hexane as a solvent instead of THF, used to prepare **17a** and **17b** in this study, should also be investigated in attempt to accommodate the $M(CO)_5$ group in the 3-position. Theoretical studies could provide a better understanding of this bonding and may reveal what effect the steric requirements of the $M(CO)_5$ unit would have on this bonding. No significant differences in the M-$C_{carbonyl}$ bond lengths in **17a** and **17b** were obvious, indicating that the *trans*-influence of the carbene and the CO ligands in these complexes is similar.

The complex chloro(2-methoxy-1-methyl-1,4-dihydro-quinolin-4-ylidene)bis(triphenylphosphine) palladium(II) tetrafluoroborate, **13a**, proved to be a very active pre-catalyst in the Mizoroki-Heck and Suzuki-Miyaura reactions when compared to the well known pre-catalysts *trans*-chloro(1,3-dimethyl-2,3-dihydro-1*H*-imidazol-2-ylidene)bis(triphenylphosphine)palladium(II) tetrafluoroborate, **3a**, *trans*-diiodo(1,3-dimethyl-2,3-dihydro-1*H*-imidazol-2-ylidene) (triphenylphosphine)palladium(II), $Pd(Cl(PPh_3)_3]BF_4$ and $Pd(Cl)_2(PPh_3)_2$. The catalytic activity of pre-catalyst **13a** should certainly be enhanced by the increase of the steric bulk of this type of ligand. Bulky ligands increase the catalytic activity of the catalyst as the oxidative addition, probably a rate determining step in the Suzuki-Miyaura reaction, of aryl halides to Pd(0) is facilitated.[27,92] Further work focusing on the mechanism of these C-C coupling reactions, particularly involving Pd(II) pre-catalysts with non-labile carbene ligands is necessary.

Quantum mechanical calculations undertaken in Marburg indicated that the palladium-carbene bond for *r*NHC ligands of the quinolinylidene-type is 20 kcal/mol stronger than that in NHC-type complexes of the standard imidazolylidene class. The exceptionally strong metal-carbene bond in complexes of the *r*NHC carbenes is mainly due to very strong metal-ligand electrostatic attraction as well as an energetically higher-lying σ-HOMO on the ligand that overlaps well and donates electrons readily. EDA-analysis indicated that these carbene ligands are strong σ-donors and weak π-acceptors.

[92] U. Christmann, R. Vilar, *Angew. Chem., Int. Ed.*, 2005, **44**, 366.

For the nickel complexes of the pyridinylidene-type, quantum mechanical calculations again unequivocally showed that the *r*NHC ligands are more strongly bonded than their NHC counterparts. The former group also shows stronger *trans*-influences. π-Donor groups α to the carbene carbon stabilise the complex against nucleophilic attack while weakening the metal-carbene bond.

All the results should find further application in C-C coupling reactions and, by further ligand design, probably also in other catalytic reactions like hydroformylation.

2.4 Experimental

2.4.1 General

All reactions were carried out under nitrogen or argon using standard vacuum-line and Schlenk techniques. Tetrahydrofuran (THF), hexane, pentane and diethyl ether were dried and deoxygenated by distillation on sodium benzophenone ketyl and dichloromethane from CaH_2. Flash column chromatography was performed with "flash grade" SiO_2 (SDS 230-400 mesh) at –10 - –15°C.

Melting points were determined on a Stuart SM P3 apparatus and are uncorrected. Mass spectra were recorded on an AMD 604 (EI, 70eV) or VG 70SEQ (FAB, 70 eV, 3-nitrobenzylalcohol matrix, resolution: 1000) instrument, the infrared spectra on a Perkin-Elmer 1600 Series FTIR spectrometer and NMR spectra on a Varian 300 FT or INOVA 600MHz spectrometer (^{1}H NMR at 300/600 MHz, ^{13}C{^{1}H} NMR at 75/150 MHz and ^{31}P{^{1}H} NMR at 121/243 MHz; δ reported relative to the solvent resonance or external reference 85% H_3PO_4). Element analyses were carried out by the Micoranalytical Laboratories at the TU Munich and in the Department of Chemistry, University of Cape Town.

$Pd(PPh_3)_4$[93], $Pt(PPh_3)_4$[94], ligand **5**[7], compound **11**, complexes **13a** and **13c**[18] and the catalyst precursors **F**[31] and **G**[95] were prepared according to literature methods. $[Me_3O][BF_4]$, $Ni(PPh_3)_4$, ligand **2** and $Pd(Cl_2)(PPh_3)_2$ (catalyst precursor **H**) were obtained from Aldrich and used without further purification.

2.4.2 2-chloro-1,3-dimethylimidazolium tetrafluoroborate, 1

2-chloro-1-methylimidazole was prepared according to a modified literature procedure.[38] Methylimidazole (0.4 cm^3, 5.0 mmol) in THF (40 cm^3) was treated with a slight access of BuLi (3.7 cm^3, 5.3 mmol) at –78°C. The slightly yellow reaction mixture was stirred for 30 minutes before CCl_4 (0.5 cm^3, 5 mmol) was added and the reaction mixture turned dark brown and was allowed to reach room temperature over 16 hours. The addition of a saturated solution of NH_4Cl (4 cm^3) followed by 50 ml diethyl ether, filtration over $MgSO_4$ and removal of solvent yielded a dark brown oily residue. This residue was adsorbed to flash silica and chromatographed over a short column (4 cm) with pentane:diethyl ether (7:3) as eluent. The intermediate (2-chloro-1-methylimidazole) was removed with THF, leaving a brown oil (1.8 g, 1.5 mmol, 30 %) after stripping of the solvent.

2-chloro-1-methylimidazole (1.75 g, 1.50 mmol) and $[Me_3O][BF_4]$ (0.22 g, 1.5 mmol) were stirred for 17 hours in THF (40 cm^3) and a precipitate formed as the THF was reduced. The precipitate was filtered off, washed with THF (4 x 15 cm^3) and dried giving an off-white powder. This powder was dissolved in dichloromethane, precipitated with diethyl ether, filtered and dried. The resulting off-white powder was washed with diethyl ether (3 x 20 cm^3) and THF (3 x 20 cm^3), dissolved in dichloromethane and filtered over dried celite. The solvent was removed to obtain a white microcrystalline powder.

---

[93] F. Ozawa in: S. Komiya (Ed), *Synthesis of Organometallic Compounds, A practical Guide*, John Wiley & Sons, Chichester, 1997, p. 286.

[94] W.A. Herrmann, K. Öfele, C.E. Zybill in: W. A. Herrmann (Ed.), *Synthetic methods of Organometallic and Inorganic Chemistry, Volume 7, Transition Metals Part 1*, Georg Thieme Verlag Stuttgart, 1997, p. 77.

[95] E.P. Urriolabeitia, *J. Chem. Educ.*, 1997, **74**, 325.

Yield: 0.308g (94 %) (28 % overall)
Melting point: 181 - 182°C

Elemental analysis (%): Calc for **1** ($C_5H_8BClF_4N_2$) (218.39): C, 27.50; H, 3.69; N, 4.95. Found: C; 27.38; H, 3.71; N, 12.90

2.4.3 Preparation of *trans*-chloro(1,3-dimethyl-2,3-dihydro-1*H*-imidazol-2-ylidene)bis(triphenylphosphine)palladium(II) tetrafluoroborate, 3a

Complex **3a** was prepared by stirring **1** (0.04 g, 0.16 mmol) and $Pd(PPh_3)_4$ (0.19 g, 0.16 mmol) in toluene at 60°C for 15 hours. The white precipitate, which formed during the reaction, was filtered off, washed well with toluene and then repeatedly with THF and diethyl ether to remove unreacted ligand **1**. Crystallisation from CH_2Cl_2 layered with pentane, yielded colourless crystals of **3a** at -20°C.

Yield: 50 % (determined by NMR)
Melting point: 255 - 260°C (decomposition)

Elemental analysis (%): Calc for **3a** ($C_{41}H_{38}BClF_4N_2P_2Pd$) (849.38): C, 57.98; H, 4.51; N, 3.30. Found: C; 58.22; H, 4.33; N, 3.51

2.4.4 Preparation of *trans*-chloro(1,3-dimethyl-2,3-dihydro-1*H*-imidazol-2-ylidene)bis(triphenylphosphine)nickel(II) tetrafluoroborate, 3b

$Ni(PPh_3)_4$ (0.19 g, 0.17 mmol) dissolved in toluene was reacted with ligand **1** (0.037 g, 0.17 mmol) at room temperature for 1.5 hours. The dark brown reaction mixture became lighter. The reaction mixture was stirred at 60°C for 16 hours. The brown precipitate that formed during the reaction was filtered over dried celite and washed with toluene (3 x 20 cm^3). The precipitate was washed through the celite with CH_2Cl_2 and the yellow filtrate was dried under vacuum yielding a yellow precipitate. The product was washed with diethyl ether (3 x 10 cm^3) and the product extracted with THF, leaving a yellow precipitate after the THF was removed. Crystallisation of the yellow precipitate

from a concentrated solution in CH_2Cl_2, layered with pentane, at –20°C yielded yellow (complex **3b**) and colourless crystals (ligand **1**). The crystals were separated mechanically. Recrystallisation of the yellow crystals yielded crystals, suitable for single crystal X-Ray determination.

Yield: 0.025g (18 %) (33 % determined by NMR)
Melting point: 184 - 190°C (decomposition)

Elemental analysis (%): Calc. for **3b** ($C_{41}H_{38}BClF_4N_2P_2Ni$) (801.65): C, 61.43; H, 4.78; N, 3.49. Found: C, 61.33; H, 4.83; N, 3.42.

2.4.5 Preparation of *trans*-chloro(1,3-dimethyl-2,3,4,5-tetrahydro-1*H*-imidazol-2-ylidene)bis(triphenylphosphine)nickel(II) tetrafluoroborate, 4b

$Ni(PPh_3)_4$ (0.39g, 0.35 mmol) dissolved in toluene was reacted with ligand **2** (0.097g, 0.35 mmol) in the same manner as complex **4b**, with the exception that the microcrystalline powder obtained was recrystallised from CH_2Cl_2, layered with pentane, without any further attempts at purification. The yellow (complex **4b**) and colourless crystals (ligand **2**) were separated mechanically. The yellow crystals were suitable for single crystal X-Ray determination.

Pectora roborant cultus recti

Yield: 0.079g (26 %) (47 % determined by NMR)
Melting point: 185 - 195°C (decomposition)

Elemental analysis (%): Calc. for **4b** ($C_{41}H_{40}BClF_4N_2P_2Ni$) (803.67): C, 61.27; H, 5.02; N, 3.49. Found: C, 61.21; H, 5.18; N, 3.60.

2.4.6 Preparation of compounds (carbene precursors) 6 and 7

Ligands **6** and **7** were prepared by the alkylation of the ligand precursors as described in literature.[7] Ligand **6** was prepared as follows: The oxonium salt $[Me_3O][BF_4]$ (0.96 g, 6.6 mmol) was added to chloroquinoline (1.1 g, 6.5 mmol) in a CH_2Cl_2:CH_3CN (3:1) solution (40 cm^3), over a period of 1.5 hours at room temperature. The reaction mixture was stirred overnight. The solvent was removed

under vacuum and the residue was washed with THF (50 cm^3) and three more portions of THF (3 x 15 cm^3) to yield a white microcrystalline powder. The resulting white powder was dried under high vacuum.

The same procedure was employed to prepare compound **7** with 2-chlorolepidin (0.89 g, 5.0 mmol) and $[Me_3O][BF_4]$ (0.74 g, 5.0 mmol) as starting materials.

Yield: Ligand **6** 0.99 g (85%) Melting point: 138 - 139°C
Ligand **7** 0.84 g (87%) Melting point: 156°C

Elemental analysis (%): Calc. for **6** ($C_{10}H_9BClF_4N$) (265.44): C, 45.25; H, 3.42; N, 5.28. Found: C, 45.19; H, 3.42; N, 4.96. Calc. for **7** ($C_{11}H_{11}BClF_4N$) (279.47): C, 47.27; H, 3.97; N, 5.01. Found: C, 47.51; H, 4.11; N, 4.83.

2.4.7 Preparation of *trans*-chloro(1-methyl-1,2-dihydro-pyridin-2-ylidene)bis(triphenylphosphine)palladium(II) tetrafluoroborate, 8a

$Pd(PPh_3)_4$ (0.46 g, 0.40 mmol) and ligand **5** (0.086 g, 0.40 mmol) were suspended in toluene (40 cm^3) and the mixture was stirred at 60°C for 17 hours. The yellow reaction mixture became almost colourless, the white precipitate was filtered off and washed with toluene (2 x 10 cm^3). The white microcrystalline powder was dried under vacuum. Crystallisation from a CH_2Cl_2/pentane solution (-20°C) gave the pale yellow crystals of complex **8a** suitable for single crystal X-ray determination.

Yield: 0.25 g (74 %)
Melting point: 209 - 216°C (decomposition)

Elemental analysis (%): Calc. for **8a** ($C_{42}H_{37}NClBF_4P_2Pd$) (846.37): C, 59.60; H, 4.41; N, 1.65. Found: C, 59.23; H, 4.40; N, 1.59.

2.4.8 Preparation of *trans*-chloro(1-methyl-1,2-dihydro-pyridin-2-ylidene)bis(triphenylphosphine)nickel(II) tetrafluoroborate, 8b

$Ni(PPh_3)_4$ (0.36 g, 0.32 mmol) and compound **5** (0.070 g, 0.32 mmol) were suspended in toluene (40 cm^3) and the mixture was stirred at 60°C for 17 hours. The brown reaction mixture became light brown, with the formation of a brown precipitate. This precipitate was filtered over dried celite and washed with toluene (3 x 20 cm^3). The product was washed through the celite with CH_2Cl_2, the yellow filtrate concentrated and the product precipitated with pentane. The yellow precipitate was filtered off and dried under vacuum. Crystallisation of this microcrystalline powder from CH_2Cl_2/pentane solution (-20°C) produced the yellow crystals of complex **8b** suitable for single crystal X-Ray determination.

Yield: 0.13 g (51 %)
Melting point: 164 - 170°C (decomposition)

Elemental analysis (%): Calc. for **8b** ($C_{42}H_{37}NClBF_4P_2Ni$) (798.65): C, 63.16; H, 4.67; N, 1.75. Found: C, 62.90; H, 4.87; N, 1.76.

Pectora roborant cultus recti

2.4.9 Preparation of *trans*-chloro(1-methyl-1,2-dihydro-quinolin-2-ylidene)bis(triphenylphosphine)palladium(II) tetrafluoroborate, 9a

Complex **9a** was prepared from $Pd(PPh_3)_4$ (0.42 g, 0.36 mmol) and ligand **6** (0.096 g, 0.36 mmol) in similar fashion as complex **8a**. The white precipitate was dried under vacuum and precipitated again from a concentrated CH_2Cl_2 solution with pentane. The white fluffy powder was filtered off and dried under vacuum. Crystallisation from concentrated CH_2Cl_2 solutions layered with pentane at room temperature and –20°C yielded colourless crystals of ***trans*-9a** and ***cis*-9a** respectively, suitable for single crystal X-ray determination.

Yield: 0.26 g (81 %)
Melting point: 202 - 208°C (decomposition)

Elemental analysis (%): Calc. for **9a** ($C_{46}H_{39}NClBF_4P_2Pd$) (896.43): C, 61.63; H, 4.39; N, 1.56. Found: C, 61.40; H, 4.52; N, 1.59.

2.4.10 Preparation of *trans*-chloro(1-methyl-1,2-dihydro-quinolin-2-ylidene)bis(triphenylphosphine)nickel(II) tetrafluoroborate, 9b

The procedure followed for **8b** was used to prepare complex **9b** using $Ni(PPh_3)_4$ (0.34 g, 0.31 mmol) and ligand **6** (0.082 g, 0.31 mmol). Complex **9b** was isolated as a red-purple microcrystalline powder by precipitation from a dark red CH_2Cl_2 solution with pentane. Complex **9b** could not be obtained analytically pure as it decomposes slowly during the crystallisation from a CH_2Cl_2/pentane solution. The melting point and elemental analysis of complex **9b** was therefore not determined.

Yield: 0.16 g (60 %)

2.4.11 Preparation of *trans*-chloro(1,4-dimethyl-1,2-dihydro-quinolin-2-ylidene)bis(triphenylphosphine)palladium(II) tetrafluoroborate, 10a

$Pd(PPh_3)_4$ (0.44 g, 0.38 mmol) and ligand **7** (0.11 g, 0.38 mmol) were suspended in toluene (40 cm^3) and a red violet precipitate started to form almost immediately. The reaction mixture was stirred overnight at room temperature and the yellow colour of the $Pd(PPh_3)_4$ disappeared almost completely. The resultant pinkish precipitate was filtered off and washed with toluene (3 x 20 cm^3) until all the $Pd(PPh_3)_4$ was washed out. This precipitate was dissolved in CH_2Cl_2 and filtered through celite. The red-purple solution was concentrated and product was precipitated with the addition of pentane. The precipitate was collected by filtration and then dried *in vacuo*, to yield **10a** as a red-purple microcrystalline material.

Yield: 0.29 g (85 %)
Melting point: 140 - 146°C (decomposition)

Elemental analysis (%): Calc. for **10a** ($C_{47}H_{41}NClBF_4P_2Pd$) (910.46): C, 62.00; H, 5.54; N, 1.54. Found: C, 61.47; H, 4.79; N, 1.14.

2.4.12 Preparation of *trans*-chloro(1,4-dimethyl-1,2-dihydro-quinolin-2-ylidene)bis(triphenylphosphine)nickel(II) tetrafluoroborate, 10b

Complex **10b**, a pink microcrystalline powder, was prepared in the same way as **8b** and **9b**, using $Ni(PPh_3)_4$ (0.395 g, 0.36 mmol) and ligand **7** (0.10 g, 0.36 mmol). The product was precipitated from a dark purple CH_2Cl_2 solution with pentane and collected by filtration. The dark-purple microcrystalline material was dried under vacuum. Similar to **9a**, complex **10b** could not be obtained analytically pure as it also decomposed in solution during the recrystallisation from a CH_2Cl_2 solution layered with pentane. The melting point and elemental analysis of **10b** was not determined.

Yield: 0.20 g (64 %)

2.4.13 Preparation of 4-chloro-1-methylpyridinium tetrafluoroborate, 12

An aqueous solution of 4-chloropyridine hydrochloride (2.5 g, 16.6 mmol) was treated with a 1 M NaOH (1.0 g, 25 cm^3 H_2O) solution followed by an extraction with diethyl ether (3 x 30 cm^3). The ether extract was washed with a saturated aqueous NaCl solution, filtered over $MgSO_4$ and concentrated to a colourless oil. This oil, 4-chloropyridine, (0.74 g, 6.5 mmol) dissolved in a CH_2Cl_2:CH_3CN (3:1) solution (40 cm^3), was reacted immediately with $[Me_3O][BF_4]$ (0.96 g, 6.5 mmol) in one portion in a brown Schlenk tube at –78°C. The reaction was stirred for 16 hours as the temperature was allowed to reach room temperature. The solvent was removed under vacuum and the white microcrystalline powder, **12**, was washed with THF (50 cm^3) and then dried under high vacuum.

Yield: 0.68 g (81 %)
Melting point: 82 - 83°C

Elemental analysis (%): Calc. for **12** ($C_6H_7BClF_4N$) (215.38): C, 33.46; H, 3.28; N, 6.50. Found: C, 33.50; H, 3.27; N, 6.50.

2.4.14 Preparation of *trans*-chloro(2-methoxy-1-methyl-1,4-dihydro-quinolin-4-ylidene)bis(triphenylphosphine)nickel(II) tetrafluoroborate, 13b

Following the same procedure as for the preparation of complex **8b**, complex **13b** was prepared from $Ni(PPh_3)_4$ (0.34 g, 0.31 mmol) and ligand precursor **11** (0.091 g, 0.31 mmol) as starting materials. Crystallisation of the yellow microcrystalline powder from a CH_2Cl_2 solution layered with pentane at –20°C yielded yellow crystals of **13b** suitable for single crystal X-Ray determination.

Yield: 0.18 g (66 %)
Melting point: 145 - 149°C (decomposition)

Elemental analysis (%): Calc. for **13b** ($C_{47}H_{41}BClF_4NOP_2Ni$) (878.73): C, 64.24; H, 4.70; N, 1.59. Found: C, 63.81; H, 4.91; N, 1.63.

2.4.15 Preparation of *trans*-chloro(1-methyl-1,4-dihydro-pyridin-4-ylidene)bis(triphenylphosphine)palladium(II) tetrafluoroborate, 14a

The same procedure as used for the preparation of complex **8a** was employed to prepare complex **14a**, as a microcrystalline material, from $Pd(PPh_3)_4$ (0.513 g, 0.44 mmol) and ligand precursor **12** (0.096 g, 0.44 mmol).

Yield: 0.29 g (78 %)
Melting point: 163 - 166°C (decomposition)

Elemental analysis (%): Calc. for **14a** ($C_{42}H_{37}NClBF_4P_2Pd$) (846.37): C, 59.60; H, 4.41; N, 1.65. Found: C, 59.72; H, 4.51; N, 1.68.

2.4.16 Preparation of *trans*-chloro(1-methyl-1,4-dihydro-pyridin-4-ylidene)bis(triphenylphosphine)nickel(II) tetrafluoroborate, 14b

$Ni(PPh_3)_4$ (0.458 g, 0.41 mmol) was reacted with ligand **12** (0.089 g, 0.41 mmol) in toluene (40 cm^3) at room temperature for 5 hours. The brown precipitate was filtered over dried celite and washed with toluene (3 x 20 cm^3). The product was washed through the celite with CH_2Cl_2 resulting in a yellow filtrate, which was concentrated, and a precipitation by the addition of pentane was attempted. Very little precipitate formed and thus the solvents were removed under vacuum yielding an off-yellow microcrystalline powder. Crystallisation of **14b** from CH_2Cl_2/pentane solution (-20°C) gave the yellow crystals suitable for single crystal X-Ray determination.

Yield: 0.02 g (6 %)
Melting point: 123 - 125°C (decomposition)

Elemental analysis (%): Calc. for **14b** ($C_{42}H_{37}BClF_4NP_2Ni$) (798.65): C, 63.16; H, 4.67; N, 1.75. Found: C, 63.23; H, 4.57; N, 1.80.

Pectora roborant cultus recti

2.4.17 Preparation of CH=C(C=NCMe$_2$CH$_2$O)SC(Me)=CH, 16

Lithium diisopropylamide (LDA) prepared from diisopropylamine (0.26 cm^3, 1.9 mmol) and *n*-BuLi (1.3 cm^3, 1.9 mmol, 1.4 M) in THF at –78°C (20 min) was added to ligand **15** dissolved in THF at –78°C. The reaction mixture turned yellow and was stirred at – 78°C for 1 hour followed by the addition of $CF_3SO_3CH_3$ (0.20 cm^3, 1.9 mmol). After stirring the reaction mixture at –78°C the Schlenk tube was removed from the dry ice bath and allowed to reach room temperature. The solvent was removed under vacuum, leaving ligand **16** (and unreacted ligand **15**) as a cream precipitate. It was not possible to separate ligand **15** and **16** with column chromatography and this precipitate was used without further purification.

Yield: 80 % (determined by NMR)

2.4.18 Preparation of $(CO)_5Cr\{\overline{CSC(CNMeCMe_2CH_2O)}CHCH\}$, 17a

Ligand **15** (0.22 g, 1.2 mmol) dissolved in THF was treated with *n*-BuLi (0.90 cm^3, 1.3 mmol, 1.5 M) at –78°C for 15 min. The temperature was raised to –30°C and the yellow reaction mixture was stirred for 40 minutes. $[(CO)_5CrBr][NEt_4]$ (0.49 g, 1.2 mmol) dissolved in THF (at –30°C) was added to the reaction mixture and this was stirred for 2 hours after which the solvent was removed under vacuum. The residue was dissolved in CH_2Cl_2 again, cooled down to –50°C and $CF_3SO_3CH_3$ (0.14 cm^3, 1.2 mmol) was added drop wise. The reaction mixture was allowed to reach room temperature slowly, then filtered over dried silica (2 cm) and dried under vacuum. The residue was chromatographed on a flash silica column at –15°C with hexane:ether (1:1) as eluent. Complex **17a** was removed from the column with CH_2Cl_2 after all the other fractions were washed out. Crystallisation from a CH_2Cl_2/pentane solution (-20°C) gave the yellow orange crystals of complex **17a** suitable for single crystal X-Ray determination.

Yield: 0.02 g (6 %)
Melting point: 154 - 160°C (decomposition)

Elemental analysis (%): Calc. for **17a** ($C_{15}H_{13}NO_6SCr$) (387.33): C, 46.51; H, 3.38; N, 3.62. Found: C, 46.33; H, 3.29; N, 3.58.

2.4.19 Preparation of $(CO)_5W\{\overline{CSC(CNMeCMe_2CH_2O)}CHCH\}$, 17b

Ligand **15** (0.56 g, 3.1 mmol) was reacted with *n*-BuLi (2.3 cm^3, 3.7 mmol, 1.6 M) in THF at –78°C for 15 min. The temperature was elevated to –30°C, stirred for 30 minutes before $[(CO)_5WCl][NEt_4]$ (1.6 g, 3.1 mmol) dissolved in THF (at –30°C) was added the reaction mixture. After stirring the reaction mixture for 2 hours at –30°C, the temperature was lowered to –50°C and $CF_3SO_3CH_3$ (0.35 cm^3, 3.1 mmol) was added drop wise. This was stirred for 30 minutes at –50°C, then allowed to reach room temperature and the solvent was removed under vacuum. The dark yellow residue was dissolved in CH_2Cl_2, filtered over a short florosil column and dried under vacuum. Column chromatography over flash silica with CH_2Cl_2:hexane (5:2) at –15°C yielded an orange band (fraction 2) as complex **17b**. This fraction was not pure and was dissolved in ether,

filtered over dried flash silica and washed with ether to remove impurities. Compound **17b** was removed from the column with CH_2Cl_2.

Yield: 0.16 g (10 %)
Melting point: 175°C (decomposition)

Elemental analysis (%): Calc. for **17b** ($C_{15}H_{13}NO_6SW$) (519.17): C, 34.70; H, 2.52; N, 2.70. Found: C, 34.17; H, 2.48; N, 2.75.

2.4.20 Attempted preparation of $(CO)_5Cr\{\underline{CC(\overline{COCH_2CMe_2NMe})SCMeCH}\}$, I

In an attempt to prepare complex **I**, the same procedure used as in the synthesis of complex **17a** was followed with ligand precursor **16** (0.2 g, 1.0 mmol), *n*-BuLi (0.84 cm^3, 1.1 mmol, 1.4 M), $[(CO)_5CrCl][NEt_4]$ (0.37 g, 1.0 mmol) and $CF_3SO_3CH_3$ (0.12 cm^3, 1.0 mmol) as starting materials. The residue was chromatographed over a short column (6 cm) at room temperature and the non-polar fractions were washed out with hexane. The yellow band that stayed on the column was washed out with CH_2Cl_2 and identified as complex **17a**. The three fractions were separated on a flash silica column at –15°C with hexane as eluent but none could be identified as complex **I**.

Pectora roborant cultus recti

2.4.21 Attempted preparation of $(CO)_5W\{\underline{CC(\overline{COCH_2CMe_2NMe})SCMeCH}\}$, II

Complex **II** was prepared using the same procedure as for complex **17b** with ligand precursor **16** (0.2 g, 1.0 mmol), *n*-BuLi (0.84 cm^3, 1.1 mmol, 1.4 M), $[(CO)_5WCl][NEt_4]$ (0.51 g, 1.0 mmol) and $CF_3SO_3CH_3$ (0.12 cm^3, 1.0 mmol). The residue was chromatographed over a short column (6 cm) at room temperature and four fractions were removed with a diethyl ether:hexane (1:1) solution. The yellow band that stayed on the column was washed out with CH_2Cl_2 and identified as complex **17b**. The four fractions were separated on a flash silica column at –15°C with diethyl ether:hexane (1:1) as eluent but could not be identified as complex **II**.

2.4.22 Single crystal X-Ray determinations

The crystal data collection and refinement details for complexes **3a**, **3b**, **4b**, **8a**, **8b**, ***trans*-9a**, ***cis*-9a**, **13b**, **13c**, **14a**, **14b**, **17a**, **17b** and $[PtCl(PPh_3)_3]BF_4$ are summarised in Tables 2.42 to 2.46. Data sets for **13c** and **17b** were collected on an Enraf-Nonius Kappa CCD diffractometer[96] and the other data sets on a Bruker SMART Apex CCD diffractometer[97] with graphite-monochromated Mo-K_α radiation (λ = 0.71073 Å) each. Data reduction was carried out with standard methods from the software packages DENZO-SMN[98] and Bruker SAINT[99] respectively. Empirical corrections were performed using SCALEPACK[100] and SMART data were treated with SADABS.[101,102] The structures were solved by direct methods (**8a**, ***trans*-9a**, ***cis*-9a**, **8b**, **14b**, **17a**), the partial structure expansion method (**3a**, **3b**, **4b**, **13b**, **13c**, **14a**, $[PtCl(PPh_3)_3]BF_4$) or interpretation of a Patterson synthesis (**17b**), which yielded the position of the metal atoms, and conventional Fourier methods. All non-hydrogen atoms were refined anisotropically by full-matrix least squares calculations on F^2 using SHELXL-97[103] within the X-Seed environment (except for **4b** and **17a**).[104] The hydrogen atoms were fixed in calculated positions. POV-Ray for Windows was used to generate the various figures of the three complexes at the 50% probability level.

Complexes **4b** and **17a** were refined as twins using SHELXL-97.[103] The crystal lattice of three complexes contains CH_2Cl_2 molecules that are disordered over two positions (the respective site occupancy factors given in parenthesis) namely **3b**, one CH_2Cl_2 molecule (0.57 and 0.47); **8a**, two CH_2Cl_2 molecules (0.60 and 0.40 for both molecules); ***cis*-9a**, one CH_2Cl_2 (0.51 and 0.49 for one Cl only). Contributions of another disordered CH_2Cl_2 in the unit cell of ***cis*-9a** were taken into account by the SQEEZE method.[105] The unit cell of complex **13c** contains a CH_2Cl_2 molecule, which does

---

[96] COLLECT, Data collection software, Nonius BV Delft, The Netherlands, 1998.

[97] SMART, Data collection software (version 5.629), Bruker AXS Inc., Madison, WI, 2003.

[98] Z. Otwinowski, W. Minor, *Methods Enzymol.*, 1997, **276**, 307.

[99] SAINT, Data reduction software (version 6.45) Bruker AXS Inc., Madison, WI, 2003.

[100] L.J. Ferrugia, *J. Appl. Crystallogr.*, 1999, **32**, 837.

[101] R.H. Blessing, *Acta Crystallogr., Sect. A*, 1995, **51**, 33.

[102] SADABS (version 2.05) Bruker AXS Inc., Madison, WI, 2002.

[103] G.M. Sheldrick, SHELX-97. Program for crystal structure analysis, Univ. of Göttingen, Germany, 1997.

[104] L.J. Barbour, *J. Supramol. Chem*. 2001, **1**, 189.

[105] A.L. Spek, *J. Appl. Cryst.*, 2003, **36**, 7.

not occupy the position fully (85%). Some atoms in the BF_4^- counter ion in complexes ***cis*-9a** (the B atom and one F atom, site occupancy factors 0.62 and 0.38) and **13c** (three F atoms, site occupancy factors 0.52 and 0.48) are disordered over two positions.

Additional information regarding these crystal structures is available from Prof H.G. Raubenheimer, Department of Chemistry, University of Stellenbosch.

2.4.23 Catalysis

2.4.23.1 Heck Reaction

A constant ratio of sodium acetate (0.25 g, 3.0 mmol) and aryl halide (0.32 g, 2.0 mmol bromobenzene) as well as diethyleneglycol-di-*n*-butylether (0.10 g) was placed in a Schlenk tube equipped with a stirring bar under a nitrogen atmosphere. Then *n*-butylacrylate (0.43 cm^3, 3.0 mmol) and 2 cm^3 degassed DMAc (dimethylacetamide) were added at 130 °C. After 10 minutes, the catalyst solution was added against a positive stream of nitrogen. To terminate the reaction the mixture was allowed to cool to room temperature and 3 cm^3 of water was added. The water phase was extracted thrice with 2 cm^3 of dichloromethane and the organic fraction dried over $MgSO_4$. Conversions and yields were determined by GC-MS using diethyleneglycol-di-*n*-butylether as internal standard.

2.4.23.2 Suzuki reaction

Phenylboronic acid (0.29 g, 2.4 mmol) and potassium carbonate (0.42g, 3.0 mmol) were placed in a Schlenk tube equipped with a stirring bar under nitrogen. 2.0 mmol aryl halide (e.g. 0.37 g bromoanisole), diethyleneglycol-di-*n*-butylether (0.10 g) and degassed xylene (2 cm^3) were added. After stirring at 130°C for 10 min, the catalyst solution was added against a positive stream of nitrogen. To end the reaction, the mixture was allowed to cool to room temperature and 3 cm^3 of

water was added. The water phase was extracted three times with 2 cm^3 of diethyl ether and the organic phase dried over $MgSO_4$.

Table 2.42 Crystallographic data for complexes **3a**, **3b** and **4b**

	3a	**3b**	**4b**
Empirical formula	$C_{43}H_{42}BCl_5F_4N_2P_2Pd$	$C_{43}H_{42}BCl_5F_4N_2NiP_2$	$C_{42}H_{42}BCl_3F_6N_2NiP_3$
Formula weight ($g.mol^{-1}$)	1019.19	971.50	946.75
Crystal system	Monoclinic	Monoclinic	Triclinic
Space group	$P2_1$	$P2_1$	P-1
a (Å)	9.1549(12)	9.0700(7)	12.6204(19)
b (Å)	21.553(3)	21.5846(17)	18.109(3)
c (Å)	11.6267(14)	11.4553(9)	20.641(3)
α (°)	90	90	108.180(3)
ß (°)	93.233(2)	94.326(3)	96.018(3)
γ (°)	90	90	100.588(3)
Volume ($Å^3$)	2290.5(5)	2236.0(3)	4338.5(11)
Z	2	2	4
Calculated density ($g.cm^{-3}$)	1.478	1.443	1.449
Wave length (Å)	0.71073	0.71073	0.71073
Temperature (K)	210(2)	100(2)	193(2)
Absorption coefficient (mm^{-1})	0.816	0.854	0.801
Crystal size (mm)	0.30 x 0.20 x 0.20	0.20 x 0.15 x 0.10	0.20 x 0.15 x 0.12
θ range for data collection (°)	$1.75 \leq \theta \leq 28.29$	$2.44 \leq \theta \leq 28.29$	$1.22 \leq \theta \leq 25.35$
Index range, *hkl*	$-12 \leq h \leq 9$	$-9 \leq h \leq 11$	$-15 \leq h \leq 14$
	$-27 \leq k \leq 27$	$-27 \leq k \leq 22$	$-21 \leq k \leq 21$
	$-15 \leq l \leq 14$	$-15 \leq l \leq 15$	$-24 \leq l \leq 24$
Reflections collected	14503	14192	24540
Independent reflections	9019	7622	24540
Parameters	553	517	1040
Goodness of fit	1.019	1.047	0.970
Largest peak	0.938	1.512	0.913
Deepest hole	-1.081	-2.100	-1.196
R1 [$I>2\sigma(I)$]	0.0569	0.603	0.0652
wR (all data)	0.1167	0.1426	0.1610

Table 2.43 Crystallographic data for complexes **8a**, **10** and ***trans*** **9a**

	8a	**8b**	***Trans*-9a**
Empirical formula	$C_{44.50}H_{42}BCl_6F_4NP_2Pd$	$C_{44}H_{41}BCl_5F_4NNiP_2$	$C_{47}H_{41}BCl_3F_4NP_2Pd$
Formula weight ($g.mol^{-1}$)	1058.64	968.49	981.31
Crystal system	Triclinic	Orthorhombic	Orthorhombic
Space group	*P*-1	*Pnma*	$Pca2_1$
a (Å)	11.897(2)	18.114(4)	31.977(3)
b (Å)	13.008(3)	21.802(5)	12.8745(13)
c (Å)	17.193(3)	11.028(2)	10.7781(11)
α (°)	73.05(3)	90	90
ß (°)	76.83(3)	90	90
γ (°)	65.23(3)	90	90
Volume ($Å^3$)	2293.8(8)	4355.4(16)	4437.2(8)
Z	2	4	4
Calculated density ($g.cm^{-3}$)	1.533	1.477	1.469
Wave length (Å)	0.71073	0.71073	0.71073
Temperature (K)	100(2)	273(2)	100(2)
Absorption coefficient (mm^{-1})	0.873	0.877	0.722
Crystal size (mm)	0.30 x 0.15 x 0.15	0.20 x 0.15 x 0.10	0.20 x 0.10 x 0.10
θ range for data collection (°)	$1.25 \leq \theta \leq 28.33$	$1.87 \leq \theta \leq 28.30$	$2.03 \leq \theta \leq 25.68$
Index range, *hkl*	$-15 \leq h \leq 15$	$-24 \leq h \leq 22$	$-38 \leq h \leq 25$
	$-17 \leq k \leq 17$	$-27 \leq k \leq 26$	$-15 \leq k \leq 15$
	$-22 \leq l \leq 22$	$-14 \leq l \leq 13$	$-12 \leq l \leq 13$
Reflections collected	26190	25645	23605
Independent reflections	10444	5300	8144
Parameters	607	281	635
Goodness of fit	1.100	1.131	1.030
Largest peak	2.341	1.846	0.739
Deepest hole	-0.707	-1.399	-0.568
R1 [$I>2\sigma(I)$]	0.419	0.0584	0.0440
wR (all data)	0.0987	0.1559	0.0909

Table 2.44 Crystallographic data for complexes ***cis cis-9a***, **13b** and **13c**

	***Cis*-9a**	**13b**	**13c**
Empirical formula	$C_{47}H_{41}BCl_3F_4NP_2Pd$	$C_{49}H_{45}BCl_5F_4NNiOP_2$	$C_{52}H_{49}BCl_{11}F_4NOP_2Pt$
Formula weight ($g.mol^{-1}$)	981.31	1048.57	1437.71
Crystal system	Triclinic	Orthorhombic	Monoclinic
Space group	*P*-1	*Pbcm*	$P2_1/n$
a (Å)	14.562(3)	10.8783(9)	11.4430(2)
b (Å)	16.041(3)	19.9993(16)	19.1450(2)
c (Å)	18.605(3)	22.3327(18)	27.2989(3)
α (°)	94.746(3)	90	90
ß (°)	95.891(3)	90	95.48(1)
γ (°)	92.326(3)	90	90
Volume ($Å^3$)	4302.8(13)	4858.7(7)	5953.19(14)
Z	4	4	4
Calculated density ($g.cm^{-3}$)	1.515	1.433	1.604
Wave length (Å)	0.71073	0.71073	0.71073
Temperature (K)	100(2)	100(2)	173(2)
Absorption coefficient (mm^{-1})	0.745	0.793	2.954
Crystal size (mm)	0.25 x 0.10 x 0.10	0.15 x 0.10 x 0.10	0.30 x 0.25 x 0.15
θ range for data collection (°)	$1.69 \leq \theta \leq 25.35$	$1.82 \leq \theta \leq 28.25$	$2.46 \leq \theta \leq 27.00$
Index range, *hkl*	$-17 \leq h \leq 17$	$-14 \leq h \leq 14$	$-14 \leq h \leq 14$
	$-19 \leq k \leq 19$	$-21 \leq k \leq 26$	$-24 \leq k \leq 24$
	$-22 \leq l \leq 22$	$-29 \leq l \leq 25$	$-34 \leq l \leq 34$
Reflections collected	42500	29503	65762
Independent reflections	15704	5903	12910
Parameters	1089	318	659
Goodness of fit	1.192	1.024	1.208
Largest peak	1.644	0.851	2.820
Deepest hole	-1.310	-0.580	-1.198
R1 [$I>2\sigma(I)$]	0.0890	0.0665	0.0546
wR (all data)	0.2011	0.1437	0.1629

Table 2.45 Crystallographic data for complexes **14a**, **14b** and **17a**

	14a	**14b**	**17a**
Empirical formula	$C_{43}H_{39}BCl_3F_4NP_2Pd$	$C_{43.50}H_{40}BCl_4F_4NNiP_2$	$C_{15}H_{13}CrNO_6S$
Formula weight ($g.mol^{-1}$)	931.25	926.03	387.32
Crystal system	Triclinic	Monoclinic	Monoclinic
Space group	*P*-1	$P2_1/n$	$P2_1/n$
a (Å)	9.359(3)	9.7256(12)	9.425(4)
b (Å)	11.552(3)	19.822(3)	14.328(4)
c (Å)	19.987(5)	21.939(3)	12.631(4)
α (°)	90.159(4)	90	90
ß (°)	94.623(4)	92.392(3)	94.787(50
γ (°)	106.670(4)	90	90
Volume ($Å^3$)	2062.7(10)	4225.9(9)	1699.7(10)
Z	2	4	4
Calculated density ($g.cm^{-3}$)	1.499	1.456	1.514
Wave length (Å)	0.71073	0.71073	0.71073
Temperature (K)	100(2)	100(2)	100(2)
Absorption coefficient (mm^{-1})	0.722	0.839	0.825
Crystal size (mm)	0.20 x 0.1 x 0.1	0.20 x 0.15 x 0.10	0.30 x 0.20 x 0.10
θ range for data collection (°)	$2.28 \leq \theta \leq 28.16$	$1.39 \leq \theta \leq 25.06$	$2.15 \leq \theta \leq 25.35$
Index range, *hkl*	$-12 \leq h \leq 12$	$-11 \leq h \leq 11$	$-11 \leq h \leq 11$
	$-14 \leq k \leq 14$	$-23 \leq k \leq 23$	$-17 \leq k \leq 17$
	$-26 \leq l \leq 25$	$-19 \leq l \leq 26$	$-15 \leq l \leq 15$
Reflections collected	19197	22008	8291
Independent reflections	8972	7474	8222
Parameters	497	524	229
Goodness of fit	1.040	0.997	0.961
Largest peak	1.433	0.794	0.880
Deepest hole	-1.275	-0.666	-0.708
R1 [$I>2\sigma(I)$]	0.0755	0.0684	0.0660
wR (all data)	0.1708	0.1376	0.1684

Table 2.46 Crystallographic data for complexes **17b**, and **26**

	17b	$[PtCl(PPh_3)_3]BF_4$
Empirical formula	$C_{15}H_{13}NO_6SW$	$C_{56}H_{49}BCl_5F_4P_3Pt$
Formula weight ($g.mol^{-1}$)	519.17	1274.01
Crystal system	Orthorhombic	Monoclinic
Space group	$P2_1nb$	$P2_1/n$
a (Å)	9.53190(10)	17.7782(10)
b (Å)	14.7075(2)	12.1641(7)
c (Å)	12.6130(2)	25.5252(15)
α (°)	90	90
ß (°)	90	105.1790(10)
γ (°)	90	90
Volume ($Å^3$)	1768.22(4)	5327.4(5)
Z	4	4
Calculated density ($g.cm^{-3}$)	1.950	1.588
Wave length (Å)	0.71073	0.71073
Temperature (K)	173(2)	100(2)
Absorption coefficient (mm^{-1})	6.680	3.026
Crystal size (mm)	0.20 x 0.11 x 0.10	0.20 x 0.15 x 0.10
θ range for data collection (°)	$3.85 \leq \theta \leq 26.00$	$1.65 \leq \theta \leq 28.29$
Index range, *hkl*	$-11 \leq h \leq 11$	$-23 \leq h \leq 22$
	$-18 \leq k \leq 18$	$-14 \leq k \leq 15$
	$-15 \leq l \leq 15$	$-33 \leq l \leq 31$
Reflections collected	3320	32192
Independent reflections	3320	12333
Parameters	243	632
Goodness of fit	0.980	1.007
Largest peak	0.291	2.315
Deepest hole	-0.613	-2.137
R1 [$I>2\sigma(I)$]	0.0178	0.0657
wR (all data)	0.0393	0.1341

Chapter 3

New results concerning the preparation and structure of unsymmetric *N*-heterocyclic carbene complexes of rhodium

Abstract

Free carbenes, produced from the reaction of [EMIM]Br, [PMIM]Br or [BMIM]Br with an excess of KO^{t}Bu, reacted with $[Rh(Cl)COD]_2$ to yield three non-symmetrical products for each reaction. These were bis(carbene) complexes, $[Rh(NHC)_2COD]Br$, bromo-mono(carbene) complexes, Rh(Br)COD(NHC), and chloro-mono(carbene) complexes, Rh(Cl)COD(NHC) where NHC is 1-R-3-methyl-2,3-dihydro-1*H*-imidazol-2-ylidene (R = ethyl or propyl or butyl). [Rh(Br)COD(NHC)] forms as a result of substitution of a chloride ligand by a Br^--anion. Carbonyl complexes, *cis*-$[Rh(CO)_2X(NHC)]$ (X = Br or Cl; NHC = 1-ethyl-3-methyl-2,3-dihydro-1*H*-imidazol-2-ylidene) have been prepared and these compounds undergo isomerisation in solution to yield the corresponding *trans*-$[Rh(CO)_2X(NHC)]$ compounds.

These compounds were fully characterised and the crystal structures *of cis*-[(η^4-1,5-cyclooctadiene)bis(1-butyl-3-methyl-2,3-dihydro-1*H*-imidazol-2-ylidene)rhodium(I)] bromide, bromo(η^4-1,5-cyclooctadiene)(1-methyl-3-propyl-2,3-dihydro-1*H*-imidazol-2-ylidene) rhodium(I) and *cis*-[(η^4-1,5-cyclooctadiene)bis(1-butyl-3-methyl-2,3-dihydro-1*H*-imidazol-2-ylidene)rhodium(I)] bromide were determined.

3.1 Introduction and Aims

3.1.1 General

Arduengo reported the first stable *N*-heterocyclic carbene (NHC)[1] and since then it has been established that the stability of these free carbenes is primarily dependent on the pπ-pπ interaction between the carbene carbon and the adjacent heteroatoms.[2] The isolation of several

[1] A.J. Arduengo,III, R.L. Harlow, M. Kline, *J. Am. Chem. Soc.*, 1991, **113**, 361.

[2] W.A. Herrmann, C. Köcher, *Angew. Chem., Int. Ed., Engl.*, 1997, **36**, 2162.

free carbenes confirmed that steric,[3] aromatic[4] and cyclic[5] requirements were not crucial to their stability. The majority of such carbenes have a singlet ground state (**i**) while there are few triplet ground state carbenes (**ii**) but they belong to another family.[2,6] The singlet state of NHC's have been confirmed with theoretical studies.[7]

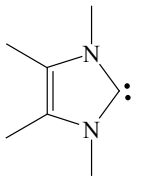

(**i**)

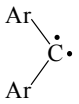

(**ii**)

Free carbenes prepared from imidazolium and imidazolinium salts are the most common. The imidazolium salts are usually prepared by two main methods (Scheme 3.1).[8] The reaction of potassium imidazolide with one molar equivalent alkyl halide produces the 1-alkylimidazole. Subsequent alkylation in the 3-position is achieved by the reaction with another mole quantity alkyl halide (equation 1). This reaction allows the introduction of *N*-substituents that are similar or different but is restricted to primary alkyl halides. Imidazolium salts can also be prepared by ring formation of primary amines, glyoxal and formaldehyde (equation 2). In this manner other substituents can be introduced but the method is restricted to identical *N*-substituents. *N*-functionalised heterocyclic carbenes with a donor atom (P, O, N) incorporated into one or both the *N*-substituents are also available from precursors prepared according to equations 1 and 2.[9,10] Thiazole, pyrazole and triazole also serve as precursors for free carbenes.[11,12,13]

Pectora roborant cultus recti

---

[3] A.J. Arduengo,III, H.V.R. Dias, R.L. Harlow, M. Kline, *J. Am. Chem. Soc.*, 1992, **114**, 5530.

[4] A.J. Arduengo,III, J.R. Goerlich, W.J. Marshall, *J. Am. Chem. Soc.*, 1995, **117**, 11027.

[5] R.W. Alder, P.R. Allen, M. Murray, G. Orpen, *Angew. Chem., Int. Ed., Engl.*, 1996, **35**, 1121.

[6] D. Bourissou, O. Guerret, F.P. Gabbai, G. Bertrand, *Chem. Rev.*, 2000, **100**, 39.

[7] D.A. Dixon, A.J. Arduengo,III, *J. Phys. Chem.*, 1991, **95**, 4180.

[8] T. Weskamp, V.P.W. Böhm, W.A. Herrmann, *J. Organomet. Chem.*, 2000, **600**, 12.

[9] W.A. Herrmann, C. Köcher, L.J. Gooβen, G.R.J. Artus, *Chem. Eur. J.*, 1996, **2**, 1627.

[10] W.A. Herrmann, L.J. Gooβen, M Spiegler, *Organometallics*, 1998, **17**, 2162.

[11] A.J. Arduengo,III, J.R. Goerlich, W.J. Marshall, Liebigs Ann./Recueil, 1997, 365.

[12] J. Schultz, E. Herdtweck, W.A. Herrmann, *Organometallics*, 2004, **23**, 6084.

[13] D. Enders, H. Gielen, J. Runsink, K. Breuer, S. Brode, K. Boehm, *Eur. J. Inorg. Chem.*, 1998, 913.

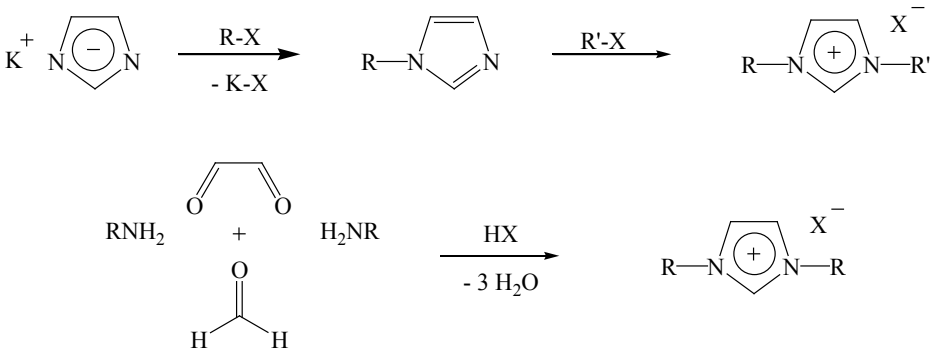

Various pathways are available to generate the free carbenes. Most generally,[8] deprotonation of azolium salts with an external base (potassium *tert*-butoxide or sodium hydride) or basic anions {e.g. alkoxo ligands from μ-alkoxo complexes of (COD)rhodium(I)} (COD = η^4-1,5-cyclooctadiene) produce free carbenes *in situ*. Azole-thiones can be converted into the corresponding carbenes by reaction with elemental sodium or potassium.[14]

Transition metal complexes

Preformed, free carbenes react with a variety of transition metals to yield the corresponding carbene complexes. These nucleophilic carbene ligands cleave dimeric complexes with bridging ligands like halides, carbon monoxide or acetonitrile. Free carbenes can also substitute ligands like phosphines (PR_3) and CO in transition metal complexes. The thermal cleavage of electron-rich olefins by various transition metal complexes also generates carbene complexes.[8,15] Carbene complexes of an array of transition metals such as cobalt, iron, palladium and rhodium to name but a few, are known.[2,6,16] Rhodium(I) carbene complexes are the main focus of this chapter.

The synthesis of rhodium carbene complexes is well established and various routes used by different authors towards these complexes are illustrated in Scheme 3.1.[8,17,18] The NHC's cleave the dimeric rhodium complexes, $[Rh(Cl)COD]_2$ or $[Rh(Cl)(CO)_2]_2$, to yield the corresponding COD or carbonyl mono(carbene) complexes (**iii** or **iv**). The local excess of the two applicable

[14] N. Kuhn, T. Kratz, *Synthesis*, 1993, 561.

[15] M.J. Doyle, M.F. Lappert, P.L. Pye, P. Terreros, *J. Chem. Soc., Dalton Trans.*, 1984, 2355.

[16] H. van Rensburg, R.P. Tooze, D.F. Foster, A.M.Z. Slawin, *Inorg. Chem.*, 2004, **43**, 2004.

[17] A. Neveling, G.R. Julius, S. Cronje, C. Esterhuysen, H.G. Raubenheimer, *Dalton Trans.*, 2005, 181.

[18] W.A. Herrmann, M. Elison, J. Fischer, C. Köcher, G.R.J. Artus, *Chem. Eur. J.*, 1996, **2**, 772.

reagents is important and determines which products are formed. The slow addition of the NHC's to $[Rh(Cl)COD]_2$ (now in local excess) will mainly produce the neutral mono(carbene) complex (**iii**). If the NHC is in excess (2L), the mono(carbene) complex (**iii**) as well as the bis(carbene) complex (**vi**) can be isolated.

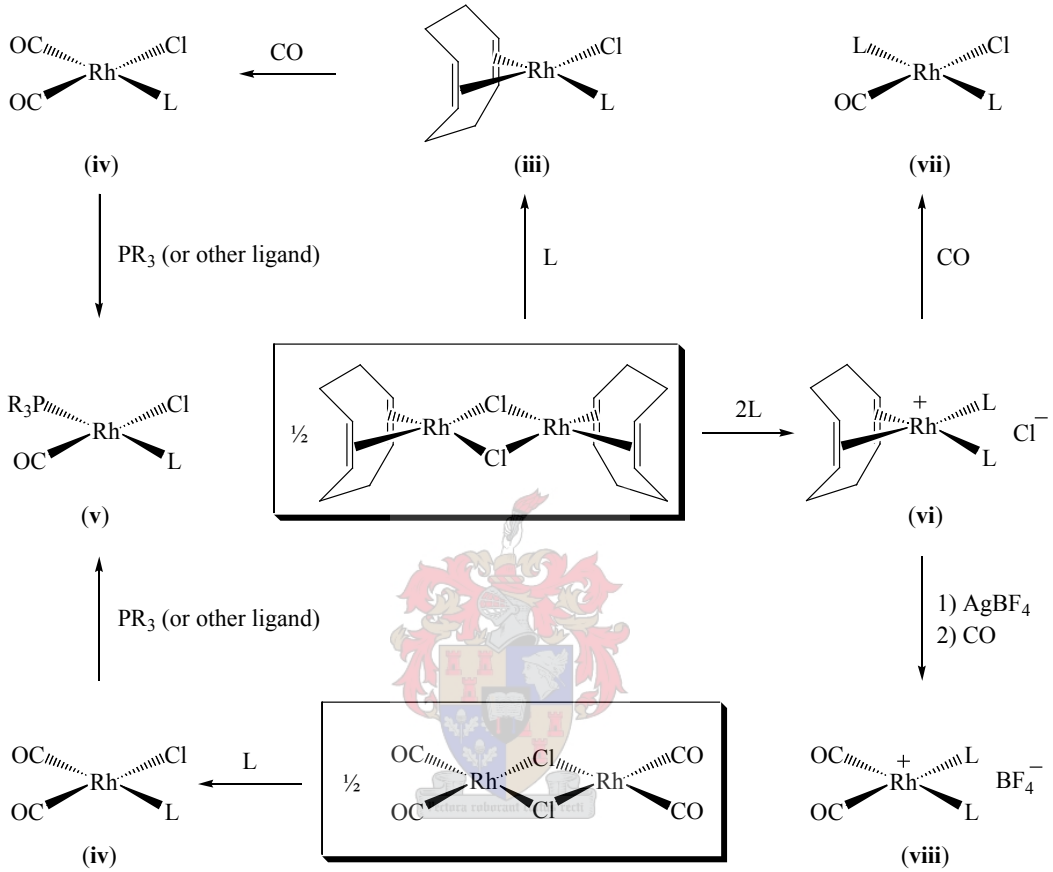

Scheme 3.1 {L = *N*-heterocyclic carbene (NHC) in this investigation}

The carbonyl carbene complex (**iv**) can be prepared by the substitution of the COD ligand with two carbonyls when CO gas is bubbled through a solution of the COD{mono(carbene)} complex. This same reaction with the bis(carbene) complex produces the carbonyl bis(carbene) complex (**vii**) with the counter ion (Cl^-) now bonded to rhodium. The carbonyl bis(carbene) complex (**viii**) can be obtained if the initially uncoordinated Cl^--ion is replaced by BF_4^-. A carbonyl ligand can also be substituted by a phosphine ligand (or another ligand with two donating electrons such as an amine, imine, a thione or even another NHC) to form a carbene($2e^-$ donor ligand) complex (**v**).[17] The carbonyl *trans* to the NHC is replaced first because the NHC has a greater *trans*-effect than the halide (Cl^-). Despite modifications to the standard NHC's their coordination to rhodium would follow the reaction paths presented in Scheme 3.1. Bis(carbene) complexes are prepared using bridging carbene ligand (L^L instead of 2L). Mata

reported that bidentate coordination of bis(carbene) ligands with long $(CH_2)_n$ linkers is preferred and dinuclear monodentately-coordinated complexes are formed when $n = 1$ or 2.[19] *N*-functionalised heterocyclic carbenes could potentially act as bidentate ligands if the donor atom in the *N*-substituent coordinates to the metal with an available coordination site. Removal of the chloride from (COD)Rh(NHC)Cl by $TlPF_6$ (or possibly $AgBF_4$) would provide exactly such a coordination site.[9]

Catalysis

As mentioned previously, *N*-heterocyclic carbenes are established ligand alternatives for the widely used phosphines in pre-catalysts for various catalytic processes. The catalytic properties of these NHC complexes are highlighted and well summarised in the literature.[2,6,20] The properties of *N*-heterocyclic carbene complexes of rhodium substantiate their importance as pre-catalysts in homogeneous catalysis. The complexes are very robust and are air and moisture stable. These NHC ligands are easily accessible and are not as sensitive as phosphine ligands, which are easily oxidised in the presence of air and moisture. The NHC ligands also do not dissociate from the metal during catalytic reactions as phosphines sometimes do. No excess of the NHC ligands is thus required to prevent the decomposition of the catalyst in contrast to the excess of phosphine ligands that are critically necessary for the stability of rhodium phosphine complexes in catalysis. Furthermore, NHC ligands increase the electron density on the rhodium relative to phosphines and, therefore, lowers the activity of these catalysts. Higher activities and greater stabilities were achieved for mixed rhodium carbene-phosphine complexes. [2,6,21]

Complexes of the type (COD)Rh{=$\overline{\text{CN(R)CH=CHN}}$(R)}(Cl), $(CO)_2$Rh{=$\overline{\text{CN(R)CH=CHN}}$(R)}(Cl) and [(COD)(Cl)Rh{=$\overline{\text{CN(R)CH=CHN}}$(R)}]$_2(CH_2)_2$ (R = Me or cyclohexyl) as catalyst precursors in the hydroformylation of olefins (propene, 1-hexene, 2-hexene and styrene) have been patented.[22] The rhodium carbene-phosphine complexes (PPh_3)(L)Rh{=$\overline{\text{CN(Ar)CH=CHN}}$(Ar)}(Cl) (L = PPh_3 or CO, Ar = 2,4,6-trimethylbenzene) have

---

[19] J.A. Mata, A.R. Chianese, J.R. Miecznikowski, M. Poyatos, E. Peris, J.W. Faller, R.H. Crabtree, *Organometallics*, 2004, **23**, 1253.

[20] W.A. Herrmann, *Angew. Chem., Int. Ed., Engl.*, 2002, **41**, 1290.

[21] W.A. Herrmann, L.J. Gooβen, G.R.J. Artus, C. Köcher, *Organometallics*, 1997, **16**, 2472.

[22] Hoechst AG (DE) (W.A. Herrmann, M. Elison, J. Fischer, C. Köcher) EP 0.719.753 (1996), EP 0.721.953 (1996), US 5.663.451 (1997); Hoechst AG (DE) (W.A. Herrmann, J. Fischer, M. Elison, K. Öfele, C. Köcher) US 5.728.839.

been tested as pre-catalysts in the hydroformylation of styrene showing high selectivities with *n*/*i* ratios higher than 95:5.[23] Members of our group recently reported a comparable study of the homogeneous hydroformylation of 1-hexene employing square planar mono(thione), mono(carbene), bis(carbene), thione(carbene), thione(phosphine) and carbene(phosphine) rhodium(I) complexes as catalyst precursors.[17] The selectivity for all these complex types were low with the *n*/*i* ratio close to 50:50. The thione complex $(CO)_2Rh\{S=\overline{CN(^iPr)C(Me)=C(Me)N}(^iPr)\}(Cl)$ (^{i}Pr = isopropyl) was the most active (TOF > 167 h^{-1} after 6 hours)[24] of all the complexes tested indicating that further tailoring, more specifically by introducing steric factors, could make such ligands competitive. This thione complex, however, was inactive when the ionic liquid [BMIM]BF_4 (1-butyl-3-methylimidazolium tetrafluoroborate) was used as solvent.

Water-soluble *N*-functionalised rhodium complexes have shown their potential as catalysts in the biphasic catalysis being used in the Ruhrchemie/Rhône-Poulene hydroformylation process.[25]

3.1.2 Aims of this study

The NMR data obtained for the rhodium carbene complex, chloro(η^4-1,5-cyclooctadiene)(1-butyl-3-methyl-2,3-dihydro-1*H*-imidazol-2-ylidene)rhodium(I), showed two sets of signals for all protons and carbons in its NMR spectra.[26] The existence of rotamers and restricted rotation around the Rh-$C_{carbene}$ bond are invoked in explaining the results. No X-ray data are available.

The uncertainty still surrounding the information around this complex, led to the present study in a further attempt to understand the obtained results. The synthesis and characterisation of a range of rhodium carbene complexes (including the one above) was embarked upon. The salts 1-ethyl-3-methylimidazolium bromide, [EMIM]Br, 1-methyl-3-propylimidazolium, [PMIM]Br and 1-butyl-3-methylimidazolium bromide, [BMIM]Br, were chosen as carbene precursors, to establish at what chain length of substituent such restricted rotation around the Rh-$C_{carbene}$ would appear.

---

[23] A.C. Chen, A. Decken, C.M. Crudden, *Organometallics*, 2000, **19**, 3459

[24] TOF = (mol aldehydes formed/mol catalyst) h^{-1}, Conditions (80°C, 8 MPa, 6h, catalyst:substrate 1:1000, solvent: toluene).

[25] W.A. Herrmann, L.J. Gooβen, M. Spiegler, *J. Organomet. Chem.*, 1997, **547**, 357.

[26] A. Neveling, *Ph.D. Dissertation*, University of Stellenbosch, 2003.

The synthesis and unambiguous characterisation of rhodium carbene complexes with [EMIM]Br, [PMIM]Br, [BMIM]Br, and [BMIM]BF_4 as carbene precursors, were the major goals of this study. Replacement COD ligand by two CO ligands was also envisaged. It was imperative to compliment the NMR and MS data with X-ray crystal structure determinations where possible.

In future, the catalytic activity of such complexes in the hydroformylation of olefins, in normal organic solvents as well as ionic liquids, could also be examined.

3.2 Results and discussion

3.2.1 Synthesis of complexes 18a - 23b

The imidazolium salts were prepared according to literature methods by heating *N*-methylimidazole with an excess of RBr (R = Et, Pr or Bu) in toluene at 65 - 70 °C to form [EMIM]Br, [PMIM]Br and [BMIM]Br.[27] The formed ionic liquids were deprotonated with potassium *tert*-butoxide (KO^{t}Bu) at room temperature to form the corresponding free carbene.[8] $[Rh(Cl)COD]_2$ was added directly to a solution of the free carbene to produce complexes **18a**, **19a**, **19b**, **20a**, **21a**, **21b**, **22a**, **23a** and **23b** (Scheme 3.2).

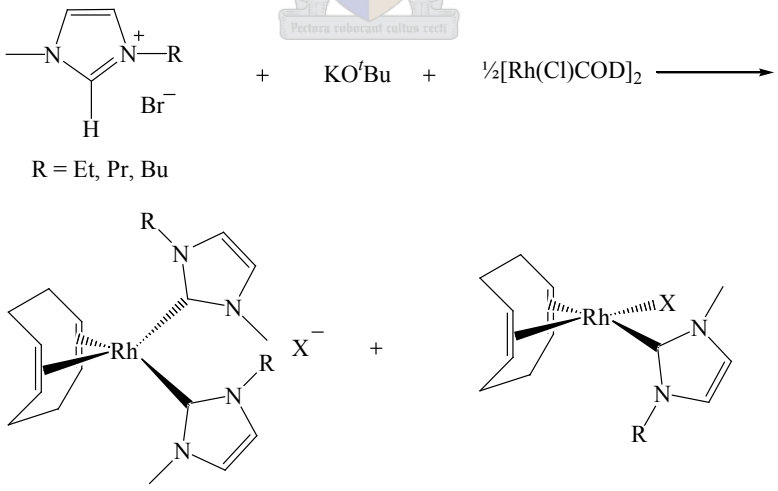

Scheme 3.2 (**a**: X = Br; **b**: X = Cl)

[27] N.E. Leadbeater, H.M. Torenius H. Tye, *Tetrahedron*, 2003, **59**, 2253.

The unsymmetric bis(carbene) rhodium complexes (**18a**, **20a** and **22a**) not mentioned in the previous study) formed immediately upon addition of the $[Rh(Cl)COD]_2$ as precipitates and were isolated by filtration. Complexes **19a**, **21a** and **23a** formed by substitution of chloride bonded to the rhodium by bromide stemming from the ionic liquids. The mono(carbene) complexes (e.g. **19a, 19b**) in each experiment were separated on a short silica column by flash chromatography with ether as eluent. In addition, complex **23b** was also prepared, as sole product by reacting the free carbene generated from $[BMIM]BF_4$ (different counterion)[27,28] with $[Rh(Cl)COD]_2$ (equation 3). No isolable precipitate formed here after addition of the $[Rh(Cl)COD]_2$ as observed in reactions with [EMIM]Br, [PMIM]Br and [BMIM]Br when preparing complexes **18a**, **19a**, **19b**, **20a**, **21a**, **21b**, **22a**, **23a** and **23b**. This result indicates the important role played by the counterion in these synthetic steps.

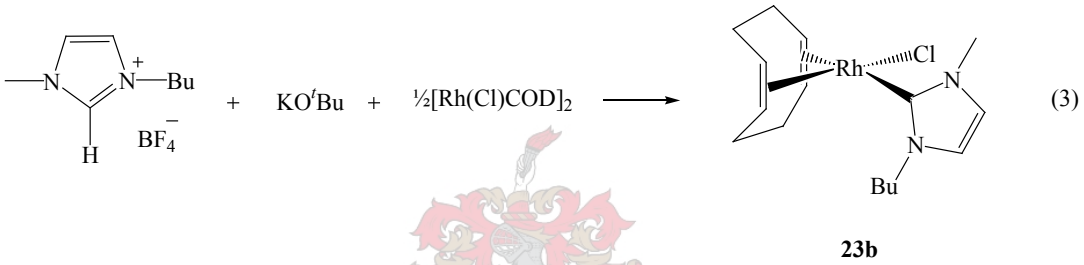

(3)

23b

All the complexes are soluble in more polar organic solvents like CH_2Cl_2 and acetone but some (**18a**, **20a** and **22a**) are insoluble in diethyl ether and THF and not one of them dissolves in non-polar solvents like pentane.

3.2.2 Spectroscopic characterisation of complexes 18a - 23b

NMR spectroscopy

The correct assignment of the signals in the ^1H and ^{13}C NMR spectra for complexes **18a - 23b** was accomplished with ghsqc (gradient heteronuclear single quantum coherence) NMR spectra. NMR data for the [EMIM]Br, [PMIM]Br and [BMIM]Br have been reported previously.[29]

---

[28] N.E. Leadbeater, H.M. Torenius, *J. Org. Chem.*, 2002, **67**, 3145.

[29] E.A. Turner, C.C. Pye, R.D. Singer, *J. Phys. Chem.*, 2003, **107**, 2277.

*3.2.2.1 Cis-[(η^4-1,5-cyclooctadiene)bis(1-ethyl-3-methyl-2,3-dihydro-1**H**-imidazol-2-ylidene)rhodium(I)]bromide, 18a*

NMR data for complex **18a** are summarised in Table 3.1. A set of signals for each of the two ylidene ligands in the complex is observed both in the ^{1}H and ^{13}C NMR spectra and it is very clear that they are not equivalent. The alkene protons for one carbene ligand appear at δ 7.05 and differ slightly from those in the other carbene ligand. The two protons attached to C^{6} and $C^{6'}$ appear at δ 4.27 (both ligands) and 4.42 or 4.61 and these protons in each set (A and A') are diastereotopic.[30] Proton A experiences geminal coupling with A' and in a like manner A' with A and each proton also couples with the three methyl protons (X) giving rise to an $AA'X_3$ spin system and thus two multiplets are observed. Similar diastereotopic NCH_2 protons have been reported by Crabtree and co-workers for chloro(η^4-1,5-cyclooctadiene)(1,3-dibutyl-2,3-dihydro-1*H*-imidazol-2-ylidene)rhodium(I).[31] According to the two-dimensional ghsqc NMR spectrum the two olefinic protons H^{6} and $H^{6'}$ at δ 4.27, assigned to approximately the same multiplet, do appear at very slightly different chemical shifts. The olefinic protons of the COD ligand appear as four multiplets, which could not be assigned to individual protons with certainty. The molecular structure of **18a** (see section 3.2.5.1) shows that these protons are in chemically different environments as the two non-equivalent carbene ligands (at least in the solid state) are almost perpendicular to the square plane, formed by the two carbene carbons, the rhodium atom and the centers of the two COD double bonds, with the ethyl groups pointing in the same direction while the methyl groups are pointing in the other direction. There is thus no mirror plane dissecting the rhodium atom and the centers of the C11-C12 and C15-C16 bonds. The six multiplets (δ 2.55 - 2.04, Table 3.1) were assigned to the aliphatic protons. Again, as for the olefinic protons, no unambiguous assignments could be made. However, the two protons of the carbon atoms are in chemically different environments, each appearing as a multiplet.

---

[30] D.L. Pavia, G.M. Lampman, G.S. Kriz, *Introduction to Spectroscopy*, 3rd Edition, Harcourt College Publishers, Fort Worth, 2001, p. 270.

[31] A.R. Chianese, X. Li, M.C. Janzen, J.W. Faller, R.H. Crabtree, *Organometallics*, 2003, **22**, 1663.

Table 3.1 ^{1}H and ^{13}C NMR data of complex **18a** measured in CD_2Cl_2

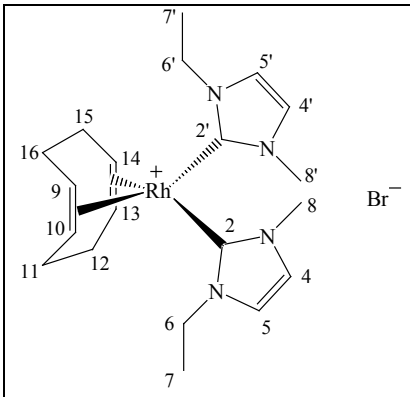

Assignment	δ / ppm	Assignment	δ / ppm
^{1}H NMR		**^{13}C NMR**	
H^4, H^5; $H^{4'}$, $H^{5'}$	7.05 (2H, m), 7.11 (2H, m)	C^2, $C^{2'}$	180.3 (d, J_{Rh-C} = 53.7 Hz),
$H^{6'}$, H^6	4.61 (1H, m), 4.27 (1H, m),		180.4 (d, J_{Rh-C} = 53.8 Hz)
	4.42 (1H, m), 4.27 (1H, m)	C^4, C^5, $C^{4'}$, $C^{5'}$	123.8 (s), 120.8 (s),
-HC=CH- (COD)	4.42 (1H, m), 4.27 (1H, m),		123.9 (s), 120.5 (s)
	4.11 (1H, m)	-HC=CH- (COD)	90.4 (d, J_{Rh-C} = 8.6 Hz),
H^8, $H^{8'}$	4.08 (s), 4.02 (s)		89.5 (d, J_{Rh-C} = 7.3 Hz),
$-H_2C-CH_2-$ (COD)	2.51 (1H, m), 2.43 (2H, m),		88.9 (d, J_{Rh-C} = 8.6 Hz),
	2.35 (1H, m), 2.28 (1H, m),		88.3 (d, J_{Rh-C} = 8.6 Hz)
	2.18 (2H, m), 2.08 (1H, m)	C^6, $C^{6'}$	46.1 (s), 45.9 (s)
H^7, $H^{7'}$	1.42 (3H, m), 1.33 (3H, m)	C^8, $C^{8'}$	38.5 (s),
			38.8 (d, J_{Rh-C} = 2.5 Hz)
		$-H_2C-CH_2-$ (COD)	32.3 (s), 31.0 (s), 31.1(s),
			29.8 (s)
		C^7, $C^{7'}$	16.0 (s), 16.0 (s)

The protons H^7 and $H^{7'}$ were observed as triplet-like multiplets although one would expect a doublet of doublets due to coupling of H^7 to the two diastereotopic H^6 protons. These triplet-like multiplets were observed probably as a result of the overlap of the doublets and their equal coupling constants. The apparent first order signals (triplets) are classified as multiplets because the intensity ratios of the individual signals do not reflect the intensity ratios that are expected for these signals derived from the (n + 1)-rule.[32] The chemical shifts of the signals for H^7 and H^8 (as well as $H^{7'}$ and $H^{8'}$) are found at expected positions.

[32] D.L. Pavia, G.M. Lampman, G.S. Kriz, *Introduction to Spectroscopy*, 3rd Edition, Harcourt College Publishers, Fort Worth, 2001, p. 134.

Two doublets at ca. δ 180 in the ^{13}C NMR spectrum of **18a** were assigned to the carbene carbons of the two ligands. The coupling constants (^{103}Rh - ^{13}C-coupling) for both the carbene ligands are the same (53.8 Hz) and compare well with similar coupling constants reported for rhodium carbene complexes in literature.[9,17,33] All the other carbon atoms of the carbene ligand have expected chemical shifts. The signal for one set of NMe carbons surprisingly shows a long-range ^{103}Rh - ^{13}C-coupling of 2.5 Hz. The four non-equivalent olefinic carbon atoms (C^9, C^{10}, C^{13} and C^{14}) resonate each as a doublet at δ 90.42 - 88.24 with ^{103}Rh - ^{13}C-coupling constants of ca. 8.6 Hz. These chemical shifts are similar to those reported for the olefinic carbons in *cis*-[(η^4-1,5-cyclooctadiene)bis(1,3-dimethyl-2,3-dihydro-1*H*-imidazol-2-ylidene)rhodium(I)] chloride by Herrmann and co workers.[18] They did, however, not report any rhodium-carbon couplings. Each aliphatic carbon atom (C^{11}, C^{12}, C^{15} and C^{16}) is situated in a chemically different environment.

3.2.2.2 Bromo(η^4-1,5-cyclooctadiene)(1-ethyl-3-methyl-2,3-dihydro-1H-imidazol-2-ylidene)rhodium(I), 19a, and chloro(η^4-1,5-cyclooctadiene)(1-ethyl-3-methyl-2,3-dihydro-1H-imidazol-2-ylidene)rhodium(I), 19b

The NMR data of complexes **19a** and **19b** are compiled in Tables 3.2 and 3.3. The signals in the ^{1}H and ^{13}C NMR spectra of **19a** and **19b** were assigned completely and in similar fashion as for chloro(η^4-1,5-cyclooctadiene)(1-benzyl-3-methyl-2,3-dihydro-1*H*-imidazol-2-ylidene) rhodium(I).[34] The two *N*-substituents in the majority of the known (COD)Rh(NHC)Cl complexes are similar and only a few examples of asymmetric carbene complexes, where these substituents are different, are known. The NMR spectra of the former are simplified due to the symmetry in these complexes. The lack of symmetry in the latter causes the atoms in particular the COD ligand, generally to be in different chemical environments and is clearly observed in the NMR experiments.[9,13,35] Few imidazole-derived carbene complexes of the type (COD)Rh(NHC)Cl with different alkyl substituents on the two nitrogens (e.g. methyl, ethyl, butyl) are known and then the NMR analysis are incomplete.[9]

---

[33] M.V. Barker, S.K. Brayshaw, B.W. Skelton, A.H. White, *Inorg. Chim. Acta*, 2004, **357**, 2841.

[34] G.R. Julius, *M.Sc. Thesis*, University of Stellenbosch, 2003, p. 65.

[35] A.W. Coleman, P.B. Hitchcock, M.F. Lappert, R.K. Maskell, J.H. Müller, *J. Organomet. Chem.*, 1985, **296**, 173.

Table 3.2 ^{1}H NMR data of complexes **19a** and **19b** in CD_2Cl_2

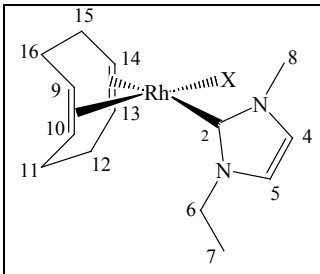

X = Br **19a**
X = Cl **19b**

Assignment	δ / ppm **19a**	δ / ppm **19b**
H^4, H^5	6.89 (2H, m)	6.88 (1H, m), 6.87 (1H, m)
H^{13}, H^{14}	4.99 (2H, m)	4.91 (2H, m)
H^6	4.63 (1H, m), 4.40 (1H, m)	4.64 (1H, m), 4.44 (1H, m)
H^8	4.00 (3H, s)	4.04 (3H, s)
H^9, H^{10}	3.34 (2H, m)	3.32 (1H, m), 3.28 (1H, m)
-HCH-, equatorial, COD	2.35 (4H, m)	2.41 (4H, m)
-HCH-, axial, COD	1.90 (4H, m)	1.94(4H, m)
H^7	1.47 (m)	1.49 (m)

The NMR data of complexes **19a** and **19b** are discussed together. H^{13} and H^{14} shows one multiplet compared to similar protons in complex **18a** where each olefinic proton resonates as a multiplet. The lower field strength than for H^9 and H^{10} is due to the greater *trans*-influence of the carbene ligand when compared to the Cl^- ligand. These assignments were confirmed in the ghsqc NMR spectrum of **19b** where the multiplet for H^{13} and H^{14} was correlated with the two doublets of C^{13} and C^{14} and the signals assigned to $H^9$and H^{10} were correlated with the two doublets assigned to C^9 and C^{10}. The ^{103}Rh - ^{13}C coupling constants for C^{13} and C^{14} ($^1J_{Rh\text{-}C}$ = ca. 7 Hz) are smaller than the ^{103}Rh - ^{13}C coupling constants for C^9 and C^{10} ($^1J_{Rh\text{-}C}$ = ca. 14 Hz) also showing the greater *trans*-influence of the carbene ligand compared to Cl^-. These assignments and coupling constants are similar to those of comparable complexes X(η^4-1,5-cyclooctadiene)(1,3-dimethyl-2,3-dihydro-1*H*-imidazol-2-ylidene)rhodium(I) (X = Cl, Br, I, NCO and N_3).[33] Lappert also reported that a ligand with a greater *trans*-influence is expected to lower the coupling constant.[15] C^{13} and C^{14} thus have more sp^2 character than C^9 and C^{10}, which posess more sp^3 character, because they are more loosely bound to the rhodium atom. Typical olefinic protons and carbons (more sp^2 character) resonate at lower fields than protons and carbons that are more aliphatic in character.[36] Corresponding differences in bond lengths are

[36] B.E. Mann, B.F. Taylor, *^{13}C NMR Data for Organometallic Compounds* (Eds. P.M. Maitlis, F.G.A. Stone, R. West), Academic Press, London, 1981, p 16.

confirmed by crystal structure determinations of (COD)Rh(NHC)Cl complexes reported in literature[18,33] as again in the crystal structure of **21a** (see section 3.2.5.2). The two protons, H^6, are diastereotopic and are observed as two multiplets, similar to H^6 and $H^{6'}$ in complex **18a**. The H^7 protons were observed as a triplet-like multiplet similar to corresponding protons in **18a**.

The aliphatic ring protons of the COD ligand are represented by two miltiplets at δ 2.35 and δ 1.90 in the ^{1}H NMR spectrum of **19a** and at δ 2.41 and δ 1.49 in the spectrum of **19b**. The multiplet at lower field strength was assigned to the four protons (A and A') that are equatorial to the double bond of the COD ligand because these protons are deshielded as a result of the anisotropic effect of the double bond.[37] The axial protons (B and B') are shielded due to the anisotropic effect of the double bond and appear at higher field. The multiplet assigned to the equatorial protons displays greater complexity than the multiplet at higher field, assigned to the axial protons. According to the Karplus-concept, coupling over three bonds is at a maximum when the dihedral angle of the two C-H bonds is 0° or 180°.[38] At these two angles, the overlap of the C-H bond orbitals is at a maximum. When the two C-H bonds are perpendicular to each other, the orbitals of these particular bonds do not overlap, thus there is little or no coupling between the two protons. The dihedral angle between the equatorial protons and the olefinic protons (Q) is approximately 180° (or 0°) in the COD ligand of **19a** and **19b**. The equatorial protons couple with the olefinic protons in addition to coupling with the aliphatic axial protons giving rise to an AA'BB'Q_2 spin system. The probable orientation of these protons can be seen in the crystal structure of complex **21a** (see section 3.2.5.2, the hydrogen atoms in the crystal structure were fixed in calculated positions and these positions were used as a guideline in the interpretation of the NMR spectra). The axial protons are orientated at a dihedral angle of 90° to the olefinic protons and only couple with the equatorial protons, with no or little coupling to the olefinic protons and display a less complicated AA'BB' spin system.

The chemical shifts of the protons in the ^{1}H NMR spectrum of complex **19a** and **19b** are very similar, with the exception of H^4 and H^5. In complex **19a** the signals for H^4 and H^5 resonate together as a multiplet whereas in **19b** these protons are better resolved and appeared as a multiplet each. In a similar fashion, H^9 and H^{10} appear as one multiplet for **19a** but as two multiplets for **19b**.

---

[37] D.L. Pavia, G.M. Lampman, G.S. Kriz, *Introduction to Spectroscopy*, 3rd Edition, Harcourt College Publishers, Fort Worth, 2001, p. 127.

[38] D.L. Pavia, G.M. Lampman, G.S. Kriz, *Introduction to Spectroscopy*, 3rd Edition, Harcourt College Publishers, Fort Worth, 2001, p. 225.

The ^{13}C NMR data of complexes **19a** and **19b** are summarised in Table 3.3. The chemical shifts for the carbene ligand in **19a** and **19b** as well as the aliphatic carbons compare well with the corresponding signals in complex **18a**. The chemical shifts as well as the coupling constants for the doublets assigned to the olefinic carbons of the COD ligand experience the greater *trans*-influence of the carbene ligand (greater *trans*-influence, smaller coupling constant) when compared to the halides (smaller *trans*-influence, larger coupling constant) as discussed above. The resonances for C^6 – C^8 are normal.[35]

Table 3.3 ^{13}C NMR data of complexes **19a** and **19b** in CD_2Cl_2

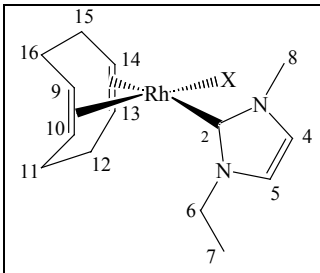

X = Br **19a**
X = Cl **19b**

Assignment	δ / ppm **19a**	δ / ppm **19b**
C^2	182.3 (d, J_{Rh-C} = 50.1 Hz)	182.4 (d, J_{Rh-C} = 50.0 Hz)
C^5, C^4	122.7 (s), 120.0 (s)	122.4 (s), 119.9 (s)
C^{13}, C^{14}	97.8 (d, J_{Rh-C} = 6.5 Hz),	98.3 (d, J_{Rh-C} = 6.1. Hz),
	97.6 (d, J_{Rh-C} = 7.4 Hz)	98.1 (d, J_{Rh-C} = 7.3 Hz)
C^9, C^{10}	69.2 (d, J_{Rh-C} = 11.1 Hz),	68.1 (d, J_{Rh-C} = 14.7 Hz),
	69.0 (d, J_{Rh-C} = 11.1 Hz)	68.0 (d, J_{Rh-C} = 14.7 Hz)
C^6	45.7 (s)	45.8 (s)
C^8	37.8 (s)	37.8 (s)
$-H_2\underline{C}-CH_2-$ (COD)	33.1 (s), 32.9 (s), 29.4 (s), 29.3 (s)	33.3 (s), 33.2 (s), 29.2 (s)
C^7	16.2 (s)	16.5 (s)

The signals in the ^{13}C NMR spectra of **19a** and **19b** are similar. The ^{103}Rh - ^{13}C-coupling constant of the doublets assigned to C^9 and C^{10} is slightly smaller for **19a**. Only three signals are observed for the aliphatic carbons (C^{11}, C^{12}, C^{15} and C^{16}) in **19b** in contrast to the expected four signals that were observed for **19a**. The singlet at δ 29.2 has a greater intensity than the two other singlets (which are of equal intensity) indicating that it represents two chemically equivalent aliphatic carbon atoms. Since intensity of a signal in a ^{13}C NMR spectrum does not necessarily correlate to the number of carbon atoms it represents, therefore, this result was confirmed by two-dimensional ghsqc NMR spectroscopy. The coupling constants for the

doublets that represent C^{13} and C^{14} in **19a** and **19b** are the same, indicating that Br^- and Cl^- exhibit a rather similar *trans*-influence.

*3.2.2.3 Cis-[(η^4-1,5-cyclooctadiene)bis(1-methyl-3-propyl-2,3-dihydro-1**H**-imidazol-2-ylidene)rhodium(I)]bromide, 20a*

The NMR data for complex **20a** are summarised in Table 3.4. The signals in both the ^1H and ^{13}C NMR spectra of **20a** were assigned in the same manner as for complex **18a**. Similar to the spectrum for **18a**, a set of signals is observed for each carbene ligand. C^2 and $C^{2'}$ appear as one doublet in the ^{13}C NMR spectrum. With the *N*-substituent changed from ethyl in complex **18a** to propyl in complex **20a** an extra set of signals is present for the additional CH_2. H^5 and H^4 (as well as $H^{4'}$ and $H^{5'}$) are well resolved. The two protons of one saturated carbon in the COD ligand are assigned to two multiplets, indicating that these two protons are in different chemical environments.

The H^6 and $H^{6'}$ protons (A and A') are diastereotopic and are seen as two multiplets at δ 4.05 and δ 4.31 or δ 4.52 due to geminal coupling as well as further coupling to the diastereotopic H^7 and $H^{7'}$ protons (B and B') respectively that result in a possible AA'BB' spin system for H^6 and $H^{6'}$ each. H^7 and $H^{7'}$ show two multiplets (δ 1.77 – 1.95) and a single sextet-like multiplet (δ 1.75 for 2H) respectively. Geminal coupling of the diastereotopic protons H^7 and $H^{7'}$ followed by coupling to H^6 and $H^{6'}$ and further coupling with the methyl protons, H^8 and $H^{8'}$ (C) can be described as an AA'BB'C_3 spin system. Precise overlap of the resultant higher order signals yields this sextet-like multiplet. The H^8 and $H^{8'}$ protons couple to the diastereotopic H^7 and $H^{7'}$ protons and are the triplet-like multiplets in the spectrum. These multiplets are observed as a result of the overlap of the expected doublet of doublets. Crabtree and co-workers reported the *N*CH_2 protons as diastereotopic in chloro(η^4-1,5-cyclooctadiene)(1,3-dibutyl-2,3-dihydro-1*H*-imidazol-2-ylidene)rhodium(I) but do not mention the rest of the CH_2 protons of the butyl substituent as being diastereotopic as well.[31]

Table 3.4 ^{1}H and ^{13}C NMR data of complex **20a** in CD_2Cl_2

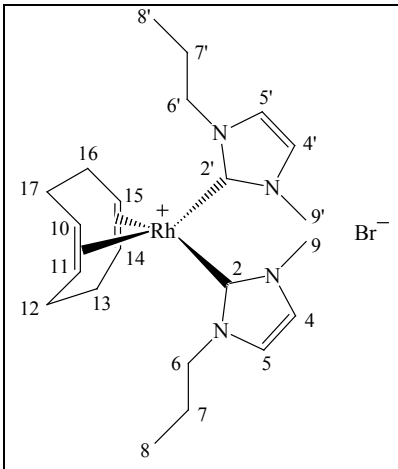

Assignment	δ / ppm	Assignment	δ / ppm
^{1}H NMR		**^{13}C NMR**	
H^4, H^5; $H^{4'}$, $H^{5'}$	7.13 (1H, d, $^3J_{H-H}$ 2.0 Hz),	C^2	180.7 (d, J_{Rh-C} = 53.7 Hz)
	7.05 (1H, d, $^3J_{H-H}$ 1.7 Hz),	C^4, C^5; $C^{4'}$, $C^{5'}$	123.8 (s), 120.9 (s)
	7.11 (1H, d, $^3J_{H-H}$ 1.9 Hz),		123.7 (s), 121.3 (s)
	7.02(1H, d, $^3J_{H-H}$ 2.0 Hz)	-HC=CH- (COD)	90.7 (d, J_{Rh-C} = 7.3 Hz),
H^6, $H^{6'}$	4.52 (1H, m), 4.31 (1H, m), 4.05		89.7 (d, J_{Rh-C} = 7.3 Hz),
	(2H, m)		89.0 (d, J_{Rh-C} = 7.3 Hz),
H^9, $H^{9'}$	4.09 (3H, s), 4.01(3H, s)		88.3 (d, J_{Rh-C} = 8.6 Hz)
-HC=CH- (COD)	4.42 (2H, m), 4.28 (1H, m),	C^6, $C^{6'}$	52.9 (s), 52.8 (s)
	4.05 (1H, m)	C^9, $C^{9'}$	38.8 (s), 38.7 (s)
$-H_2C-CH_2-$ (COD)	2.51 (1H, m), 2.42 (2H, m),	$-H_2C-CH_2-$ (COD)	32.7 (s), 31.2 (s), 31.1 (s),
	2.32 (2H, m), 2.18 (2H, m),		29.6 (s)
	2.06 (1H, m)	C^7, $C^{7'}$	24.4 (s), 24.1 (s)
H^7, $H^{7'}$	1.77 - 1.95 (2H, 2 x m)	C^8, $C^{8'}$	11.4 (s), 11.3 (s)
	1.75 (2H, m),		
H^8, $H^{8'}$	1.05 (3H, t, $^3J_{HH}$ = 7.5 Hz),		
	0.96 (3H, t, $^3J_{HH}$ = 7.4 Hz)		

3.2.2.4 Bromo(η^4-1,5-cyclooctadiene)(1-methyl-3-propyl-2,3-dihydro-1H-imidazol-2-ylidene)rhodium(I), 21a, and chloro(η^4-1,5-cyclooctadiene)(1-methyl-3-propyl-2,3-dihydro-1H-imidazol-2-ylidene)rhodium(I), 21b

The signals in the ^{1}H and ^{13}C NMR spectra (Table 3.5 and 3.6 respectively) of **21a** and **21b** are identical and were assigned similar to those in **19a** and **19b**. The chemical shifts for H^{10} and H^{11} are better resolved than the ones in **19a** and appear as two multiplets. Again, second order

multiplets are observed for H^6, H^7 and H^8 in **21a** and **21b**, due to the presence of diastereotopic protons H^6 and H^7.

Table 3.5 ^{1}H NMR data of complexes **21a** and **21b** in CD_2Cl_2

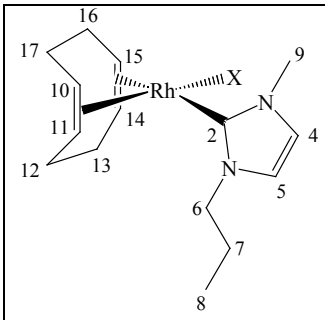

X = Br **21a**
X = Cl **21b**

Assignment	δ / ppm **21a**	δ / ppm **21b**
H^4, H^5	6.88 (2H, m)	6.87 (2H, m)
H^6	4.47 (1H, m), 4.32 (1H, m)	4.48 (1H, m), 4.30 (1H, m)
H^9	4.00 (3H, s)	4.03 (3H, s)
H^{14}, H^{15}	4.99 (2H, m)	4.90 (2H, m)
H^{10}, H^{11}	3.38 (1H, m), 3.30 (1H, m)	3.32 (1H, m), 3.23 (1H, m)
-HCH-, equatorial, COD	2.35 (4H, m)	2.38 (4H, m)
-HCH-, axial, COD	1.75 - 2.08 (4H, m)	2.09 - 1.76 (4H, m)
H^7	1.75 - 2.08 (2H, 2 x m)	2.09 - 1.76 (2H, 2 x m)
H^8	1.01 (3H, m)	1.01 (3H, m)

The olefinic carbons (C^{14} and C^{15}) of **21a** show only one doublet (δ 97.7) in contrast to the other mono(carbene) complexes **19a**, **19b**, **21b**, **23a** and **23b** wherein, however, small (≤ 0.2 ppm) differences are apparent. The ^{103}Rh - ^{13}C coupling constants for the doublets assigned to the olefinic carbons, again reflect the greater *trans*-influence of the carbene ligand compared to Cl^-.

Table 3.6 ^{13}C NMR data of complexes **21a** and **21b** in CD_2Cl_2

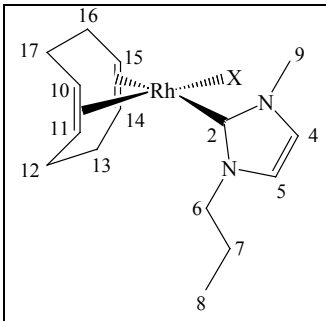

X = Br **21a**
X = Cl **21b**

Assignment	δ / ppm **21a**	δ / ppm **21b**
C^2	182.7 (d, J_{Rh-C} = 50.2 Hz)	182.8 (d, J_{Rh-C} = 50.8 Hz)
C^5, C^4	122.6 (s), 120.7 (s)	122.3 (s), 120.6 (s)
C^{14}, C^{15}	97.7 (d, J_{Rh-C} = 6.7. Hz)	98.3 (d, J_{Rh-C} = 7.1 Hz), 98.2 (d, J_{Rh-C} = 7.0 Hz)
C^{10}, C^{11}	69.4 (d, J_{Rh-C} = 14.7 Hz), 68.8 (d, J_{Rh-C} = 14.1 Hz)	68.4 (d, J_{Rh-C} = 14.9 Hz), 67.8 (d, J_{Rh-C} = 14.8 Hz)
C^6	52.6 (s)	52.6 (s)
C^9	37.9 (s)	37.9 (s)
$-H_2\underline{C}-CH_2-$ (COD)	33.2 (s), 32.6 (s), 29.6 (s), 29.1 (s)	33.4 (s), 32.9 (s), 29.3 (s), 28.9 (s)
C^7	24.3 (s)	24.5 (s)
C^8	11.4 (s)	11.4 (s)

3.2.2.5 Cis-[(η^4-1,5-cyclooctadiene)bis(1-butyl-3-methyl-2,3-dihydro-1H-imidazol-2-ylidene) rhodium(I)]bromide, 22a

The assignment of the signals in the ^1H and ^{13}C NMR spectra of **22a** was carried out in the same way as for **18a**. Two sets of signals for the chemically different carbene ligands in **22a** are found (Table 3.7) as in compounds **18a** and **20a**. No unexpected changes in the chemical shifts are obvious. The CH_2 protons of the butyl substituents are diastereotopic and appear as higher order multiplets as the CH_2 protons in **20a - 21b**. The diastereotopic protons of H^7 and $H^{7'}$ couple to their neighbouring diastereotopic protons H^6, H^8 and $H^{6'}$, $H^{8'}$ respectively and show two multiplets. H^8 and $H^{8'}$ exhibit two multiplets representing an AA'BB'C_3 spin system as obtained for H^7 and $H^{7'}$ in **20a**. Triplet-like multiplets are assigned to H^9 and $H^{9'}$ in the same fashion as was done for H^8 and $H^{8'}$ in **20a - 21b** and H^7 and $H^{7'}$ in **18a - 19b**. The two protons of one aliphatic carbon are in chemically different environments and exhibit two separate chemical shifts (multiplets) in the ^1H NMR spectrum of **22a**, which is similar to the situation in complex **20a**.

Table 3.7 ^{1}H and ^{13}C NMR data of complex **22a** in CD_2Cl_2

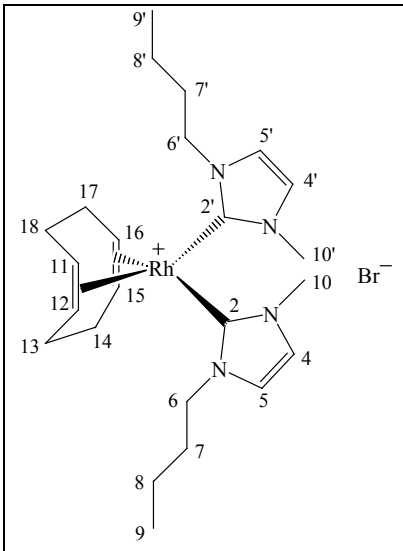

Assignment	δ / ppm	Assignment	δ / ppm
^{1}H NMR		**^{13}C NMR**	
H^4, H^5, $H^{4'}$, $H^{5'}$	7.02 (2H, m), 7.13 (2H, m)	C^2, $C^{2'}$	180.5 (d, J_{Rh-C} = 53.7 Hz),
H^6, $H^{6'}$	4.63 (1H, m), 4.44 (1H, m),		180.5 (d, J_{Rh-C} = 53.7 Hz)
	4.06 (1H, m), 4.01 (1H, m)	C^4, C^5, $C^{4'}$, $C^{5'}$	123.6 (s), 121.2 (s),
H^{10}, $H^{10'}$	4.08 (3H, s), 4.03 (3H, s)		123.9 (s), 120.9 (s)
-HC=CH- (COD)	4.39 (1H, m), 4.29 (1H, m),	-HC=CH- (COD)	90.2 (d, J_{Rh-C} = 7.4 Hz),
	4.23 (1H, m), 4.13 1H, m)		89.6 (d, J_{Rh-C} = 8.6 Hz),
$-H_2C-CH_2-$ (COD)	2.47 (2H, m), 2.37 (2H, m),		88.8 (d, J_{Rh-C} = 7.3 Hz),
	2.28 (1H, m), 2.11 (1H, m)		88.4 (d, J_{Rh-C} = 8.6 Hz)
H^7, $H^{7'}$	1.64 – 1.92 (1H, m; 3H, m)	C^6, $C^{6'}$	51.2 (s)
H^8, $H^{8'}$	1.36 – 1.54 (4H, 2 x m)	C^{10}, $C^{10'}$	38.9 (s), 38.7 (s)
H^9, $H^{9'}$	1.04 (3H, m),	C^7, $C^{7'}$	33.0 (s), 33.1 (s)
	1.00 (3H, m)	$-H_2C-CH_2-$ (COD)	32.2 (s), 31.2 (s), 31.1 (s),
			30.0 (s)
		C^8, $C^{8'}$	20.5 (s), 20.4 (s)
		C^9, $C^{9'}$	13.9 (s), 13.8 (s)

In similar fashion as to complex **18a** the two carbene carbons of **22a** resonate separately as a doublet each (both at δ 180.5) with the chemical shifts and coupling constants that are indistinguishable from the corresponding signals for **18a** and **20a**. The chemical shifts of the singlets assigned to C^4, C^5, $C^{4'}$ and $C^{5'}$ are normal. Four signals for the non-equivalent olefinic carbons (C^{11}, C^{12}, C^{15} and C^{16}) and aliphatic carbons (C^{13}, C^{14}, C^{17} and C^{18}) are observed for

22a, in the same fashion as for **18a** and **20a**. The ^{103}Rh-^{13}C coupling for the olefinic carbons were the same because of the same type of carbene ligand that is coordinated *trans* to these carbons. C^6 and $C^{6'}$ resonate as one singlet at δ 51.16 and this is confirmed by the two-dimensional ghsqc NMR spectrum of **22a**. The signals for both sets of butyl carbons appear where expected.

*3.2.2.6 Bromo(η^4-1,5-cyclooctadiene)(1-butyl-3-methyl-2,3-dihydro-1*H*-imidazol-2-ylidene) rhodium(I), 23a, and chloro(η^4-1,5-cyclooctadiene)(1-butyl-3-methyl-2,3-dihydro-1*H*-imidazol-2-ylidene)rhodium(I), 23b*

The very nearly indistinguishable NMR data for complexes **23a** and **23b** are summarised in Table 3.8 and Table 3.9. The assignment of the signals observed in the ^{1}H NMR spectrum for the carbene ligand was done similarly as for complex **20a** and **22a** and was substantiated by the ghsqc NMR spectrum of complex **23b**. The rest of the signals in the ^{1}H and ^{13}C NMR spectra can be assigned using the same principles as for compounds **19a** and **19b**. The NCH_2 protons are diastereotopic in keeping with all the complexes reported in this chapter and appear as two multiplets in the ^{1}H NMR spectra of **23a** and **23b**. Second order multiplets are further assigned to the diastereotopic H^7 and H^8 as well as to H^9 in similar manner to the spectrum of complex **22a**. The olefinic protons H^{15} and H^{16} resonate together as a multiplet while the other olefinic protons H^{11} and H^{12} appear as a muliplet each. This is consistent with the corresponding signals for complexes **19a**, **19b**, **21a** and **21b**.

Table 3.8 ^{1}H NMR data of complexes **23a** and **23b** in CD_2Cl_2

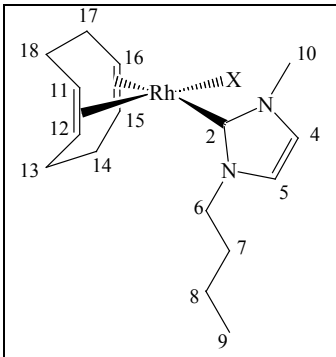

X = Br **23a**
X = Cl **23b**

Assignment	δ / ppm **23a**	δ / ppm **23b**
H^4, H^5	6.87 (2H, m)	6.86 (2H, m)
H^6	4.48 (1H, m), 4.40 (1H, m)	4.50 (1H, m), 4.43 (1H, m)
H^{10}	4.00 (3H, s)	4.03 (3H, s)
H^{15}, H^{16}	4.99 (2H, m)	4.91 (2H, m)
H^{11}, H^{12}	3.40 (1H, m), 3.30 (1H, m)	3.34 (1H, m), 3.25 (1H, m)
-HCH-, equatorial, COD	2.38 (4H, m)	2.40 (4H, m)
-HCH-, axial, COD	1.95 (4H, m)	1.90 (4H, m)
H^7	1.82 (2H, m)	1.90 (2H, m)
H^8	1.47 (2H, m)	1.47 (2H, m)
H^9	1.03 (3H, m)	1.03 (3H, m)

The chemical shifts and coupling constants of the carbene signals are normal. The olefinic carbons (C^{15} and C^{16}) resonate at lower field with smaller ^{103}Rh - ^{13}C coupling when compared to the other two olefinic carbons (C^{11} and C^{12}). This is typical for these complexes due to the larger *trans*-influence of the carbene ligand when compared to the halides, as discussed for complexes **19a** and **19b**. The four singlets assigned to the aliphatic COD carbons indicate that each carbon is in a different chemical environment.

Table 3.9 ^{13}C NMR data of complexes **23a** and **23b** in CD_2Cl_2

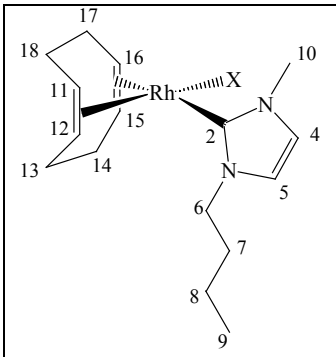

X = Br **23a**
X = Cl **23b**

Assignment	δ / ppm **23a**	δ / ppm **23b**
C^2	182.1 (d, J_{Rh-C} = 50.0 Hz)	182.5 (d, J_{Rh-C} = 50.0 Hz)
C^5, C^4	122.3 (s), 120.4 (s)	122.2 (s), 120.4 (s)
C^{15}, C^{16}	97.6 (d, J_{Rh-C} = 7.3 Hz),	98.2 (d, J_{Rh-C} = 7.3 Hz),
	97.4 (d, J_{Rh-C} = 6.1 Hz)	98.0 (d, J_{Rh-C} = 7.4 Hz)
C^{11}, C^{12}	69.4 (d, J_{Rh-C} = 14.6 Hz),	68.4 (d, J_{Rh-C} = 14.6 Hz),
	68.6 (d, J_{Rh-C} = 14.7 Hz)	67.6 (d, J_{Rh-C} = 14.7 Hz)
C^6	50.6 (s)	50.7 (s)
C^{10}	37.9 (s)	37.9 (s)
C^7	33.1 (s)	33.3 (s)
-H_2C-CH_2- (COD)	33.4 (s), 32.5 (s), 29.7 (s), 29.0 (s)	33.6 (s), 32.8 (s), 29.5 (s), 28.8 (s)
C^8	20.4 (s)	20.4 (s)
C^9	13.9 (s)	13.9 (s)

Pectora roborant cultus recti

Mass spectrometry

The FAB-MS data for the bis(carbene) complexes (**18a**, **20a**, and **22a**) appear in Table 3.10. All of these complexes display the same fragmentation pattern. The cation is observed as the base peak. The loss of the COD ligand is followed by the loss of one of the carbene ligands.

Table 3.10 Mass spectrometry data for complexes **18a, 20a** and **22a**

Complex	m/z	Relative intensity (%)	Fragment ion
18a	431	100	$[M - Br]^+$
	323	17	$[M - Br - COD]^+$
	213	7	$[Rh\{=\overline{CN(Me)CH=CHN}(Et)\}]^+$
	111	22	$[EMIM]^+$
20a	459	100	$[M - Br]^+$
	347	19	$[M - Br - COD]^+$
	225	13	$[Rh\{=\overline{CN(Me)CH=CHN}(Pr)\}]^+$
	125	14	$[PMIM]^+$
22a	487	100	$[M - Br]^+$
	377	14	$[M - Br - COD]^+$
	239	21	$[Rh\{=\overline{CN(Me)CH=CHN}(Bu)\}]^+$
	139	17	$[BMIM]^+$

The fragmentation patterns for the mono(carbene) complexes (**19a**, **19b**, **21a**, **21b**, **23a** and **23b**), shown in Table 3.11 are exactly the same. The molecular ion is observed, followed by the loss of the halide (Br or Cl). The third fragment forms after the loss of a COD ligand. The carbene ligand fragment forms the base peak.

Table 3.11 Mass spectrometry data for complexes **19a, 19b, 21a, 21b, 23a** and **23b**

Complex	m/z	Relative intensity (%)	Fragment ion
19a	400	33	M^+
	321	46	$[M - Br]^+$
	212	11	$[M - Br - COD]^+$
	111	100	$[EMIM]^+$
19b	356	22	M^+
	321	59	$[M - Cl]^+$
	207	10	$[M - Cl - COD]^+$
	111	100	$[EMIM]^+$
21a	414	17	M^+
	335	31	$[M - Br]^+$
	224	15	$[M - Br - COD]^+$
	125	100	$[PMIM]^+$
21b	370	22	M^+
	335	50	$[M - Cl]^+$
	225	48	$[M - Cl - COD]^+$
	125	100	$[PMIM]^+$
23a	428	21	M^+
	349	39	$[M - Br]^+$
	239	40	$[M - Br - COD]^+$
	139	100	$[BMIM]^+$
23b	384	19	M^+
	349	39	$[M - Cl]^+$
	239	52	$[M - Cl - COD]^+$
	139	100	$[BMIM]^+$

3.2.3 Synthesis of complexes 24a, 24b, 25a and 25b

Complexes **24a** and **24b** were prepared by bubbling CO gas through a CH_2Cl_2 solution of **19a** and **19b** respectively (Scheme 3.3). These two complexes were separated from $[Rh(X)COD]_2$ (X = Cl or Br], which formed during the reaction, on a short flash silica column. Complexes **24a** and **24b** could not be obtained pure as they both contained an unknown compound **III** (observed by NMR spectroscopy).

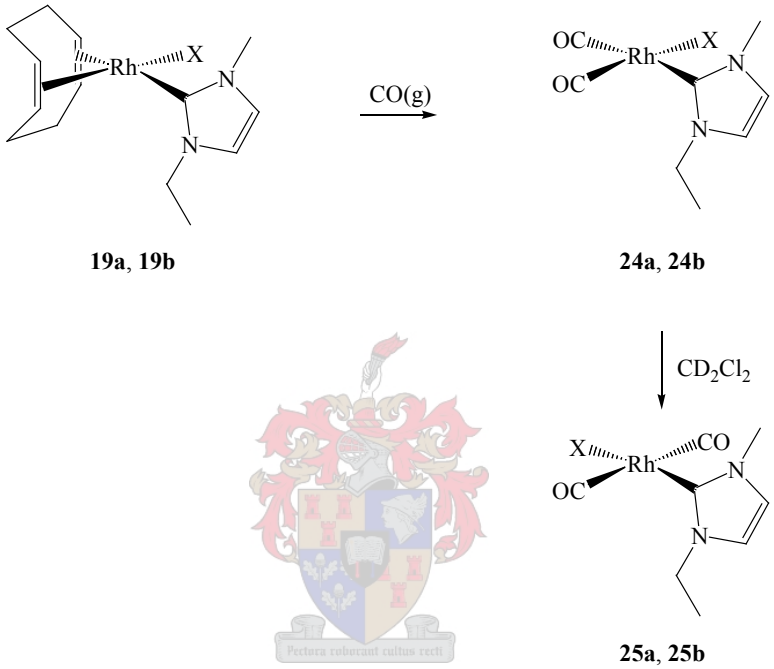

Scheme 3.3 (a: X = Br, b: X = Cl)

Complexes **25a** and **25b** irreversibly formed spontaneously in solution as a result of the rearrangement of the CO-substituted complexes **24a** and **24b** respectively. Isomerisation of **24a** is much faster than that of **24b**, probably because Br^- ligand is a better leaving group than Cl^- ligand. It is not certain at this point whether the isomerisation proceed *via* the associative or dissosiative mechanism. The lack of steric crowding of the rhodium and the availability of an empty *p* orbital perpendicular to the molecular plane may favour the associative mechanism.[39]

These complexes are soluble in polar solvents (dichloromethane and acetone) and not soluble in non-polar solvents (pentane and hexane).

---

[39] B.E. Douglas, D.H. McDaniel, J.J. Alexander, *Concepts and Models for Inorganic Chemistry*, 2nd Edition, Wiley & Sons, New York, 1983, p 74.

3.2.4 Spectroscopic characterisation of complexes 24a, 24b, 25a and 25b

NMR spectroscopy

*3.2.4.1 Cis-bromo(dicarbonyl)(1-ethyl-3-methyl-2,3-dihydro-1*H*-imidazol-2-ylidene) rhodium(I), 24a, and cis-chloro(dicarbonyl)(1-ethyl-3-methyl-2,3-dihydro-1*H*-imidazol-2-ylidene)rhodium(I), 24b*

As expected the ^{1}H and ^{13}C NMR data for the two complexes are similar (Table 3.12) since the NMR data of the parent analogues **19a** and **19b** do not differ very much. The signals for H^5 and H^4 appear slightly downfield and H^7 and H^8 slightly upfield in the ^{1}H NMR spectra of both **24a** and **24b** when compared to the chemical shifts of these signals in **19a** and **19b**. Compounds **24a** and **24b** show as a multiplet and a quartet (due to coupling with H^7) for protons H^6 respectively, indicating that these protons are not diastereotopic as they were in **19a** and **19b**. This occurrence could be attributed to the fact that the CO ligands do not impose the same sterical influence on these protons as the COD ligand does in **19a** and **19b**.

C^9 resonates as a doublet at δ ~187 and C^{10} at δ ~183 in the ^{13}C NMR spectra of **24a** and **24b**. This assignment is based on the difference in *trans*-influence of the carbene ligand and the halides (Cl and Br). The carbene ligand has a greater *trans*-influence than the halides and the ^{103}Rh - ^{13}C coupling constant for the doublet assigned to C^9 (J_{Rh-C} = 54 Hz) should be smaller than that for the doublet assigned to C^{10} (J_{Rh-C} = 75 Hz). The doublets at δ ca. 174 (J_{Rh-C} = 43 Hz) belong to the carbene atom C^2. C^2 appears upfield (Δδ = 8) compared to C^2 in both **19a** and **19b** and the coupling constant for the ^{103}Rh - ^{13}C coupling is 7 Hz smaller than for C^2 in **19a** and **19b** (J_{Rh-C} ~ 50 Hz). This atom has a smaller coupling constant now because CO has a greater *trans*-influence than the carbene ligand and an even greater *trans*-influence than the halides. These assignments and chemical shifts are consistent with those recently reported by the group of Crabtree.[19] These chemical shifts and coupling constants also compare well with those for chloro(dicarbonyl)(1,3-diisopropyl-4,5-dimethyl-2,3-dihydro-1*H*-imidazol-2-ylidene)rhodium(I)[17] and those (except for the carbene signal) for chloro(dicarbonyl){(*tert*-butyl)bis(diisopropylamino)ylidene}rhodium(I).[40] Herrmann, however, reports only one doublet

[40] V. Lavallo, J. Mafhouz, Y. Canac, B. Donnadieu, W.W. Schoeller, G. Bertrand, *J. Am. Chem. Soc.*, 2004, **126**, 8670.

(J_{Rh-C} ~ 75 Hz) for both the carbonyl carbons in chloro(dicarbonyl)(1,3-dimethyl-2,3-dihydro-1*H*-imidazol-2-ylidene)rhodium(I).[18]

Table 3.12 ^{1}H and ^{13}C NMR data of complexes **24a** and **24b** in CD_2Cl_2

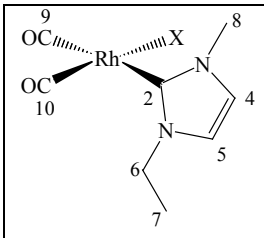

X = Br **24a**
X = Cl **24b**

Assignment	δ / ppm **24a**	δ / ppm **24b**
^{1}H NMR		
H^4, H^5	7.05 (1H, d, $^{3}J_{HH}$ = 1.9 Hz),	7.04 (1H, d, $^{3}J_{HH}$ = 1.9 Hz),
	7.01 (1H, d, $^{3}J_{HH}$ = 1.8 Hz)	7.01 (1H, d, $^{3}J_{HH}$ = 1.9 Hz)
H^6	4.28 (2H, m)	4.31 (2H, q, $^{3}J_{HH}$ = 7.3 Hz)
H^8	3.83 (3H, s)	3.87 (3H, s)
H^7	1.43 (3H, t, $^{3}J_{HH}$ = 7.4 Hz)	1.44 (3H, t, $^{3}J_{HH}$ = 7.4 Hz)
^{13}C NMR		
C^9	187.1 (d, J_{Rh-C} = 53.7 Hz)	186.6 (d, J_{Rh-C} = 53.7 Hz)
C^{10}	182.1 (d, J_{Rh-C} = 76.3 Hz)	183.4 (d, J_{Rh-C} = 74.1 Hz)
C^2	173.2 (d, J_{Rh-C} = 42.3 Hz)	174.2 (d, J_{Rh-C} = 43.1 Hz)
C^5, C^4	123.6 (s), 121.3 (s)	123.4 (s), 121.2 (s)
C^6	46.4	46.5 (s)
C^8	38.6	38.5 (s)
C^7	16.0	16.3 (s)

*3.2.4.2 Trans-bromo(1-ethyl-3-methyl-2,3-dihydro-1*H*-imidazol-2-ylidene)-trans-(dicarbonyl)rhodium(I), 25a, and trans-chloro(1-ethyl-3-methyl-2,3-dihydro-1*H*-imidazol-2-ylidene)-trans-(dicarbonyl)rhodium(I), 25b*

The NMR data of complexes **25a** and **25b** are very similar (Table 3.13). In the ^{1}H NMR spectrum of **25a** and **25b**, H^4 and H^5 are observed as one multiplet, whereas the signals, due to these protons, are well resolved in the spectra of **24a** and **24b**. H^6 and H^8 in both **25a** and **25b** resonate somewhat downfield (Δδ 0.36, Δδ 0.24 respectively) compared to the same protons in **24a** and **24b.**

Table 3.13 ^{1}H and ^{13}C NMR data of complexes **25a** and **25b** in CD_2Cl_2

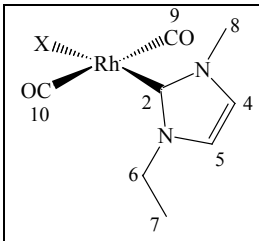

X = Br **25a**
X = Cl **25b**

Assignment	δ / ppm **25a**	δ / ppm **25b**
^{1}H NMR		
H^4, H^5	7.03 (2H, m)	7.01 (2H, m)
H^6	4.66 (2H, q, $^{3}J_{HH}$ = 7.3 Hz)	4.65 (2H, q, $^{3}J_{HH}$ = 7.3 Hz)
H^8	4.08 (3H, s)	4.09 (3H, s)
H^7	1.52 (3H, t, $^{3}J_{HH}$ = 7.3 Hz)	1.53 (3H, t, $^{3}J_{HH}$ = 7.3 Hz)
^{13}C NMR		
C^2	185.4 (d, J_{Rh-C} = 86.9 Hz)	185.4 (d, J_{Rh-C} = 86.2 Hz)
C^9, C^{10}	172.1 (d, J_{Rh-C} = 58.6 Hz)	170.9 (d, J_{Rh-C} = 60.0 Hz)
C^5, C^4	122.9 (s), 120.7 (s)	122.9 (s), 120.7 (s)
C^6	46.3 (s)	46.4 (s)
C^8	38.7 (s)	38.7 (s)
C^7	16.2 (s)	16.4 (s)

Doublets at δ 185.4 are due to the carbene carbons of **25a** and **25b**. C^2 in the spectrum of **25a** appears downfield by 13.1 ppm compared to the chemical shift of C^2 in **24a** with the rhodium-carbon coupling constant of 44.6 Hz larger than the same coupling in **24a**. The signal for C^2 in **25b** is shifted downfield by 11.2 ppm and the coupling constant for the rhodium-carbon coupling is 43.9 Hz, larger than that of C^2 in **24b**. The coupling constants are larger because the carbene ligand is located *trans* to the halide (in **24a** and **24b** the carbene ligand is located *trans* to a CO ligand) and halides have a much smaller *trans*-influence than the CO ligand. Only one signal is observed for the carbonyl carbons in the ^{13}C NMR spectra of **25a** and **25b** at δ 172.1 (J_{Rh-C} = 58.6 Hz) and 170.9 (J_{Rh-C} = 60.0 Hz) respectively. The CO ligands are now in the same chemical environment and because of their greater *trans*-influence have a smaller rhodium-carbon coupling constant. These signals appear upfield compared to the two signals observed for both **24a** and **24b**. This information together with the one ν(CO) absorption band observed in the IR-spectra of these complexes (Table 3.16) support the postulated structures of **25a** and **25b**. The resonances of the other signals in the ^{13}C NMR spectrum of **25a** and **25b** compare well with those of **24a** and **24b**.

A set of signals of an unknown compound **III**, were observed in the spectra of **24a**, **24b**, **25a** and **25b**. The concentration of this complex is very low and the signals do not change when **24a** converts to **25a** and **24b** to **25b**. As a result of the low concentration of **III**, not all its chemical shifts were clearly observed in the ^{13}C NMR spectrum but the observed signals correspond to those of a carbene ligand. No other information could be obtained. The NMR data for **III** are reported in the experimental section 3.4.9.

Mass spectrometry

The general fragmentation patterns for complexes **24a**, **24b** and **25b** are illustrated in Table 3.14. The loss of the halide is followed by the sequential loss of the two CO ligands. A second fragmentation pattern is observed for complex **24a** where the sequential loss of two CO ligands and Br are indicated. Recombination of fragments occurs in the mass spectrometer and the $[(CO)_2Rh\{=\overline{CN(Me)CH=CHN}(Et)\}_2]^+$ fragment forms when the MS spectra of **24a** and **25b** are recorded. The fragmentation pattern of this fragment is characterised by the sequential loss of the CO ligands. Despite several attempts, no FAB-MS data could be obtained for complex **25a** possibly due to decomposition of the complex.

Pectora roborant cultus recti

Table 3.14 Mass spectrometry data for complexes **24a** - **25b**

Complex	m/z	Relative intensity (%)	Fragment ion
24a	269	13	$[M - Br]^+$
	241	9	$[M - Br - CO]^+$
	213	15	$[M - Br - 2CO]^+$
	111	100	$[EMIM]^+$
	320	5	$[M - CO]^+$
	292	4	$[M - 2CO]^+$
	213	15	$[M - 2CO - Br]^+$
	111	100	$[EMIM]^+$
	379	14	$[(CO)_2Rh\{=\overline{CN(Me)CH=CHN(Et)}\}_2]^+$
	351	9	$[(CO)Rh\{=\overline{CN(Me)CH=CHN(Et)}\}_2]^+$
	323	5	$[Rh\{=\overline{CN(Me)CH=CHN(Et)}\}_2]^+$
24b	269	21	$[M - Cl]^+$
	241	10	$[M - Cl - CO]^+$
	213	12	$[M - Cl - 2CO]^+$
	111	23	$[EMIM]^+$
25b	269	44	$[M - Cl]^+$
	241	30	$[M - Cl - CO]^+$
	213	52	$[M - Cl - 2CO]^+$
	111	100	$[EMIM]^+$
	379	83	$[(CO)_2Rh\{=\overline{CN(Me)CH=CHN(Et)}\}_2]^+$
	351	41	$[(CO)Rh\{=\overline{CN(Me)CH=CHN(Et)}\}_2]^+$
	323	18	$[Rh\{=\overline{CN(Me)CH=CHN(Et)}\}_2]^+$

Infrared spectroscopy

Two bands in the infrared spectra of **24a** and **24b** (Table 3.15) are observed as expected for the two CO ligands because they are not chemically equivalent. The vibration frequencies of these bands are determined by the σ-donation and π-acceptor ability of the carbene ligand. A very 'basic' carbene ligand is characterised by strong σ-donation of the carbon to the metal while

little π-back-donation from the metal to the ligand takes place.[40,41] Thus a very basic ligand (carbene ligand in our case) would effect a low wave number of the CO-stretching frequencies. The infrared stretching frequencies for the CO ligands in chloro(dicarbonyl)(1,3-diisopropyl-4,5-dimethyl-2,3-dihydro-1*H*-imidazol-2-ylidene)rhodium(I), (**A**),[17] chloro(dicarbonyl)(1,3-methyl-2,3-dihydro-1*H*-imidazol-2-ylidene)rhodium(I), (**B**),[18] and chloro(dicarbonyl)[(*tert*-butyl)bis(diisopropylamino)ylidene)rhodium(I), (**C**),[40] are also listed in Table 3.15. It is clear from this data that the basicity (and thus bonding characteristics) of the carbene ligands in **24a**, **24b**, **A** and **B** are comparable while the carbene ligand in **C** is more basic than these four carbene ligands. As mentioned in Chapter 1, the carbene ligand in **C**, the most basic carbene ligand, induces higher electron density at the metal center and thus results in lower ν(CO) frequencies.

Table 3.15 The infrared data of complexes **24a** and **24b** in CH_2Cl_2

Complex	ν(CO) / cm^{-1}	
24a	2079 (s)	2000 (s)
24b	2081 (s)	2000 (s)
A	2076 (s)	1996 (s)
B	2076 (s)	2006 (s)
C	2057 (s)	1984 (s)

The CO ligands are in the *trans* positions in **25a** and **25b** and only one band is observed (Table 3.16). These very strong π-acceptor CO ligands are mutually removing electron density from the metal into their π*-orbitals, lowering the C-O bond orders and consequently the CO-stretching frequencies.

[41] K. Denk, P. Sirch, W.A. Herrmann, *J. Organomet. Chem.*, 2002, **649**, 219.

Table 3.16 The infrared data of complexes **25a** and **25b** in CH_2Cl_2

Complex	ν(CO) / cm^{-1}
25a	1957 (s)
25b	1958 (s)

3.2.5 Crystal and molecular structure determinations by single crystal X-ray diffraction

Crystallisation of cis-[(η^4-1,5-cyclooctadiene)bis(1-ethyl-3-methyl-2,3-dihydro-1*H*-imidazol-2-ylidene)rhodium(I)] bromide, **18a**, and cis-[(η^4-1,5-cyclooctadiene)bis(1-butyl-3-methyl-2,3-dihydro-1*H*-imidazol-2-ylidene)rhodium(I)] bromide, **22a,** from CH_2Cl_2/pentane solutions (-20°C) produced yellow crystals suitable for single crystal X-ray determination. Single crystals of bromo(η^4-1,5-cyclooctadiene)(1-methyl-3-propyl-2,3-dihydro-1*H*-imidazol-2-ylidene)rhodium(I), **21a** were obtained when diethyl ether was slowly removed, under reduced pressure, from the fraction containing **21a**, after column chromatography. The hydrogen atoms, counter ions and the solvent molecules are omitted from the Figures 3.1 and 3.5 for clarity (except the hydrogen atoms of compound **21a** in Figure 3.3). Hydrogen atoms are also not shown in the packing diagrams of the complexes in Figures 3.2, 3.4 and 3.6. There are no short intermolecular contacts in the unit cells of **18a**, **21a** and **22a**. The molecules in the crystal lattice are organised by Van der Waals forces.

Pectora roborant cultus recti

*3.2.5.1 The crystal and molecular structure of cis-[(η^4-1,5-cyclooctadiene)bis(1-ethyl-3-methyl-2,3-dihydro-1*H*-imidazol-2-ylidene)rhodium(I)]bromide,* ***18a***

Figure 3.1 shows one of the two independent molecules in the unit cell of **18a**. The two carbene ligands are orientated in such a way that the ethyl groups are pointing in the same direction with their methyl groups bent towards each other. The ethyl groups in the other independent molecule are also on the same side, but one ethyl group is pointing away from the other carbene ligand. This difference between the two independent molecules is illustrated by the torsion angles C(11)-N(11)-C(14)-C(15) [126.0(8)°] and C(21)-N(21)-C(24)-C(25) [-122.3(9)°] in the molecule depicted here and C(41)-N(41)-C(44)-C(45) [114.6(8)°] and C(51)-N(51)-C(54)-C(55) [115.2(10)°] for the other independent molecule. The dihedral angles of the independent molecules differ significantly. Deviations from the least square planes through the carbene ligands are smaller [0.001(1) - 0.017(6) and 0.003(6) - 0.014(6) Å] in the independent molecule

shown in Figure 3.1 than the other independent molecule of **18a** [0.087(7) - 0.680(7) and 0.062(7) - 0.641(9) Å]. The bond lengths and angles of the two independent molecules are the same and only those of one are listed in Table 3.17.

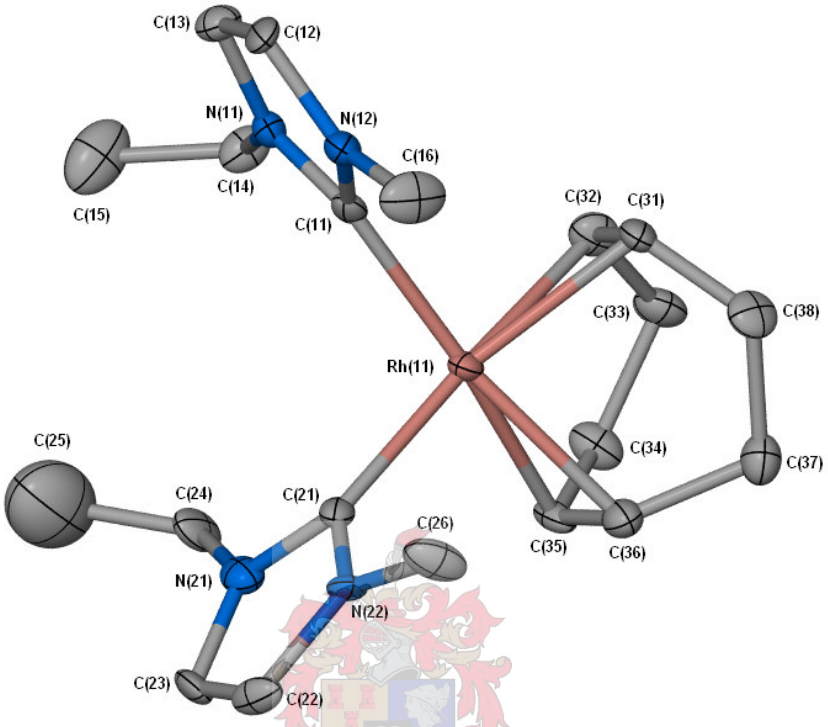

Figure 3.1 Molecular structure of **18a**, showing the numbering scheme, generated in POV-Ray

The molecular structure of **18a** compares well with that of *cis*-[(η^4-1,5-cyclooctadiene)bis(1,3-dimethyl-2,3-dihydro-1*H*-imidazol-2-ylidene)rhodium(I)] chloride, (**D**),[18] and *cis*-[(η^4-1,5-cyclooctadiene)bis(1,3,4,5-tetramethyl-2,3-dihydro-1*H*-imidazol-2-ylidene)rhodium(I)] chloride, (**E**).[17] The rhodium atom resides in a square planar environment defined by the carbene carbons [C(11) and C(21)] and the two centres of the two COD double bonds. The Rh-$C_{carbene}$ bond lengths [2.046(7) and 2.054(8) Å] do not differ significantly from those of one independent molecule of **D** [2.053(8) and 2.059(8) Å] and with those in **E** [2.059(4) and 2.051(4) Å]. The C(11)-Rh(11)-C(21) angle of 96.1(3)° in **18a** compares well with the corresponding angle in **D** [94.4(3)°] but is significantly larger than the same angle in **E** [88.43(13)°]. No apparent reason for the difference in these angles could be found. The carbene ligands are not orientated perpendicular to the square coordination plane of the rhodium atom. The torsion angles C(21)-Rh(11)-C(11)-N(12) [85.9(7)°] and C(11)-Rh(11)-C(21)-N(22) [-102.0(7)°] illustrate that the carbene ligands are bent away from the ideal 90° because of the close proximity of the ethyl substituents of each other. As two carbene ligands are located *trans* to the COD ligand the Rh-

COD distances are not expected to differ. The Rh-COD distances do not differ significantly from the corresponding bonds in **D** and **E**.

Table 3.17 Selected bond lengths (Å) and angles (°) of one of the two independent molecules in the asymmetric unit of **18a**

Rh(11)-C(11)	2.046(7)	N(12)-C(16)	1.454(10)
Rh(11)-C(21)	2.054(8)	N(11)-C(14)	1.476(9)
Rh(11)-C(31)	2.170(7)	C(14)-C(15)	1.514(12)
Rh(11)-C(32)	2.187(8)	C(21)-N(21)	1.357(9)
Rh(11)-C(35)	2.193(8)	C(21)-N(22)	1.358(9)
Rh(11)-C(36)	2.192(8)	N(22)-C(22)	1.404(9)
C(11)-N(11)	1.370(9)	N(21)-C(23)	1.377(9)
C(11)-N(12)	1.353(10)	C(22)-C(23)	1.338(11)
N(12)-C(12)	1.384(9)	N(22)-C(26)	1.463(10)
N(11)-C(13)	1.382(9)	N(21)-C(24)	1.458(10)
C(12)-C(13)	1.334(11)	C(24)-C(25)	1.496(15)
C(11)-Rh(11)-C(21)	96.1(3)	C(11)-N(12)-C(12)	112.3(7)
C(11)-Rh(11)-C(31)	88.2(3)	C(11)-N(12)-C(16)	123.4(6)
C(11)-Rh(11)-C(32)	91.2(3)	C(11)-N(11)-C(14)	125.1(6)
C(21)-Rh(11)-C(35)	87.0(3)	N(11)-C(14)-C(15)	111.0(7)
C(21)-Rh(11)-C(36)	88.4(3)	N(21)-C(21)-N(22)	104.2(6)
C(31)-Rh(11)-C(36)	81.5(3)	C(21)-N(21)-C(23)	111.6(7)
C(32)-Rh(11)-C(35)	81.6(3)	N(21)-C(23)-C(22)	107.2(7)
N(11)-C(11)-N(12)	103.0(6)	N(22)-C(22)-C(23)	106.5(7)
C(11)-N(11)-C(13)	111.1(6)	C(21)-N(22)-C(22)	110.6(6)
N(11)-C(13)-C(12)	107.3(7)	C(21)-N(22)-C(26)	125.7(6)
N(12)-C(12)-C(13)	106.3(7)	C(21)-N(21)-C(24)	124.2(6)
		N(21)-C(24)-C(25)	114.5(9)

Pectora roborant cultus recti

The packing of the molecules of **18a** in the unit cell viewed along the a-axis (A) and c-axis (B) is shown in Figure 3.2. The two independent molecules in the asymmetric unit are stacked in pairs on top of each other, along the a-axis. Layers of molecules parallel to the b-axis are formed with the molecules orientated in such a way that the COD ligand points in one direction in one layer and the opposite direction in the following layer. The view along the c-axis in Figure 3.2 (B) shows the orientation of the COD ligands and also that they are situated on top of each other.

The bromide counter ions and CH_2Cl_2 solvent molecules are located in the cavities formed as a result of the packing of the cations in the unit cell (B).

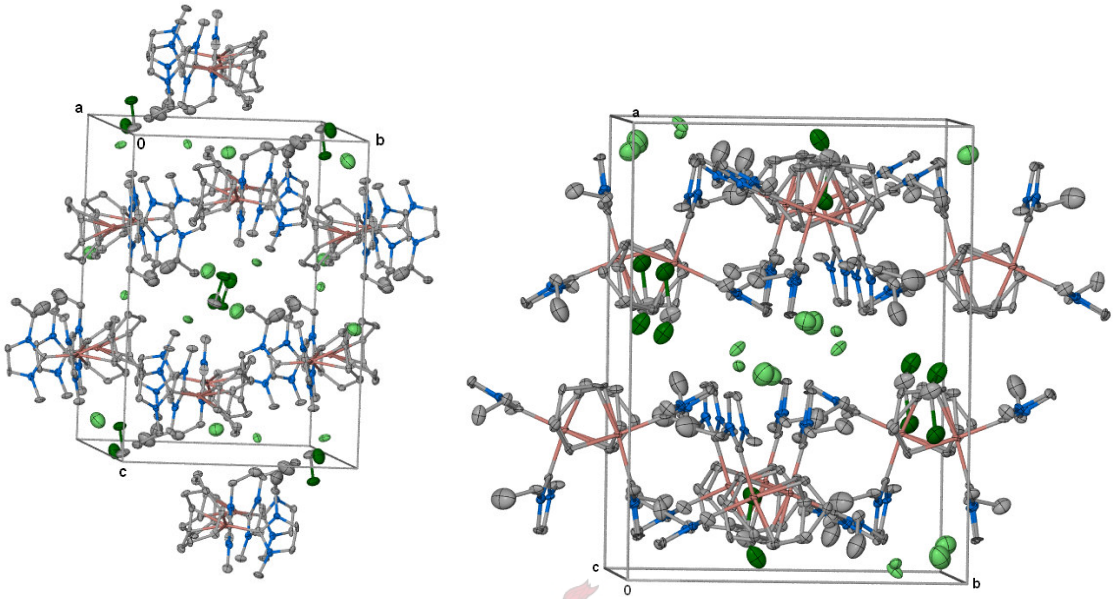

A B

Figure 3.2 Packing diagram of molecules of **18a** along the a-axis (A) and the c-axis (B)

*3.2.5.2 The crystal and molecular structure of bromo(η^4-1,5-cyclooctadiene)(1-methyl-3-propyl-2,3-dihydro-1*H*-imidazol-2-ylidene)rhodium(I),* ***21a***

The molecular structure of the square planar complex **21a** is shown in Figure 3.3. The carbene carbon, Br-atom and the centers of the olefinic bonds of the COD ligand define the square planar environment around the rhodium atom. Selected bond lengths and angles are summarised in Table 3.18. The crystal structures of various rhodium carbene complexes of the type (COD)Rh(NHC)X (NHC = *N*-heterocyclic carbene, X = halide), wherein the *N*-substituents are similar every time, have been reported.[9,18,33] The Rh-$C_{carbene}$ bond [2.016(5)Å] and the Rh-Br bond [2.504(1) Å] compare well with those in known structures bromo(η^4-1,5-cyclooctadiene)(1,3-dimethyl-2,3-dihydro-1*H*-imidazol-2-ylidene)rhodium(I), [Rh-$C_{carbene}$ = 2.023(2) Å, Rh-Br = 2.498(1) Å],[33] and bromo(η^4-1,5-cyclooctadiene)[1,3-di-(methoxycarbonylmethyl)-2,3-dihydro-1*H*-imidazol-2-ylidene) rhodium(I), [Rh-$C_{carbene}$ = 2.021(3) Å, Rh-Br = 2.494(1) Å].[25] The Rh-carbene bond also compares well with those in the crystal structures of a few other rhodium complexes of similar types in literature.[9,18,33]

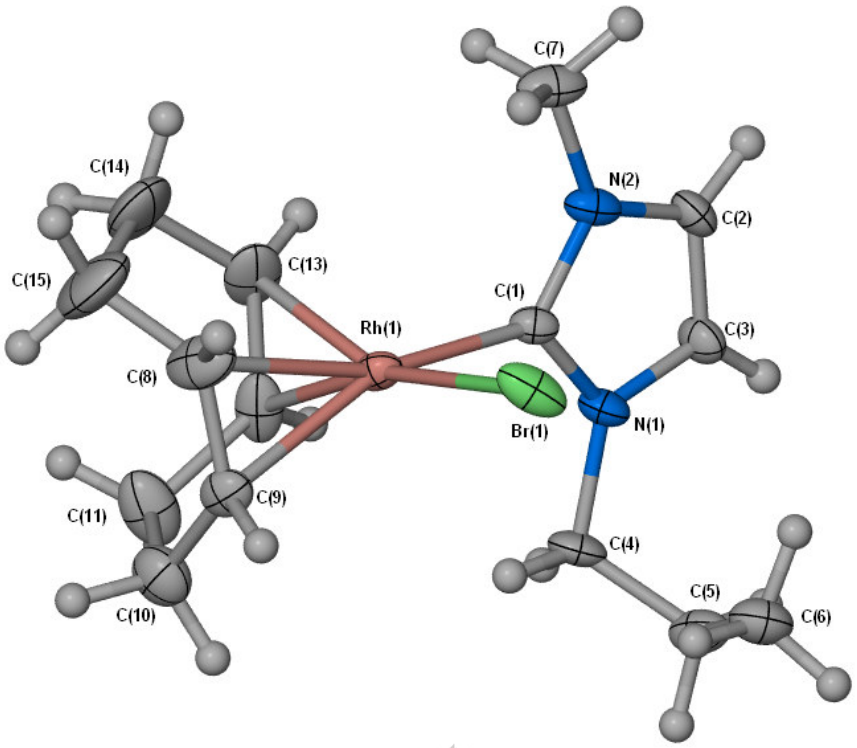

Figure 3.3 Molecular structure of **21a**, showing the numbering scheme, generated in POV-Ray

The difference in *trans*-influence of the carbene ligand and the Br^- ligand is illustrated in the difference of the Rh-C_{COD} distances. The Rh(1)-C(8) [2.211(6) Å] and Rh(1)-C(9) [2.197(5) Å] bond lengths (*trans* to the carbene ligand) are significantly longer than the Rh(1)-C(12) [2.117(6) Å] and Rh(1)-C(13) [2.088(6) Å] distances [*trans* to Br(1)] and confirms that the carbene ligand has a greater *trans*-influence than the Br^- ligand. The Rh(1)-C(8) and Rh(1)-C(9) bond lengths fall into the range (2.175 – 2.205 Å) reported for Rh-C_{COD} distances *trans* to the carbene ligand.[41] The carbene ligand is orientated almost perpendicular to the coordination plane with the dihedral angle Br(1)-Rh(1)-C(1)-N(2) of -83.4 (1)° which is smaller than those [-87.6(2) and –86.8(1)°] reported[33] for similar complexes. This difference probably results from the longer propyl substituent, that must be accommodated in the unit cell, instead of the methyl substituents as in the reported structures.

Table 3.18 Selected bond lengths (Å) and angles (°) for **21a**

Rh(1)-C(1)	2.016(5)	N(2)-C(2)	1.377(7)
Rh(1)-Br(1)	2.504(1)	C(2)-C(3)	1.347(8)
Rh(1)-C(8)	2.211(6)	C(3)-N(1)	1.383(6)
Rh(1)-C(9)	2.197(5)	N(1)-C(4)	1.471(6)
Rh(1)-C(12)	2.117(6)	C(4)-C(5)	1.516(9)
Rh(1)-C(13)	2.088(6)	C(5)-C(6)	1.504(9)
C(1)-N(1)	1.358(6)	N(2)-C(7)	1.468(7)
C(1)-N(2)	1.363(6)		
C(1)-Rh(1)-Br(1)	88.5(2)	C(1)-N(1)-C(3)	111.1(4)
C(1)-Rh(1)-C(12)	91.9(2)	N(1)-C(3)-C(2)	106.9(5)
C(1)-Rh(1)-C(13)	90.4(2)	N(2)-C(2)-C(3)	106.4(5)
Br(1)-Rh(1)-C(8)	93.0(2)	C(1)-N(2)-C(2)	111.8(4)
Br(1)-Rh(1)-C(9)	92.7(2)	C(1)-N(2)-C(7)	123.6(5)
C(8)-Rh(1)-C(13)	81.9(3)	C(1)-N(1)-C(4)	124.3(4)
C(9)-Rh(1)-C(12)	81.8(2)	N(1)-C(4)-C(5)	112.2(5)
N(1)-C(1)-N(2)	103.7(4)	C(4)-C(5)-C(6)	114.8(5)

The packing diagram of the molecules of **21a** in the unit cell is shown in Figure 3.4. The molecules are stacked on top of each other along the a-axis (A) and b-axis (B). The molecules pack in an alternating fashion along the b-axis, with the carbene ligand pointing up and down but the carbene ligands are packed next to each other with the methyl groups overlapping. The molecules are centered on the corners of the unit cell with other molecules in the center of the unit cell (A).

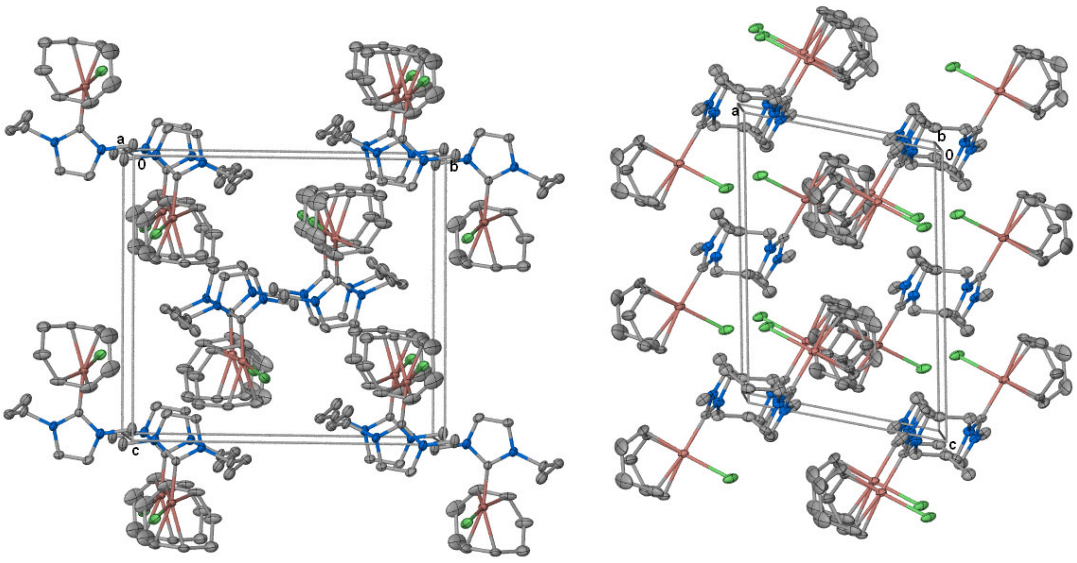

A B

Figure 3.4 Packing diagram of the molecules of **21a** along the a-axis (A) and the b-axis (B)

*3.2.5.3 The crystal and molecular structure of cis-[(η⁴-1,5-cyclooctadiene)bis(1-butyl-3-methyl-2,3-dihydro-1*H*-imidazol-2-ylidene)rhodium(I)]bromide,* ***22a***

The molecular structure of the square planar complex **22a** (Figure 3.5) compares well with that of **18a**, **D**[18] and **E**.[17] Selected bond lengths and angles are listed in Table 3.19 and Table 3.20 respectively. The Rh-$C_{carbene}$ distances [2.050(6) and 2.053(6) Å] do not differ significantly from those in **18a** [2.046(7) and 2.053(8) Å], **D** [2.053(8) and 2.059(8) Å] and **E** [2.059(4) and 2.051(4) Å]. The C(11)-Rh(1)-C(21) angle of 90.0(2)° is significantly smaller than the same angle in **18a** [96.1(3)°] and **D** [94.4(3)°] larger than that in **E** [88.4(1)°]. The two carbene ligands are orientated not quite perpendicular to the square plane defined by Rh(1), C(11), C(21) and the centers of C(31)-C(32) and C(35)-C(36). The torsion angles C(21)Rh(1)-C(11)-N(12) [81.4(6)°] and C(11)-Rh(1)-C(21)-N(22) [-94.9(6)°] indicate that the carbene ligands are considerably bent away from 90° probably in order to accommodate the large butyl substituent in the packing diagram. Similar to complex **18a** the Rh-C_{COD} distances in **22a** do not differ significantly.

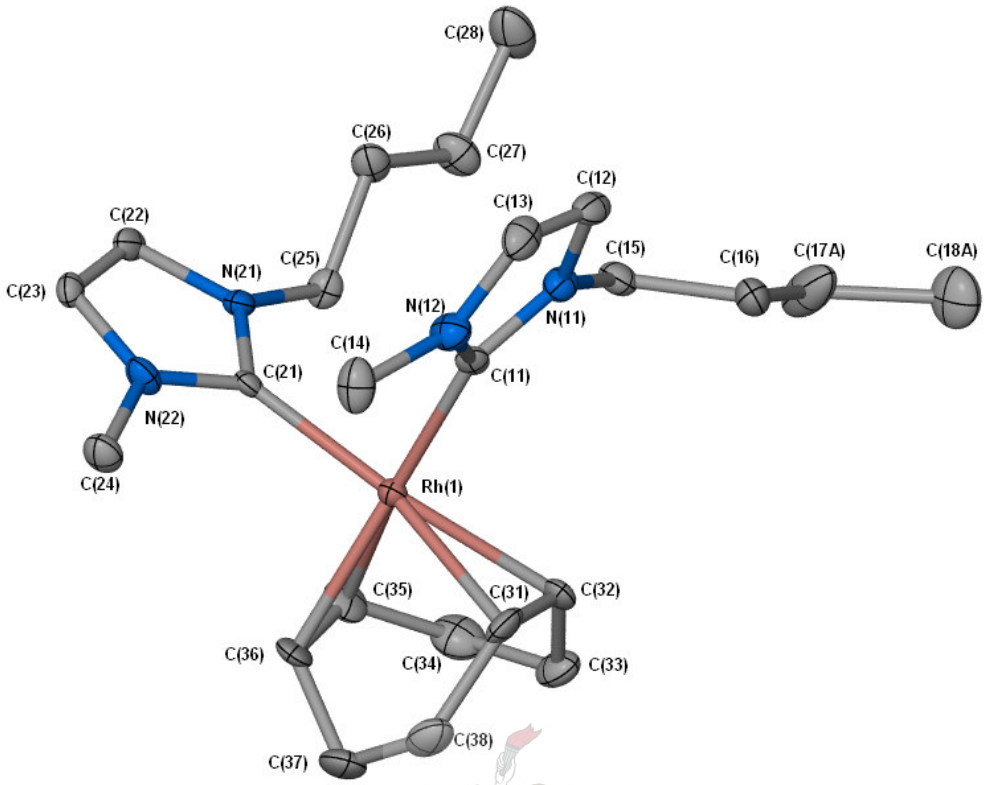

Figure 3.5 Molecular structure of **22a**, showing the numbering scheme, generated in POV-Ray

Table 3.19 Selected bond lengths (Å) of complex **22a**

Rh(1)-C(11)	2.050(6)	C(15)-C(16)	1.525(9)
Rh(1)-C(21)	2.053(6)	C(16)-C(17A)	1.537(11)
Rh(1)-C(31)	2.178(6)	C(17A)-C(18A)	1.690(12)
Rh(1)-C(32)	2.195(7)	C(21)-N(21)	1.351(8)
Rh(1)-C(35)	2.186(7)	C(21)-N(22)	1.358(8)
Rh(1)-C(36)	2.198(6)	N(22)-C(23)	1.388(8)
C(11)-N(11)	1.359(8)	N(21)-C(22)	1.397(8)
C(11)-N(12)	1.348(8)	C(22)-C(23)	1.333(9)
N(12)-C(13)	1.382(9)	N(22)-C(24)	1.465(8)
N(11)-C(12)	1.393(8)	N(21)-C(25)	1.464(8)
C(12)-C(13)	1.335(10)	C(25)-C(26)	1.516(9)
N(12)-C(14)	1.466(9)	C(26)-C(27)	1.516(9)
N(11)-C(15)	1.455(8)	C(27)-C(28)	1.517(10)

Table 3.20 Selected bond angles (°) of complex **22a**

C(11)-Rh(1)-C(21)	90.0(2)	N(12)-C(13)-C(12)	106.7(6)
C(11)-Rh(1)-C(31)	90.5(3)	C(11)-N(12)-C(14)	124.8(6)
C(11)-Rh(1)-C(32)	93.3(3)	C(11)-N(11)-C(15)	126.5(5)
C(21)-Rh(1)-C(35)	90.5(3)	N(21)-C(21)-N(22)	104.2(5)
C(21)-Rh(1)-C(36)	92.7(2)	C(21)-N(21)-C(22)	111.1(5)
C(31)-Rh(1)-C(36)	81.5(3)	N(21)-C(22)-C(23)	106.6(5)
C(32)-Rh(1)-C(35)	80.8(3)	N(22)-C(23)-C(22)	107.0(5)
N(11)-C(11)-N(12)	104.0(5)	C(21)-N(22)-C(23)	111.1(5)
C(11)-N(11)-C(12)	110.8(5)	C(21)-N(22)-C(24)	126.4(5)
N(11)-C(12)-C(13)	111.7(6)	C(21)-N(21)-C(25)	124.8(5)

Figure 3.6 shows the packing of the molecules of **22a** in the unit cell viewed down the a-axis (A) and b-axis (B). There are eight molecules around the four long sides (two per side) of the unit cell. The molecules are arranged precisely on top of each other when viewed along the a-axis and b-axis with the bromide anions located in the spaces between the molecules. In the layers parallel to the a-axis and b-axis the carbene ligands in one layer are directed to the carbene ligands in the next layer.

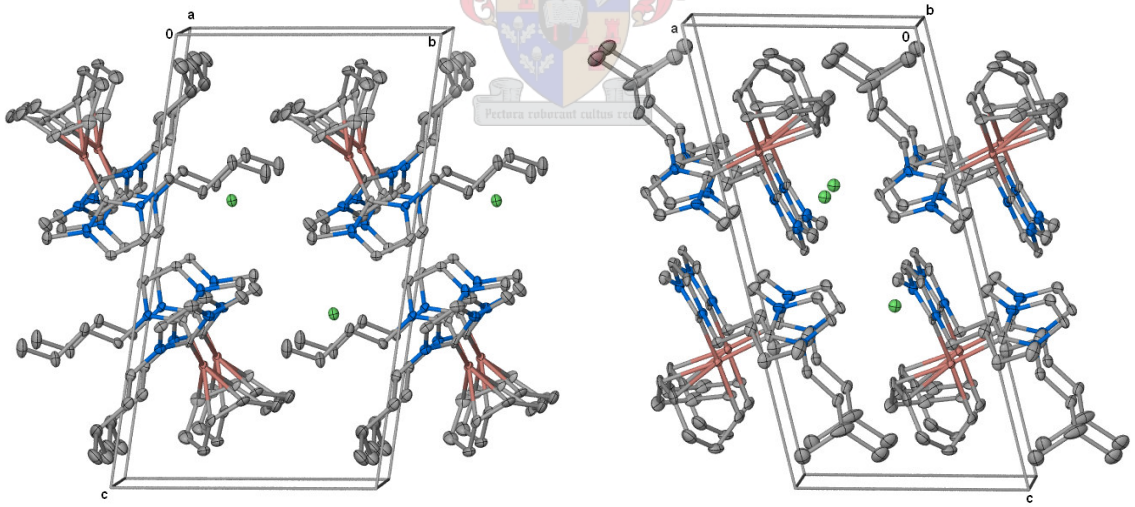

A B

Figure 3.6 Packing diagram of the molecules of **22a** along the a-axis (A) and the b-axis (b)

3.3 Conclusions and future work

Free carbenes, produced from the reaction of [EMIM]Br, [PMIM]Br or [BMIM]Br with an excess of KO^{t}Bu, reacted with $[Rh(Cl)COD]_2$ to yield three non-symmetrical products for each reaction. These were rhodium bis(carbene) complexes (**18a**, **20a** or **22a**), bromo-mono(carbene) complexes (**19a**, **21a** or **23a**) and chloro-mono(carbene) complexes (**19b**, **21b** or **23b**). The bromo complexes formed *via* the substitution of a chloride ligand bonded to rhodium with a Br^--ion, stemming from the imidazolium salts. The reaction of the free carbene, generated from $[BMIM]BF_4$, with $[Rh(Cl)COD]_2$, however, produced only one product namely the mono(carbene) complex **23b**. No significant formation of the bis(carbene) complex was observed. X-ray crystal structures of **18a**, **21a** and **22a** were also determined (carried out by the author himself).

The NMR data of the bis(carbene) complexes (**18a**, **20a** and **22a**) clearly showed two sets of signals for the two non-equivalent carbene ligands. Due to the different chemical environments of the carbene ligands and the difference in the *N*-substituents, the carbon atoms of the COD ligand are also in chemically different environments. The NMR data of the mono(carbene) complexes are naturally different from that of the bis(carbene) complexes in that only one set of peaks are observed for the carbene ligand. The assignment of the signals in the NMR spectra was confirmed by two-dimensional ghsqc NMR spectra. From this data we also conclude that there is no rotation around the Rh-$C_{carbene}$ bond in any of these COD complexes. It is clear from these results that the NMR data previously reported for chloro(η^4-1,5-cyclooctadiene)(1-butyl-3-methyl-2,3-dihydro-1*H*-imidazol-2-ylidene)rhodium(I)[26] fits the structure of the bis(carbene) complex rather than that of the proposed mono(carbene) complex. The structures of **18a**, **22a**, confirmed by X-ray single crystal diffraction, further substantiate our findings. This study has, therefore, resolved the uncertainty attached to a previous investigation and in addition showed the halide exchange that occurs under the chosen conditions.

The *trans*-influence of the carbene ligands, the halides and CO are clearly illustrated in the ^{103}Rh - ^{13}C coupling constants in the ^{13}C NMR spectra of the mono(carbene) complexes of rhodium. The coupling of rhodium with the COD or CO carbons *trans* to the carbene is smaller than the coupling of the rhodium with the COD or CO carbons *trans* to the halides (bromide and chloride). The coupling of rhodium with the carbene carbon in the *cis*-carbonyl complexes **24a** and **24b** (the CO is *trans* to the carbene ligand) is smaller than the former ^{103}Rh - ^{13}C coupling constants. Based on these coupling constants, the CO has the largest *trans*-influence, followed

by the carbene ligand and then the halides. The Rh-C_{COD} bond lengths in the crystal structure of **21a** confirm this difference in *trans*-influence. The Rh-C_{COD} distances *trans* to the carbene ligand is significantly longer than the Rh-C_{COD} distances *trans* to the halide (bromide in this case), illustrating the larger *trans*-influence of the carbene ligand compared to bromide. The ligands can be arranged in decreasing order of *trans*-influence as follows: CO > carbene > halide.

The COD ligand in **19a** and **19b** were substituted by CO ligands to produce **24a** and **24b**. The mechanism for the isomerisation of the two *cis*-carbonyl complexes to complexes **25a** and **25b** respectively is still unknown. A detailed kinetic study is required to unravel this mechanism. The isomerisation of **24a** was much faster than that of **24b**.

Further work is required to fully understand the mechanism and kinetics of this *cis*-*trans* isomerisation. The growing of single crystals of the complexes, for X-ray structure determinations, would greatly help such an investigation. The activity of the complexes, described in this chapter, as pre-catalysts for the hydroformylation of olefins should be investigated.

3.4. Experimental

3.4.1 General

The general techniques described in Section 2.4.1, Chapter 2, are also applied to the work in this chapter. KO^{t}Bu was purchased from Aldrich and used without further purification. [EMIM]Br, [PMIM]Br, [BMIM]Br, [BMIM]BF_4[27,28] and $[Rh(Cl)COD]_2$[42] were synthesised according to literature methods. The yield for complexes **18a - 23b** varied when the reactions were repeated for a second time. Complexes **18a - 24b** were all isolated as yellow microcrystalline material.

[42] W.A. Herrmann, C. Zybill, *Synthetic Methods of Organometallic and Inorganic Chemistry, Volume 1, Literature, Laboratory Techniques, and Common Starting Materials*, (Eds. W.A. Herrmann, A. Salzer), Georg Thieme Verlag, Stuttgart, 1996, p 150.

3.4.2 Synthesis of *cis*-[(η^4-1,5-cyclooctadiene)bis(1-ethyl-3-methyl-2,3-dihydro-1*H*-imidazol-2-ylidene)rhodium(I)]bromide, 18a, bromo(η^4-1,5-cyclooctadiene)(1-ethyl-3-methyl-2,3-dihydro-1*H*-imidazol-2-ylidene)rhodium(I), 19a, and chloro(η^4-1,5-cyclooctadiene)(1-ethyl-3-methyl-2,3-dihydro-1*H*-imidazol-2-ylidene)rhodium(I), 19b

[EMIM]Br (0.20 g, 1.0 mmol) dissolved in 30 cm^3 THF was reacted with KO^{t}Bu (0.18 g, 1.6 mmol) at room temperature for three hours. $[Rh(Cl)COD]_2$ (0.25 g, 0.51 mmol) was added as a solid to the light yellow reaction mixture with a white suspension. A yellow precipitate formed immediately and the reaction mixture was stirred for two hours at room temperature. The precipitate was filtered of over dry celite and washed four times with THF. The precipitate was washed through the celite with CH_2Cl_2 and dried *in vacuo* to yield complex **18a**. The THF filtrate was dried *in vacuo* and the resultant residue contained $[Rh(Cl)COD]_2$ and complexes **19a** and **19b**. These three complexes were separated on a short flash silica column (7 cm) with diethyl ether as eluent, fraction 1 contained $[Rh(Cl)COD]_2$, fraction 2, complex **19a** and fraction 3, complex **19b**. Microcrystalline materials were obtained after the solutions were stripped of solvent under vacuum. Crystallisation from a concentrated CH_2Cl_2 solution layered with pentane at -20 °C yielded yellow crystals of **18a** suitable for single crystal X-ray structure determination.

Yield: Complex **18a** 0.16 g (30 %) Melting point: 154 - 160 °C (decomposition)
Complex **19a** 0.065 g (16 %) Melting point: 144 - 151 °C (decomposition)
Complex **19b** 0.090 g (25 %) Melting point: 159 - 162 °C (decomposition)

Elemental analysis (%): Calc. for **18a** ($C_{20}H_{32}BrN_4Rh$) (511.30): C, 46.98; H, 6.31; N, 10.96. Found: C, 47.22; H, 6.28; N, 10.90. Calc. for **19a** ($C_{14}H_{22}BrN_2Rh$) (401.15): C, 41.92; H, 5.53; N, 6.98. Found: C, 41.77; H, 5.44; N, 6.89. Calc. for **19b** ($C_{14}H_{22}ClN_2Rh$) (356.70): C, 47.14; H, 6.22; N, 7.85. Found: C, 47.06; H, 6.25; N, 7.77.

3.4.3 Synthesis of *cis*-[(η^4-1,5-cyclooctadiene)bis(1-methyl-3-propyl-2,3-dihydro-1*H*-imidazol-2-ylidene)rhodium(I)]bromide, 20a, bromo(η^4-1,5-cyclooctadiene)(1-methyl-3-propyl-2,3-dihydro-1*H*-imidazol-2-ylidene)rhodium(I), 21a, and chloro(η^4-1,5-cyclooctadiene)(1-methyl-3-propyl-2,3-dihydro-1*H*-imidazol-2-ylidene)rhodium(I), 21b

Complexes **20a** - **21b** were prepared in the same fashion as complexes **18a** - **19b** using [PMIM]Br (0.18 g, 0.86 mmol), KO^{t}Bu (0.15 g, 1.3 mmol) and $[Rh(Cl)COD]_2$ (0.21 g, 0.43 mmol) as starting materials. Suitable crystals for single crystal X-ray structure determination of

21a were obtained when the solvent of fraction 2 was reduced under reduced pressure after column chromatography.

Yield: Complex **20a** 0.14 g (29 %) Melting point: 148 °C (decomposition)
Complex **21a** 0.10 g (28 %) Melting point: 135 - 141 °C (decomposition)
Complex **21b** 0.083 g (22 %) Melting point: 143 - 147 °C (decomposition)

Elemental analysis (%): Calc. for **20a** ($C_{22}H_{36}BrN_4Rh$) (539.36): C, 48.99; H, 6.73; N, 10.39. Found: C, 48.86; H, 6.61; N, 10.19. Calc. for **21a** ($C_{15}H_{24}BrN_2Rh$) (415.17): C, 43.39; H, 5.83; N, 6.75. Found: C, 43.11; H, 5.90; N, 6.67. Calc. for **21b** ($C_{15}H_{24}ClN_2Rh$) (370.72): C, 48.60; H, 6.53; N, 7.56. Found: C, 48.45; H, 6.32; N, 7.62.

3.4.4 Preparation of *cis*-[(η^4-1,5-cyclooctadiene)bis(1-butyl-3-methyl-2,3-dihydro-1*H*-imidazol-2-ylidene)rhodium(I)]bromide, 22a, bromo(η^4-1,5-cyclooctadiene)(1-butyl-3-methyl-2,3-dihydro-1*H*-imidazol-2-ylidene)rhodium(I), 23a, and chloro(η^4-1,5-cyclooctadiene)(1-butyl-3-methyl-2,3-dihydro-1*H*-imidazol-2-ylidene)rhodium(I), 23b

The procedure followed for complexes **18a - 19b** was used to prepare complexes **22a - 23b** from [BMIM]Br (0.14 g, 0.62 mmol), KO^{t}Bu (0.10 g, 0.92 mmol) and $[Rh(Cl)COD]_2$ (0.16 g, 0.32 mmol). Crystallisation of **22a** from a CH_2Cl_2/pentane solution (-20°C) produced yellow crystals suitable for single crystal X-ray determination.

Yield: Complex **22a** 0.077 g (22 %) Melting point: 135 - 138 °C (decomposition)
Complex **23a** 0.054 g (19 %) Melting point: 139 - 142 °C (decomposition)
Complex **23b** 0.042 g (17 %) Melting point: 120 - 128 °C (decomposition)

Elemental analysis (%): Calc. for **22a** ($C_{24}H_{40}BrN_4Rh$) (567.41): C, 50.80; H, 7.11; N, 9.87. Found: C, 50.92; H, 6.94; N, 9.91. Calc. for **23a** ($C_{16}H_{26}BrN_2Rh$) (429.20): C, 44.77; H, 6.11; N, 6.53. Found: C, 44.56; H, 5.92; N, 6.59. Calc. for **23b** ($C_{16}H_{26}ClN_2Rh$) (384.75): C, 49.95; H, 6.81; N, 7.28. Found: C, 50.23; H, 6.95; N, 7.17.

3.4.5 Preparation of chloro(η^4-1,5-cyclooctadiene)(1-butyl-3-methyl-2,3-dihydro-1*H*-imidazol-2-ylidene)rhodium(I), 23b

[BMIM]BF_4 (0.14 g, 0.636 mmol) dissolved in 30 cm^3 THF was reacted with KO^{t}Bu (0.11 g, 0.97 mmol) at room temperature for two hours. The reaction mixture turned yellow immediately upon the addition of the KO^{t}Bu. [Rh(Cl)COD]$_2$ (0.16 g, 0.31 mmol) was added as a solid to the reaction mixture with no significant formation of a precipitate. The reaction mixture was filtered over dried celite after stirring for a further two hours at room temperature. Complex **23b** was separated from [Rh(Cl)COD]$_2$ on a short column (7 cm) with diethyl ether as eluent. The solvent were removed in vacuo.

Yield: 0.15 g (62%)
Melting point: 120 - 128 °C (decomposition)

Elemental analysis (%): Calc. for **23b** ($C_{16}H_{26}ClN_2Rh$) (384.75): C, 49.95; H, 6.81; N, 7.28. Found: C, 49.90; H, 6.91; N, 7.32.

3.4.6 Preparation of *cis*-bromo(dicarbonyl)(1-ethyl-3-methyl-2,3-dihydro-1*H*-imidazol-2-ylidene)rhodium(I), 24a

Carbon monoxide was bubbled through a yellow solution of **19a** (0.078 g, 0.19 mmol) in 25 cm^3 of CH_2Cl_2 for 30 minutes after which the solvent was removed. Complex **24a** was separated as fraction 2 from [Rh(X)COD]$_2$ (X = Cl or Br) (fraction 1), which formed during the reaction, on a short flash silica column with diethyl ether as eluent. The melting point and elemental analysis of **24a** (as well as **24b**, **25a** and **25b**) was not determined because of the presence of an unknown complex **III**.

Yield of crude product: 0.043 g (63 %)

3.4.7 Preparation of *cis*-chloro(dicarbonyl)(1-ethyl-3-methyl-2,3-dihydro-1*H*-imidazol-2-ylidene)rhodium(I), 24b

The same procedure as above was employed to prepare complex **24b** from **19b** (0.053g, 0.15 mmol).
Yield of crude product: 0.030 g (66 %)

3.4.8 Preparation of *trans*-bromo(dicarbonyl)(1-ethyl-3-methyl-2,3-dihydro-1*H*-imidazol-2-ylidene)rhodium(I), 25a, and *trans*-chloro(dicarbonyl)(1-ethyl-3-methyl-2,3-dihydro-1*H*-imidazol-2-ylidene)rhodium(I), 25b

Complexes **25a** and **25b** formed as rearranged products in CD_2Cl_2 from **24a** and **24b** respectively. Complex **25a** and **25b** are brown microcrystalline materials. Complex **25a** formed at a much faster rate than complex **25b**.

Yield of crude product: Complex **25a** 0.031 g (72 %)
Complex **25b** 0.020 g (66 %)

3.4.9 NMR details of unknown complex III

^{1}H NMR (CD_2Cl_2): 6.69 (2H, m), 4.49 (2H, m), 4.00 (3H, s), 1.43 (3H, t, $^3J_{H-H}$ = 7.2 Hz). ^{13}C NMR (CD_2Cl_2): 125.3 (s), 120.5 (s), 46.0 (s), 38.4 (s).

3.4.10 X-ray structure determinations

The crystal data collection and refinement details for complexes **18a**, **21a** and **22a** are summarised in Table 3.21. All the data sets were collected on a Bruker SMART Apex CCD diffractometer[43] with graphite-monochromated Mo-K_α radiation (λ = 0.71073 Å) each. Data reduction was carried out with standard methods from the software package Bruker SAINT.[44] Emperical corrections were performed using SCALEPACK[45] and SMART data were treated with SADABS.[46,47] All three structures were solved by direct methods, which yielded the position of the metal atoms, and conventional Fourier methods. All non-hydrogen atoms were refined anisotropically by full-matrix least squares calculations on F^2 using SHELXL-97[48] within the X-Seed environment.[49] The hydrogen atoms were fixed in calculated positions. POV-Ray

---

[43] SMART Data collection software (version 5.629), Bruker AXS Inc., Madison, WI, 2003.

[44] SAINT, Data reduction software (version 6.45) Bruker AXS Inc., Madison, WI, 2003.

[45] L.J. Ferrugia, *J. Appl. Crystallogr.*, 1999, **32**, 837.

[46] R.H. Blessing, *Acta Crystallogr., Sect. A*, 1995, **51**, 33.

[47] SADABS (version 2.05) Bruker AXS Inc., Madison, WI, 2002.

[48] G.M. Sheldrick, SHELX-97. Program for crystal structure analysis, Univ. of Göttingen, Germany, 1997.

[49] L.J. Barbour, *J. Supramol. Chem*. 2001, **1**, 189.

for Windows was used to generate the various figures of the three complexes at the 50% probability level.

The electron densities for the two bromide atoms of complex **18a** are each disordered over two sites with site occupation factors of 0.70 and 0.30 for one bromide and 0.79 and 0.21 for the other bromide. The methyl group of one butyl substituent in complex **22a** was disordered over two sites with occupation factors of 0.52 and 0.48 respectively. This structure also contains disordered CH_2Cl_2 solvent molecules. Contributions of these solvent molecules were taken into account by the squeeze method included in the program PLATON[50] (N: Total Potential Solvent Accessible Area Vol 173.1 Ang^3; Electron Count / Cell = 55).

Additional information regarding these crystal structures is available from Prof H.G. Raubenheimer, Department of Chemistry, University of Stellenbosch.

[50] A.L. Spek, *Acta Crystallogr., Sect. A*, 1990, **46**, C34.

Table 3.21 Crystallographic data for complexes **18a**, **21a** and **22a**

	18a	**21a**	**22a**
Empirical formula	$C_{41}H_{64}Br_2Cl_2N_8Rh_2$	$C_{15}H_{18}BrN_2Rh$	$C_{24}H_{40}BrN_4Rh$
Formula weight ($g.mol^{-1}$)	1105.54	409.13	567.42
Crystal system	Monoclinic	Monoclinic	Triclinic
Space group	$P2_1/n$	$P2_1/n$	P-1
a (Å)	18.4428(15)	9.0128(12)	8.7416(12)
b (Å)	13.7078(12)	13.9582(19)	10.5132(14)
c (Å)	18.8336(16)	12.9764(17)	16.855(2)
α (°)	90.00	90.00	92.973(3)
ß (°)	91.206(2)	101.989(2)	103.143(3)
γ (°)	90.00	90.00	110.644(2)
Volume ($Å^3$)	4760.3(7)	1596.9(4)	1396.7(3)
Z	4	4	2
Calculated density ($g.cm^{-3}$)	1.543	1.702	1.349
Wave length (Å)	0.71073	0.71073	0.71073
Temperature (K)	100(2)	100(2)	100(2)
Absorption coefficient (mm^{-1})	2.521	3.560	2.058
Crystal size (mm)	0.10 x 0.10 x 0.10	0.20 x 0.15 x 0.10	0.20 x 0.10 x 0.10
θ range for data collection (°)	$1.84 \leq \theta \leq 25.35$	$2.17 \leq \theta \leq 28.27$	$2.28 \leq \theta \leq 25.35$
Index range, *hkl*	$-22 \leq h \leq 19$	$-11 \leq h \leq 7$	$-10 \leq h \leq 10$
	$-16 \leq k \leq 15$	$-18 \leq k \leq 18$	$-12 \leq k \leq 12$
	$-22 \leq l \leq 22$	$-17 \leq l \leq 17$	$-20 \leq l \leq 20$
Reflections collected	25240	9655	13730
Independent reflections	8666	3653	5070
Parameters	525	175	286
Goodness of fit	1.022	1.139	1.085
Largest peak	1.445	2.160	1.547
Deepest hole	-0.774	-1.447	-1.305
Final R indices [$I>2\sigma(I)$]	0.0683	0.0549	0.0577
R indices (all data)	0.1426	0.1546	0.1238

Chapter 4

Cyclisations and other reactions of α-deprotonated, Fischer-type aminocarbene complexes in the presence of chlorophosphine

Abstract

The anionic Fischer-type aminocarbene complexes $[(CO)_5Cr=C(NMe_2)CH_2]Li$ (M = Cr or W) react with $ClPPh_2$ to produce acyclic compounds $(CO)_5M=C(NMe_2)CH_2PPh_2$, and four-membered chelates $(CO)_4M=C(NMe_2)CH_2PPh_2$ as well as the bridged complex $(CO)_5Cr=C(NMe_2)CH_2P(Ph_2)Cr(CO)_5$. Cyclisation, to afford the four membered chelates occurs much faster for Cr than for W. The four-membered aminocarbene-phosphine chelates represent the first examples of structurally characterised C,P-chelate carbene complexes.

4.1 Introduction and aims

4.1.1 General

The stoichiometric reactions of transition metal carbene complexes were already well established in the 1980's![1] The structure of Fischer-type carbene complexes and their anions have been extensively studied and the most important contributing structures for a chosen compound are depicted in Scheme 4.1. The π-interaction between the carbene carbon and its substituents is important for the stability of these complexes as this reduces the electron deficiency on the carbene carbon.[2] Structure (**iii**) makes the most important contribution when X is a heteroatom and especially when $X = NR_2$. The backdonation from the heteroatom to the carbene carbon (p_z orbital in valence bond terms) is, for example, more significant in amino carbene complexes than in alkoxy carbene complexes. In general carbene complexes are formulated as shown in structure (**i**).

[1] F.J. Brown, *Prog. Inorg Chem.*, 1980, **27**, 1.

[2] U. Schubert, *Coord. Chem. Rev.*, 1984, **55**, 261.

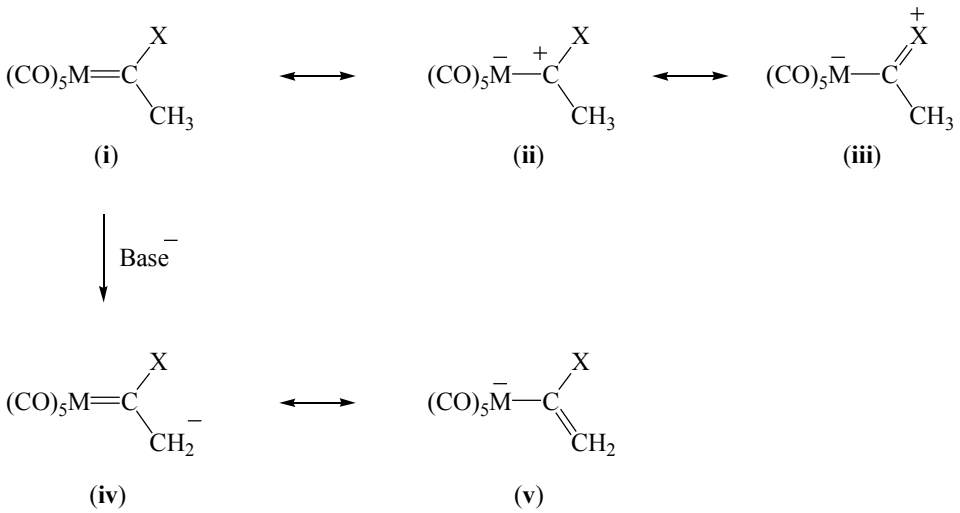

Scheme 4.1 (X = OR, NR_2 or SR with R = organic moiety)

Deprotonation of the carbene complex with a base (for example *n*-BuLi) yields the anion (**iv**) that can be stabilised with the negative charge located on the metal carbonyl moiety – delocalisation into the electron sink of carbonyls not shown (**v**) (Scheme 4.1). The air and water stable salt of such a stabilised anion, $[(CO)_5Cr{=}C(OMe)CH_2][N(PPh_3)_2]$, has been isolated in the group of Casey.[3] The acidity of the protons α to the carbene carbon can be used to synthesise various new Fischer-type carbene complexes that are inaccessible *via* various preparative methods known in the literature such as the alkylation of lithium metallates, alkylation of neutral acyl complexes, nucleophilic additions to carbynes and coordinated isonitriles to name a few.[1] The reaction of the $[(CO)_5Cr{=}C(OMe)CH_2]^-$ anion with epoxide yields such a carbene complex (Scheme 4.2). A consecutive deprotonation of carbene complex (**vi**) followed by reaction with acetaldehyde afford carbene complex (**vii**). The synthesis of lactones (**viii**) via oxidative cleavage of the carbene bond is also known.[4]

[3] C.P. Casey, R.L. Anderson, *J. Am. Chem. Soc.*, 1974, **96**, 1230.

[4] C.P. Casey, W.R. Burnsworld, *J. Organomet. Chem.*, 1975, **102**, 175.

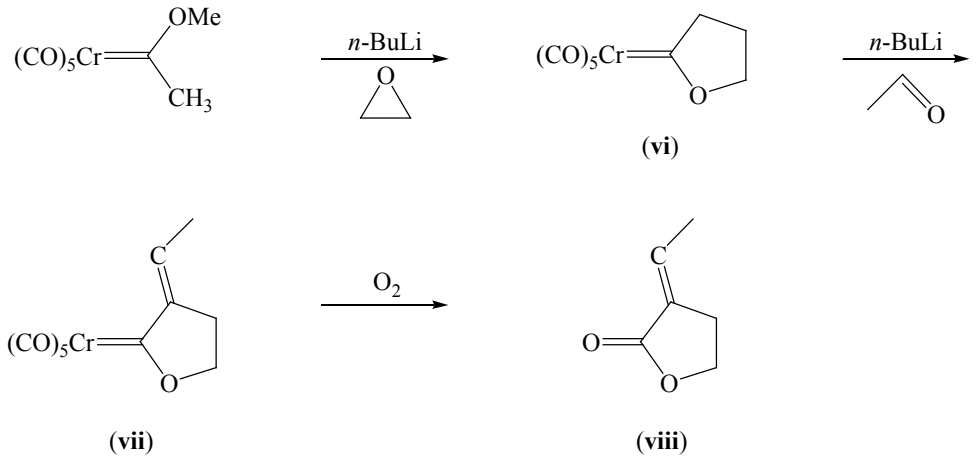

Scheme 4.2

The formation of dialkylation products has been a problem during the alkylation of carbene anions.[5,6] The alkylation of $[(CO)_5Cr=C(OMe)CH_2]^-$ with bromoacetate yields 37% of the monoalkylation product, $(CO)_5Cr=C(OMe)CH_2CH_2CO_2CH_3$, and 20% of the dialkylation product, $(CO)_5Cr=C(OMe)CH\{CH_2CO_2CH_3\}_2$.[5]

Modifications to the Fischer-type carbene complexes potentially allow them to be used as either cationic or neutral, monodentate or bidentate ligands towards another metal center, producing a 'complex of a complex' as is shown in Scheme 4.3. Such a complex of complexes can be tailored in various ways. Both metals M^1 and M^2 with their ligands can be varied. The donor groups X and Y can be altered as well as the size of the chelate ring formed upon coordination of this bidentate ligand (Fischer carbene) to M^2.

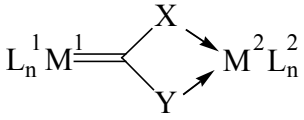

Scheme 4.3

[5] C.P. Casey, R.L. Anderson, *J. Organomet. Chem.*, 1974, **73**, C28.

[6] C.P. Casey, W.R. Burnsworld, *J. Organomet. Chem.*, 1976, **118**, 309.

Du Toit *et al.* have prepared complexes of complexes where the Fischer carbene acted as an anionic ligand and was bonded to the second metal in a monodentate (**ix**) or bidentate fashion (**x**) (Scheme 4.4).[7,8] Complex (**xi**) is an active pre-catalyst in the co-polymerization of ethylene and 1-pentene.

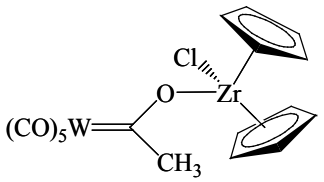

(**ix**)

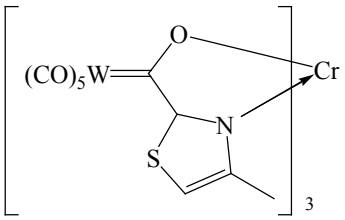

(**x**)

Scheme 4.4

In our quest to further tailor neutral carbene complexes towards being monodentate or bidentate ligands, donor atoms were incorporated in the carbene side chain as a first step. Aminocarbene complex anions are less likely to be stabilized by delocalisation of negative charge on to the metal (formation of **v**, Scheme 4.1) than alkoxycarbene anions due to significant existing donation of non-bonding electrons into the p_z orbitals of the carbene carbons from the N atoms (as mentioned before). Put differently, an aminocarbene complex anion is more reactive than a corresponding alkoxycarbene anion because of less competition for the electrons on the deprotonated carbon. No pre-activation of the aminocarbene complex anions, therefore, is required and they give better results in aldol reactions as well as in Michael-additions.[9] Due to the backdonation from the N atom to the carbene atom, the lone pair will, however, be less available for coordination to a second metal.

A P atom has previously been incorporated β to the carbene carbon of Fischer carbene complexes.[10] Since heterometallocyclic compounds resulted from the work reported here, it needs to be mentioned that five and six-membered carbene-phosphine chelates have previously been

[7] N. Luruli, V. Grumel, R. Brüll, A. Du Toit, H. Pasch, A.J. Van Reenen, H.G. Raubenheimer, *J. Pol. Sci., Part A: Pol. Chem.*, 2004, **42**, 5121.

[8] A. Du Toit, M. Du Toit, S. Cronje, H.G. Raubenheimer, C. Esterhuysen, A.M. Crouch, J. An, L. van Niekerk, *Dalton Trans.*, 2004, 1173.

[9] K.H. Dötz, J. Pfeifer in: M. Beller, C. Bolm (Eds), *Transition Metals for Organic Synthesis*, Vol. 1, Wiley-VCH, Weinheim, 1998, p 335.

[10] H.G. Raubenheimer, G.J. Kruger, H.W. Viljoen, S. Lotz, *J. Organomet. Chem.*, 1986, **314**, 281.

reported.[10,11,12] The four-membered members of the family are, however, still lacking. Four-membered carbene-amine chelates are known from the work of Dötz and Kreiter[13] and Barluengo and coworkers[14] and are shown as (**xi**) and (**xii**) respectively in Scheme 4.5. The formation of compound (**xi**) involves reaction of $(CO)_5M{=}C(OMe)Ph$ (M = Cr or W) with bis(diethylamino)acetylene in *n*-Bu_2O at 70 – 90°C. The reaction of $(CO)_5Cr{=}C(OR^*)C(Me){=}CH$ { R*OH = (±)-menthol} with trimethylsilyldiazomethane ($TMSCHN_2$) at –50°C to room temperature affords complex (**xii**).

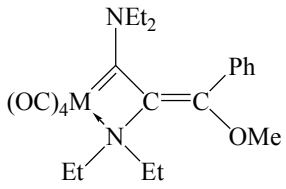

(**xi**)

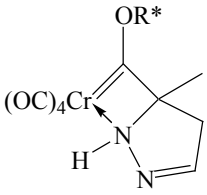

(**xii**)

Scheme 4.5 (M = Cr or W; R*OH = (±)-menthol)

4.1.2 Aims of this study

The most important goal of the investigation was to modify the standard (dimethylaminomethylcarbene)pentacarbonylchromium(0) and (dimethylaminomethylcarbene)-pentacarbonyltungsten(0) Fischer-type carbene complexes by introducing a soft P donor atom into the carbene side chain, to characterise the formed product and to investigate the formed products in order to establish whether internal CO-substitution is possible. By deprotonation of the CH-acidic complex α to the carbene carbon followed by reaction with $ClPPh_2$ such C-P-bonding could be achieved

Such Fischer-type carbene complexes that contain soft P donor atoms could serve as models for other similar carbene complexes with alkoxy groups that could then be modified (aminolysis) and

[11] S. Maiorana, A. Papagni, E. Licandro, D. Perdicchia, C. Baldoli, C. Graiff, A. Tiripicchio, *Inorg. Chim. Acta*, 1999, **296**, 236.

[12] K. Issberner, E. Niecke, E. Wittchow, K.H. Dötz, M. Nieger, *Organometallics*, 1997, **16**, 2370.

[13] K.H. Dötz, C.G. Kreiter, *Chem. Ber.*, 1976, **109**, 2026.

[14] J. Barluenga, F. Fernández-Marí, A.L. Viado, E. Aguilar, B. Olano, S. García-Granda, C. Moya-Rubiera, *Chem. Eur. J.*, 1999, **5**, 883.

N-deprotonated as future bidentate ligands. In certain instances even the neutral compounds could be utilized in such a capacity. Bonding of the phosphine to the already-present central metal by folding back to it, would indicate that the P-atoms are available as soft donors. Eventually catalytic applications (by future fine tuning) could come into play.

4.2 Results and discussion

4.2.1 Synthesis of complexes 26a, 26b, 27a, 27b and 28a

Deprotonation of the aminocarbene complexes, $(CO)_5M{=}C(NMe_2)Me$ (M = Cr or W), at –78°C with BuLi, followed by the treatment with $ClPPh_2$ afforded the targeted compounds, $(CO)_5M{=}C(NMe_2)CH_2PPh_2$, **26a** and **26b**, respectively (Scheme 4.6).[10] Only product **26b** could be isolated in a satisfactory yield. The chromium analogue could barely be isolated and characterised before it converted completely into the four-membered carbene-phosphine chelate, **27a**, which was then also the main product of this reaction. The conversion of **26b**, into **27b** occurred much slower (albeit even at -20°C in solution). These cyclisations represent the first observation of four-membered carbene-phosphine chelate formation. The phosphorus atom in **26a** also reacted intermolecularly by carbene substitution to give the dinuclear product **28a**. This reaction was not observed for **26b**.

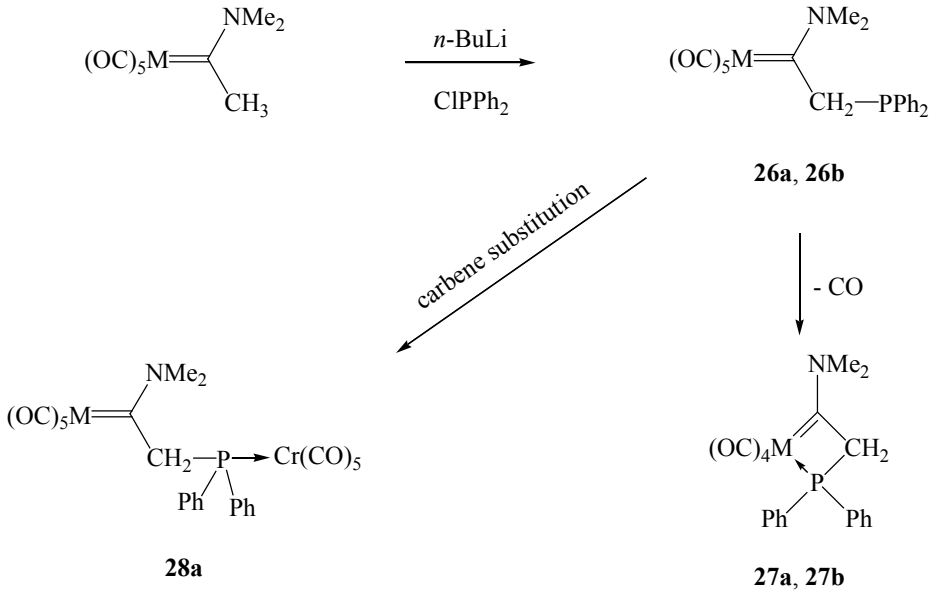

Scheme 4.6 (**a**: M = Cr, **b**: M = W)

All the complexes are soluble in polar organic solvents (dichloromethane and acetone), whereas **27a** and **27b** are less soluble in pentane and hexane. The chromium carbene-phosphine chelate, **27a**, is a surprisingly stable compound and shows no reaction with CS_2, Ph-C≡N, Ph-C≡CH or $MeNHNH_2$. These electron-rich reagents are known to participate in insertion into the metal-carbon bond of heteroatom-stabilised Fischer-type carbene complexes.[15]

4.2.2 Spectroscopic characterisation of complexes 26a, 26b, 27a, 27b and 28a

NMR spectroscopy

4.2.2.1 $(CO)_5Cr=C(NMe_2)CH_2PPh_2$, 26a, $(CO)_5W=C(NMe_2)CH_2PPh_2$, 26b

The NMR data of complexes **26a** and **26b** are summarised in Table 4.1. The ^1H NMR data for the two complexes do not differ much. The phenyl protons resonate as a multiplet. The CH_2 protons appear as a doublet ($^2J_{P-H}$ = 2.0 Hz) due to geminal coupling with the P atom. This coupling constant is much smaller than the range (7 - 14 Hz) normally observed for this type of protons. In general, ^2J geminal coupling constants increase as the angle between the two atoms that experience coupling, decreases. The small coupling constant thus suggests that the H-C-P angle must be in the order of 120°.[16]

Two signals for the NMe_2 protons are observed for both complexes as a result of significant π-interaction of the N atom to give the $C_{carbene}$-N bond significant double bond character (as mentioned in the introduction).[17,18] The signal at higher field (δ 2.54) is assigned to *cis*-NMe and the one at δ 3.67 to *trans*-NMe. The NMe_2 protons in **26a** experience long range coupling to the P atom with coupling constants of 2.2 and 0.5 Hz. Only the *trans*-NMe protons in **26b** couples with the P atom, while the *cis*-NMe protons appear as a singlet.

---

[15] W.D. Wulff, V. Dragisich, J.C. Huffman, R. W. Haesler, D.C. Yang, *Organometallics*, 1989, **8**, 2196; H. Fischer, S. Zeuner, *J. Organomet. Chem.*, 1987, **327**, 63; R. Aumann, E. Kuckert, *Chem. Ber.*, 1987, **120**, 1939; E. O. Fischer, R. Aumann, *Angew. Chem., Int. Ed., Engl.*, 1967, **6**, 181.

[16] D.L. Pavia, G.M. Lampman, G.S. Kriz, *Introduction to Spectroscopy*, 3rd Edition, Harcourt College Publishers, Fort Worth, 2001, p. 221.

[17] E. Moser, E.O. Fischer, *J. Organomet. Chem.*, 1968, **13**, 387.

[18] D.W. Macomber, P. Madhukar, R.D. Rogers, *Organometallics*, 1989, **8**, 1275.

Table 4.1 ^{1}H, ^{13}C and ^{31}P NMR data of **26a** and **26b** in CD_2Cl_2

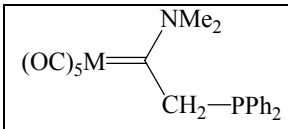

M = Cr **26a**
M = W **26b**

Assignment	δ / ppm **26a**	δ / ppm **26b**
^{1}H NMR		
Ph	7.45 (10H, m)	7.45 (10H, m)
CH_2	4.04 (2H, d, $^{2}J_{P-H}$ = 2.0 Hz)	4.13 (2H, d, $^{2}J_{P-H}$ = 2.0 Hz)
trans-NMe	3.67 (3H, d, $^{5}J_{P-H}$ = 2.2 Hz)	3.67 (3H, d, $^{5}J_{P-H}$ = 2.1 Hz)
cis-NMe	2.54 (3H, d, $^{5}J_{P-H}$ = 0.5 Hz)	2.54 (3H, s)
^{13}C NMR		
$C_{carbene}$	271.2 (d, $^{2}J_{P-C}$ = 16.8 Hz)	253.0 (d, $^{2}J_{P-C}$ = 18.2 Hz, J_{W-C} = 95.2 Hz)
CO_{trans}	224.1 (s)	203.7 (s, J_{W-C} = 125.4 Hz)
CO_{cis}	218.9 (d, $^{4}J_{P-C}$ = 2.8 Hz)	200.0 (d, $^{4}J_{P-C}$ = 4.3 Hz, J_{W-C} = 127.7 Hz)
C_{ipso}	137.2 (d, J_{P-C} = 19.6 Hz)	137.1 (d, J_{P-C} = 18.6 Hz)
C_{ortho}	133.6 (d, $^{2}J_{P-C}$ = 20.5 Hz)	133.5 (d, $^{2}J_{P-C}$ = 20.5 Hz)
C_{para}	129.9 (s)	129.8 (s)
C_{meta}	129.4 (d, $^{3}J_{P-C}$ = 6.5 Hz)	129.2 (d, $^{3}J_{P-C}$ = 6.5 Hz)
CH_2	54.2 (m)	56.0 (d, J_{P-C} = 24.2 Hz)
trans-NMe	53.5 (s)	56.6 (d, $^{4}J_{P-C}$ = 2.8 Hz)
cis-NMe	43.4 (d, $^{4}J_{P-C}$ = 1.8 Hz)	42.1 (d, $^{4}J_{P-C}$ = 1.8 Hz)
^{31}P NMR		
PPh_2	-14.9 (s)	-12.7 (s)

Pectora roborant cultus recti

The carbene carbon of **26a** resonates at δ 271.2 as a doublet in the ^{13}C NMR spectrum. The chemical shift of the carbene carbon is typical for chromium aminocarbene complexes.[23,19] The coupling constant of the carbene carbon with the P atom is 16.8 Hz agreeing with $^{2}J_{P-C}$ reported for similar chromium carbene complexes.[20] The chemical shifts of the signals for the CO ligands are normal.[23,19,21] The *trans*-CO carbon signal (δ 224.1) does not show coupling with the P atom while the *cis*-CO carbons (δ 218.9) couple with the P atom (2.8 Hz). The phenyl carbons appear as

[19] R. Imwinkelried, L.S. Hegedus, *Organometallics*, 1988, **7**, 702.

[20] R. Streubel, S. Priemer, J. Jeske, P.G. Jones, *J. Organomet. Chem.*, 2001, **617 - 618**, 423.

[21] C. Kelly, M.R. Terry, A. Kaplan, G.L. Geoffroy, N. Lugan, R. Mathieu, B.S. Haggerty, A.L. Rheingold, *Inorg. Chim. Acta*, 1992, **198 - 200**, 601.

doublets, as result of coupling with the P atom. The *para*-phenyl carbon, however, appears as a singlet. The CH_2 carbon resonates as a multiplet at δ 54.2; a phosphorus-carbon coupling constant could not be determined. The singlet at δ 53.5 has been assigned to *trans*-NMe and the doublet ($^4J_{P-C}$ = 1.8 Hz) at δ 43.5 to *cis*-NMe.

The doublet at δ 253.0 in the ^{13}C NMR spectrum of **26b** is due to the carbene carbon and this resonance is normal for tungsten aminocarbene complexes.[23,12,18,22] Phosphorus-carbon coupling ($^2J_{P-C}$ = 18.2 Hz) and tungsten-carbon coupling (J_{W-C} = 95.2 Hz) are present for this carbon. As in **26a**, the *trans*-CO carbon does not experience coupling to the P atom but shows tungsten-carbon coupling of 125.4 Hz. *Cis*-CO appears as a doublet at δ200.0 showing both phosphorus-carbon (4.3 Hz) and tungsten-carbon coupling (127.7 Hz). These chemical shifts and tungsten-carbon coupling constants are similar to reported values.[12] The CH_2 carbon (δ 56) couples with the P atom and has a coupling constant of 24.2 Hz. Each carbon of the NMe_2 group appears as a doublet due to coupling to the P atom with coupling constants of 2.8 and 1.8 Hz respectively. These coupling constants compare well to those observed for **26a**.

The P atoms in **26a** and **26b** resonate as singlets at δ -14.9 and -12.7 respectively in the ^{31}P NMR spectra of the two complexes.

The NMR data of complex **26a** (Table 4.2) have also been recorded in $(CD_3)_2CO$. The data are similar to the data in CD_2Cl_2. The signal for the CH_2 carbon is, however, now a well-resolved doublet with a ^{31}P - ^{13}C coupling constant of 24.2 Hz. This coupling constant is the same as the one determined for **26b**.

[22] D.W. Macomber, P. Madhukar, *J. Organomet. Chem.*, 1992, **433**, 279.

Table 4.2 ^{1}H, ^{13}C and ^{31}P NMR data of **26a** in $(CD_3)_2CO$

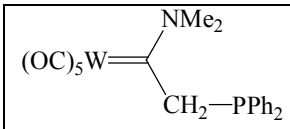

Assignment	δ / ppm	Assignment	δ / ppm
^{1}H NMR		**^{13}C NMR**	
Ph	7.49 (10H, m)	$C_{carbene}$	268.7 (d, $^{2}J_{P-C}$ = 18.2 Hz)
CH_2	4.18 (2H, d, $^{2}J_{P-H}$ = 2.5 Hz)	CO_{trans}	225.0 (s)
trans-NMe	3.80 (3H, d, $^{5}J_{P-H}$ = 2.2 Hz)	CO_{cis}	219.8 (d, $^{4}J_{P-C}$ = 3.0 Hz)
cis-NMe	2.73 (3H, d, $^{5}J_{P-H}$ = 0.7 Hz)	C_{ipso}	138.5 (d, J_{P-C} = 19.8 Hz)
		C_{ortho}	134.7 (d, $^{2}J_{P-C}$ = 21.3 Hz)
^{31}P NMR		C_{para}	130.9 (s)
PPh_2	-14.0 (s)	C_{meta}	130.3 (d, $^{3}J_{P-C}$ = 7.6 Hz)
		CH_2	55.4 (d, J_{P-C} = 24.2 Hz)
		trans-NMe	55.1 (s)
		cis-NMe	44.7 (d, $^{4}J_{P-C}$ = 3.1 Hz)

4.2.2.2 $(CO)_4Cr=C(NMe_2)CH_2PPh_2$, 27a, $(CO)_4W=C(NMe_2)CH_2PPh_2$, 27b

The NMR data of complexes **27a** and **27b** are summarised in Table 4.3. The signals in the ^{1}H NMR spectra of the two complexes are also comparable. The phenyl protons appear as two multiplets whereas they were one multiplet for both **26a** and **26b**. The phenyl groups are in chemically different environments as a result of the coordination of the P atom to a metal (Cr or W). The CH_2 protons of **27a** and **27b** are slightly deshielded when compared to the same signals in **26a** and **26b** due to this coordination. Likewise to **26a** and **26b**, the CH_2 protons resonate as doublets but the coupling constants ($^{2}J_{P-H}$ = 9.2 Hz for both complexes) are greater than that observed for **26a** and **26b** ($^{2}J_{P-H}$ = 2.0 Hz). The coupling constant of 9.2 Hz falls in the range (7 - 14 Hz) predicted for geminal coupling between ^{1}H and ^{31}P.[16] *Cis*-NMe and *trans*-NMe in **27a** resonate as singlets. These protons do not experience ^{31}P - ^{1}H coupling as was noted for **26a**. Only the *trans*-NMe protons of **27b** display coupling but a multiplet is observed for them instead of the expected doublet.

Table 4.3 ^{1}H, ^{13}C and ^{31}P NMR data of **27a** and **27b**

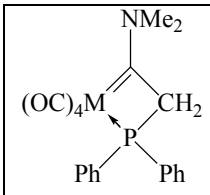

M = Cr **27a**
M = W **27b**

Assignment	δ / ppm **27a**	δ / ppm **27b**
^{1}H NMR		
Ph	7.65 (4H, m), 7.48 (6H, m)	7.63 (4H, m), 7.49 (6H, m)
CH_2	4.31 (2H, d, $^{2}J_{P-H}$ = 9.2 Hz)	4.48 (2H, d, $^{2}J_{P-H}$ = 9.2 Hz)
trans-NMe	3.69 (3H, s)	3.58 (3H, m)
cis-NMe	3.20 (3H, s)	3.17 (3H, s)
^{13}C NMR		
$C_{carbene}$	270.3 (d, $^{2}J_{P-C}$ = 4.8 Hz)	243.4 (d, $^{2}J_{P-C}$ = 13.0 Hz)
$CO_{cis\ to\ P}$	232.9 (d, $^{2}J_{P-C}$ = 16.1 Hz)	217.0 (d, $^{2}J_{P-C}$ = 7.4 Hz)
$CO_{trans\ to\ P}$	232.4 (d, $^{2}J_{P-C}$ = 2.9 Hz)	215.0 (d, $^{2}J_{P-C}$ = 26.0 Hz, J_{W-C} = 130.0 Hz)
CO_{axial}	223.1 (d, $^{2}J_{P-C}$ = 13.2 Hz)	205.4 (d, $^{2}J_{P-C}$ = 7.4 Hz, J_{W-C} = 131.0 Hz)
C_{ipso}	136.2 (d, J_{P-C} = 43.5 Hz)	135.1 (d, J_{P-C} = 33.4 Hz)
C_{ortho}	132.3 (d, $^{2}J_{P-C}$ = 12.3 Hz)	132.7 (d, $^{2}J_{P-C}$ = 13.9 Hz)
C_{para}	130.4 (d, $^{4}J_{P-C}$ = 1.8 Hz)	130.6 (d, $^{4}J_{P-C}$ = 1.9 Hz)
C_{meta}	129.0 (d, $^{3}J_{P-C}$ = 10.4 Hz)	129.2 (d, $^{3}J_{P-C}$ = 10.2 Hz)
CH_2	58.0 (d, J_{P-C} = 32.1 Hz)	61.7 (d, J_{P-C} = 36.2 Hz)
trans-NMe	50.2 (s)	52.8 (s)
cis-NMe	41.6 (s)	40.5 (s)
^{31}P NMR		
PPh_2	6.6 (s)	-38.0 (s, J_{W-P} = 182.1 Hz)

The doublet at δ 270.3 in the ^{13}C NMR spectrum of **27a** is assigned to the carbene carbon. Despite the chelate formation that would have had a shielding effect on the carbene carbon the chemical shift of this carbon does not differ from the carbene carbon in **26a**. The phosphorus-carbon coupling ($^{2}J_{P-C}$ = 4.8 Hz) for the carbene carbon in **27a** is however smaller than that in **26a** ($^{2}J_{P-C}$ = 16.8 Hz). The CO ligand *cis* to the coordinated P atom appears as a doublet at δ 232.9 with a ^{31}P - ^{13}C coupling constant of 16.1 Hz while the CO *trans* to the P atom at δ 232.4 has a much smaller coupling (2.9 Hz). The two axial CO ligands appear as a doublet. Only three signals for the CO ligands in **27a** are observed apposed to four signals shown for a tetracarbonyl chromium complex with another bidentate carbene-phosphine ligand.[11] The tetracarbonyl chromium carbene complex

(**xi**) in Scheme 4.5 shows three signals with similar chemical shifts as in complex **27a**.[13] All the phenyl carbons in **27a** couple to the P atom and have been assigned according to the ^{31}P - ^{13}C coupling constants. The CH_2 carbon resonates as a doublet at δ 58.0, slightly downfield (Δδ 3.8) from the signal for CH_2 in **26a**. This deshielding results from the electron donation from the P atom to Cr. The ^{31}P - ^{13}C coupling of 32.1 Hz is greater than the same coupling (J_{P-C} = 24.2 Hz) for **26a**. As in **26a**, *trans*-NMe and *cis*-NMe appear as singlet each in the ^{1}H NMR spectrum of **27a**.

The signal for the carbene carbon of **27b** appears at δ 243.5 in the ^{13}C NMR spectrum, 9.6 ppm upfield from the signal for the carbene carbon in **26b**. Chelate formation increases the electron density on the W atom and the carbene atom becomes more shielded by backdonation than in **26b**. The ^{31}P - ^{13}C coupling constant of 13 Hz, for this doublet, is smaller than in **26b** ($^{2}J_{P-C}$ = 18.2 Hz). This decrease upon chelate formation is also observed for **27a**. The doublets at δ 217 and δ 205.4 are assigned to the CO *cis* to the P atom and the axial CO ligands respectively. The CO *trans* to the P atom resonates as a doublet at δ 215, with a coupling constant of 26 Hz, which is larger than the coupling constant for the former CO ligands. This is in contrast to the situation in **27a** where the coupling constant for the CO *trans* to the P atom is much smaller than the constants for the other CO ligands. Only the CO *trans* to the P atom and the axial CO ligands experience coupling with tungsten (J_{W-C} = 131.0 Hz). The chemical shifts and coupling constants of the carbene signals and the CO signals compare well with those reported for a tetracarbonyl tungsten carbene complex, $(CO)_4W$=C(NCH$_2$CH$_2$CH$_2$CH$_2$)C(D)=C(Ph)P(Ph)C{Ph}=CPh, **A**, with a bidentate carbene-phosphine ligand even though four signals for the CO ligands are reported.[12] Analogous to **27a**, the *cis* and *trans* NMe carbons appear as a singlet each. Again, chelate formation has a deshielding effect (Δδ 5.1) on CH_2 and the ^{31}P - ^{13}C coupling (J_{P-C} = 36.2 Hz) is greater than that observed for **26b** (J_{P-C} = 24.2 Hz).

The ^{31}P NMR chemical shift of **27a** (δ 6.6) appears downfield (Δδ 22) compared to the same signal in the ^{31}P NMR spectrum of **26a** as a result of the backfolding and coordination of the phosphorus atom to the Cr. The opposite was found for the tungsten complex **27b** where the signal (δ -38) appears at a more upfield position (Δδ 25) compared to **26b**.

4.2.2.3 $(CO)_5Cr=C(NMe_2)CH_2P(Ph_2)Cr(CO)_5$, 28a

The NMR data of complex **28a** are summarized in Table 4.4. The phenyl protons appear as two multiplets, identical to those for **27a** and **27b**. The CH_2 protons show coupling of 6.5 Hz to the P atom, which is smaller than the same coupling in **27a** and **27b** ($^2J_{P\text{-}H}$ = 9.2 Hz). A smaller H-C-P angle should result in greater geminal coupling but the opposite is observed for **28a**.[16] The H-C-P angle of 107.5°, obtained from the crystal structure of **28a** (Section 4.2.3.3), is smaller than the same angle in **27a** (112.4°) and **27b** (112.1°). This phenomenon is probably the result of the coordination of the phosphorus atom to $Cr(CO)_5$. NMe_2 resonates as two singlets in a like manner to complexes **26a - 27b**.

Table 4.4 ^1H, ^{13}C and ^{31}P NMR data of **28a** in CD_2Cl_2

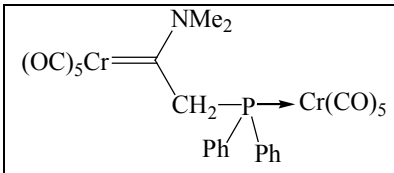

Assignment	δ / ppm	Assignment	δ / ppm
^{1}H NMR		**^{13}C NMR**	
Ph	7.66 (4H, m), 7.52 (6H, m)	$CO_{trans\ to\ P}$	221.6 (d, $^2J_{P\text{-}C}$ = 6.5 Hz)
CH_2	4.56 (2H, d, $^2J_{P\text{-}H}$ = 6.5 Hz)	$CO_{trans\ to\ carbene}$	217.1 (s)
trans-NMe	3.38 (3H, s)	$CO_{cis\ to\ P}$	217.0 (d, $^2J_{P\text{-}C}$ = 19.5 Hz)
cis-NMe	2.86 (3H, s)	$CO_{cis\ to\ carbene}$	216.7 (s)
		C_{ipso}	135.0 (d, $J_{P\text{-}C}$ = 35.3 Hz)
^{31}P NMR		C_{ortho}	133.4 (d, $^2J_{P\text{-}C}$ = 11.1 Hz)
PPh_2	55.1 (s)	C_{para}	131.2 (d, $^4J_{P\text{-}C}$ = 1.8 Hz)
		C_{meta}	129.1 (d, $^3J_{P\text{-}C}$ = 9.3 Hz)
		trans-NMe	56.0 (s)
		cis-NMe	47.0 (s)

The low intensity signal for the carbene carbon is not observed in the ^{13}C NMR spectrum of **28a**. The CO ligands *trans* and *cis* to the carbene ligand have been assigned to the singlets at δ 217.1 and 216.7 respectively while the CO ligands *trans* and *cis* to the P atom appear as doublets at δ 221.6 and 217.0 respectively. The coupling constant for the doublet that has been assigned to the CO ligands *cis* to the P atom is greater than that for the CO *trans* to the P atom. This is consistent with

the couplings observed for **26a**, **26b**. The chemical shifts for the CO carbons are similar to those in **26a** and in $(CO)_5Cr=C(NMe_2)CH_2S(Me)Cr(CO)_5$ (*vide infra*).[23] The signals for the phenyl carbons also have the same chemical shifts and coupling constants as those in **27a** and **27b**. The signal for the CH_2 in **28a** is not visible and is probably obscured by the signal for CD_2Cl_2. The NMe_2 carbons each appears as a singlet.

The P atom in **28a** is deshielded and appears at δ 55.1 upon coordination of the P atom to a $Cr(CO)_5$ group. This signal in the ^{31}P NMR spectrum of **28a** is downfield from the signals for **26a** and **27a** (Δδ 70 and 48.5 respectively).

Mass spectrometry

Table 4.5 Mass spectrometry data for complexes **26a**, **26b** and **28a**

Complex	m/z	Relative intensity (%)	Fragment ion
26a	447	1	M^+
	419	3	$[M - CO]^+$
	391	2	$[M - 2CO]^+$
	363	1	$[M - 3CO]^+$
	335	4	$[M - 4CO]^+$
	307	15	$[M - 5CO]^+$
26b	551	67	$[M - CO]^+$
	4.23	4	$[M - 2CO]^+$
	495	100	$[M - 3CO]^+$
	467	52	$[M - 4CO]^+$
	439	91	$[M - 5CO]^+$
28a	419	6	$[M - Cr(CO)_5 - CO]^+$
	391	5	$[M - Cr(CO)_5 - 2CO]^+$
	363	3	$[M - Cr(CO)_5 - 3CO]^+$
	335	10	$[M - Cr(CO)_5 - 4CO]^+$
	307	78	$[M - Cr(CO)_5 - 5CO]^+$

[23] E. Stander, *M. Sc. Thesis*, University of Stellenbosch, 2005.

The molecular ion peak was observed for complexes **26a**, **27a** and **27b** but not for **26b** and **28a** (Tables 4.5 and 4.6). The fragmentation patterns for all the complexes are characterised by the sequential loss of the carbonyl ligands. In **28a** CO loss is preceded by the expulsion of the $Cr(CO)_5$ fragment.

Table 4.6 Mass spectrometry data for complexes **27a** and **27b**

Complex	m/z	Relative intensity (%)	Fragment ion
27a	419	13	M^+
	391	5	$[M - CO]^+$
	363	5	$[M - 2CO]^+$
	335	20	$[M - 3CO]^+$
	307	60	$[M - 4CO]^+$
27b	551	56	M^+
	495	100	$[M - 2CO]^+$
	467	51	$[M - 3CO]^+$
	439	100	$[M - 4CO]^+$

Infrared spectroscopy

The IR spectra of all compounds in the ν(CO) region (Table 4.7) are typical for either octahedral transition metal pentacarbonyl or tetracarbonyl compounds. The spectra of the pentacarbonyl complexes **26a** and **26b** are similar to those of the starting compounds (dimethylaminomethylcarbene)pentacarbonylchromium(0) and its tungsten analogue in terms of the relative intensities of the infrared active bands and their stretching frequencies. Groups on the carbon atom α to the carbene carbon are too remote to change the local symmetry of the $M(CO)_5$ unit and thus do not cause a change in the IR active bands. Five infrared active bands were observed for **26a** and **26b** instead of the expected four bands due to the C_{4v} local symmetry of the $M(CO)_5$ unit.[24,25,26] The B_2 vibration, that is normally only Raman active, becomes infrared active

[24] S. Lotz, *Ph.D. Dissertation*, Rand Afrikaans University, 1978.

[25] J.A. Connor, E.O. Fischer, *J. Chem. Soc. (A)*, 1969, 578.

[26] E.O. Fischer, H-J. Kollmeier, *Chem. Ber.*, 1971, **104**, 1339.

because these complexes do not have exact C_{4v} symmetry. Five bands for the CO vibrations have been previously reported for other complexes containing the $M(CO)_5$ unit.[27,28]

Table 4.7 The IR data of complexes **26a**, **26b**, **27a**, **27b** and **28a** in CH_2Cl_2

Complex	ν(CO) / cm^{-1} (Intensity)	Assignment
26a	2051.6 (m)	$A_1^{(1)}$
	1997.2 (vw)	B_1
	1963.1 (sh)	B_2
	1923.0 (s)	E
	1855.8 (sh)	$A_1^{(2)}$
26b	2059.5 (m)	$A_1^{(1)}$
	2006.6 (w)	B_1
	1963.1 (sh)	B_2
	1919.8 (s)	E
	1846.7 (w)	$A_1^{(2)}$
27a	1997.8 (m)	$A_1^{(1)}$
	1899.6 (sh)	$A_1^{(2)}$
	1890.1 (s)	B_1
	1848.6 (m)	B_2
27b	2006.7 (m)	$A_1^{(1)}$
	1898.6 (s)	B_1
	1846.0 (m)	B_2
28a	2064.2 (w)	$A_1^{(1)}$
	2053.8 (w)	$A_1^{(1)}$
	1980.8 (sh)	E
	1937.9 (s)	E

[27] C.P. Casey, A.J. Shusterman, *Organometallics*, 1985, **4**, 736.

[28] D. Rieger, S.D. Lotz, U. Kernbach, S. Schröder, C. André, W.P. Fehlhammer, *Inorg. Chim. Acta*, 1994, **222**, 275.

Four infrared active bands are also expected for the $M(CO)_4$ unit because of its approximate C_{2v} local symmetry.[10,24] The infrared spectrum of **27a** shows these expected four bands. The infrared spectrum of **27b** exhibits only three bands and this could be due to the overlap of the strong B_1 band and the $A_1^{(2)}$ band. Two sets of $A_1^{(1)}$ and E bands are observed in the spectra of the tetracarbonyl complex **28a**. The bands with the larger wave numbers are assigned to the phosphine section (ν = 2064.2 and 1980.8 cm^{-1}) and the others (at ν = 2053.8 and 1937.9 cm^{-1}) to the carbene part of the carbene-phosphine bridged dinuclear complexes. The infrared spectrum of **28a** is similar to that of $(CO)_5Cr=C(NMe_2)CH_2S(Me)Cr(CO)_5$ (*vide infra*).[23]

4.2.3 Crystal and molecular structure determinations by single crystal X-ray diffraction

The incorporation of sulfur in the carbene side chain of an aminocarbene of tungsten and chromium has been accomplished concomitant with this work.[23] Reaction of the aminocarbene complex anions, $[(CO)_5M=C(NMe_2)CH_2]^-$ (M = Cr or W), with the thiosulfonium salt, $[Me_2(MeS)S]BF_4$ furnishes the desired complexes, $(CO)_5M=C(NMe_2)CH_2SMe$. The double sulfonated products, $(CO)_5M=C(NMe_2)CH(SMe)_2$, are also present. The sulfur donor atom also coordinated intramolecularly and intermolecularly *via* carbonyl and carbene substitution respectively to a metal center to form $(CO)_4\overline{M=C(NMe_2)CH_2SMe}$ and $(CO)_5M=C(NMe_2)CH_2S(Me)M(CO)_5$. In the latter complex the carbene ligand acted as a monodentate ligand towards the second metal. The crystal structures of $(CO)_4\overline{M=C(NMe_2)CH_2SMe}$ (M = Cr or W) and $(CO)_5Cr=C(NMe_2)CH_2S(Me)Cr(CO)_5$ will be compared to the structures of the corresponding complexes, determined in this study.

Crystalisation of the tetracarbonyl complexes **27a** and **27b** from CH_2Cl_2/pentane solutions and complex **28a** from a diethyl ether/hexane solution yielded yellow crystals suitable for single crystal X-ray determination. The hydrogen atoms are omitted from the Figures 4.1, 4.3 and 4.5 for clarity. Hydrogen atoms are also not shown in the packing diagrams of the complexes in Figures 4.2, 4.4 and 4.6. There are no short intermolecular contacts in the unit cells of **27a**, **27b** and **28a**. The molecules in the in the unit cells of all three complexes are organised by Van der Waals forces.

*4.2.3.1 The crystal and molecular structure of $(CO)_4\overline{Cr=C(NMe_2)CH_2PPh_2}$, **27a***

The molecular structure of **27a** is shown in Figure 4.1, with selected bond lengths and angles summarized in Table 4.8. No other examples of C,P-four-membered chelates could be found in the

literature. Complex **27a** displays approximate octahedral coordination geometry. The largest digression from the ideal angle of 180° is shown by the ligand-metal-ligand angles that involve the atoms of the four-membered ring, namely C(6)-Cr(1)-P(1) [168.1(1)°] and C(5)-Cr(1)-C(1) [166.0(1)°]. Such large deviations are apparently required for the formation of the four-membered ring. The angle C(7)-Cr(1)-C(8) [176.1(1)°] is bent away from the non-carbonyl ligands to accommodate the steric demand that this chelating ligand imposes. The bite angle in the chelating ligand, C(1)-Cr(1)-P(1) [68.2(1)°], is much smaller than 90° but compares well with the bite angles of a carbene-thioether chelate in $(CO)_4\overline{Cr{=}C(NMe_2)CH_2}SMe$ [69.7(1)°].[23] The bite angles in the five-membered carbene-phosphine chelate of chromium, $[(CO)_4\overline{Cr{=}C(NH_2)C(OEt){=}CHPPh_2}]$, **B**, [79.3(1)°][10] and six-membered carbene-phosphine chelate, $[(CO)_4\overline{Cr{=}C(CH_2R)N(Me)CH_2CH(Ph)PPh_2}]$ {R = *p*$NO_2C_6H_4$-CH(OH)-}, **C**, [91.4(2)°][11], are larger, as expected for larger chelate rings. The maximum deviation from the least square plane calculated through C(1), C(2), P(1) and Cr(1) is by C(1) [0.103(1) Å] and C(2) [-0.115(1) Å]. C(2) lies 0.304(3) Å below the plane through C(1), P(1) and Cr(1). This out of plane bending is required to accommodate the strain in the four-membered ring.

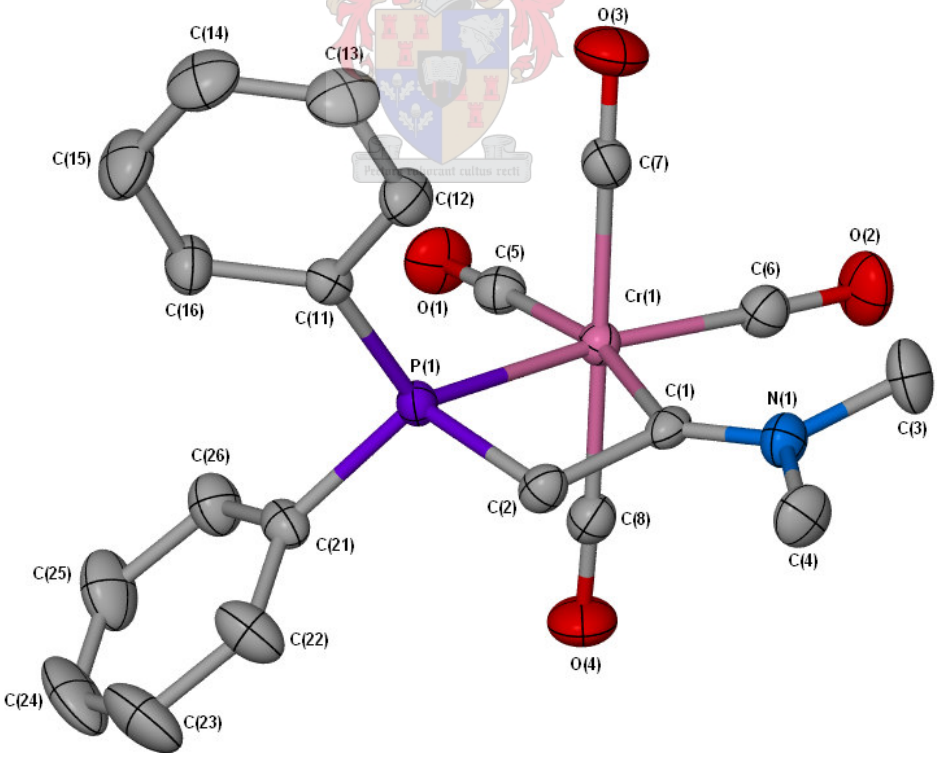

Figure 4.1 Molecular structure of **27a**, showing the numbering scheme, generated in POV-Ray

The Cr-$C_{carbene}$ distance of 2.107(2) Å in **27a** falls within the 2.10 – 2.15 Å range reported for other aminocarbene complexes of chromium.[2,11,29] The Cr-P distance [2.359(1) Å] in **27a** is surprisingly near to those of five and six-membered carbene-phosphine chelates of chromium, **B**, and **C**, [2.379(2) Å and 2.352(1) Å respectively].[10,11] The normality of the Cr-$C_{carbene}$ and Cr-P distances illustrates that the strain in this four-membered ring is alleviated by the out of plane bending of C(2), as mentioned above, rather than by a shortening in these two bonds. The $C_{carbene}$-N distance [1.309(3) Å] reflects its double bond character, which is also evident in the ^{1}H and ^{13}C NMR spectra of **26a** (Section 4.2.2.1).[29] The Cr(1)-C(5) [1.855(2) Å] and Cr(1)-C(6) [1.851(2) Å] bond lengths are the same but are significantly shorter than Cr(1)-C(7) [1.885(2)] and Cr(1)-C(8) [1.888(2) Å]. This illustrates the greater *trans*-influence of the CO ligand when compared to the phosphine and the carbene ligands that exhibit similar *trans*-influences.

Table 4.8 Selected bond lengths (Å) and angles (º) for **27a**

Cr(1)-C(1)	2.107(2)	Cr(1)-C(5)	1.855(2)
Cr(1)-P(1)	2.359(1)	Cr(1)-C(6)	1.851(2)
C(1)-C(2)	1.518(3)	Cr(1)-C(7)	1.885(2)
C(2)-P(1)	1.838(2)	Cr(1)-C(8)	1.888(2)
C(1)-N(1)	1.309(3)	C(5)-O(1)	1.151(3)
N(1)-C(3)	1.470(5)	C(6)-O(2)	1.159(3)
N(1)-C(4)	1.473(3)	C(7)-O(3)	1.148(3)
		C(8)-O(4)	1.142(3)
C(1)-Cr(1)-P(1)	68.2(1)	C(6)-Cr(1)-P(1)	168.1(1)
Cr(1)-C(1)-C(2)	105.8(1)	C(8)-Cr(1)-C(7)	176.1(1)
Cr(1)-C(1)-N(1)	137.6(2)	C(5)-Cr(1)-C(1)	166.0(1)
C(1)-C(2)-P(1)	96.5(1)	C(3)-N(1)-C(4)	113.2(2)
C(2)-P(1)-Cr(1)	87.0(1)	N(1)-C(1)-C(2)	116.6(2)

The packing of the molecules of **27a** viewed along the a-axis (A) and b-axis (B) is shown in Figure 4.2. The molecules are packed on top of each other and form layers parallel to both axis. The molecules are also packed in an up-down alternating fashion (A).

[29] P.E. Baikie, E.O. Fischer, O.S. Mills, *J. Chem. Soc., Chem. Commun.*, 1967, 1199.

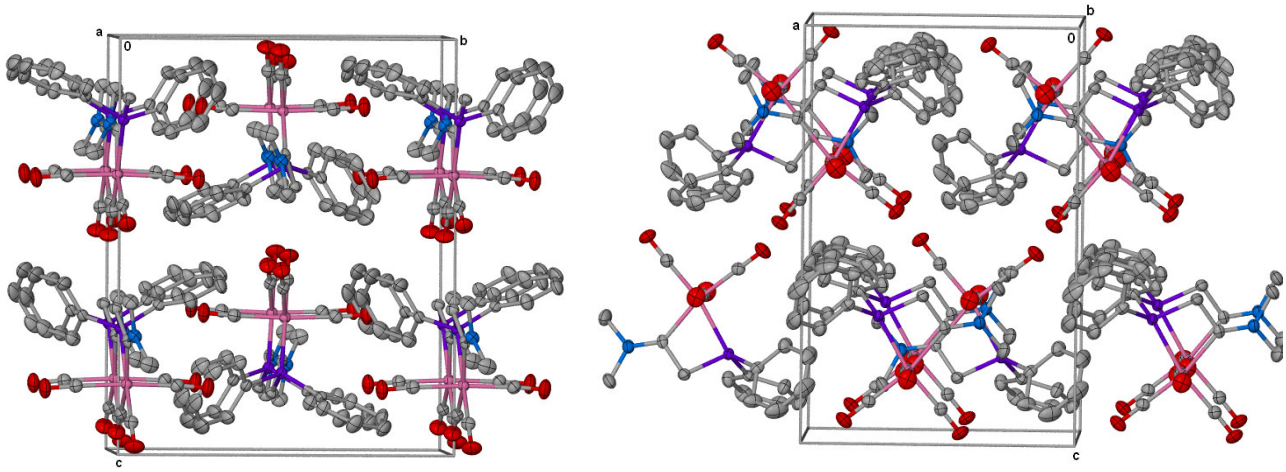

A B

Figure 4.2 The packing diagram of the molecules of **27a** in the unit cell, viewed along the a-axis (A) and the b-axis (B)

*4.2.3.2 The crystal and molecular structure of $(CO)_4W{=}C(NMe_2)CH_2PPh_2$, **27b***

Compounds **27b** (Figure 4.3) and **27a** are isostructural and these complexes, therefore, display similar characteristics. Selected bond lengths and angles for **27b** are listed in Table 4.9. The largest divergence from the ideal 180° for ligand-metal-ligand angles, expected for octahedral complexes, is experienced by C(6)-W(1)-P(1) [165.3(1)°] and C(5)-W(1)-C(1) [164.1(1)°], similar to the result for **27a** while the angle C(7)-Cr(1)-C(8) [176.9(1)°] is bent away from the non-carbonyl ligands. The bite angle of the chelating ligand, C(1)-W(1)-P(1) [64.9(1)°], is much smaller than 90° and compares well with the bite angle of the carbene thioether chelate in $(CO)_4W{=}C(NMe_2)CH_2SMe$ [66.1 (1)].[23] C(2) [-0.116(2) Å] and C(1) [0.104(2) Å] exhibit maximum deviation from the least square plane calculated through C(1), C(2), P(1) and W(1). C(2) is bent away by 0.289(5) Å from the plane through C(1), P(1) and W(1) to accommodate the strain in the four-membered ring.

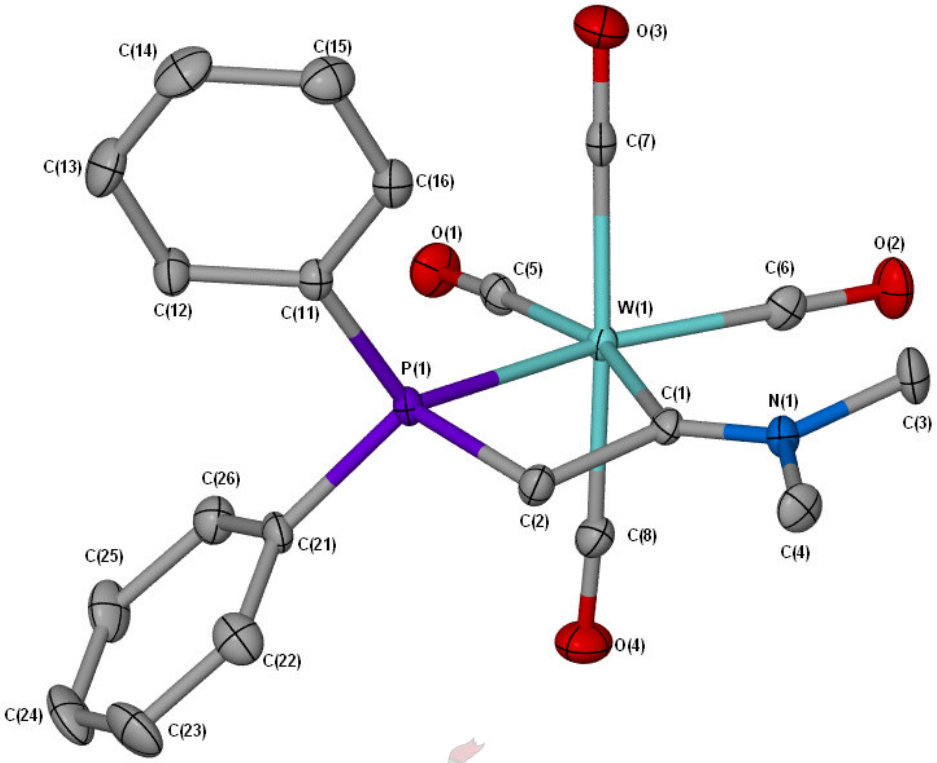

Figure 4.3 Molecular structure of **27b**, showing the numbering scheme, generated in POV-Ray

The W-$C_{carbene}$ bond length [2.237(3) Å] compares well with others reported in literature [2.20 - 2.28 Å] for aminocarbene complexes while the W-P bond length [2.495(1) Å] is only slightly shorter than reported values [2.51 - 2.53 Å] for comparable compounds.[12,18,20,30,31] As in **27a**, the strain in the four-membered ring is greatly relieved through the out of plane bending of C(2) instead of a dramatic change in the W-$C_{carbene}$ and W-P bond lengths. These two distances compare well with those reported for the five-membered carbene-phosphine chelate, **A**, [W-$C_{carbene}$, 2.223(7) Å and W-P, 2.507(2) Å][12] but is longer than the values reported for a the three-membered carbene-phosphine chelate, $(CO)_4\overline{W=C(NEt_2)P}(Ph)Me$, [W-$C_{carbene}$, 2.108(10) Å and W-P, 2.465(3) Å].[32] The indistinguishable W(1)-C(5) [1.990(4) Å] and W(1)-(C(6) [1.985(4) Å] distances are significantly shorter than W(1)-C(7) [2.026(3) Å] and W(1)-C(8) [2.034(3) Å] due to the smaller *trans*-influence of the phosphine and carbene ligands when compared to the CO ligands.

[30] B. Fuss, M. Dede, B. Weibert, H. Fisher, *Organometallics*, 2002, **21**, 4425.

[31] T. Weidmann, K. Sünkel, W. Beck, *J. Organomet. Chem.*, 1993, **459**, 219.

[32] E.O. Fischer, R. Reitmeier, K. Ackermann, *Angew. Chem. Int. Ed. Engl.*, 1983, **22**, 411.

Table 4.9 Selected bond lengths (Å) and angles (°) for **27b**

W(1)-C(1)	2.237(3)	W(1)-C(5)	1.990(4)
W(1)-P(1)	2.495(1)	W(1)-C(6)	1.985(4)
C(1)-C(2)	1.522(4)	W(1)-C(7)	2.026(3)
C(2)-P(1)	1.833(4)	W(1)-C(8)	2.034(3)
C(1)-N(1)	1.309(4)	C(5)-O(1)	1.164(4)
N(1)-C(3)	1.465(4)	C(6)-O(2)	1.158(4)
N(1)-C(4)	1.472(4)	C(7)-O(3)	1.154(4)
		C(8)-O(4)	1.143(4)
C(1)-W(1)-P(1)	64.9(1)	C(6)-W(1)-P(1)	165.3(1)
W(1)-C(1)-C(2)	106.5(2)	C(8)-W(1)-C(7)	173.9(1)
W(1)-C(1)-N(1)	136.3(2)	C(5)-W(1)-C(1)	164.7(1)
C(1)-C(2)-P(1)	98.3(2)	C(3)-N(1)-C(4)	112.1(3)
C(2)-P(1)-W(1)	88.0(1)	N(1)-C(1)-C(2)	117.2(3)

Complexes **27a** and **27b** are isostructural and the packing diagram in the unit cells of these complexes are the same. Figure 4.4 illustrates this (compare with the packing of **27a**, Figure 4.2). The molecules are packed on top of each other and form layers parallel to both axis. The molecules are also packed in an up–down alternating fashion (A).

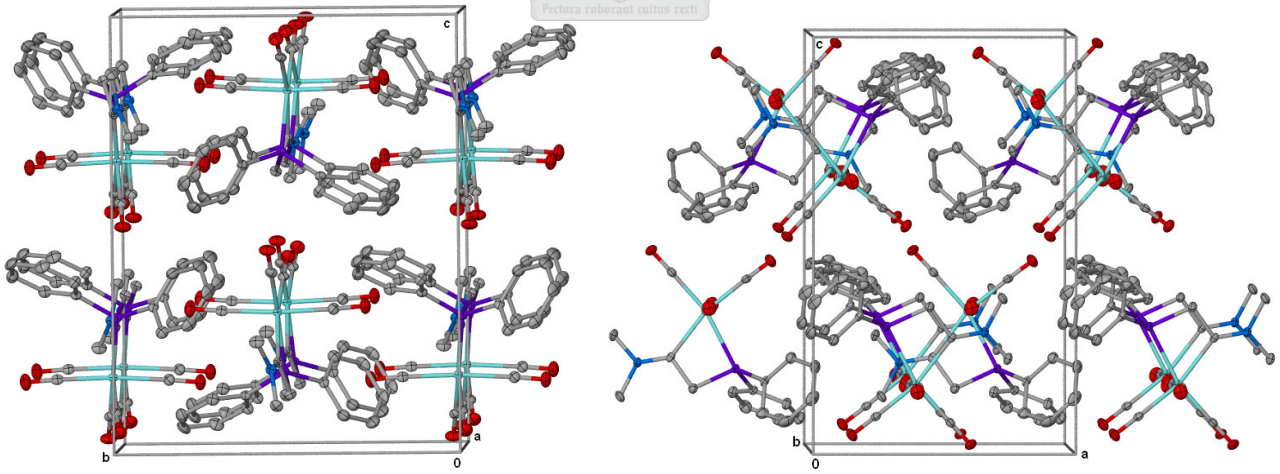

A B

Figure 4.4 The packing diagram of the molecules of **27b** in the unit cell, viewed along the a-axis (A) and the b-axis (B)

4.2.3.3 The crystal and molecular structure of $(CO)_5Cr=C(NMe_2)CH_2P(Ph_2)Cr(CO)_5$, ***28a***

The molecular structure of **28a** is shown in Figure 4.5 and selected bond lengths and angles are given in Table 4.10. The octahedral environment of the Cr atoms is somewhat distorted as illustrated by the angles C(8)-Cr(1)-C(9) [172.1(1)°], C(13)-Cr(2)-C(14) [173.2(1)°] and C(12)-Cr(2)-C(11) [174.8(1)°] that are well bent away from the ideal 180°. These deviations occur to accommodate the steric requirements in the complex and are most pronounced when the non-carbonyl ligand is a carbene. Two of the angles in the bridge between the metal centers in **28a**, C2-P1-Cr2 [117.1(1)°] and C1-C2-P1 [119.7(2)°] are larger than the expected sp^3 angle of 109.5° and thus appear to be opened to accommodate the two $Cr(CO)_5$ groups in this dinuclear compound. In $(CO)_5Cr=C(NMe_2)CH_2S(Me)Cr(CO)_5$ this effect is less marked, C1-C2-S1 [114.6(1)°] and not visible in C2-S1-Cr2 [108.2(1)°] (S1 is approximately sp^3 hybridised).[23] The planes containing Cr, equatorial carbonyl groups [(C(5), C(6), C(7) and C(10), C(13), C(14)] and the phosphine ligand or carbene ligand in **4** form an angle of 79.5(1) and 53.5(2)° respectively with the plane defined by Cr1-C2-P1. Similarly, planes containing Cr, equatorial carbonyl groups and the thioether ligand or carbene ligand in $(CO)_5Cr=C(NMe_2)CH_2S(Me)Cr(CO)_5$ form angles of 58.9(1) and 61.1(1)° respectively with the plane defined by C2-Cr2-S1.[23]

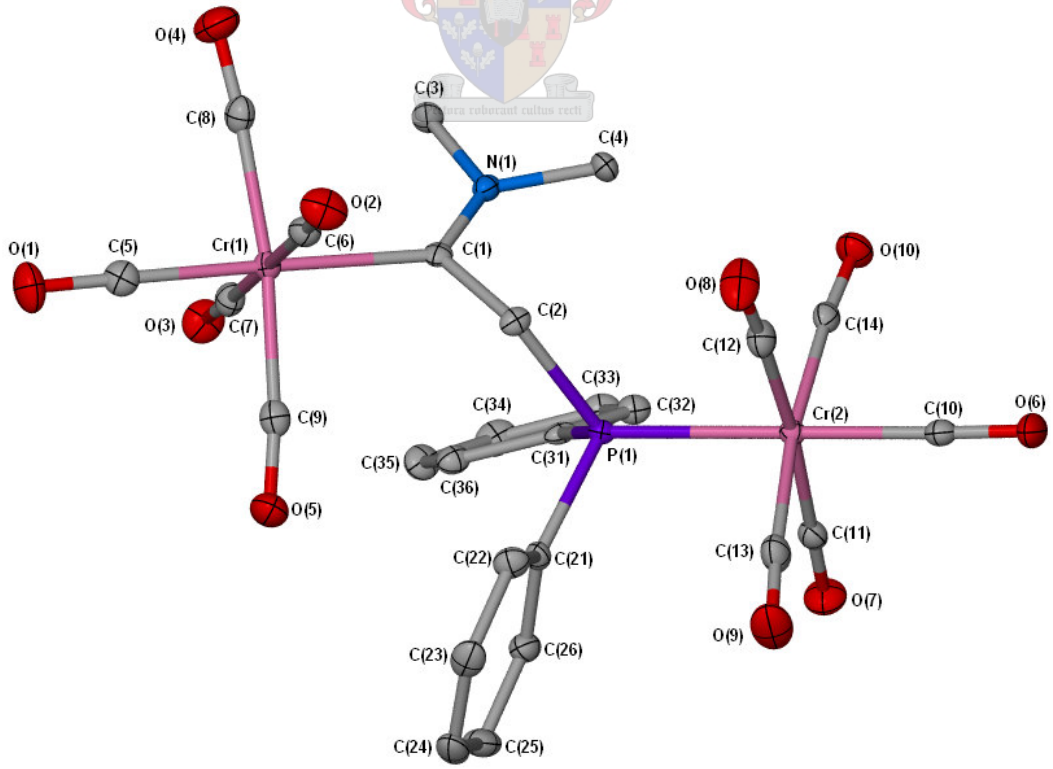

Figure 4.5 Molecular structure of **28a**, showing the numbering scheme, generated in POV-Ray

The Cr-$C_{carbene}$ bond distance in **28a** [2.143(3) Å] compares well with that of **27a** [2.107(2) Å] and $(CO)_5Cr=C(NMe_2)CH_2S(Me)Cr(CO)_5$ [2.129(2) Å][23] and these distances compare well with reported Cr-$C_{carbene}$ distances [2.10 – 2.15 Å] in aminocarbene complexes of chromium.[2] The Cr-P bond length in **28a** [2.401(1) Å] is longer than in **27a** [2.359(1) Å] and slightly shorter than the Cr-P separation in $PPh_3(CO)_4Cr=C(OMe)Me$ [2.42 Å].[33] This bond in **28a** is longer than the same bond in **27a**, because the former does not experience strain due to chelate formation.

Table 4.10 Selected bond lengths (Å) and angles (º) for **28a**

Cr(1)-C(1)	2.143(3)	Cr(2)-C(11)	1.908(3)
Cr(2)-P(1)	2.401(1)	Cr(2)-C(12)	1.889(3)
C(1)-C(2)	1.529(4)	Cr(2)-C(13)	1.910(3)
C(2)-P(1)	1.891(3)	Cr(2)-C(14)	1.891(3)
C(1)-N(1)	1.311(3)	C(5)-O(1)	1.157(3)
N(1)-C(3)	1.475(3)	C(6)-O(2)	1.134(3)
N(1)-C(4)	1.476(3)	C(7)-O(3)	1.139(3)
Cr(1)-C(5)	1.851(3)	C(8)-O(4)	1.144(3)
Cr(1)-C(6)	1.921(3)	C(9)-O(5)	1.143(3)
Cr(1)-C(7)	1.898(3)	C(10)-O(6)	1.146(3)
Cr(1)-C(8)	1.901(3)	C(11)-O(7)	1.136(3)
Cr(1)-C(9)	1.904(3)	C(12)-O(8)	1.146(3)
Cr(2)-C(10)	1.864(3)	C(13)-O(9)	1.140(3)
		C(14)-O(10)	1.145(3)
Cr(1)-C(1)-C(2)	117.1(2)	C(1)-Cr(1)-C(5)	177.4(1)
C(1)-C(2)-P(1)	119.7(2)	C(8)-Cr(1)-C(9)	172.1(1)
C(2)-P(1)-Cr(2)	117.1(1)	C(7)-Cr(1)-C(6)	179.8(1)
Cr(1)-C(1)-N(1)	128.0(2)	C(12)-Cr(2)-C(11)	174.8(1)
N(1)-C(1)-C(2)	114.5(2)	C(10)-Cr(2)-P(1)	179.5(1)
C(3)-N(1)-C(4)	109.7(2)	C(13)-Cr(2)-C(14)	173.2(1)

The Cr(1)-C(5) [1.851(3) Å] and Cr(2)-C(10) [1.864(3) Å] distances are the same but significantly shorter than the other Cr-$C_{carbonyl}$ bond lengths, with Cr(2)-C(12) at 1.889(3) Å being the shortest.

[33] O.S. Mills, A.D. Redhouse, *J. Chem. Soc., Chem. Commun.*, 1966, 815.

This again underlines the similarity in *trans*-influence of the carbene and phosphine ligands and the fact that CO has a greater *trans*-influence than both these ligands.

The packing of the molecules of **28a** in the unit cell is shown in Figure 4.6. The molecules are packed on top of each other, forming layers along the a-axis (A) as well as the b-axis (B). Diethyl ether molecules fill some of the voids in the unit cell.

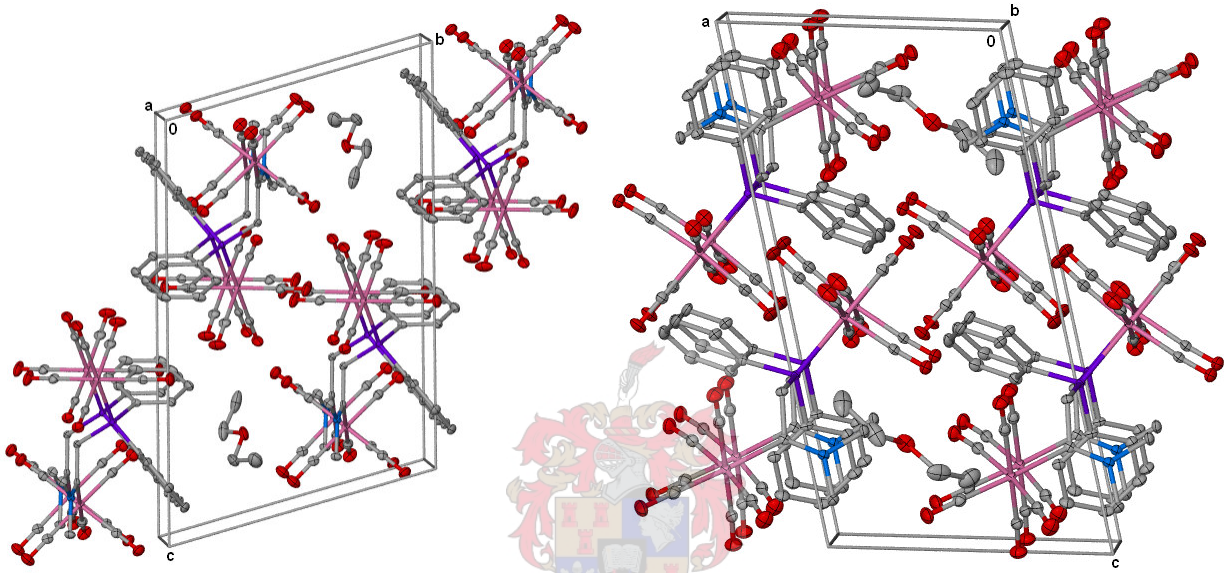

Figure 4.6 The packing diagram of the molecules of **28a** in the unit cell, viewed along the a-axis (A) and the b-axis (B)

4.2.4 An attempt to coordinate the newly formed carbene complex 26b to other metal centers

Carbene complex **26b** could potentially act as a mono or bidentate ligand through the soft P and/or hard N donor atoms. Soft transition metals have a greater affinity towards P donors than towards N donors.[34] Reaction of two molar equivalents of PPh_3 with one molar equivalent of $[RhClCOD]_2$ quantitatively yielded $(COD)Rh(Cl)PPh_3$.[35] The same reaction was carried out with **26b** as phosphine ligand (equation 1) but no coordination took place. The four-membered chelate complex

[34] V.F. Kuznetsov, G.A. Facey, G.P.A. Yap, H. Alper, *Organometallics*, 1999, **18**, 4706.

[35] J. Chatt, L.M. Venanzi, *J. Chem. Soc.*, 1957, 4735.

27b resulted almost quantitatively as the main product while no evidence for the formation of **IVb** was obtained.

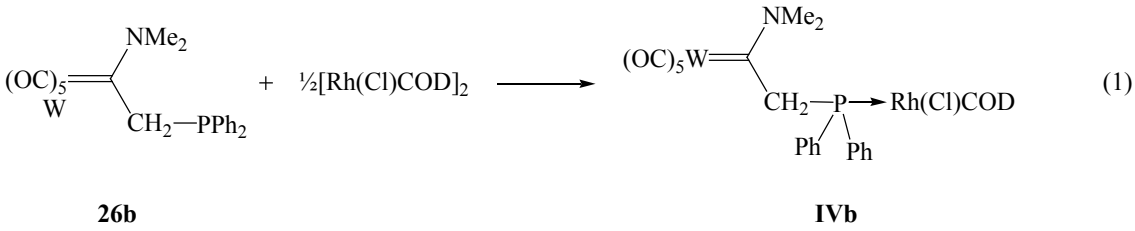

(1)

26b **IVb**

Coordination of the P and N donor atoms of ligands to various metal centers are known.[36,37,38] The reaction of **26b** with $CODPtCl_2$ to prepare **Vb** was also attempted (equation 2).[36] Again, complex **27b** was identified as the sole product rather than the complex of complexes, **Vb**. It is clear that similar reactions should, in future, only be attempted when cyclisation can be excluded as a reaction pathway – probably by simple phosphine substitution of one (preferably *cis*) CO ligand.

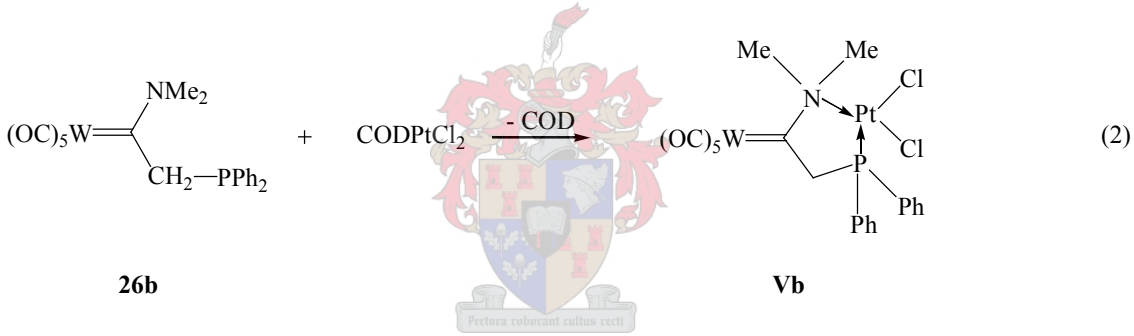

(2)

26b **Vb**

4.3 Conclusions and future work

The reaction of the deprotonated Fischer-type amino carbene complexes $[(CO)_5M{=}C(NMe_2)CH_2]Li$ (M = Cr or W) with $ClPPh_2$ produced the desired amino-phosphine Fischer-type carbene complexes, $(CO)_5M{=}C(NMe_2)CH_2PPh_2$ (M = Cr or W). Only the tungsten complex of this type (**26b**) could be obtained in a reasonable yield, since the chromium analogue (**26a**) quickly converted to the novel four-membered carbene-phosphine chelate, $(CO)_4\overline{Cr{=}C(NMe_2)CH_2PPh_2}$ (**27a**). $(CO)_5Cr{=}C(NMe_2)CH_2PPh_2$ (**26a**) was characterised before this conversion to **27a** was completed.

[36] A. Habtemariam, B. Watchman, B.S. Potter, R. Palmer, S. Parsons, A. Parkin, P.J. Sadler, *J. Chem. Soc., Dalton Trans.*, 2001, 1306.

[37] L. Crociani, G. Bandoli, A. Dolmella, M. Basato, B. Corain, *Eur. J. Inorg. Chem.*, 1998, 1811.

[38] M. Valentini, K. Selvakumar, M. Wörle, P.S. Pregosin, *J. Organomet. Chem.*, 1999, **587**, 244.

$(CO)_5W{=}C(NMe_2)CH_2PPh_2$ (**26b**) also converted to $(CO)_4W{=}C(NMe_2)CH_2PPh_2$ (**27b**) but at a much slower rate. $(CO)_5Cr{=}C(NMe_2)CH_2P(Ph)_2Cr(CO)_5$ (**28a**) was also isolated from the reaction mixture of **26a**. The four-membered chelate (**27a**) is very stable and did not show any insertion reaction with CS_2, Ph-C≡N, Ph-C≡CH or $MeNHNH_2$. The four-membered aminocarbene-phosphine chelates (**27a** and **27b**) represent the first examples of structurally characterised C,P-chelate carbene complexes. The Cr-$C_{carbonyl}$ bond length *trans* to the phosphine atom and *trans* to carbene carbon in **28a** are similar but significantly shorter than the other Cr-$C_{carbonyl}$ bond distances (CO *trans* to CO). This confirmed that the carbene and the phosphine ligand exhibit similar *trans*-influences and that CO has a greater *trans*-influence than both these ligands.

Coordination of the amino-phosphine carbene complex, **26b**, to rhodium and platinum was unsuccessful and the four-membered chelate, **27b**, was identified as the main product of these reactions. Intramolecular chelation is preferred to coordination involving another metal.

In order to achieve the coordination of such a amino-phosphine carbene complex to another metal, further tailoring of this complex is required to prevent the formation of the four-membered chelates. A possible solution could be the substitution of a carbonyl ligand with a ligand such as PPh_3, preferably before the introduction of the phosphine group to the carbene side chain. The loss of a third carbonyl ligand is unlikely. Other donor atom combinations, for example P and S should also be explored by using thiocarbenes as starting materials.

The formation of the four-membered chelates could also be followed kinetically to obtain more quantitative information regarding differences in reactivity between chromium and tungsten. Such a study should be underpinned and complimented by a theoretical study.

4.4 Experimental

4.4.1 General

The general techniques described in Section 2.4.1 were also applied to the work in this chapter. $Cr(CO)_6$, $W(CO)_6$, and $ClPPh_2$ were purchased from commercial suppliers and used without further

purification. *n*-BuLi, purchased from Aldrich was standardised before use.[39] The complexes, (dimethylaminomethylcarbene)pentacarbonylchromium(0) and its tungsten analogue, were prepared according to literature procedures.[40,41]

4.4.2 Preparation of $(CO)_5Cr=C(NMe_2)CH_2PPh_2$, 26a, $(CO)_4\overline{Cr=C(NMe_2)CH_2PPh_2}$, 27a, and $(CO)_5Cr=C(NMe_2)CH_2P(Ph_2)Cr(CO)_5$, 28a

$(CO)_5Cr=C(NMe_2)CH_3$ (0.36 g, 1.4 mmol) was treated with *n*-BuLi (0.97 cm^3, 1.5 M, 1.5 mmol) in THF at -78°C and stirred for 45 minutes before $ClPPh_2$ (0.25 cm^3, 1.4 mmol) dissolved in THF was added dropwise *via* a dropping funnel to the reaction mixture. The reaction mixture became darker and was stirred at -78°C for 1 hour and allowed to reach room temperature overnight. The THF was removed *in vacuo* and the oily residue chromatographed with diethyl ether/hexane (1:2) as eluent. The first fraction collected contained complex **28a**, the second fraction **26a** and the last yellow fraction **27a**. In spite of the bulk of **26a** converting (90 % conversion) to **27a** during overnight stirring, quantities suitable for characterisation could be obtained. Repetition of the reaction and stirring for less than 4 hours yielded 0.25 g (40 %) of **26a**, 0.06 g (10 %) of **27a** and 0.04 g (4 %) of **28a**. Removal of the solvent yielded **26a** as a yellow oil (not pure, contains **27a**) and **27a** and **28a** as yellow microcrystalline materials. Crystallisation of **27a** from a CH_2Cl_2/pentane solution and **28a** from a diethyl ether/hexane (1:2) solution (-20°C) gave the yellow crystals suitable for single crystal X-ray determination.

Pectora roborant cultus recti

Yield: Complex **26a** 0.061 g (10 %)
Complex **27a** 0.29 g (50 %) Melting point: 151°C (decomposition)
Complex **28a** 0.035 g (4 %) Melting point: 110 - 115ºC (decomposition)

Elemental analysis (%): Calc. for **27a** ($C_{20}H_{18}NO_4PCr$) (419.33): C, 57.29; H, 4.33; N, 3.34. Found: C, 57.32; H, 4.23; N, 3.64. Calc. for **28a** ($C_{26}H_{18}NO_{10}PCr_2$) (639.3): C, 48.84; H, 2.84; N, 2.19. Found: C, 48.62; H, 2.73; N, 2.23.

---

[39] M.R. Winkle, J.M Lansinger, R.C. Ronald, *J.Chem. Soc., Chem. Commun.*, 1980, 87.

[40] F. Kreissl, in: W. A. Herrmann (Ed.), *Synthetic methods of Organometallic and Inorganic Chemistry, Volume 7, Transition Metals Part 1*, Georg Thieme Verlag, Stuttgart, 1997, p. 127.

[41] E.O. Fischer, M. Leupold, *Chem. Ber.*, 1972, **105**, 599.

4.4.3 Preparation of $(CO)_5W=C(NMe_2)CH_2PPh_2$, 26b, and $(CO)_4\overline{W=C(NMe_2)CH_2P}Ph_2$, 27b

Complexes **26b** and **27b** were prepared in the same way as **26a** and **27a** using $(CO)_5W=C(NMe_2)CH_3$ (0.46g, 1.2 mmol), *n*-BuLi (0.85 cm^3, 1.4 M, 1.2 mmol) and $ClPPh_2$ (0.21 cm^3, 1.2 mmol) as starting materials. The two products were separated by column chromatography with hexane/ether (1:1) as eluent. Fraction 1 contained **26b** and fraction 3 (which formed during the chromatography) **27b**. Complexes **26b** and **27b** were obtained as yellow microcrystalline materials after the fractions were dried under vacuum. Crystallisation from a concentrated CH_2Cl_2 solution layered with pentane at -20 °C yielded yellow crystals of **27b**, suitable for single crystal X-ray determination.

Yield: Complex **27b** 0.34 g (50 %) Melting point: 124°C (decomposition).
Complex **28b** 0.10 g (15 %) Melting point: 100°C (decomposition)

Elemental analysis (%): Calc. for **26b** ($C_{21}H_{18}NO_5PW$) (579.19): C, 43.55; H, 3.13; N, 2.42. Found: C, 43.64; H, 2.80; N, 2.68. Calc. for **27b** ($C_{20}H_{18}NO_4PW$) (551.18): C, 43.58; H, 3.29; N, 2.54. Found: C, 43.50; H, 3.43; N, 2.26.

4.4.4 Attempted preparation of $(CO)_5W=C(NMe_2)CH_2P(Ph_2)Rh(Cl)(COD)$, IVb

$[Rh(Cl)COD]_2$ (0.062 g, 0.13 mmol) was added to **26b** (0.12g, 0.25 mmol), dissolved in CH_2Cl_2 (15 cm^3) and the solution turned deep red. After 2 hours of stirring at room temperature the solvent was removed under vacuum, leaving a brown residue. The brown residue was chromatographed over a short (7 cm) column with ether as eluent. Two yellow fractions were collected, with fraction 2 identified as **27b** based on the IR spectra recorded.

4.4.5 Attempted preparation of $(CO)_5W=C\overline{(NMe_2)CH_2P(Ph_2)}PtCl_2$, Vb

Complex **26a** (0.080 g, 0.14 mmol), dissolved in CH_2Cl_2 was reacted with $CODPtCl_2$ (0.052 g, 0.14 mmol). The reaction mixture became more intense yellow and after 1 hour of stirring at room temperature, the solvent was removed resulting in a yellow residue. The IR spectrum of this residue

indicated complex **27a** as the major carbonyl-containing product. No further purification was carried out.

4.4.6 X-ray structure determinations

The crystal data collection and refinement details for complexes **27a**, **27b** and **28a** are summarised in Table 4.11. Data sets for **27a** were collected on an Enraf-Nonius Kappa CCD diffractometer[42] and the other data sets on a Bruker SMART Apex CCD diffractometer[43] with graphite-monochromated Mo-K_α radiation (λ = 0.71073 Å) each. Data reduction was carried out with standard methods from the software packages DENZO-SMN[44] and Bruker SAINT[45] respectively. Emperical corrections were performed using SCALEPACK[46] and SMART data were treated with SADABS.[47,48] The structures were solved by direct methods (**27a** and **28a**) or the interpretation of a Patterson synthesis (**27b**), which yielded the position of the metal atoms, and conventional Fourier methods. All non-hydrogen atoms were refined anisotropically by full-matrix least squares calculations on F^2 using SHELXL-97[49] within the X-Seed environment.[50] The hydrogen atoms were fixed in calculated positions. POV-Ray for Windows was used to generate the various figures of the three complexes at the 50% probability level.

Additional information regarding these crystal structures is available from Prof H.G. Raubenheimer, Department of Chemistry, University of Stellenbosch.

[42] COLLECT, Data collection software, Nonius BV Delft, The Netherlands, 1998.

[43] SMART, Data collection software (version 5.629), Bruker AXS Inc., Madison, WI, 2003.

[44] Z. Otwinowski, W. Minor, *Methods Enzymol.*, 1997, **276**, 307.

[45] SAINT, Data reduction software (version 6.45) Bruker AXS Inc., Madison, WI, 2003.

[46] L.J. Ferrugia, *J. Appl. Crystallogr.*, 1999, **32**, 837.

[47] R.H. Blessing, *Acta Crystallogr., Sect. A*, 1995, **51**, 33.

[48] SADABS (version 2.05) Bruker AXS Inc., Madison, WI, 2002.

[49] G.M. Sheldrick, SHELX-97. Program for crystal structure analysis, Univ. of Göttingen, Germany, 1997.

[50] L.J. Barbour, *J. Supramol. Chem*. 2001, **1**, 189.

Table 4.11 Crystallographic data for complexes **27a**, **27b** and **28a**

	27a	**27b**	**28a**
Empirical formula	$C_{20}H_{18}CrNO_4P$	$C_{20}H_{18}NO_4PW$	$C_{30}H_{18}Cr_2NO_{11}P$
Formula weight ($g.mol^{-1}$)	419.32	551.17	703.42
Crystal system	Orthorhombic	Orthorhombic	Triclinic
Space group	$P2_12_12_1$	$P2_12_12_1$	P-1
a (Å)	10.6320(10)	10.0998(13)	9.308(2)
b (Å)	12.4850(2)	12.5224(17)	11.521(3)
c (Å)	15.5747(2)	15.921(2)	17.044(4)
α (°)	90.00	90.00	102.914(4)
ß (°)	90.00	90.00	99.139(4)
γ (°)	90.00	90.00	109.336(3)
Volume ($Å^3$)	1976.24(4)	2013.6(5)	1626.3(6)
Z	4	4	2
Calculated density ($g.cm^{-3}$)	1.409	1.818	1.437
Wave length (Å)	0.71073	0.71073	0.71073
Temperature (K)	173(2)	273(2)	100(2)
Absorption coefficient (mm^{-1})	0.684	3.560	0.775
Crystal size (mm)	0.15 x 0.10 x 0.10	0.20 x 0.15 x 0.10	0.15 x 0.15 x 0.10
θ range for data collection (°)	$3.08 \leq \theta \leq 27.47$	$2.07 \leq \theta \leq 28.31$	$1.99 \leq \theta \leq 28.24$
Index range, *hkl*	$-13 \leq h \leq 13$	$-13 \leq h \leq 7$	$-12 \leq h \leq 12$
	$-16 \leq k \leq 16$	$-14 \leq k \leq 15$	$-15 \leq k \leq 15$
	$-20 \leq l \leq 20$	$-21 \leq l \leq 20$	$-22 \leq l \leq 21$
Reflections collected	4498	12489	18400
Independent reflections	4498	4663	7401
Parameters	244	246	408
Goodness of fit	1.040	0.948	1.021
Largest peak	0.351	1.241	0.712
Deepest hole	-0.370	-0.510	-0.347
Final R indices [$I>2\sigma(I)$]	0.0310	0.0213	0.0466
R indices (all data)	0.0789	0.0447	0.1167